Analysis of the role of MreC and MreD in *Staphylococcus aureus*

By

Xing Ma MSc

A thesis submitted for the degree of Doctor of Philosophy

July 2016

Department of Molecular Biology and Biotechnology,

University of Sheffield, Firth Court, Western Bank, Sheffield, S10 2TN

Summary

Cell division is an essential process that is required for bacterial proliferation and is thus an important target for the development of new antimicrobial agents. Bacterial cell division has mainly been studied in rod-shaped microorganisms, where a complex macromolecular machine, termed the divisome, mediates the division process. Cell division requires the coordination of components from the cytoplasm, through the membrane, to the cell wall where synthesis of new peptidoglycan takes place. *Escherichia coli* and *Bacillus subtilis* divisomes involve multiple essential components, mostly of unknown function.

Staphylococcus aureus is a coccus that divides by binary fission in three orthogonal planes. As *S. aureus* is a clinically significant pathogen. The search for new drug targets against this organism is crucial. Although *S. aureus* contains many homologues of the cell division machinery components of *B. subtilis* and *E. coli*, their roles in peptidoglycan dynamics are mostly unknown. In rod shaped cells, the MreC trans-membrane dimer interacts with MreD and forms an MreCD complex which contacts the penicillin-binding proteins (PBPs) and is required for elongation in *S. aureus*. In this study, the role of MreC and MreD in cell growth and division of *S. aureus* has been determined. BACTH revealed that MreC and MreD interact with several divisome components, indicating that in *S. aureus*, these proteins are likely to have a role in peptidoglycan synthesis during division. Specific antibody revealed MreC localise with the cell wall. GFP fusion analysis and immunolocalisation experiments demonstrated that MreCD may transiently localise to the division site and localisation patterns suggest that it might identify previous or potential planes of division by recognising specific forms of peptidoglycan architecture. In-frame deletions of *mreC* and *mreD* were successfully generated in *S. aureus*, suggesting they are not essential for cell viability. However, a role in the cell division is highly possible and discussed.

Acknowledgements

Publications from this study

Garcia-Lara J., Weihs F., Ma X., Walker L., Chaudhuri R.R., Kasturiarachchi J., Crossley H., Golestanian R. & Foster S.J. (2015) Supramolecular structure in the membrane of *Staphylococcus aureus*. *Proc Natl Acad Sci U S A*. 2015 Dec 22;112(51):15725-30. doi: 10.1073/pnas.1509557112. Epub 2015 Dec 7.

Abbreviations

3D	Three dimentional
A	Absorbance
AFM	Atomic force microscopy
Ala	Alanine
Amp	Ampicillin
AMP	Adenosine monophosphate
APS	Ammonium persulphate
ATP	Adenosine triphosphate
BACTH	Bacterial adenylate-cyclase two hybrid
BCIP	5-bromo-4-chloro-3-indolyl phosphate
BHI	Brain heart infusion
Bis-pNPP	bis-p-nitrophenyl phosphate
bp	Base pair
BSA	Bovine serum albumin
Cam	Chloramphenicol
CBP	Calmodulin-binding protein
cfu	Colony forming units
CHIPS	Chemotaxis inhibitory protein
CIP	Calf intestinal alkaline phosphatase
cm	Centimetres
CoA	Co-enzyme A
dH2O	Distilled water
DIG	Digoxigenin
DMF N,	N-dimethylformamide
DMSO	Dimethyl sulphoxide
dNTP	Deoxyribosenucleoside
EDTA	Ethylenediamine tetra-acetic acid
EMP	Embden–Meyerhof–Parnas
Ery	Erythromycin
FRAP	Fluorescence recovery after photobleaching
g	Grams
GAP	Glyceraldehyde-3-phosphate
GAPDH	Glyderaldehyde-3-phosphate dehydrogenase
GFP	Green fluorescent protein
GMP	Guanosine monophosphate

GTP	Guanosine triphosphate
GTPase	Guanosine triphosphate hydrolase
h	Hours
His	Histidine
HMW	High molecular weight
HPLC	High performance liquid chromatography
IgG	Immunoglobulin G
Ile	Isoleucine
IPP	Isopentenyl diphosphate
IPTG	Isopropyl β-D-1-thiogalactopyranoside
Kan	Kanamycin
kb	Kilobase pairs
kDa	Kilodaltons
Km	Michaelis constant
kV	Kilovolts
l	Litre
LB	Luria-Bertani medium
Lin	Lincomycin
LMW	Low molecular weight
LTA	Lipoteichoic acid
M	Molar
mA	Milliamps
mbar	Millibars
MCS	Multiple cloning site
mg	MilliGrams
MIC	Minimum inhibitory concentration
min	Minutes
ml	Millilitres
mM	Millimolar
mm	Millimetres
mol	Moles
mRNA	Messenger RNA
MRSA	Methicillin-resistant Staphylococcus aureus
MSCRAMM	Microbial surface components recognising adhesive matrix molecules
MSSA	Methicillin-sensitive Staphylococcus aureus
MU	4-Methyl umbelliferone
MUG	4-methylumbelliferyl-β-D-galactopyranoside

6

MW	Molecular weight
NA	Nutrient agar
NAD	Nicotinamide adenine dinucleotide
NADPH	Reduced form of nicotinamide adenine dinucleotide phosphate
NB	Nutrient broth
NBT	Nitroblue tetrazolium
NCBI	National Centre for Biotechnology Information
Neo	Neomycin
°C	Degrees Celsius
OD600	Optical density at 600 nm
ORF	Open reading frame
P	Phosphate
PAGE	Polyacrylamide gel electrophoresis
PBP	Penicillin-binding protein
PBS	Phosphate buffered saline
PCR	Polymerase chain reaction
Pfu	Plaque forming units
PG	Peptidoglycan
PI	Isoelecric point
PSpac	Spac promoter
PVDF	Polyvinylidene difluoride
RBS	Ribosome binding site
RNA	Ribonucleic acid
RNase	Ribonuclease
rpm	Revolutions per minute
RT	Room temperature
s	Seconds
SAM	S-adenosylmethionine
SDS	Sodium dodecyl sulphate
SEDS	Separation, elongation, division and sporulation family
Spec	Spectinomycin
TAE	Tris-acetate EDTA
Taq	Thermostable DNA polymerase derived from Thermus aquaticus
TBS	Tris-buffered saline
TCA	Tricarboxylic acid
TE	Tris-EDTA

TEMED N,N,	N'N'-tetramethyl-ethylenediamine
Tet	Tetracycline
Thr	Threonine
TIGR	The Institute of Genomic Research
TMDH	Transposon-mediated differential hybridisation
Tris	Tris(hydroxymethyl)aminomethane
tRNA	Transfer RNA
TSB	Tryptic soya broth
UV	Ultraviolet
V	Volts
v/v	Volume for volume
Van-FL BODIPY	FL conjugated vancomycin
VISA	Vancomycin-insensitive *S. aureus*
VRE	Vancomycin-resistant enterococcus
VRSA	Vancomycin-resistant *S. aureus*
w/v	Weight for volume
WTA	Wall teichoic acid
xg	x Gravity
X-Gal	5-bromo-4-chloro-3-indolyl-β-D-galactopyranoside
Xyl	Xylose
μF	Microfarad
μg	MicroGrams
μl	Microlitre
Φ	Phage

11

Table of Figures

List of Tables

1   Chapter 1 Introduction

1.1   Bacterial morphology

The shapes of bacteria are highly diverse as shown in Fig. 1.1. For example, there are straight rods, such as *Escherichia coli* and *Bacillus subtilis*, curved rods with or without tapered ends and a polar stalk at one end, such as *Caulobacter crescentus* and *Vibrio cholerae*, respectively. There are apparently spherical bacteria, such as *Neisseria gonorrhoeae* and *Staphylococcus aureus*, whereas, some are ovococci, such as *Streptococcus pneumoniae*. Cell shape is ultimately coordinated by genetic and epigenetic information and various physical constraints (Margolin 2009). Understanding the control of cell shape is essential for the study of cell biology at the molecular level. For instance, chromosomal replication and segregation is coordinated with division to make sure that each daughter cell receives an equal amount of genetic information. If the cell shape is altered then this coordination can be disrupted.

1.1.1   The cell wall

In most bacteria the cell wall is the major component of the cell that defines its shape and acts as an exoskeleton (Holtje 1998). Since the cell membrane is delicate, it is retained by the cell wall made of porous and rigid material, such as peptidoglycan (also known as murein) laying immediately outside of the cytoplasmic membrane (Fig. 1.2). Peptidoglycan is a polymer of disaccharides (glycan) cross-linked by short chains of amino acids (peptide) (Typas *et al.* 2012). The peptidoglycan sacculus is the main determinant of bacterial morphology since isolated sacculi retain the cell shape (Turner *et al.* 2014). Peptidoglycan synthesis and hydrolysis compensate to each other to allow the insertion of the newly synthesized material without infinite thickening of cell wall. The process is ultimately coordinated by bacterial cytoskeletal elements, often including actin-like MreB and the tubulin-like FtsZ (Typas *et al.* 2012).

The overall cell wall structure differs between the Gram-positive bacteria (those that retain the purple crystal violet dye when subjected to the Gram-staining procedure) and Gram-negative bacteria (those do not retain the crystal violet) (Fig. 1.2). The Gram-positive bacteria cell wall is thick (20 – 80 nm) and consists of several layers of peptidoglycan and anionic polymers, such as teichoic acids and lipoteichoic acids running perpendicular to the peptidoglycan sheets and covalently linked to the peptidoglycan or inserted in the adjacent cell membrane (Fig. 1.2 A). In comparison, the Gram-negative cell wall is thin (7-10 nm) and composed of a single layer of peptidoglycan surrounded by an outer membrane which contains lipopolysaccharide (LPS or endotoxin), a unique component to Gram-negative

bacteria that is responsible for antigenic properties (Fig. 1.2 B). Gram-negative cell wall lacks teichoic acid (Holtje 1998).

1.1.2   Physical constraints limit the cell shape

The evolutionary morphological diversity of bacteria has been was partially selected by physical constraints. For example, *C. crescentus* developed stalks to extend the surface area for nutrient foraging in nutrient-limited environments (Wagner *et al.* 2006). Another physical key constraint is turgor pressure, which results from lower water activity in the cytoplasm relative to the outside environment. For example, the pressure can reach as high as 3 megapascals in Gram-positive bacteria (Margolin 2009). In order to counteract such a high turgor, the cell wall must be oriented to be unbreakable (Margolin 2009).

Physical pressures were historically thought to be the main selective constraints for prokaryotes, since prokaryotes were supposed to lack a cytoskeleton and were less complex than eukaryotes. However, sequencing of multiple genome and labelling with fluorescent proteins has uncovered the importance of an apparent prokaryotic cytoskeleton, which is probably as highly organised and complex as the eukaryotic cytoskeleton (Lewis 2004).

1.2   The growth of the cell wall

The growth of cylindrical bacteria occurs via incorporation of peptidoglycan precursors into the existing cell wall mainly occurring during elongation as well as regular cell division (den Blaauwen *et al.* 2008), characterised by the two-competing-sites model (Lleo *et al.* 1990). Ovococci grow mainly via their division septa and also certain length extension, whereas cocci grow apparently mostly via division septa (Zapun *et al.* 2008; Zhou *et al.* 2015).

Family	Species	Shape	MreB	MreC	MreD	RodZ	DivIVA
γ-proteo	*Escherichia coli*		+	+	+	+	-
γ-proteo	*Vibrio cholerae*		+	+	+	+	-
γ-proteo	*Francisella tularensis*		-	-	-	-	-
β-proteo	*Neisseria gonorrhoeae*		-	-	-	-	-
β-proteo	*Bordetella pertussis*		+	+	+	+	-
α-proteo	*Sinorhizobium meliloti*		-	-	-	-	-
α-proteo	*Caulobacter crescentus*		+	+	+	+	-
α-proteo	*Rickettsia typhi*		+	+	-	+	-
ε-proteo	*Helicobacter pylori*		+	+	-	-	-
Firmicutes	*Bacillus subtilis*		+	+	+	+	+
Firmicutes	*Staphylococcus aureus*		-	+	+	+	+
Firmicutes	*Streptococcus pyogenes*		-	-	-	+	+
Mollicutes	*Mycoplasma pneumoniae*		-	-	-	-	-
Actino-bacteria	*Corynebacterium glutamicum*		-	-	-	-	+
Spirochetes	*Borrelia burgdorferi*		+	+	-	+	-
Cyano-bacteria	*Anabaena variabilis*		+	+	+	+	-

Figure 1-1 Phylogeny of some shape-determining proteins across representative bacteria, adapted from Margolin (2009).

The bacteria are gathered by family. For each bacteria, classic cell shape is drawn (not to scale). The presence or absence of MreB, MreC, MreD, RodZ or DivIVA in different bacteria as determined by STRING COG was described in (Alyahya *et al.* 2009).
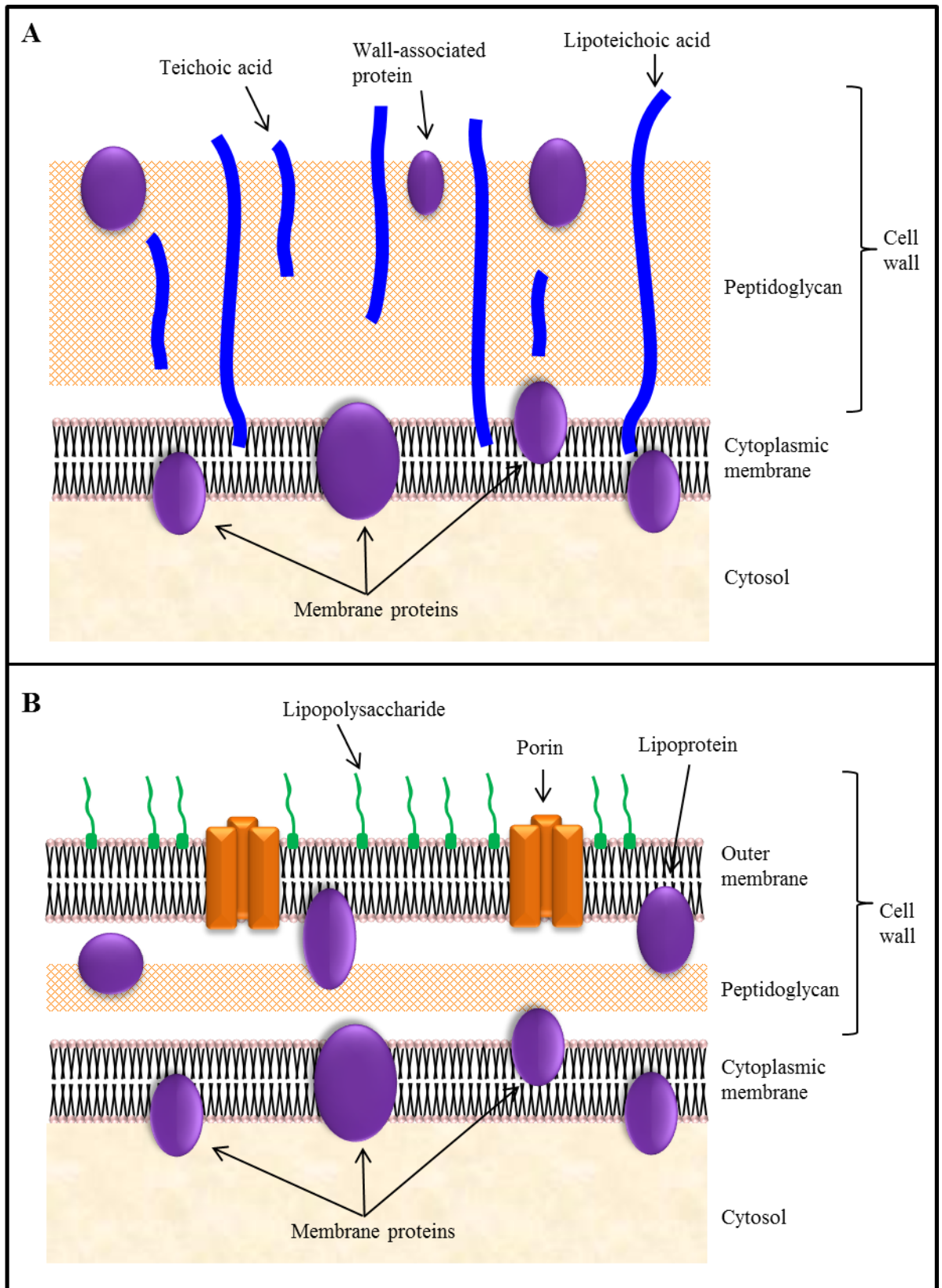
Figure 1-2 Schematic of the cell wall in Gram-negative and Gram-positive bacteria, modified from Brock biology of Microorganisms 2006.

A.   Gram-positive bacterium cell wall

B.   Gram-negative bacterium cell wall

1.2.1 Control of cylindrical elongation in rod-shaped bacteria

In rod-shaped bacteria such as *E. coli* and *B. subtilis*, growth is precisely controlled by sequential switching between two morphogenetic systems, elongation and septation (Fig. 1.4 A). At the time of cell elongation, cell size doubles by peptidoglycan synthesis along the sidewall, maintaining constant cell diameter (Grover *et al.* 1977) (Fig. 1.4A).

Many proteins have been identified in the control of cell morphology using mutagenesis technologies. Deletion of *mreB* (for murein region 'e') leads to spherical cell formation in *E. coli* (Levin *et al.* 1992), *B. subtilis* (Varley & Stewart 1992) and *Salmonella typhimurium* (Costa & Anton 1999). The *mreC* and *mreD* genes, found on the same operon as *mreB,* are also required for the maintenance of rod shape in *E. coli* (Wachi *et al.* 1987; Wachi *et al.* 1989), *B. subtilis* (Leaver & Errington 2005), and *S. typhimurium* (Costa & Anton 1999). *pbp2* and/or *rodA* mutants appeared to be unable to elongate in *B. subtilis* (Henriques *et al.* 1998), *S. typhimurium* (Costa & Anton 1999) and the ovococcus *Streptococcus thermophilus* (Thibessard *et al.* 2002). The shape defect associated with absence of the above proteins suggested that these proteins have a role in cell wall synthesis.

MreB is highly conserved among most of the rod shaped bacteria (Margolin 2009). Bioinformatic studies showed that the bacterial protein MreB contains the sequence motifs that are conserved in the actin super-family, as well as StbA (ParM) and FtsA (Bork *et al.* 1992), which will be discussed later. The crystal structure of MreB from *Thermotoga maritima* showed that MreB and actin are highly likely derived from a common ancestral sequence (van den Ent *et al.* 2001). Both *in vitro* and *in vivo* studies showed that MreB and its *B. subtilis* paralogues MreBH and Mbl (MreB like) polymerise to form highly dynamic helical filaments (Jones *et al.* 2001; Carballido-Lopez & Errington 2003; Defeu Soufo & Graumann 2004; Gitai *et al.* 2004; Kruse *et al.* 2005; Slovak *et al.* 2005) and bind to and hydrolyse ATP, as actin does (Esue *et al.* 2005). MreB forms cables in a helical pattern which extended much of the length of the cell (Jones *et al.* 2001), this is similar to the pattern of new peptidoglycan incorporation shown by fluorescent vancomycin labelling (Daniel & Errington 2003). MreB cables form a double helix that extends the length of the cell wall during elongation, the cables then collapse to generate two MreB rings that surround the FtsZ ring during cell division and reassemble into new cables in the daughter cells (Vats & Rothfield 2007). The above findings indicate that MreB acts as an apparent cytoskeletal element that directs lateral peptidoglycan synthesis. Later evidence suggests that MreB may not form a continuous helix but dynamic patches which polymerise across the short axis of the cell and provide localisation for peptidoglycan synthesis machinery (Dominguez-Escobar *et al.* 2011). The transmembrane proteins MreC and MreD are thought to stabilise the MreB

cytoskeleton by linking the cytosolic MreB filaments to the extracellular cell wall synthesis machinery (Divakaruni *et al.* 2005; Kruse *et al.* 2005; Leaver & Errington 2005).

Lateral cell wall synthesis is coordinated by a protein complex consisting of MreB, MreC and MreD along with PBPs and the shape, elongation, division and sporulation (SEDS) protein RodA (Kruse *et al.* 2005) (Fig. 1.3). SEDS proteins are frequently organised into operons with class B PBPs, and are proposed to be responsible for the translocation of peptidoglycan precursors from the cytoplasm to the extracellular site of synthesis (Ehlert & Holtje 1996). The localisation of cytoskeleton MreB localisation was found to be dependent on RodA, MreC and MreD, and association of MreB, MreC and MreD into a protein complex is essential for lateral growth (Kruse *et al.* 2005).

MreC has also been shown to have a helical pattern in *B. subtilis* (Leaver & Errington 2005) and *C. crescentus* (Divakaruni *et al.* 2005; Dye *et al.* 2005). Direct interactions between MreB, MreC, MreD, RodA and many PBPs have been observed by pull-down and bacterial two hybrid assays. (Kruse *et al.* 2005; Leaver & Errington 2005; van den Ent *et al.* 2006; Kawai *et al.* 2009; White *et al.* 2010). MreB, MreC and MreD also directly interact with proteins involved in synthesis of peptidoglycan precursors and in wall teichoic acid (WTA) synthesis (Mohammadi *et al.* 2007; Formstone *et al.* 2008; White *et al.* 2010). Therefore, lateral cell wall synthesis is conducted by a protein complex (Fig. 1.3) consisting of cytoskeletal components (MreB, MreC and MreD) to ensure insertion of new peptidoglycan material into the existing cell wall and proteins, such as PBPs and RodA, which are directly involved in the synthesis and insertion of new peptidoglycan into the old lateral cell wall.

RodZ localises in a helical pattern similar to MreB in *E. coli*, *B. subtilis* and *C. crescentus* ((Shiomi *et al.* 2008; Alyahya *et al.* 2009), and loss of RodZ results in spherical cells and the misassembly of MreB (Shiomi *et al.* 2008; Bendezu *et al.* 2009), suggesting that MreB and RodZ localization are dependent on each other (Margolin 2009). RodZ localises to where peptidoglycan is actively synthesised, indicating a role for RodZ in lateral cell wall synthesis (Alyahya *et al.* 2009). RodZ directly interacts with RodA, MreB and MreD, suggesting its involvement in the elongation machinery (van den Ent *et al.* 2010; White *et al.* 2010). Interestingly, pseudorevertants of *E. coli ΔrodZ* mutants acquired a near-wild-type rod-shaped phenotype, suggesting that RodZ is not indispensable for cell wall elongation (Niba *et al.* 2010).

Nascent peptidoglycan is a polymer made up of repeating disaccharides cross-linked via peptide side chains terminated by two D-alanine residues (D-ala-D-ala), which are cleaved before maturation by carboxypeptidases or certain PBPs (Matsuhashi *et al.* 1990). A

fluorescent derivative of vancomycin that binds to the D-ala-D-ala residues of newly synthesised peptidoglycan (Pinho & Errington 2003) has revealed a cylindrical incorporation pattern of labelling in *B. subtilis* (Daniel & Errington 2003; Tiyanont *et al.* 2006), *E. coli* (Varma *et al.* 2007) and *C. crescentus* (Divakaruni *et al.* 2007). No overall pattern of synthesis but a discontinuous and patchy incorporation has been observed in *E. coli* and *C. crescentus* (Turner *et al.* 2013). Total internal reflection microscopy has shown that MreB does not form a helical cytoskeletal structure but forms distinct foci, moving perpendicular and bidirectionally along the cell axis of *B. subtilis,* and labelling with vancomycin showed that peptidoglycan precursors match the MreB localisation pattern (Dominguez-Escobar *et al.* 2011; Garner *et al.* 2011). To investigate how the bacterial cytoskeleton relates to cell wall synthesis, MreB polymerisation was destroyed by an MreB-specific drug, A22 (Iwai *et al.* 2002), this leads to an alteration of cell shape suggesting that the cytoskeleton directs the pattern of new cell wall growth (Gitai *et al.* 2005). Notably, as discussed above, loss of MreB does not prevent peptidoglycan synthesis as rod-shaped cells become round by expanding their walls uniformly. In the past, Daniel and Errington (2003) showed that peptidoglycan incorporation is dependent upon the presence of Mbl but not MreB. A recent breakthrough study found that the inhibition of cell wall synthesis blocks the motility of MreB (Garner *et al.* 2011), implying that cell wall synthesis drives MreB dynamics.
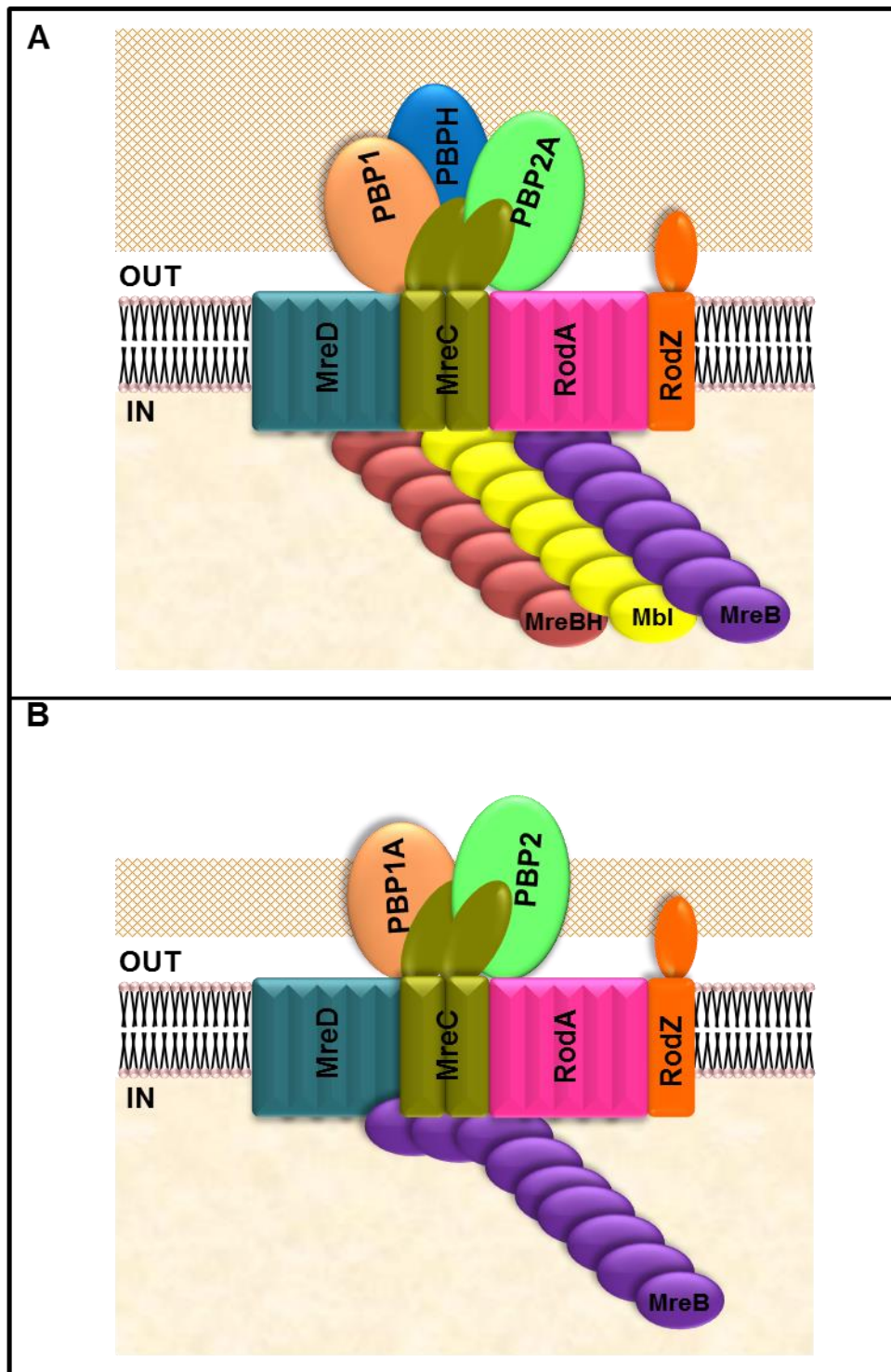
Figure 1-3 Elongation machinery of *B. subtilis* and *E. coli*

Schematic representations of the elongation machineries in *B. subtilis* (A) and *E. coli* (B). The components were determined based on protein-protein interactions and co-localisation. Not all known interactions between the elongation components are shown here. Modified from (Carballido-Lopez & Formstone 2007; Chastanet & Carballido-Lopez 2012; Typas *et al.* 2012)

1.2.2 Cell division

The second fundamental phase of bacterial cell wall growth following elongation is cell division, in which a septum is formed in the middle of the cell and generates two daughter cells (Bramhill 1997). Temporally and spatially, cell division must be tightly coupled to chromosome replication, chromosome segregation, and cell growth to ensure that each daughter cell receives a complete copy of the genetic material with high fidelity and is of the appropriate size and shape (Weart & Levin 2003). For the purpose of this study, I will focus on prokaryotic cell division and in particular three common types of Gram-positive bacterial cell shape: cylindrical, typified by *B. subtilis*; ovococci, typified by *S. pneumoniae*; and cocci, typified by *S. aureus* (Fig. 1.4).

1.2.2.1 The bacterial tubulin homolog FtsZ controls cell division and morphology

FtsZ is highly conserved in almost all prokaryotes, most archaea and also in the organelles of many eukaryotes (Osteryoung *et al.* 1998; Beech *et al.* 2000) but absent in the prokaryotes *Chlamydia*, *Aeropyrum pernix* and *Ureaplasma urealyticum* (Margolin 2000b).

FtsZ shows high sequence homology with the N-terminal GTP-binding site of eukaryotic tubulin, despite limited homology across the remaining protein sequence (de Boer *et al.* 1992a). The crystal structure of *Methanococcus jannaschii* FtsZ confirmed the protein to be a structural homologue of tubulin and suggested a cytoskeletal role for FtsZ (Lowe & Amos 1998). Like tubulin, FtsZ is a GTPase that assembles into cylindrical protofilaments utilising GTP (de Boer *et al.* 1992a; Mukherjee & Lutkenhaus 1994). However, unlike tubulin, FtsZ protofilaments do not form microtubules, because FtsZ lacks the loops involved in lateral interactions of tubulin protofilaments (Nogales *et al.* 1998).

In vitro, *E. coli* FtsZ assembles into protofilaments that are one subunit thick and 120 subunits long (Chen & Erickson 2005), and can, under some conditions, further associate into paired filaments or larger bundles of protofilaments (Erickson *et al.* 1996). Binding of the FtsZ N-terminus to GTP induces polymerisation of the protein that then activates GTP hydrolysis (Singh *et al.* 2007; Ruiz-Avila *et al.* 2013), where FtsZ acts as its own GTPase-activating protein; when assembled into protofilaments, the bottom interface of one FtsZ monomer interacts with the GTP pocket of the adjacent FtsZ monomer via a cation-coordinated loop (T7 loop) (Mukherjee et al. 2001; Scheffers and Driessen 2001; Scheffers et al. 2002).

Historically, FtsZ has been believed to serve as a scaffold (Levin and Losick, 1994) and recruits cell division components to the division site using the energy release associated with its function in GTP hydrolysis (Daniel and Errington, 2000; Lucet et al., 2000; Gueiros-Filho

and Losick, 2002), suggesting that it is probably the most critical component of the divisome (Sievers & Errington 2000; Vaughan *et al.* 2004; Singh *et al.* 2007). FtsZ was named after filamenting temperature-sensitive (Ts) mutant Z (Lutkenhaus *et al.* 1980). Mutagenesis studies of *ftsZ* in *B. subtilis* and *E. coli* showed that the cells do not form complete septa but generate long filaments, although the cells undergo normal elongation, DNA replication and chromosome segregation (Lutkenhaus *et al.* 1980; Beall & Lutkenhaus 1991; Dai & Lutkenhaus 1991). In rod shaped cells, FtsZ assembles into a cytokinetic ring called the Z ring at the cell division site on the inside of the cytoplasmic membrane when cells are dividing or prior to division (Bi & Lutkenhaus 1991; Ma *et al.* 1996). The Z ring represents the initial stage in bacterial cell division, with all other division proteins requiring FtsZ for proper localisation (Errington *et al.* 2003). A membrane-targeted form of recombinant FtsZ is sufficient for *in vitro* Z ring formation and constriction of tubular liposomes, suggesting that FtsZ provides the major force in constriction of the cell membrane (Osawa *et al.* 2008). Recently, single-molecule based super-resolution imaging revealed that *E. coli* FtsZ-ring is stabilised by a multi-layered protein network, consisting of ZapA, ZapB and MatP, which also modulates cell constriction and chromosomal segregation (Buss *et al.* 2015), suggesting that the divisome structure is not solely dictated by the FtsZ-ring.

Single-molecule based super-resolution imaging has also demonstrated that the Z ring is a compressed helical structure that is likely consisted of randomly overlapping bundles of FtsZ protofilaments, rather than one single continuous closed structure in *E. coli* (Fu *et al.* 2010). Quantitative fluorescence imaging of FtsZ found that only 30% of FtsZ formed a ring structure, whilst 70% of FtsZ was diffuse in the cytoplasm in both *E.coli* and *B.subt*ilis (Anderson *et al.* 2004). Time-lapse microscopy of FtsZ-GFP showed that FtsZ localised as a dynamic helical structure bound to the inside membrane throughout the *B. subtilis* and *E. coli* cells (Thanedar & Margolin 2004; Peters *et al.* 2007). Single molecule tracking of FtsZ-GFP illustrated that, in the time frame used, *E. coli* FtsZ molecules were stationary within the Z ring, however, very dynamic outside the Z ring structure (Niu & Yu 2008) Fluorescence recovery after photobleaching (FRAP) analysis using a FtsZ-GFP has demonstrated that, the Z ring itself was also highly dynamic in *E. coli* and *B. subtilis*, with fluorescence recovery 8 or 9 seconds, respectively (Anderson *et al.* 2004).

In the presence MreB, FtsZ shuffles from the sidewall to the division site reminiscent of the MreB relocalisation system suggesting that FtsZ may serve a similar function to MreB (Margolin 2009). Furthermore, FtsZ is involved in both septal synthesis and a subset of sidewall synthesis by recruiting the peptidoglycan synthesis machinery via PBP2 in *E. coli* and *C. crescentus* (Aaron *et al.* 2007; Varma *et al.* 2007; Vats *et al.* 2009). Both FtsZ and

MreB ensure even peptidoglycan synthetic machinery distribution, since *ftsZ⁻ E. coli* or *S. aureus* mutants synthesize a patchy cell wall (Pinho & Errington 2003). This implies, like actin, tubulin cables also play key roles in tethering the peptidoglycan synthetic machinery and therefore ensuring the new cell wall materials are precisely distributed to the correct location.

FtsZ is essential for bacterial cell shape and size (Margolin 2009). In *C. crescentus*, cell poles are tapered since FtsZ contributes significantly to cell wall elongation near the midcell, resulting in constriction instead of septation (Aaron *et al.* 2007). Before FtsZ assembles to the division site, cells grow via dispersed peptidoglycan incorporation over the entire sidewalls (Aaron *et al.* 2007). FtsZ depleted *E. coli* and *C. crescentus* mutants fail to divide and grow into long filaments (Wang *et al.* 2001; Vats & Rothfield 2007). In *B. subtilis*, mutation in UgtP, a negative regulator for FtsZ ring assembly, leads to shorter cell formation even in rich medium (Weart *et al.* 2007). In *E. coli*, a gain-of-function mutation in FtsA also generates 20% shorter cells in rich medium, by enhancing FtsZ-FtsA interactions and therefore boosting the integrity of the Z ring (Geissler *et al.* 2007).
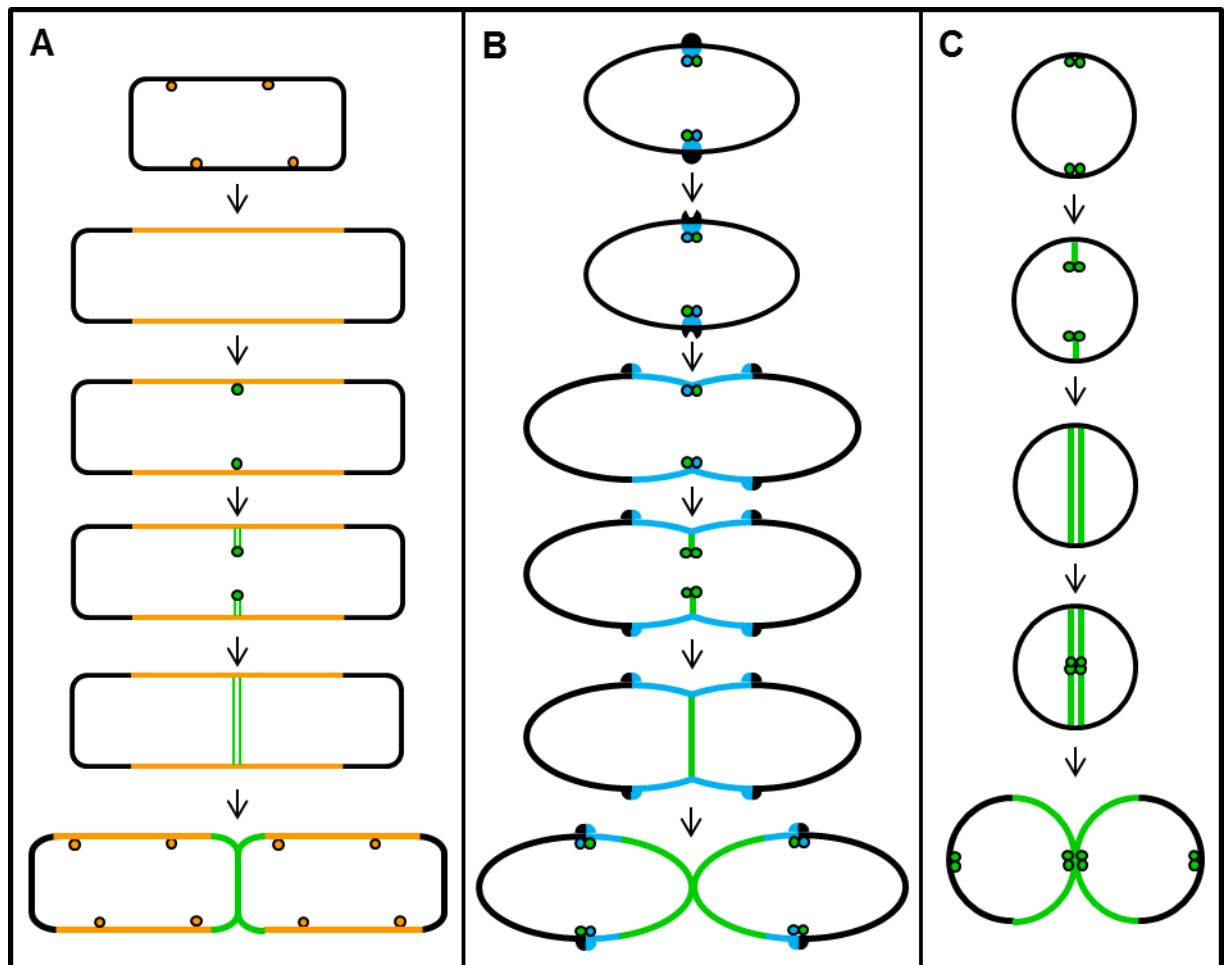
Figure 1-4 Cell wall assembly in three representative Gram-positive species

Schematic representations of cell wall assembly in Gram-positive A), rods (e.g., *B. subtilis*), B), ovococci (e.g., *S. pneumoniae*), C), and cocci (e.g., *S. aureus*). The elongation machinery is shown in orange with a black outline; the peripheral synthesis machinery is shown in cyan with black outlines; the septal synthesis machinery is represented in green with a black outline. The parental cell wall is represented in black; the nascent lateral cell wall is represented in orange; the new peripheral cell wall and the new septal cell wall are represented in cyan and green. Modified from (Zapun *et al.* 2008; Pinho *et al.* 2013).

1.2.2.2 Essentiality of bacterial cell division process

Bacterial cell division is mediated by the divisome, a complex macromolecular machine, which is formed of a number of proteins. Many cell division components have been shown to be essential for viability: ten genes involved in cell division are essential in *B. subtilis* (Kobayashi *et al.* 2003), *E. coli* (Buddelmeijer & Beckwith 2002) and *C. crescentus* (Goley *et al.* 2011), whilst six division genes are essential for growth of *S. pneumoniae* (Song *et al.* 2005).

Cell division is conserved in most prokaryotes where cells divide by binary fission with growth either occurring in between or during division. The nucleoid duplicates and segregates to opposite regions of the dividing cell. Membrane invagination occurs at midcell and the peptidoglycan septum forms, separating the two nucleoids. The cells then split, giving rise to two daughter cells of equal size. In some bacterial species, alternative mechanisms such as multiple offspring formation and budding are used, sometimes conditionally (Angert 2005).

1.2.2.3 Temporal control of bacterial cell division

Cell growth and division are precisely coordinated to make sure that cells are the right size for their developmental fate. Analysis of *Enterococcus hirae* division found that cell division initiation was independent of growth rate and chromosome replication, but occurred at a constant cell volume (Gibson *et al.* 1983). Studies of *E.coli* and *B.subtilis* found that cells

need to elongate to a certain length before chromosome segregation starts, which is a prerequisite for septum formation (Donachie & Begg 1989; Sharpe *et al.* 1998). Therefore, to ensure cells maintain the correct size and growth rate, a mechanism must exist to detect nutrient availability and signal this information to the divisome to coordinate proper temporal septum formation initiation (Wang & Levin 2009). Indeed, studies in *E. coli* and *B. subtilis* demonstrated that growth rate impacts on timing of FtsZ assembly and the period between Z ring formation and cytokinesis, suggesting FtsZ polymerises in a growth rate dependent manner (Den Blaauwen *et al.* 1999; Weart & Levin 2003). In *B.subtilis*, it was suggested that the coordination of cell size with growth rate is governed by the glucolipid biosynthesis pathway, which regulates appropriate FtsZ assembly by ensuring cells reach a 'critical mass' prior to initiating cytokinesis (Weart *et al.* 2007).

1.2.2.4 The bacterial cell division machinery

The cell division machinery has been extensively studied in the rod-shaped model organisms *E.coli* and *B.subtilis*. Whilst many components of the divisome have been identified, the precise molecular functions of many of these proteins remain to be explored. Mutagenesis and conditional lethality analysis, *in vivo* imaging, structural determination, biochemical assays and extensive two and three-hybrid screens have been powerful tools in identifying novel divisome components and elucidating their function in the division process. The key components of the divisome between different organisms are mostly conserved, whereas differences in composition of the division apparatus have seen in *E.coli* and *B.subtilis* (Fig. 1.5).

The divisome proteins can be grouped into two categorises according to their localisation and timing of participation in division; the FtsZ interacting proteins, such as FtsA, ZipA (in *E. coli*), ZapA (in *B. subtilis* and *E. coli*) and EzrA (in Gram-positive bacteria), interact directly, whereas the late division proteins depend on the FtsZ interacting proteins for localisation to the division site (Daniel *et al.* 2006).
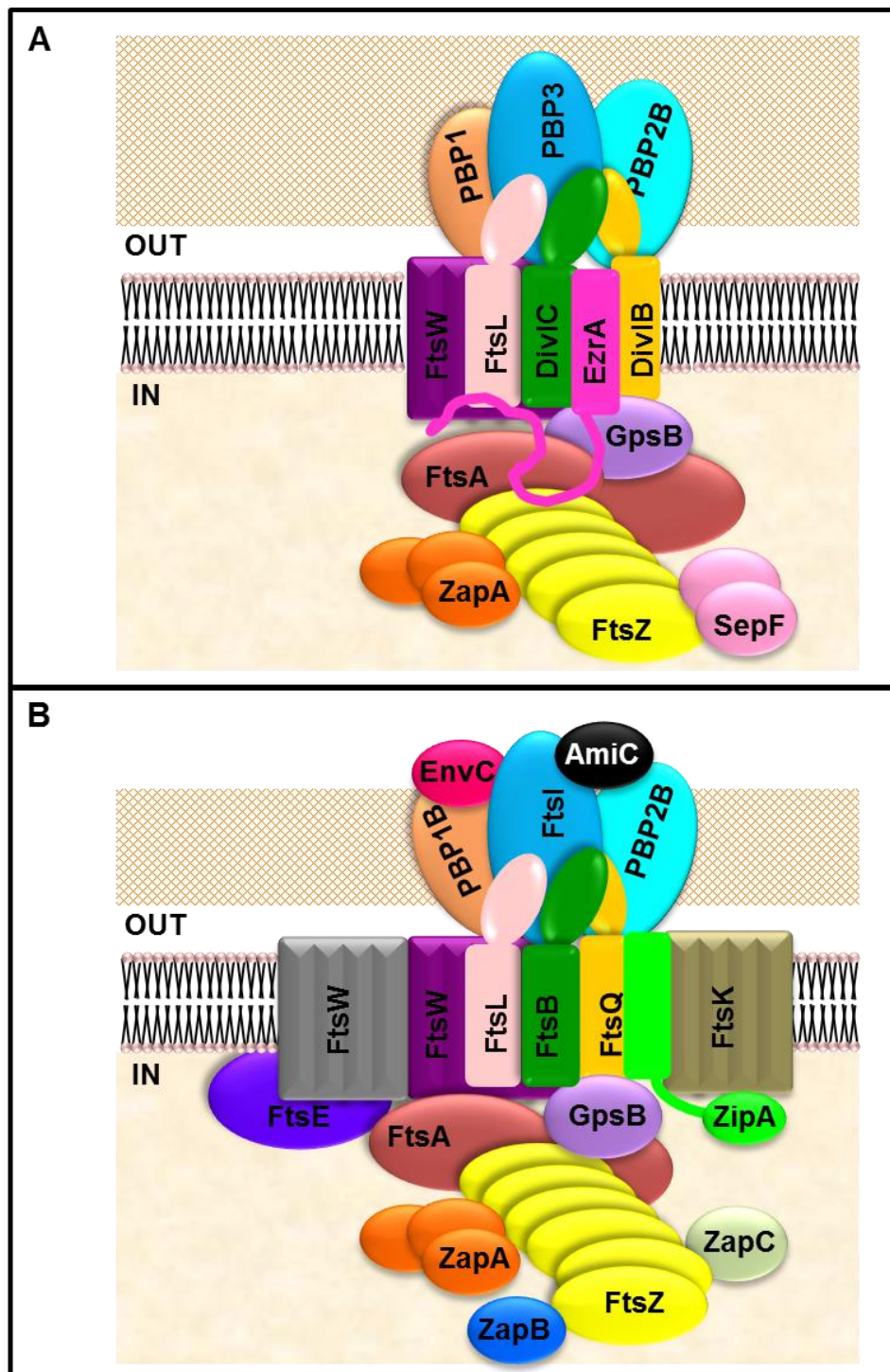
Figure 1-5 Cell division machinery of *B. subtilis* and *E. coli*

Schematic representations of the cell division machineries in *B. subtilis* (A) and *E. coli* (B). The proteins were determined based on protein-protein interactions and localisation at the midcell using fluorescent protein fusions or immunolocalisation. Not all known interactions between the division components are shown here. Analogues are shown in the same colours. Modified from (Errington *et al.* 2003; Carballido-Lopez & Formstone 2007; Adams & Errington 2009; Gamba *et al.* 2009).

1.2.2.4.1 Selection of the division site

Determination of the correct division site and the formation of the Z ring are regulated by the Min system and nucleoid occlusion, both of which inhibit Z ring polymerisation at the cell poles. These mechanisms ensure cells divide at the midcell as the default site (Weiss 2004). Z ring formation at the midcell occurs with high fidelity, as the standard deviation for the middle position is 2.6 % and 2.2 % in *E. coli* and *B. subtilis*, respectively (Yu & Margolin 1999; Migocki *et al.* 2002).

1.2.2.4.1.1 The Min system

The Min system was first identified in *E. coli*, in which mutations of the minicell locus (*minB*) resulted in minicell formation lacking genomic information (de Boer *et al.* 1989). *E. coli minB* encodes three gene products, MinC, MinD and MinE, whose coordination is required for ensuring appropriate placement of septum by blocking potential division sites specifically, including cell poles (de Boer *et al.* 1989). MinC, a division inhibitor, dimerises and interacts with FtsZ via its N-terminus (Hu *et al.* 1999; Hu & Lutkenhaus 2000), and MinD via its C-terminus (Hu & Lutkenhaus 2000). MinD, a monomeric peripheral membrane ATPase, sequesters MinC to the membrane by direct interactions (de Boer *et al.* 1991).

MinC and MinD together negatively regulate FtsZ ring formation (de Boer *et al.* 1992b). MinE, a topological specificity factor, gives site specificity to MinC and prevents its activity at midcell via interaction with MinD (de Boer *et al.* 1992b). In contrast, overexpression of MinCD leads to suppression of division and formation of aseptate filamentous cells (de Boer *et al.* 1992b).

Fluorescence microscopy using GFP fusions has shown insights into the mechanisms of MinCDE action. MinC displays rapid pole-to-pole oscillation via interaction with MinD, which oscillates from pole to pole in the presence of MinE with a periodicity of 20 s (Hu & Lutkenhaus 1999; Raskin & de Boer 1999a). In the presence of ATP, MinD polymerises in a helical array *in vitro* and *in vivo* (Hu & Lutkenhaus 2000; Shih *et al.* 2003). MinE forms a dynamic ring-like structure that also oscillates with a restricted pattern of side-to-side around the midcell (Fu *et al.* 2001). This repetitive side-to-side oscillation appears to involve sweeping of MinCD from one cell pole, and then reassembly of the MinCD complex towards the opposite pole (Fu et al. 2001; Hale et al. 2001) (Fig. 1.6A). During the sweeping action, MinE competes for MinD binding sites via stimulation of the ATPase activity of MinD, and therefore results in disassociation of MinC from the membrane (Suefuji *et al.* 2002; Lackner *et al.* 2003; Ma *et al.* 2004). Thus, due to these oscillation patterns, the time- integrated

concentration of MinC is highest at the cell polar zone blocking FtsZ assembly and lowest at midcell allowing Z ring formation.

In *B.subtilis*, homologues of MinCD are found, however a homologue of MinE was not identified (Varley & Stewart 1992). MinD oscillation is not observed, suggesting a different mechanism of Z ring placement from *E. coli* (Marston et al. 1998). Indeed, another topological specificity factor, DivIVA, is recruited to the division site at a late stage of septation and is retained at the newly-formed cell poles where DivIVA then directly recruits MinCD via MinJ, and retains the complex there, inhibiting future division at these sites (Cha & Stewart 1997; Edwards & Errington 1997; Bramkamp *et al.* 2008) (Fig. 1.6B). Like MinE, DivIVA preferably binds strongly to the curved part of membranes via its N-terminus (Lenarcic *et al.* 2009). Certain Clostridia have both MinE and DivIVA, although their role in Z ring placement is unclear (Errington *et al.* 2003). By contrast, Gram positive cocci lack the Min system altogether (Margolin 2001).
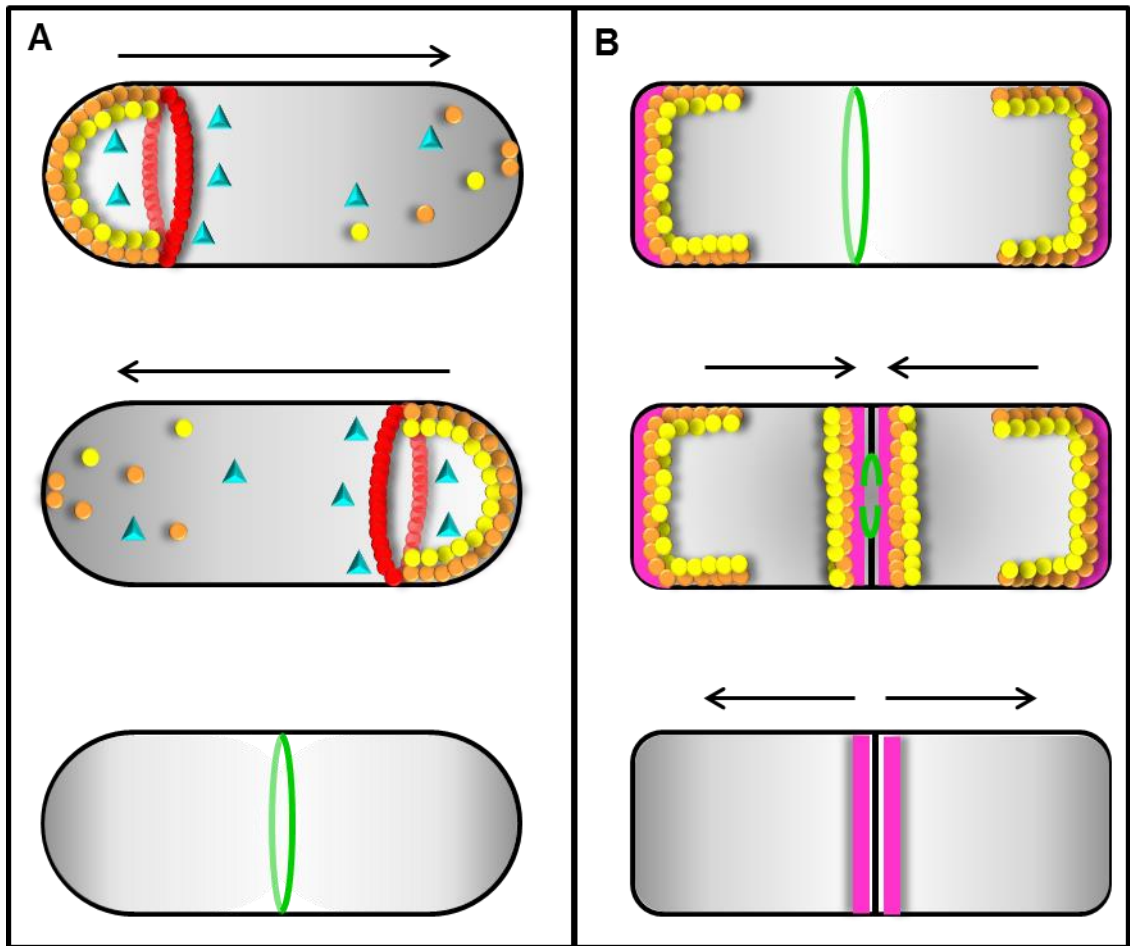
Figure 1-6 The Min system in *E. coli* and *B. subtilis*

Schematic representations of the Min system in *E. coli* (A) and *B. subtilis* (B). The Min system hinders division at the cell poles.

A. In *E. coli*, MinC (yellow) and MinD (orange) oscillate between cell poles to prevent divisome (green) assembly away from the midcell. MinCD is released from the membrane by MinE (red), which is triggered by ATP (cyan) hydrolysis. Once the nucleotide is exchanged in the cytosol, MinCD assembles at the opposite pole. The concentration of MinCD is highest at the cell poles, where it builds division restriction zones.

B. In *B. subtilis*, the MinC (yellow) / MinD complex (orange) is recruited to the poles and to the midcell by the DivIVA/MinJ complex (pink). DivIVA is stable at the midcell while the septum (green) constricts.

Modified from (Rothfield *et al.* 2005; Lutkenhaus 2012)

1.2.2.4.1.2 Nucleoid occlusion

The bacterial nucleoid occlusion model was proposed as a mechanism for selecting correct division sites (Mulder & Woldringh 1989). Cell division is inhibited in the vicinity of the nucleoid due to the production of nucleoid occlusion proteins around the nucleoid (Mulder & Woldringh 1989; Woldringh *et al.* 1990).

In a rod-shaped bacterial cell that has undergone cell division, DNA replication and segregation, three sites are available of Z-ring formation where DNA is absent: the two cell poles and the midcell (Fig. 1.7 A) (Errington *et al.* 2003). Division at the cell poles is inhibited by the Min system, leading to the midcell as the only available site for Z-ring formation (Fig. 1.7 B). Noc and SlmA were the first nucleoid occlusion factors discovered in *B. subtilis* and *E. coli* respectively (Wu & Errington 2012). Noc is only active when its C-terminus specifically binds to a Noc-binding sequence, a 14 bp palindrome in the chromosome, and its N-terminus associates with membrane simultaneously (Adams *et al.* 2015). Noc dimerises and probably physically inhibits the assembly of the cell division machinery, thereby preventing division in the region that contains the nucleoid (Adams *et al.* 2015). SlmA also forms dimers and binds to the SlmA-binding sites on the chromosome, it interferes with FtsZ polymerisation by direct interaction with FtsZ and therefore preventing Z ring formation (Tonthat *et al.* 2011). The resolution of the crystal structure of SlmA has helped in the determination of the DNA-binding site and the molecular mechanism of *E. coli* nucleoid occlusion via the assembly of the FtsZ polymer (Cho et al., 2011; Tonthat et al., 2011; Cho and Bernhardt, 2013). Interestingly, Noc and SlmA do not share sequence homology and they bind to different specific DNA binding sequences in the chromosome (Wu & Errington 2012). Thus, nucleoid occlusion plays an important role in the spatial and temporal regulation of cell division since a DNA-free midcell only results after proper DNA segregation of the newly replicated nucleoids has occurred (Errington *et al.* 2003) (Fig. 1.7 C).

In cocci where the Min system is absent, nucleoid occlusion becomes a crucial mechanism for protecting the nucleoid and determining the correct division site (Veiga *et al.* 2011). Indeed, deletion of *noc* in *S. aureus* leads to multiple Z ring formation and DNA breakage was observed in about 15% of the mutant cells (Veiga *et al.* 2011). The DNA binding sequence for the *S. aureus* Noc remains unknown (Wu & Errington 2012).
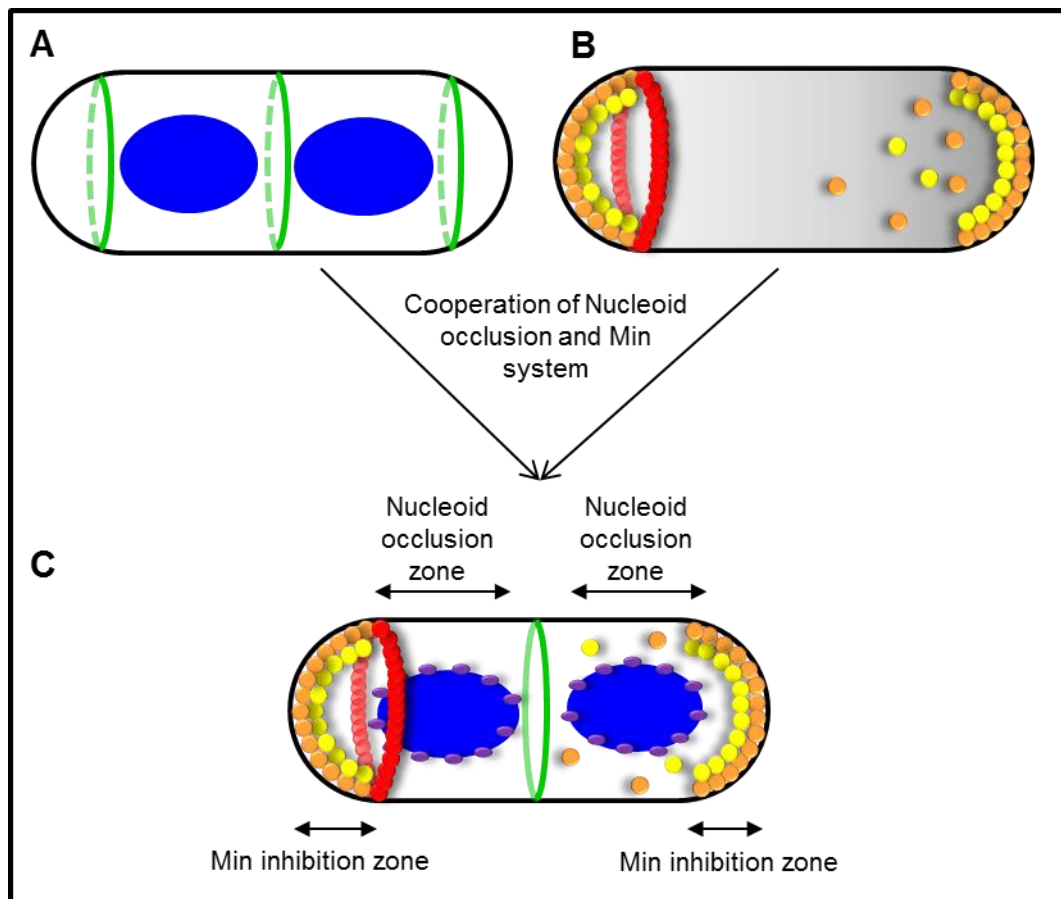
Figure 1-7 The nucleoid occlusion system in rod-shaped bacteria

Schematic representations of the nucleoid occlusion system.

A.   Once the bacterial cell undergoes cell division, DNA replication and segregation, there are three potential Z-ring formation sites (green) and at which DNA (blue) is absent: the cell poles and the midcell.

B.   Min system in *E.coli* as an example. MinC (yellow), MinD (orange) complex and MinE (red) oscillate between cell poles.

C.   Negative regulation of Z-ring formation occurs to prevent the polymerisation of FtsZ away from midcell. The Min system (yellow, orange and red) prevents division at the poles, while nucleoid occlusion proteins (purple) prevent Z-ring formation over the separated nucleoids (blue).

Modified from (Errington *et al.* 2003; Shih & Rothfield 2006).

1.2.2.4.1.3 Other systems

In addition to Min system and nucleoid occlusion mechanism, recently, ZapA-ZapB-MatP network was introduced as a third system contributing to the midcell positioning of the *E. coli* FtsZ-ring (Buss *et al.* 2015). Deletion of any one of the three proteins results in FtsZ dispersion in an extended region around the midcell (Buss *et al.* 2013). The *ter* region of chromosome moves toward the midcell at the initial stage of cell cycle and remains at the midcell until the DNA replication is completed (Mercier *et al.* 2008). MatP interacts with *ter* region of the chromosome (Mercier *et al.* 2008), it therefore localises ZapB to the midcell via direct interaction, which in turn promotes the midcell localization of ZapA and further FtsZ (Buss *et al.* 2015). Interestingly, the colocalisation of MatP and *ter* region of the chromosome is not fully abolished, in the absence of all the three division site selection systems, implying the presence of other positioning mechanisms (Buss *et al.* 2015).

1.2.2.4.2 FtsZ-interacting proteins

1.2.2.4.2.1 FtsA

The actin like FtsA is a peripheral membrane protein that possesses a C-terminal amphipathic helix anchored in the membrane (Pichoff & Lutkenhaus 2005). The *ftsA* gene is usually transcribed immediately upstream of *ftsZ* within the cell division and cell wall biosynthesis gene cluster (*dcw*) in a number of bacteria. FtsA, along with other proteins, interact with the highly conserved C terminus of FtsZ (Din *et al.* 1998). A mutagenesis study revealed that most other division proteins are dependent upon FtsA (reviewed by Errington *et al.,* 2003), suggesting an early role in tethering FtsZ, as well as other division proteins. FtsA may also either drive assembly or help control cell constriction utilising energy from ATP hydrolysis (Errington *et al.* 2003). FtsA is well conserved in most bacteria, although is not found in mycobacteria, cyanobacteria and mycoplasmas (Margolin 2000b). FtsA is essential in *E. coli* and other bacteria, but, whilst deletion of *ftsA* in *B. subtilis* leads to a severe division defect, slow growth is possible (Beall & Lutkenhaus 1992).

1.2.2.4.2.2 ZipA

ZipA was identified as an integral membrane protein in *E. coli* interacting with FtsZ found using an affinity blotting assay (Hale & de Boer 1997). ZipA is essential in *E.coli*, but poorly conserved in other organisms, with the only homologue in *Haemophilus influenzae* (RayChaudhuri 1999). The N-terminal domain of ZipA anchors to the inner cell membrane, the C-terminal domain binds to the conserved C terminus of FtsZ in the cytoplasm via hydrophobic interactions *in vivo* and *in vitro* (Hale & de Boer 1999; Mosyak *et al.* 2000; Moy

et al. 2000; Erickson 2001). Immunolocalisation studies have shown that ZipA is recruited to the Z ring at the early stage of the cell division process in an FtsZ-dependent and FtsA-independent manner, it also plays a key role in enhancing and stabilising the formation of FtsZ bundles, these suggests that ZipA is important in the recruitment of other cell division components to the septal site and/or maintaining its stability. Z ring formation occurs in the presence of either FtsA or ZipA, however, not in the absence of both proteins, indicating functional redundancy, although both proteins are required for septal constriction (Pichoff & Lutkenhaus 2002). FRAP has demonstrated that ZipA is highly dynamic, with rapid exchange between the membrane and the Z-ring (Stricker *et al.* 2002).

1.2.2.4.2.3 ZapA

ZapA is a cytoplasmic protein that is highly conserved in a various species (Gueiros-Filho & Losick 2002). ZapA localises to the division site in a FtsZ-dependent manner in both *B. subtilis* and *E. coli* and it promotes the assembly of the FtsZ-ring as it cross-links with the FtsZ polymers in addition to bundling and stabilising the Z-ring (Gueiros-Filho & Losick 2002; Monahan *et al.* 2009). ZapA becomes essential when FtsZ level are reduced or the FtsZ regulatory proteins, EzrA or DivIVA, are absent in *B. subtilis* (Gueiros-Filho & Losick 2002).

1.2.2.4.2.4 EzrA

EzrA is a transmembrane protein that is conserved among the low-GC content Gram-positive bacteria (Steele *et al.* 2011). EzrA localises to the division site in an FtsZ-dependent manner in *B. subtilis* and it probably act as a negative regulator of FtsZ-ring formation (Levin *et al.* 1999). Seven conserved amino acid residues in *B. subtilis* EzrA, are responsible for ensuring midcell localisation (Haeusser *et al.* 2007). In *S. aureus,* fluorescent microscopy has also shown that EzrA colocalised with FtsZ at the midcell (Steele *et al.* 2011). The *ezrA* gene is essential for growth of *S. pneumoniae* and *S. aureus*, it becomes essential when any one of the cell division genes, *zapA*, *noc*, *gpsB* or *sepF* are absent in *B. subtilis* (Thanassi *et al.* 2002; Steele *et al.* 2011). The absence of *S. aureus* EzrA leads to a block in peptidoglycan synthesis, and thereby delocalisation of cell division machinery, suggesting EzrA may also have a positive role in cell division (Steele *et al.* 2011). In addition, EzrA was suggested to have a role in *B. subtilis* cell elongation, as *ezrA* deleted *B. subtilis* cells have a reduced cell size (Claessen *et al.* 2008).

1.2.2.4.2.5 SepF

SepF is a cytoplasmic protein that is well-conserved in Gram-positive bacteria (Adams & Errington 2009). SepF localises to the division site in an FtsZ-dependent manner in *B. subtilis* (Hamoen *et al.* 2006). SepF directly interacts with FtsZ and induces polymerisation, bundling of the protofilament and suppression of FtsZ GTPase activity (Singh *et al.* 2008). SepF itself forms very large ring structures roughly (50 nm in diameter), which cause bundling of FtsZ protofilaments into long tubular structures similar to eukaryotic microtubules, suggesting a role for SepF in the arrangement of FtsZ filaments (Gundogdu et al. 2011). Deletion of *B.subtilis sepF* results in aberrant septum formation (Hamoen *et al.* 2006), whilst disruption of *S.pneumoniae sepF* causes an altered cell morphology (Fadda *et al.* 2003).

1.2.2.4.2.6 ZipN, ZapB and ZapC

ZipN is unique to cyanobacteria and plant chloroplasts (Koksharova & Wolk 2002). *Synechocystis zipN* gene was found to be essential for viability (Mazouni *et al.* 2004). ZipN binds to FtsZ via its N-terminal DnaJ domain (Mazouni *et al.* 2004). Both ZapB and ZapC homologues are found in a subset of γ-proteobacteria and are nonessential for viability (Baba *et al.* 2006; Ebersbach *et al.* 2008). Recruitment of ZapB to the septum is ZapA- and FtsZ-dependent, whereas ZapC is only FtsZ-dependent not ZapA or ZapB in *E. coli* (Galli & Gerdes 2010, 2012). ZapB mediates stabilisation of the lateral interactions between FtsZ protofilaments by cross-linking ZapA molecules bound to these FtsZ polymers (Galli & Gerdes 2010). In *E. coli*, ZapA-ZapB-MatP network modulates midcell positioning of the FtsZ-ring via physical interaction with the *ter* region of the chromosome (Buss *et al.* 2015). ZapC induces FtsZ protofilament bundling (Durand-Heredia *et al.* 2011; Hale *et al.* 2011) and suppresses the GTPase activity of FtsZ (Hale *et al.* 2011), thereby improving the stability of the Z-ring. Deletion of ZapC in *E. coli* altered cell morphology, as cells are elongated to some extent (Hale *et al.* 2011; Galli & Gerdes 2012).

1.2.2.4.3 Late cell division proteins

Almost all of the remaining cell division proteins, which are recruited to the septum after Z ring formation, are integral membrane proteins possessing at least one transmembrane domain. It is likely that these late division proteins are involved in synthesis, remodelling and degradation of peptidoglycan to facilitate the formation of the septum and separation of daughter cells.

1.2.2.4.3.1 Penicillin binding proteins

PBPs are enzymes involved in the last stages of septum formation. The majority of bacteria have a variable number of PBPs, and there appears to be some functional redundancies. *E. coli* has 12 PBPs, *B. subtilis* has 16 and cocci have from 4 to 7 PBPs (Wei *et al.* 2003; Pinho & Errington 2005; Zapun *et al.* 2008). PBPs are categorised into multimodular high molecular weight (HMW) PBPs, including class A and B, and monofunctional low molecular weight (LMW) PBPs (Goffin & Ghuysen 1998). Both classes of HMW PBPs possess a conserved C-terminal penicillin-binding (PB) domain with transpeptidase activity (Wei *et al.* 2003). The N-terminal domain of class A PBPs is responsible for transglycosylation that generates the glycan strands as well as the transpeptidation that builds the peptide bridges between glycan strands (Holtje 1998), distinguished from class B PBPs, whose N-terminal domain is involved in cell morphogenesis by interacting with other cell cycle proteins (Sauvage *et al.* 2008).

In *E. coli*, loss of HMW PBP class B FtsI (PBP-3) results in filamentous cells that fail to divide (Spratt 1977). FtsI has an N-terminal membrane anchor that is required for localisation and cell division (Weiss et al., 1999). Localisation of FtsI is also dependent upon its transpeptidase activity and/or substrate binding, since treatment with furazlocillin, a β-lactam that specifically binds FtsI, prohibits its association with the septum (Wang *et al.* 1998). FtsI is recruited to the division site dependent on the prior localization of FtsZ or FtsA (Wang *et al.* 1998). HMW PBP class B PBP2 mutants lose cylinder peptidoglycan synthesis forming round cells (Spratt 1975). *B. subtilis* PBP2b, an orthologue of FtsI, is essential for cell division (Yanouri *et al.* 1993; Daniel *et al.* 2000). Immunolocalisation of PBP2b and FtsI demonstrates that the proteins are associated with the septum during division (Daniel et al., 2000; Weiss et al., 1997). The two-hybrid system has shown interactions between FtsI (and PBP2B) and a number of cell division components (Di Lallo *et al.* 2003; Karimova *et al.* 2005; Daniel *et al.* 2006). In *C. crescentus,* the transpeptidase domain of PBP3 is required for appropriate septal localisation (Costa *et al.* 2008).

In *E. coli*, the class A HMW PBPs are believed to play a role in both septal and lateral cell wall peptidoglycan synthesis. However, in *B. subtilis*, the class A PBP1 shuttles between the septum and lateral cell wall during the cell cycle (Claessen *et al.* 2008) and PBP1 mutants are defective in septum formation and form filamentous cells (Pedersen *et al.* 1999), suggesting an important role in cell division.

1.2.2.4.3.2 FtsK

FtsK is well conserved in eubacteria and its homologues are also present in archaea (Bigot *et al.* 2007) FtsK is a bifunctional protein involved in both cell division and chromosome

segregation (Grenga *et al.* 2008). FtsK is essential for *E. coli* but not *B. subtilis* division (Draper *et al.* 1998; Yu *et al.* 1998). FtsK consists of a cytoplasmic C-terminal domain which is separated from the N-terminal domain by a linker that has variable length and sequence (Errington *et al.* 2003; Grenga *et al.* 2008). The N-terminal domain mediates the recruitment of other divisome components, such as FtsL and FtsQ and the C terminal domain interacts with FtsI (Grenga *et al.* 2008). The N-terminal domain is poorly conserved at the sequence level, but always contains transmembrane helices that tether the protein to the membrane (Bigot *et al.* 2007). The C-terminal domain is particularly important in chromosome segregation and translocates along DNA in an ATP-dependent manner, suggesting an involvement in pumping of DNA through the closing septum (Yu *et al.* 1998; Aussel *et al.* 2002). Furthermore, the C-terminal region has been suggested to be involved in promoting the resolution of chromosome dimers (Aussel *et al.* 2002; Bigot *et al.* 2007).

1.2.2.4.3.3   FtsW

FtsW belongs to the SEDS family of proteins, which are integral to the membrane with 10 transmembrane spans (Gerard *et al.* 2002). The genes encoding SEDS proteins are often associated with genes encoding class B PBPs: in *E. coli*, *ftsW* lies in an operon with *ftsI* and the genes encoding the elongation specific RodA and PBP2 are in another (Tamaki *et al.* 1980; Ishino *et al.* 1989; Boyle *et al.* 1997). Mutations in SEDS proteins and class B PBPs result in the same phenotype, suggesting a functional relationship (Margolin 2000b; Errington *et al.* 2003). An investigation of sequenced bacterial genomes revealed a perfect presence/absence correlation between FtsW and FtsI (PBP3), implying that their roles are closely linked (Henriques *et al.* 1998). Co-immunoprecipitation assays, Förster resonance energy transfer (FRET) analyses, peptide-based assays and bacterial-two hybrid systems (BACTH) have shown a direct interaction between PBP3 and FtsW *in vitro* and *in vivo* (Di Lallo *et al.* 2003; Karimova *et al.* 2005; Datta *et al.* 2006; Fraipont *et al.* 2011). FtsW is essential for recruitment of FtsI to the septum in *E. coli* and *Mycobacterium tuberculosis* (Mercer & Weiss 2002; Datta *et al.* 2006). SEDS proteins have been thought to function as flippases involved in the translocation of lipid II-linked peptidoglycan precursors from the cytoplasm to the external peptidoglycan-synthesising complex (Holtje 1998). A recent study showed that FtsW is required for the transportation of lipid II in *E. coli* and purified FtsW induces the translocation of lipid II in biogenic membranes, providing evidence that FtsW may be a division-specific lipid II transporter (Mohammadi *et al.* 2011).

1.2.2.4.3.4 FtsQ/DivIB

In *E. coli*, FtsQ is essential for cell division and its overproduction results in filamentation with partially formed septa when grown at the non-permissive temperature (Carson *et al.* 1991). In *B. subtilis*, *divIB*, an *ftsQ* homologue, is only essential for vegetative growth at high temperatures but is required for sporulation at all temperatures (Beall & Lutkenhaus 1989; Harry *et al.* 1993). In *S. pneumoniae*, DivIB is essential for nutrient-limited growth and deletion of *divIB* altered cell morphology to longer chains and eventually cell lysis (Le Gouellec *et al.* 2008). In *Streptomyces coelicolor*, DivIB is dispensable for mycelial growth and viability but is required for efficient conversion of aerial filaments into spores (McCormick & Losick 1996). In *S. aureus, divIB* is essential for cell viability (Chaudhuri *et al.* 2009), as depletion of DivIB results in continuously increased cells size with misplaced septa and eventual lysis (Bottomley *et al.* 2014).

ftsQ/divIB is often located in an operon of genes involved in the synthesis of peptidoglycan precursors (Zapun *et al.* 2008), its homologues are only found in bacteria possessing cell walls (Margolin 2000b), and the proteins share sequence similarity with the peptidoglycan recycling factor Mpl (MenginLecreulx *et al.* 1996), indicating a role in peptidoglycan synthesis or remodelling.

DivIB is a bitopic protein that consists of an N-terminal cytoplasmic domain, a membrane helix and a large C-terminal extracytoplasmic domain. FtsQ directly interact with FtsA and FtsK via its N-terminal domain, interaction with FtsX, FtsL, FtsB, FtsW, FtsI and FtsN was also observed by two-hybrid studies and or co-immunoprecipitation (Di Lallo *et al.* 2003; Karimova *et al.* 2005; D'Ulisse *et al.* 2007). The C-terminal domain of *B. subtilis* and *S. aureus* DivIB binds to peptidoglycan with strong affinity (Bottomley *et al.* 2014). The C-terminal domain of *E. coli* and *Yersinia enterocolitica*, is required for interactions with proteins that place FtsQ to the septum, and with proteins that are recruited by FtsQ (van den Ent *et al.* 2008).

1.2.2.4.3.5 FtsL

FtsL is essential for growth and cell division in *E. coli* and *B. subtilis*, since depletion of FtsL results in filamentous growth and eventually cell death, (Guzman *et al.* 1992; Daniel *et al.* 1998). *S. pneumoniae* FtsL was also reported to be essential for cell division (Le Gouellec *et al.* 2008). FtsL homologues are found in all bacteria with cell walls (Margolin 2000b), suggesting that the protein is probably involved in cell wall synthesis and/or remodelling.

FtsL is a small transmembrane protein with a C-terminal periplasmic domain that possesses a coiled-coiled motif, indicating that FtsL is involved in protein-protein interactions (Guzman *et al.* 1992). In *B. subtilis*, a mutagenesis study of *ftsL* showed that few, if any, residues are critical for function, implying a structural rather than catalytic role for the protein (Sievers & Errington 2000). Two-hybrid analyses have shown FtsL to interact with FtsQ, FtsI, DivIC and itself (Karimova *et al.* 2005; Daniel *et al.* 2006) and the self-interaction of FtsL has been shown biochemically through the detection of protein dimers (Ghigo & Beckwith 2000). FtsL forms a trimeric complex with DivIB/DivIC in Gram-positives, and their orthologues FtsQ/FtsB in Gram-negatives, and it is conserved in all species for which division protein interactions have been investigated (Buddelmeijer & Beckwith 2004; Noirclerc-Savoye *et al.* 2005; Daniel *et al.* 2006). Depletion of FtsL prohibits localisation of DivIB, DivIC and PBP2b to the division site (Daniel *et al.* 2000). The trimeric complex is suggested to play a direct or indirect role in peptidoglycan metabolism at the septum through interactions with PBP2B (Rowland *et al.* 2010).

In *B. subtilis*, the N-terminal cytoplasmic domain of FtsL signals the degradation of the protein, which is partially mediated by RasP (YluC), a membrane metalloprotease (Bramkamp *et al.* 2006). Mutation of YluC generates shorter cells due to earlier division, suggesting that FtsL is normally rate limiting for division (Bramkamp *et al.* 2006). Repression of FtsL expression results in an almost immediate arrest of cell division (Daniel *et al.* 1998). *ftsL* transcription is regulated by DnaA, a DNA replication initiation protein, which interrupts cell division when DNA replication is perturbed (Goranov *et al.* 2005).

1.2.2.4.3.6 FtsB/DivIC

In *B. subtilis*, *divIC*, an *ftsL*-like gene, is essential for division (Levin & Losick 1994). Native gel electrophoresis, bacterial and yeast two-hybrid analyses demonstrated that DivIC directly interacts FtsL (Sievers & Errington 2000; Daniel *et al.* 2006). DivIC is assemble to the division site in an FtsL dependent manner (Daniel *et al.* 1998) Like FtsL, DivIC is intrinsically unstable (Robson *et al.* 2002). Depletion of FtsL results a rapid loss in DivIC (Daniel *et al.* 1998), implying that DivIC may be stabilised by FtsL interaction.

In *E. coli*, *ftsB* is a homologue of *B. halodurans divIC* (Buddelmeijer & Beckwith 2002). The *ftsB* gene is essential for cell division and FtsB shows localisation to the division site co-dependent on FtsL (Buddelmeijer & Beckwith 2002). Depletion of FtsB leads to loss of FtsL (Buddelmeijer et al., 2002; Gonzalez & Beckwith, 2009) and depletion of FtsL results in

degradation of the C terminal domain of FtsB (Gonzalez & Beckwith 2009), suggesting that the proteins are dependent upon each other for stability.

1.2.2.4.3.7 FtsN

The *ftsN* gene was described in *E. coli* by the ability of its overexpression to compensate for a temperature-sensitive *ftsA* mutation, and partially compensate for temperature-sensitive mutations of *ftsI*, *ftsQ* and *ftsK* (Dai et al., 1993). Its homologues are found in *Haemophilus* species, enteric bacteria and proteobacteria (Errington *et al.* 2003; Moll & Thanbichler 2009). In *E. coli*, FtsN is essential for division, with depletion leading to filamentous growth and eventually cell death (Dai *et al.* 1993). However, in the absence of FtsN, suppressor mutants of FtsA are viable (Bernard *et al.* 2007).

The protein consists of a large periplasmic C-terminal domain, a transmembrane domain and a short cytoplasmic N-terminal domain (Dai *et al.* 1996). The N-terminal anchor and first periplasmic amino acid of FtsN are essential for cell division (Ursinus *et al.* 2004) and suppression of *ftsA*, *ftsQ*, *ftsK* and *ftsI* mutation (Goehring *et al.* 2007), whereas its C-terminal domain is required for its septal localisation, but not essential for cell division (Dai *et al.* 1996). BACTH shows that FtsN directly interacts with FtsA, FtsQ, FtsI, FtsL and FtsW (Di Lallo *et al.* 2003; Karimova *et al.* 2005). Direct interaction of FtsN with PBP1a, PBP1b and FtsI stimulate the transpeptidase and transglycosylase activities of PBP1b protein via its N-terminal domain, suggesting FtsN is involved in peptidoglycan biosynthesis (Muller *et al.* 2007). FtsN is thought to be the last of the *E.coli* essential cell division components to be recruited to the septum, as its septal localisation is dependent on the prior localization of FtsZ, FtsA, FtsI, FtsK and FtsQ (Addinall *et al.* 1997). The C-terminal domain of FtsN encodes a sporulation-related repeat domain which mediates septal localisation, and the domain localisation is dependent upon the amidases that are involved in peptidoglycan hydrolysis (Gerding *et al.* 2009; Moll & Thanbichler 2009; Arends *et al.* 2010).

1.2.2.4.3.8 FtsEX

FtsX is an integral membrane protein, and FtsE is a cytoplasmic ATPase associated with FtsX (de Leeuw *et al.* 1999). The FtsEX complex is homologous to the ATP-binding cassette (ABC)-type transporters (Schmidt *et al.* 2004; Mir *et al.* 2006). In *E. coli*, FtsE and FtsX are localised to the septum dependent upon FtsZ, FtsA and ZipA (Schmidt *et al.* 2004). In the absence of FtsEX, cells divide poorly and FtsEX downstream genes (FtsK, FtsQ, FtsI and FtsN) cannot properly target to the division site in *E. soli* (Schmidt et al., 2004). BACTH has

shown that FtsX interacts with FtsA and FtsQ (Karimova *et al.* 2005) and a co-immunoprecipitation assay has shown that FtsE interacts with FtsZ (Corbin *et al.* 2007). FtsX localises to the septum in *E. coli* cells lacking FtsE, indicating that FtsX targets FtsEX to the divisome (Arends *et al.* 2009). Lesions in the ATP-binding site of FtsE do not affect divisome assembly, but the septal ring constricted poorly, implying that FtsEX may use ATP to facilitate constriction of the ring in *E. coli* (Arends et al., 2009). Furthermore, *E. coli* FtsX interacts directly with EnvC, a peptidoglycan hydrolase, to the division site via its periplasmic loop (Yang *et al.* 2011). *ftsEX* mutants with a defect in the ATPase domain cannot separate, but are able to recruit EnvC to the septum, suggesting that the amidase activation through EnvC is impacted by the conformational changes of the FtsEX complex .

In *S. pneumoniae*, *Neisseria gonorrhoeae*, *Aeromonas hydrophila*, and *Flavobacterium johnsoniae ftsE* and/or *ftsX* mutant also exhibit division defects, implying that the FtsEX function in cell division is conserved among these organisms (Kempf & McBride 2000; Merino *et al.* 2001; Ramirez-Arcos *et al.* 2001; Sham *et al.* 2013) However, in *B. subtilis*, FtsEX has no obvious role in cell division but instead regulates entry into sporulation (Garti-Levi et al., 2008).

1.2.2.4.3.9 GpsB (YpsB)

The *gpsB* gene was first identified in *B. subtilis* as a paralogue of *divIVA*, with homologues found in several Gram-positive bacteria resulting from a gene duplication event (Tavares *et al.* 2008). Both GpsB and DivIVA possess a central coiled-coil region and share a closely related N-terminus have dixtinct C-terminal domains (Tavares et al., 2008). GpsB is membrane-associated and recruited to the division site dependent upon both early cell division components, FtsZ and FtsA, as well as the late cell division components DivIC and PBP2b (Tavares et al., 2008). This recruitment is later than for the early division proteins FtsZ, FtsA, ZapA and EzrA, and GpsB and remains associated with completed septum even after new Z-rings have started to form, though not retained at newly formed cell poles (Tavares et al., 2008).

BACTH studies have shown a direct interaction of GpsB with other cell division proteins, like PBP1 (encoded by *ponA* gene) and EzrA as well as with cell shape protein MreC (Claessen *et al.* 2008). An *ezrA/gpsB* double mutant showed severe defects in septal and lateral peptidoglycan synthesis as a result of perturbed PBP-1 localisation (Claessen *et al.* 2008). In wild-type cells, both GpsB and PBP-1 alternate between lateral wall and septal position during the cell cycle and GpsB is sufficient for localisation of PBP1 (Claessen et al.,

2008). This suggests that GpsB is probably involved in controlling the switch between elongation and division in *B. subtilis*.

1.2.2.4.4 Hierarchy of assembly of late division proteins

The assembly pathways of the late division proteins are notably different in *E. coli* and *B. subtilis*. In *E. coli*, recruitment of late cell division proteins occurs in a linear hierarchy: FtsE/X-FtsK-FtsQ-FtsB/FtsL-FtsW-FtsI-FtsN, in which the recruitment of FtsE/FtsX and FtsB/FtsL is co-dependent (Buddelmeijer and Beckwith, 2002; Errington et al., 2003; Goehring and Beckwith, 2005). Nevertheless, back-recruitment of division proteins in *E. coli* is possible (Vicente and Rico, 2006). However, the recruitment of late division proteins appears to be interdependent In *B. subtilis* and S. *pneumoniae* (Errington *et al.* 2003; Morlot *et al.* 2004). Mutation or depletion of one of the proteins results in blockage of divisome assembly, reflecting their dependency but not temporal order of assembly (Errington *et al.* 2003).

1.2.2.4.5 Separation of daughter cells

The separation of daughter cells is dependent upon cell wall hydrolases (e.g., autolysins), which cleave the peptidoglycan layer that connects the two daughter cells (Yamada *et al.* 1996). In Gram-negatives (e.g., *E. coli*), cell division occurs by a gradual constriction of the cylindrical part of the cell wall (Errington *et al.* 2003). In Gram-positives (e.g., *B. subtilis*), the new cross-wall forms from the cylindrical cell wall, and cell separation occurs after completion of septation (Errington *et al.* 2003).

In *E. coli* cell separation is carried out by LytC-type periplasmic peptidoglycan amidases AmiA/B/C (Peters *et al.* 2011; Uehara & Bernhardt 2011; Yang *et al.* 2012). AmiC localises to the midcell via its N-terminal binding to FtsN (Bernhardt & de Boer 2003) and cleaves the septal peptidoglycans, inducing cell division (Heidrich *et al.* 2001). Furthermore, the LytM factors EnvC and NlpD localise to the septum (Uehara *et al.* 2009) and activate amidases observed by *in vitro* cell wall cleavage assays (Uehara *et al.* 2010; Yang *et al.* 2012). When septal peptidoglycan synthesis was blocked in *E. coli*, amidases were not able to localise to the division ring, yet NlpD and EnvC were shown to localise (Peters *et al.* 2011). Consequently, the spatial and temporal regulation of cell separation occurs by coupling the activation of peptidoglycan hydrolase activity with the assembly of the division apparatus. In *C. crescentus,* DipM possesses a LytM endopeptidase domain at its C-terminus (Moll *et al.* 2010). DipM is suggested to be involved in envelope invagination during cell division via

septal peptidoglycan hydrolysis (Goley *et al.* 2010). LytF, LytE and CwlS of *B. subtilis* (Fukushima *et al.* 2006), RipA (endopeptidase) of *Mycobacterium smegmatis* (Hett *et al.* 2008), Atl (autolysin) of *S. aureus* (Yamada *et al.* 1996) and Cse (endopeptidase) of *S. thermophilus* (Layec *et al.* 2009) are all thought to be involved in cell wall cleavage, since depletion of these genes leads to formation of long chains or clumps of cells and failure in separation.

In addition to biological system, physical stress, such as turgor pressure, is also involved in determining the likelihood of daughter cell separation, since an increasing in cell-wall stress promotes separation, by contrast, a decrease in cell-wall stress postpones separation (Zhou *et al.* 2015).

1.2.2.4.6 Cell division in *S. aureus*

Cell division has been extensively studied in rod shaped bacteria, in particular the model organisms *B. subtilis* and *E. coli*. The cell division process amongst prokaryotes is likely conserved and much information can be obtained from comparative studies of morphologically diverse bacteria (Zapun *et al.* 2008). Lacking cylindrical elongation makes *S. aureus* a simpler model for studying cell division, since there will be less functional redundancy between proteins involved in cell wall synthesis and division process than in *B. subtilis* (Zapun *et al.* 2008).

S. aureus is a close relative of *B. subtilis*, therefore, some of the division mechanisms in *B. subtilis* are likely to be conserved in *S. aureus*. Comparison of cell division genes between *B. subtilis* and *S. aureus* shows that most of the divisome components are well conserved between the two organisms. (Table 3.1). Homologues of all of the genes essential for division in *B. subtilis* are putatively essential for growth of *S. aureus* (Chaudhuri *et al.* 2009), although some of the non-essential cell division genes are not conserved. In addition, homologues of some non-essential genes of *B. subtilis* are putatively essential for growth of *S. aureus*, indicating reduced redundancy.

S. aureus, divides in three alternating perpendicular planes, generating hemispherical daughter cells via cleavage of septum at the midcell. In *S. aureus*, FtsZ is the key determinant for morphology and accounts for the synthesis of each daughter cell (Zapun et al., 2008). Fluorescent vancomycin staining of *S.aureus* found that peptidoglycan synthesis occurs exclusively at the division site, whilst in the absence of FtsZ, peptidoglycans are delocalised throughout the *S. aureus* cell surface, most likely caused by the delocalisation of divisome components (Pinho & Errington 2003).

The Min system is absent from *S. aureus*, however a *minCD* homologue, *div*IVA, is present (Pinho & Errington, 2004). DivIVA functions as a scaffold for proteins involved in DNA segregation, cell wall synthesis, secretion, and DNA uptake in many Gram-positive bacteria (Strahl & Hamoen 2012). In *S. aureus*, DivIVA may be involved in chromosome segregation, although null mutants are unaffected in chromosome segregation or cell morphology (Pinho & Errington, 2004). The absence of a Min system is likely to be the cause of importance of the *S. aureus* homologue of *noc*. *S. aureus* cells lacking Noc form multiple Z-rings that are not placed in orthogonal planes, suggesting that nucleoid occlusion is involved in choosing the plane of the next septum (Veiga *et al.* 2011).

S. aureus has 4 PBPs, maybe due to its simpler mode of peptidoglycan synthesis during cell division. In the absence of FtsZ, PBP2 is delocalised generating enlarged cells and eventual lysis (Pinho & Errington, 2003). Recruitment of PBP2 to the division site is also dependent upon binding to its transpeptidation substrates (Pinho & Errington, 2005).

B. subtilis DivIB/DivIC/FtsL trimeric complex plays a direct role in peptidoglycan metabolism at the septum through interactions with PBP2B (Rowland *et al.* 2010; Bottomley *et al.* 2014). In *S. aureus*, DivIB is a late recruited protein of the division complex and binds directly to peptidoglycan via its extracellular domain, implying its role as a peptidoglycan binding protein (Steele *et al.* 2011; Bottomley *et al.* 2014). A high-density transposon screen for genes required for growth of *S. aureus* revealed the orthologue of *divIB* to be putatively essential for cell viability (Chaudhuri *et al.* 2009). Indeed, a conditional mutational analysis of *S. aureus divIB* showed that it is essential for growth of *S. aureus* (Bottomley *et al.* 2014). Depletion of DivIB results in enlarged cells with misplaced septa or multiple septa formed in a parallel plane and eventual lysis (Bottomley *et al.* 2014). *S. aureus* DivIC and FtsL were suggested that they might act as a peptidoglycan hydrolase activators during cell division, enhancing or activating peptidoglycan hydrolases, similar to the functions of EnvC and NlpD (Kabli 2013).

B. subtilis EzrA is not essential, however, *S. aureus* EzrA was proposed to be putatively essential in this organism (Chaudhuri *et al.* 2009). Strong positive interactions were detected between EzrA and other core components of the *S. aureus* division machinery by a bacterial two hybrid system (Steele *et al.* 2011). Its essentiality was confirmed by a condition mutagenesis study of *S. aureus* EzrA (Steele *et al.* 2011). EzrA is also required for FtsZ, PBP2 and GpsB localization, and therefore assembly of the division machinery at midcell, since under the condition of low *ezrA* expression, mid cell localisation of FtsZ and PBP2 could not be observed and GpsB delocalises (Steele *et al.* 2011).

1.3 Staphylococcal species

In 1880, *Staphylococcus* was first discovered by Sir Alexander Ogston, a Scottish surgeon, and described as bunches of grapes (*staphylo*) and grain (*kokkos*) (Archer 1998). Staphylococci are Gram-positive, nonmotile, nonsporulating, facultative anaerobes and some strains are resistant to heat and disinfectants (Hennekinne *et al.* 2012). Individual cocci are apparently spherical and have a cell diameter of 0.5-1.5μm (Harris *et al.* 2002). The cells divide in 3 orthogonal planes forming irregular clusters (Tzagoloff & Novick 1977).

The staphylococci consists of more than 40 species and mostly are non-pathogenic (DeLeo *et al.* 2009). They ubiquitously exist in the air, dust, sewage, water, and reside on environmental surfaces, humans and animals mucous membranes and skin (DeLeo *et al.* 2009; Hennekinne *et al.* 2012). However, some staphylococcal species are considered as important pathogens of warm-blooded animals, for example, *Staphylococcus epidermidis* (Otto 2012) and *S. aureus* (DeLeo *et al.* 2009), are significant in their interaction with humans.

1.3.1 *S. aureus*

In 1884, *S. aureus* was first described by Rosenbach, a German surgeon, and it was named for its golden pigmented appearance (Rosenbach 1884). *S. aureus* is a species of the genus *Staphylococcus*, family *Staphylococcaceae*, order *Bacillales*, class *Cocci*, phylum *Firmicutes*, kingdom *Bacteria* and domain *Bacteria* (Ludwig 2009). *S. aureus* has a circular chromosome of approximately 2.8 Mbp (Lowy 1998; Harris *et al.* 2002). *S. aureus* can be differentiated from other *Staphylococcus* species by the DNase and coagulase tests (Lowy 1998).

1.3.2 *S. aureus* pathogenicity

S. aureus is a most prevalent human pathogen causing a wide variety of nosocomial and community-acquired infections (Lowy 1998). For the last decades, *S. aureus* infections have increased dramatically (Rasigade & Vandenesch 2014). The severity of these infections ranges from mild skin lesions (e.g., folliculitis, impetigo and cellulitis) to invasive diseases (e.g., osteomyelitis, wound infections and metastatic complications) and toxin-mediated diseases (e.g., toxic shock syndrome, food poisoning and scaled skin syndrome) (Archer 1998; Lowy 1998; von Kockritz-Blickwede *et al.* 2008; Hennekinne *et al.* 2012).

S. aureus colonises axilla, groin, pharynx or damaged skin surfaces mucous and mostly membranes of the nasal cavity (Noble *et al.* 1967; Peacock *et al.* 2001). It is a commensal organism carried in 30% of humans (Rasigade & Vandenesch 2014). Infections occur when

a breach of the skin or mucosal barrier allows entry of *S. aureus* to soft tissues or the bloodstream (Lowy 1998). Dissemination of *S. aureus* into the bloodstream can cause *S. aureus* bacteraemia (SAB), which has has a 30 day mortality rate of approximately 23%. Higher mortality rates can be caused by antibiotic-resistant strains such as methicillin-resistant *S. aureus* (MRSA) (Mylotte & Tayara 2000; Naber 2009). The tendency of *S. aureus* to spread to other organ sites can cause metastatic infections including those of the heart (endocarditis) bone (osteomyelitis), lungs (pneumonia), joints (septic arthritis) or kidneys (Lowy 1998). Patients with Type 1 diabetes, immunocompromised patients, intravenous drug users, surgical patients and those with indwelling catheters are more prone to *S. aureus* infections (Lowy 1998). *S. aureus* also causes mastitis in animals, such as cows, goats and sheep (Le Marechal *et al.* 2011).

Virulence factors expressed by *S. aureus* are the causes of a wide range of diseases. Many surface adhesins interact with host extracellular matrix molecules acting as immune evasion molecules (Foster & Hook 1998; Lowy 1998; Harris *et al.* 2002), allowing colonisation in the anterior nares (Garcia-Lara *et al.* 2005). Protein A binds to the Fc part of antibodies, preventing recognition by the host immune system (Uhlen *et al.*, 1984; Harris *et al.,* 2002). Capsular polysaccharides, inhibitors of complement activation and chemotaxis inhibitory protein (CHIPS) also inhibit phagocytosis in different ways (Foster 2005). Membrane-damaging toxins such as cytotoxins, leukotoxins and haemolysins that lyse cells and provoke proinflammatory responses (Foster 2005). Extracellular enzymes such as proteases, coagulase and lipases, which are thought to be involved in spreading the infection and damaging the host tissue (Foster, 2005).

1.3.3   Antibiotic resistance in *S. aureus*

Before the introduction of antibiotics, the mortality rate of SAB was over 80% (Skinner & Keefer 1941). Since the beginning of the antibiotic era, the mortality rate of SAB has been improved to be just in excess of 20% over the last several decades (Chan *et al.* 2012). However, as rapidly as new antibiotics have been introduced, *S. aureus* has developed mechanisms of resistance that make them ineffective (Fig. 1.8). Therefore, *S. aureus* has been able to maintain its role as a life-threatening pathogen globally (Rasigade & Vandenesch 2014).

When penicillin was first introduced in the early 1940's, more than 94% of *S. aureus* strains were susceptible, however, about 50% of *S. aureus* isolates were resistant to penicillin by 1948 and less than 5% of *S. aureus* isolates showed sensitivity by the late 1990's (Barber &

Rozwadowska-Dowzenko 1948; Lowy 1998). *S. aureus* resistance to penicillin is due to the expression of a β-lactamase, encoded by *blaZ*, which hydrolyses the β-lactam ring of penicillin, rendering it inactive (Lowy 1998).

During the 1950s, *S. aureus* isolates resistant to the other commonly used antibiotics, such as tetracycline, streptomycin, erythromycin and chloramphenicol, also emerged shortly after the introduction of these antimicrobials into the clinic (Williams 1959). Resistance to these protein synthesis inhibitors is due to ribosome modification altering antibiotic binding affinity (tetracycline, streptomycin and erythromycin) (Lacey & Chopra 1972; Burdett 1991; Roberts *et al.* 1999), the action of efflux pumps (tetracycline and erythromycin) (Guay *et al.* 1993; Roberts *et al.* 1999) or detoxification of the antibiotic through acetylation (streptomycin and chloramphenicol) (Courvalin & Fiandt 1980; Murray & Shaw 1997).

In 1960, β-lactamase-resistant semi-synthetic penicillins were introduced to combat penicillin resistance, such as methicillin, cloxacillin and oxacillin (Rice 2006). However, in less than a year, methicillin resistant *S. aureus* (MRSA) was reported in the United Kingdom (U.K.) (Jevons *et al.* 1961). MRSA is resistant to all currently available β-lactam antibiotics (Rasigade & Vandenesch 2014). Methicillin prevents the formation of the bacterial cell wall by binding of the it's β-lactam ring to PBPs, which catalyse formation of peptidoglycan cross-links in the cell wall. Resistance is due to the acquisition of the *mecA* gene encoding PBP2a, which is able to substitute for essential transpeptidase activities as its active site has a low affinity to β-lactams (Lim & Strynadka 2002).

In 1964, gentamcin, a non- β-lactam antibiotic, was introduced to combat the problem of methicillin resistance in the U.K.; however, in the mid-1970s, resistance of *S. aureus* to gentamicin and related antibiotics, such as kanamycin and tobramycin, had been found in clinical isolates from Europe, the United States (U.S.) and Australia (Dowding 1977; Naidoo & Noble 1978; Storrs *et al.* 1988; Wright *et al.* 1998). The resistance is due to gentamicin phosphotransferase/aminoglycoside 6'-N- acetyltransferase, which modifies the antibiotic, preventing binding to the 30S ribosomal target (Dowding 1977; Rouch *et al.* 1987).

During the 1980s, fluoroquinolone antibiotics, such as clinafloxacin, pefloxacin and sparfloxacin, was developed to treat *S. aureus* infections (Entaenza et al., 1999; Khaliq and Zhanel, 2003). However, resistance developed easily soon after introduction of these antibiotics (Greenberg *et al.* 1987). The resistance is due to mutation in DNA gyrase and overexpression of NorA, a multidrug efflux protein (Kaatz *et al.* 1990; Ferrero *et al.* 1995; Ng *et al.* 1996; Charbonneau *et al.* 2006).
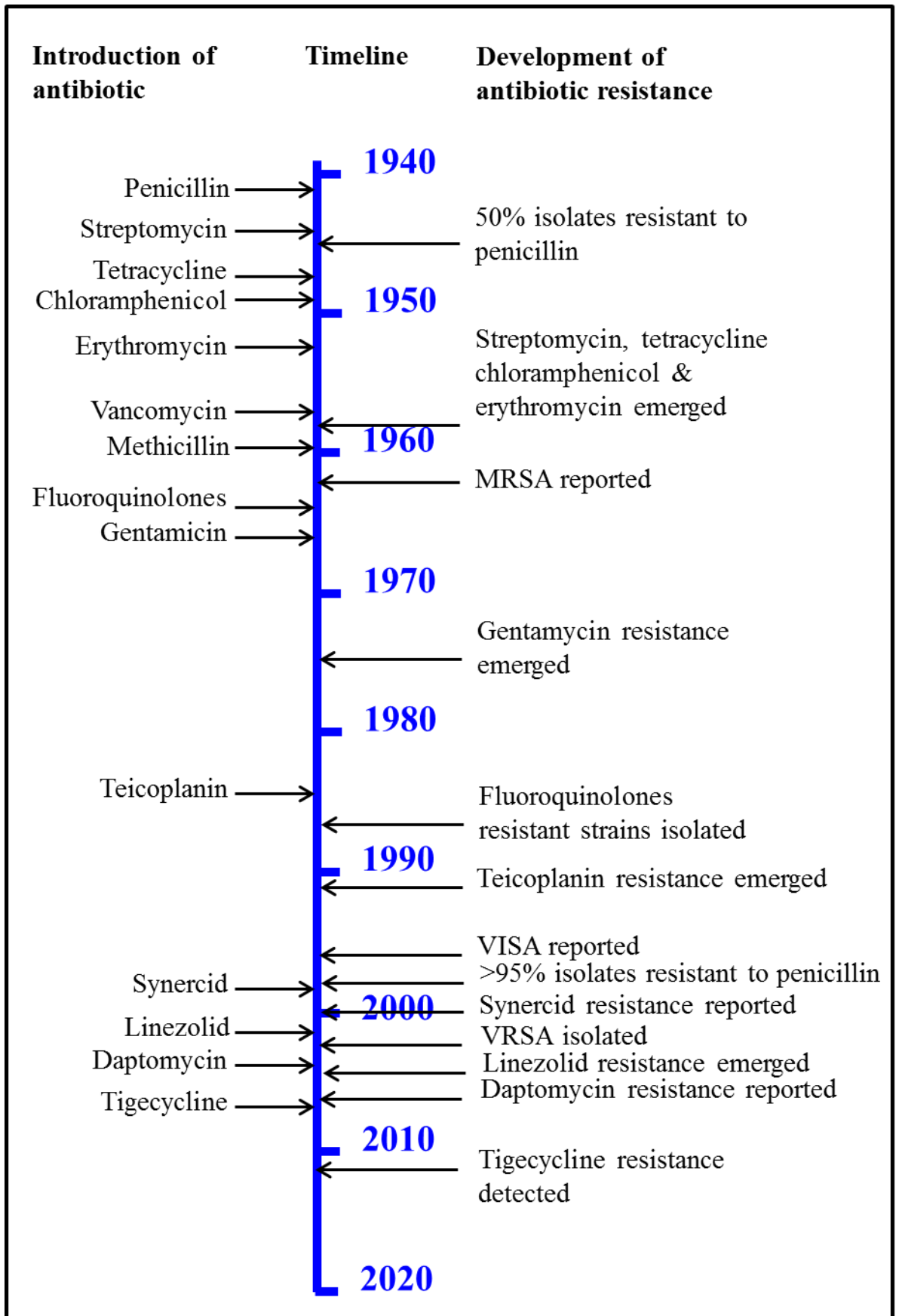
Figure 1-8 Timeline of introduction and subsequent development of resistance by *S. aureus*. Modified from Kabli (2013).

Vancomycin, a glycopeptide, was first introduced to treat drug-resistant pathogens in 1958 (Cafferkey *et al.* 1982). Glycopeptides bind to the D-ala-D-ala termini of peptidoglycan precursors preventing integration into peptidoglycan (Courvalin 2006). By late 1988, the first clinical vancomycin resistant *Enterococcus* strains were isolated (Uttley *et al.* 1988). The resistance is due to the presence of the *vanA* operon that encodes the VanH dehydrogenase and VanA ligase; responsible for the synthesis of D-Ala-D-Lac that replaces D-Ala-D-Ala and for which vancomycin has low affinity (Courvalin 2006). In 1996, Vancomycin-insensitive *S. aureus* (VISA) was first reported in Japan (Hiramatsu *et al.* 1997). VISA is due to an alteration in the synthesis of peptidoglycan, which leads to thickening of the cell wall with reduced cross-linking (Sieradzki & Tomasz 1999). This alteration sequesters vancomycin due to increased production of D-Ala-D-Ala and thus reduces the rate of diffusion of vancomycin through the cell wall (Cui *et al.* 2000; Cui *et al.* 2006; Pereira *et al.* 2007a) In 2002, the first vancomycin-resistant *S. aureus* (VRSA) was isolated as the result of conjugal transfer of the *vanA* operon from co-existing VRE (Weigel *et al.* 2003; Cui *et al.* 2006; Sievert *et al.* 2008) Although the incidence of VRSA is very rare, the level of VRSA-MRSA combination strains is on the rise, making a major threat to public health. Notably, VRSA is also resistant to other antibiotics, for instance rifampin, causing a critical situation in the control of *S. aureus* infection and making the search for new antibiotics urgent (Weigel *et al.* 2003). Like vancomycin, another glycopeptide antibiotic, teicoplanin, was also used to treat both methicillin-sensitive *S. aureus* (MSSA) and MRSA. However, teicoplanin-resistant *S. aureus* emerged in early 1990's (Kaatz *et al.* 1990).

Other therapeutic antibiotics (e.g. synercid, linezolid, daptomycin and tigecycline) have been certified to treat both MRSA and VRSA. Synercid, a combination of two streptoGramins (quinupristin and dalfopristin), inhibits protein synthesis by binding to the 50S ribosomal subunit of the ribosame (Drew *et al.* 2000). Synercid-resistant *S. aureus* strains have been reported (Werner *et al.* 2001), caused by a mutation in the L22 ribosomal protein (Malbruny *et al.* 2002). Linezolid-resistant *S. aureus* strains were isolated in the same year the antibiotic was introduced, the resistance was due to a modification in its 23S ribosomal target (Tsiodras *et al.* 2001). Daptomycin is a cyclic lipopeptide that depolarises the cell membrane (Tally *et al.* 1999; Silverman *et al.* 2003). Daptomycin-resistant strains were found 2 years later after introduction of the antibiotic in 2003 (Hayden *et al.* 2005; Mangili *et al.* 2005). Resistance is caused by perturbation of the bacterial cell wall and cell membrane, reducing the surface binding of the drug (Bayer *et al.* 2013). Tigecycline belongs to the glycylcycline class of antibiotics, is structurally similar to tetracycline but not affected by the tetracycline resistance mechanisms of ribosomal protection and efflux pumps (Petersen *et al.* 1999). Tigecycline-

resistant *S. aureus* have been reported recently in the U.K. (Hope *et al.* 2010; Kreis *et al.* 2013).

1.4   The scope of this project

There are basically two modes of cell wall growth, elongation and division, for controlling cell shape in rod shaped bacterium (Leaver & Errington 2005). Putative cytoskeletal proteins, such as MreBCD, are critically involved in controlling cell wall synthesis, determining polarity and aiding in chromosome segregation (Margolin 2009). In *S. aureus* that lacks MreB, FtsZ was suggested as the only means of recruitment and tethering of the cell wall synthetic machinery (Pinho & Errington 2003). Although *S. aureus* does not elongate and MreB is absent, it contains MreCD homologues with unknown function. The aim of this project was to determine the roles of MreC and MreD and in doing so to increase our knowledge of how cell shape is controlled in *S. aureus*. Experiments were performed using a number of molecular and biochemical approaches to study biochemical function and localisation in the cell. The interaction between proteins involved in many essential processes was also investigated and emphasised the importance of these proteins in the cell division process.

2 Chapter 2 Materials and Methods

2.1 Media and antibiotics

2.1.1 Media

All media were prepared with distilled water (dH_2O) and sterilised by autoclaving for 20 min at 121 ºC (15 pounds per square inch). All media components were bought from Oxoid and chemicals from BDH, Fisher or Sigma.

2.1.1.1 Brain heart infusion (BHI)

Brain heart infusion	37 g l^{-1}

Oxoid agar No.1 (1.5 % (w/v)) was used for BHI agar.

2.1.1.2 Luria-Bertani (LB)

Tryptone	10 g l^{-1}
Yeast Extract	5 g l^{-1}
NaCl	5 g l^{-1}

Oxoid agar No.1 (1.5 % (w/v)) was used for LB agar.

2.1.1.3 BACTH Buffered LB

Tryptone	10 g l^{-1}
Yeast Extract	5 g l^{-1}
NaCl	5 g l^{-1}
Na_2HPO_4	3.5 g l^{-1}
KH_2PO_4	1.5 g l^{-1}

pH was adjusted to 7.5 with NaOH and Oxoid agar No.1 (1 % (w/v)) was added for buffered LB agar. Once the solution had cooled after autoclaving, the filter sterilised stock solution of IPTG (0.5 mM) was added.

2.1.1.4 LK

Tryptone	10 g l^{-1}
Yeast Extract	5 g l^{-1}

KCl   7 g l^{-1}

Oxoid agar No.1 (1.5 % (w/v)) was used for LK bottom agar.

Oxoid agar No.1 (0.7 % (w/v)) was used for LK top agar.

2.1.1.5 Tryptic Soy Broth (TSB)

Tryptic soya broth   30 g l^{-1}

Oxoid agar No.1 (1.5 % (w/v)) was used for TSB agar (TSA)

2.1.1.6 ZYP-5052 Auto-induction Broth

The following solutions were prepared and autoclaved separately.

NZY	900 ml H$_2$O
NZ amines AS	10 g
Yeast extract	5 g

20 × NPS	
$(NH_4)_2SO_4$	66 g l^{-1}
KH_2PO_4	136 g l^{-1}
Na_2HPO_4	385 g l^{-1}

50 × 5052	
Glycerol	250 g l^{-1}
Glucose	25 g l^{-1}
Alpha-lactose	100 g l^{-1}

The following solutions were filter-sterilised (0.2 µm pore size) and stored at room temperature.

MgSO4	1 M
1000 × Metals Mix	
FeCl$_3$ dissolved in HCl 0.1M	0.1 M
CaCl$_2$	1 M
MnCl$_2$	1 M
ZnSO$_4$	1 M

CoCl$_2$		0.2 M
CuCl$_2$		0.1 M
NiCl$_2$		0.2 M
Na$_2$MoO$_4$		0.1 M
Na$_2$SeO$_3$		0.1 M
H$_3$BO$_3$		0.1 M

The above stock solutions and media were mix together just before use as well as appropriate antibiotics.

NZY	900 ml
20 × NPS	50 ml
50 × 5052	20 ml
MgSO4	1 ml
1000 × Metals Mix	1 ml

2.1.2 Antibiotics

All antibiotics used in this study are listed in Table 2.1. Stock solutions were filter-sterilised (0.2 µm pore size) and stored at -20°C. For use in agar plates, the antibiotic stock solutions were added to the media once cooled to below 55°C. For use in liquid media, the antibiotic

Antibiotic	Abbrivation	Stock concentration (g L^{-1})	Solvent	*E. coli* working concentration (mg L^{-1})	*S. aureus* working concentration (mg L^{-1})
Ampicillin	Amp	100	sd H$_2$O	100	-
Chloramphenicol	Cat	25	100% (v/v) ethanol	15	30 or 10
Erythromycin	Erm	5	100% (v/v) ethanol	-	5
Kanamycin	Kan	50	sdH$_2$O	-	50
Lincomycin	Lin	25	50% (v/v) ethanol	-	25
Neomycin	Neo	50	sdH$_2$O	-	50
Spectinomycin	Spec	300	sdH$_2$O	-	300
Tetracycline	Tet	5	100% (v/v) ethanol	-	10

stock solutions were added just before use.

Table 2.1 Antibiotic stock solutions and concentrations

2.2 Bacterial strains and plasmids

2.2.1 *S. aureus* strains

The *S. aureus* strains used in this study are listed in Table 2.2. Strains were grown from –80 °C Microbank (Pro-lab Diagnostics) stocks on either BHI or TSB agar plates, containing antibiotics to maintain resistance markers where necessary. For short-term storage, plates were kept at 4°C. A single colony was place into Microbank stocks for long-term storage at -80°C.

For growth in liquid media, strains were grown aerobically at 37 °C. Strains carrying temperature-sensitive plasmids were grown at 28°C or 30°C for pIMAY or pMAD, respectively. For standard growth, a single well isolated colony was used to inoculate 5 ml liquid medium in a sterile 25 ml Universal bottle. The culture was grown at 37 °C, overnight with shaking at 250 rpm. This culture was then sub-cultured in 50 ml fresh medium in a sterile 250 ml conical flask to OD_{600} 0.01. Strains were then grown at 37 °C with shaking at 250 rpm.

Strain	Relevant genotype/Markers	Source
RN4220	Restriction deficient transformation recipient	Kreiswirth *et al.* (1983)
SH1000	Functional *rsbU*$^+$ derivative of 8325-4	Horsburgh *et al.* (2002)
SJF3830	Newman *spa*$^-$ *sbi*$^-$, Kan^R, Erm^R	Lab stock
LC102	SH1000 *spa::tet* Tet^R	Cooper *et al.* (2009)
JGL220	SH1000 *noc-GFP*$^+$ Erm^R	
JGL227	SH1000 *ezrA-GFP*$^+$ Erm^R	Kasturiarachchi, unpublished
JGL228	SH1000 *gpsB-GFP*$^+$ Erm^R	Kasturiarachchi, unpublished
JGL229	SH1000 *mreC-GFP*$^+$ Erm^R	Kasturiarachchi, unpublished
JGL260	SH1000 *plsY-GFP*$^+$ Erm^R	Kasturiarachchi, unpublished
VF85	SH1000 *spa::tet ezrA-GFP*$^+$ pGL485 Tet^R Erm^R Cat^R	(Steele *et al.* 2011)
VF94	SH1000 *gpsB-GFP*$^+$ pGL485 Erm^R Cat^R	(Steele *et al.* 2011)
VF95	SH1000 *noc-GFP*$^+$ pGL485 Erm^R Cat^R	(Steele *et al.* 2011)
SJF2100	SH1000 *mreC-GFP*$^+$ P$_{spac}$-*mreC* Erm^R	This study

Strain	Relevant genotype/Markers	Source
SJF2101	SH1000 *mreD-GFP*[+] P$_{spac}$-*mreD* Erm^R	This study
SJF2164	SH1000 *plsY-GFP*[+] P$_{Spac}$-*plsY* Cat^R	(Garcia-Lara *et al.* 2015)
SJF2625	SH1000 *mreCD:: kan* Kan^R	This study
SJF2626	SH1000 *mreCD:: kan* Kan^R	This study
SJF2687	RN4220 *mreC-GFP*[+] *mreC*[-] Spec^R	This study
SJF2688	RN4220 *mreC-GFP*[+] Spec^R	This study
SJF2691	RN4220 *mreD-GFP*[+] *mreD*[-] Spec^R	This study
SJF2692	RN4220 *mreD-GFP*[+] Spec^R	This study
SJF2976	SH1000 *mreD::kan* Kan^R	This study
SJF2977	SH1000 *mreD::kan* Kan^R	This study
SJF3189	SH1000 containing pGL485 Cat^R	This study
SJF3191	SH1000 containing pGL620 Cat^R	This study
SJF3193	SH1000 containing pGL621 Cat^R	This study
SJF3195	SH1000 containing pGL631 Cat^R	This study
SJF3200	SJF2625 containing pGL620 Cat^R	This study
SJF3202	SJF2625 containing pGL621 Cat^R	This study
SJF3205	SJF2625 containing pGL631 Cat^R	This study
SJF3207	SJF2625 containing pGL485 Cat^R	This study
SJF3208	SJF2976 containing pGL621 Cat^R	This study
SJF3210	SJF2976 containing pGL485Cat^R	This study
SJF3285	SH1000 *mreCD:: kan ezrA-GFP*[+] P$_{Spac}$-*ezrA* Kan^R Erm^R	This study
SJF3286	SH1000 *mreD::kan* Kan^R *ezrA-GFP*[+] P$_{Spac}$-*ezrA* Kan^R Erm^R	This study
SJF3729	Newman *mreCD:: kan* Kan^R	This study
SJF3731	Newman *mreD::kan* Kan^R	This study
SJF3933	SH1000 *cdsA-GFP*[+] P$_{Spac}$-*cdsA* Erm^R	This study
SJF4098	SH1000 *mreC*[-]	This study
SJF4103	SH1000 *mreC*[-] *ezrA-GFP*[+] P$_{Spac}$-*ezrA* Kan^R Erm^R	This study
SJF4105	SH1000 *mreC*[-] *cdsA-GFP*[+] P$_{Spac}$-*cdsA* Cat^R	This study
SJF4109	SH1000 *mreC*[-] *gpsB-GFP*[+] P$_{Spac}$-*gpsB* Kan^R Erm^R	This study
SJF4114	SH1000 *mreCD:: kan* Kan^R *noc-GFP*[+]	This study
SJF4116	SH1000 *mreC*[-] *noc-GFP*[+]	This study
SJF4117	SH1000 *mreD::kan* Kan^R *noc-GFP*[+]	This study

Strain	Relevant genotype/Markers	Source
SJF4120	SH1000 *mreD::kan gpsB-GFP*[+] P$_{Spac}$-*gpsB* Kan[R] Erm[R]	This study
SJF4121	SH1000 *mreCD::kan gpsB-GFP*[+] P$_{Spac}$-*gpsB* Kan[R] Erm[R]	This study
SJF4123	SH1000 *mreD::kan cdsA-GFP*[+] P$_{Spac}$-*cdsA* Kan[R] Erm[R]	This study
SJF4125	SH1000 *mreCD::kan cdsA-GFP*[+] P$_{Spac}$-*cdsA* Kan[R] Erm[R]	This study
SJF4127	SH1000 *mreD::kan plsY-GFP*[+] P$_{Spac}$-*plsY* Kan[R] Erm[R]	This study
SJF4128	SH1000 *mreCD::kan plsY-GFP*[+] P$_{Spac}$-*plsY* Kan[R] Erm[R]	This study
SJF4129	SH1000 *mreC*[-] *plsY-GFP*[+] P$_{Spac}$-*plsY* Cat[R]	This study

Table 2.2 *S. aureus* strains used in this study **Erm[R], erythromycin resistant; Tet[R], tetracycline resistant; Kan[R], kanamycin resistant; Cat[R], chloramphenicol resistant.**

2.2.2 *E. coli* strains

The *E. coli* strains used in this study are shown in Table 2.3. Standard growth and storage conditions were the same as for *S. aureus* strains (Charpter 2.2.1) except that LB was used as the growth medium. All strains were grown at 37ºC.

Strain	Relevant genotype/Markers	Source
TOP10	F[-] *mcr &(mrr-hsdRMS-mcrBC)* φ 80 *lacZ &M15 &lacX74 recA1 deoR araD139 &(ara-leu) 7697 galK rpsL* (StrR) *endA1 nupG*	Invitrogen
DC10B	F[-] *endA1 recA1 Δdcm galE15 galK16 nupG rpsL ΔlacX74 Φ80lacZΔM15 araD139 Δ(ara,leu)7697 mcrA Δ(mrr-hsdRMS-mcrBC) λ*[-]	Kindly provided by I. Monk
BL21 (DE3)	F[-] *ompT gal [dcm] [lon] hsdSB (rB- mB-)* (DE3)	Novagen
BTH101	F[-] *cya99 araD139 galE15 galK16 rpsL1* (StrR) *hsdR2 mcrA1 mcrB1*	Karimova *et al*., 1998
SJF2253	TOP10 containing pGL598a Amp[R] Kan[R] Erm[R]	This study
SJF2254	TOP10 containing pGL598a Amp[R] Kan[R] Erm[R]	This study
SJF2255	TOP10 containing pGL598b Amp[R] Kan[R] Erm[R]	This study
SJF2256	TOP10 containing pGL598b Amp[R] Kan[R] Erm[R]	This study
SJF2673	TOP10 containing pGL607b Amp[R] Kan[R]	This study
SJF2674	TOP10 containing pGL607b Amp[R] Kan[R]	This study
SJF2923	TOP10 containing pGL613 Amp[R] Kan[R]	This study
SJF2924	TOP10 containing pGL613 Amp[R] Kan[R]	This study
SJF2927	TOP10 containing pGL620 Spec[R] Cat[R]	This study

Strain	Relevant genotype/Markers	Source
SJF2928	TOP10 containing pGL620 Spec^R Cat^R	This study
SJF2933	TOP10 containing pGL621 Spec^R Cat^R	This study
SJF2934	TOP10 containing pGL621 Spec^R Cat^R	This study
SJF3187	TOP10 containing pGL631 Spec^R Cat^R	This study
SJF3188	TOP10 containing pGL631 Spec^R Cat^R	This study
SJF3582	F- *gyrA462 endA1 glnV44 Δ(sr1-recA)mcrB mrr hsdS20(rB-, mB-) ara14 galK2 lacY1 proA2 rpsL20(Smr) xyl5 Δleu mtl1* DB3.1 containing pKOR1	This study
SJF2950	BTH101 containing pGL571 & pALB5 Amp^R Kan^R	This study
SJF2951	BTH101 containing pGL573 & pALB5 Amp^R Kan^R	This study
SJF2952	BTH101 containing pGL546 & pALB5 Amp^R Kan^R	This study
SJF2953	BTH101 containing pUT18c & pALB5 Amp^R Kan^R	This study
SJF2955	BTH101 containing pGL570 & pALB5 Amp^R Kan^R	This study
SJF2956	BTH101 containing pALB4 & pALB5 Amp^R Kan^R	This study
SJF3226	BTH101 containing pALB15 & pALB5 Amp^R Kan^R	This study
SJF3228	BTH101 containing pALB15 & pALB7 Amp^R Kan^R	This study
SJF3243	BTH101 containing pGL557 & pALB4 Amp^R Kan^R	This study
SJF3244	BTH101 containing pGL568 & pALB7 Amp^R Kan^R	This study
SJF3245	BTH101 containing pGL564 & pALB7 Amp^R Kan^R	This study
SJF3246	BTH101 containing pGL559 & pALB4 Amp^R Kan^R	This study
SJF3250	BTH101 containing pGL564 & pALB5 Amp^R Kan^R	This study
SJF3251	BTH101 containing pGL568 & pALB5 Amp^R Kan^R	This study
SJF3254	BTH101 containing pGL572 & pALB5 Amp^R Kan^R	This study
SJF3256	BTH101 containing pGL572 & pALB7Amp^R Kan^R	This study
SJF3260	BTH101 containing pGL570 & pALB7 Amp^R Kan^R	This study
SJF3300	BTH101 containing pALB14 & pALB5 Amp^R Kan^R	This study
SJF3304	BTH101 containing pALB14 & pALB7 Amp^R Kan^R	This study
SJF3309	BTH101 containing pALB12 & pALB7 Amp^R Kan^R	This study
SJF3314	BTH101 containing pGL545 & pALB7 Amp^R Kan^R	This study
SJF3316	BTH101 containing pGL542 & pALB11 Amp^R Kan^R	This study
SJF3317	BTH101 containing pGL551 & pALB11 Amp^R Kan^R	This study
SJF3323	BTH101 containing pALB9 & pALB4 Amp^R Kan^R	This study
SJF3325	BTH101 containing pALB10 & pALB5 Amp^R Kan^R	This study

Strain	Relevant genotype/Markers	Source
SJF3335	BTH101 containing pALB10 & pALB7 Amp^R Kan^R	This study
SJF3339	BTH101 containing pGL549 & pALB11 Amp^R Kan^R	This study
SJF3340	BTH101 containing pGL541 & pALB11 Amp^R Kan^R	This study
SJF3343	BTH101 containing pGL546 & pALB7 Amp^R Kan^R	This study
SJF3344	BTH101 containing pGL545 & pALB5 Amp^R Kan^R	This study
SJF3347	BTH101 containing pGL550 & pALB4 Amp^R Kan^R	This study
SJF3355	BTH101 containing pALB4 & pALB7 Amp^R Kan^R	This study
SJF3356	BTH101 containing pUT18c & pALB7 Amp^R Kan^R	This study
SJF3337	BTH101 containing pALB11 & pALB5 Amp^R Kan^R	This study
SJF3338	BTH101 containing pGL555 & pALB11 Amp^R Kan^R	This study
SJF3341	BTH101 containing pGL554 & pALB11 Amp^R Kan^R	This study
SJF3357	BTH101 containing pALB6 & pALB7 Amp^R Kan^R	This study
SJF3358	BTH101 containing pGL571 & pALB7 Amp^R Kan^R	This study
SJF3361	BTH101 containing pGL573 & pALB7 Amp^R Kan^R	This study
SJF3362	BTH101 containing pALB8 & pALB4 Amp^R Kan^R	This study
SJF3400	BTH101 containing pGL554 & pALB4 Amp^R Kan^R	This study
SJF3401	BTH101 containing pGL549 & pALB4 Amp^R Kan^R	This study
SJF3402	BTH101 containing pGL556 & pALB4 Amp^R Kan^R	This study
SJF3406	BTH101 containing pGL560 & pABL4 Amp^R Kan^R	This study
SJF3408	BTH101 containing pGL551 & pALB4 Amp^R Kan^R	This study
SJF3409	BTH101 containing pALB3 & pALB4 Amp^R Kan^R	This study
SJF3411	BTH101 containing pGL555 & pALB4 Amp^R Kan^R	This study
SJF3461	BTH101 containing pALB6 & pALB5 Amp^R Kan^R	This study
SJF3466	BTH101 containing pALB3 & pALB11 Amp^R Kan^R	This study
SJF3467	BTH101 containing pGL556 & pALB11 Amp^R Kan^R	This study
SJF3468	BTH101 containing pGL560 & pALB11Amp^R Kan^R	This study
SJF3469	BTH101 containing pALB8 & pALB11 Amp^R Kan^R	This study
SJF3470	BTH101 containing pGL553 & pALB11 Amp^R Kan^R	This study
SJF3471	BTH101 containing pALB11 & pALB7 Amp^R Kan^R	This study
SJF3473	BTH101 containing pGL557 & pALB11 Amp^R Kan^R	This study
SJF3474	BTH101 containing pGL558 & pALB11 Amp^R Kan^R	This study
SJF3477	BTH101 containing pGL558 & pALB4 Amp^R Kan^R	This study
SJF3479	BTH101 containing pGL553 & pALB4 Amp^R Kan^R	This study
SJF3480	BTH101 containing pKT25 & pALB4 Amp^R Kan^R	This study

Strain	Relevant genotype/Markers	Source
SJF3602	BTH101 containing pGL635 & pALB5Amp^R Kan^R	This study
SJF3609	BTH101 containing pGL633 & pALB11 Amp^R Kan^R	This study
SJF3624	BTH101 containing pUT18c & pKT25 Amp^R Kan^R	This study
SJF3627	BTH101 containing pGL542 & pALB4 Amp^R Kan^R	This study
SJF3697	BTH101 containing pUT18 & pKT25 Amp^R Kan^R	This study
SJF3703	BTH101 containing pGL365 & pALB7 Amp^R Kan^R	This study
SJF3793	BTH101 containing pALB9 & pALB11 Amp^R Kan^R	This study
SJF3950	BL21 containing pXIM10 Amp^R	This study
SJF3853	BTH101 containing pKT25 & pALB11 Amp^R Kan^R	This study
SJF3975	BTH101 containing pGL565 & pALB7 Amp^R Kan^R	This study
SJF3976	BTH101 containing pALB12 & pALB5 Amp^R Kan^R	This study
SJF3977	BTH101 containing pALB30 & pALB5 Amp^R Kan^R	This study
SJF3978	BTH101 containing pALB30 & pALB7 Amp^R Kan^R	This study
SJF3979	BTH101 containing pALB2 & pALB5Amp^R Kan^R	This study
SJF3980	BTH101 containing pALB2 & pALB7 Amp^R Kan^R	This study
SJF3981	BTH101 containing pGL550 & pALB11 Amp^R Kan^R	This study
SJF3983	BTH101 containing pGL541 & pALB4 Amp^R Kan^R	This study
SJF3984	BTH101 containing pGL552 & pALB4 Amp^R Kan^R	This study
SJF3985	BTH101 containing pGL552 & pALB11 Amp^R Kan^R	This study
SJF3986	BTH101 containing pALB24 & pALB4 Amp^R Kan^R	This study
SJF3987	BTH101 containing pALB24 & pALB11 Amp^R Kan^R	This study
SJF3988	BTH101 containing pGL632 & pALB4 Amp^R Kan^R	This study
SJF3989	BTH101 containing pATL3 & pALB7 Amp^R Kan^R	This study
SJF3990	BTH101 containing pGL562 & pALB7 Amp^R Kan^R	This study
SJF3991	BTH101 containing pATL3 & pALB5 Amp^R Kan^R	This study
SJF3992	BTH101 containing pGL633 & pALB4 Amp^R Kan^R	This study
SJF3993	BTH101 containing pATL1 & pALB4 Amp^R Kan^R	This study
SJF3994	BTH101 containing pATL1 & pALB11 Amp^R Kan^R	This study

Table 2.3 *E. coli* strains used in this study

2.2.3   Plasmids

Plasmids used in this study are shown in Table 2.4. All plasmid DNA was purified using QIAGEN kits following the manufacturer's instructions (Charpter 2.7.2 & 2.7.3) and was stored in elution buffer or sdH2O at -20°C.

Plasmid	Relevant genotype/Markers	Source
pXIM4	pET-21d containing a 542 bp of entire *S. aureus mreD*; Amp^R	This study
pXIM6	pUT18 containing T18 fused in frame to the 3' end of *S. aureus mreC*; Amp^R	This study
pXIM7	pUT18 containing T18 fused in frame to the 3' end of *S. aureus mreD*; Amp^R	This study
pXIM8	pKNT25 containing T25 fused in frame to the 3' end of *S. aureus mreC*; KanR	This study
pXIM9	pKNT25 containing T25 fused in frame to the 3' end of *S. aureus mreD*; KanR	This study
pXIM10	pET-21d containing a 745 bp fragment of *S. aureus mreC*; Amp^R	This study
pKT25	Derivative of low copy-number pSU40, carrying the first 224 amino acids of *B. subtilis* CyaA (T25 fragment), upstream of a multiple cloning site; Kan^R	Karimova et al., 2001
pKNT25	Derivative of low copy-number pSU40, carrying gene encoding the first 224 amino acids of CyaA (T25 fragment), downstream of a multiple cloning site; Kan^R	Karimova et al., 2001
pUT18	Derivative of high copy-number pUC19, carrying gene encoding amino acids 225 to 399 of CyaA (T18 fragment), downstream of a multiple cloning site; Amp^R	Karimova et al., 2001
pUT18c	Derivative of high copy-number pUC19, carrying gene encoding amino acids 225 to 399 of CyaA (T18 fragment), upstream of a multiple cloning site; Amp^R	Karimova et al., 2001
pKT25-zip	pKT25 containing T25 fused in frame to the 5' end of the leucine zipper of *GC84*; Kan^R	Karimova *et al.,* 2001
pUT18C-zip	pUT18C containing T18 fused in frame to the 5' end of the leucine zipper of *GC84*; Amp^R	Karimova *et al.,* 2001
pET21d	His$_6$-tag Over-expression vector, Amp^R	Novagen
pMAD	*E. coli-S. aureus* shuttle vector with temperature-sensitive replication origin in *S. aureus* and constitutively expressed thermostable β-galactosidase gene	Arnaud *et al.*, 2004
pOB	Cloning vector containing *erm*^{R} gene	Horsburgh *et al.*, 2002

Strain	Relevant genotype/Markers	Source
pKOR1	Cloning vector containing tet^R, cat^R, amp^R genes and a temperature-sensitive replicon for Gram positive bacteria (pE194ts)	(Bae & Schneewind 2006)
pIMAY	Cloning vector containing a temperature-sensitive replicon for Gram positive bacteria (*repBCAD*) and the tetracycline-inducible antisense *secY* region (*anti-secY*) Cat^R	(Monk *et al.* 2012)
pGL433b	Vector containing *kan*^{R} gene	Jorge Garcia-Lara, unpublished
pGL485	Cat^R derivative of *E. coli-S. aureus* shuttle vector pMJ8426, carrying *E. coli lacI* gene under the control of a constitutive promoter; Spec^R (*E. coli*),Cam^R (*S. aureus*)	(Steele *et al.* 2011)
pGL541	pKT25 containing T25 fused in frame to the 5' end of *S. aureus ftsA*; Kan^R	(Steele *et al.* 2011)
pGL542	pKT25 containing T25 fused in frame to the 5' end of *S. aureus ftsL*; Kan^R	(Steele *et al.* 2011)
pGL545	pUT18C containing T18 fused in frame to the 5' end of *S. aureus ftsA*; AmpR	(Steele *et al.* 2011)
pGL546	pUT18C containing T18 fused in frame to the 5' end of *S. aureus ftsL*;Amp^R	(Steele *et al.* 2011)
pGL550	pKT25 containing T25 fused in frame to the 5' end of *S. aureus pbpA*; Kan^R	(Steele *et al.* 2011)
pGL551	pKT25 containing T25 fused in frame to the 5' end of *S. aureus divIC*; Kan^R	(Steele *et al.* 2011)
pGL552	pKT25 containing T25 fused in frame to the 5' end of *S. aureus EzrA*; Kan^R	(Steele *et al.* 2011)
pGL553	pKT25 containing T25 fused in frame to the 5' end of *S. aureus parC*; Kan^R	(Steele *et al.* 2011)
pGL554	pKT25 containing T25 fused in frame to the 5' end of *S. aureus parE*; Kan^R	(Steele *et al.* 2011)
pGL555	pKT25 containing T25 fused in frame to the 5' end of *S. aureus yneS*; Kan^R	(Steele *et al.* 2011)
pGL556	pKT25 containing T25 fused in frame to the 5' end of *S. aureus pbp3*; Kan^R	(Steele *et al.* 2011)

Strain	Relevant genotype/Markers	Source
pGL557	pKT25 containing T25 fused in frame to the 5' end of *S. aureus gpsB*; Kan[R]	(Steele *et al.* 2011)
pGL558	pKT25 containing T25 fused in frame to the 5' end of *S. aureus ypsA*; Kan[R]	(Steele *et al.* 2011)
pGL559	pKT25 containing T25 fused in frame to the 5' end of *S. aureus sepF*; Kan[R]	(Steele *et al.* 2011)
pGL560	pKT25 containing T25 fused in frame to the 5' end of *S. aureus noc*; Kan[R]	(Steele *et al.* 2011)
pGL562	pUT18C containing T18 fused in frame to the 5' end of *S. aureus ftsZ*;Amp[R]	(Steele *et al.* 2011)
pGL564	pUT18C containing T18 fused in frame to the 5' end of *S. aureus divIC*;Amp[R]	(Steele *et al.* 2011)
pGL568	pUT18C containing T18 fused in frame to the 5' end of *S. aureus yneS*;Amp[R]	(Steele *et al.* 2011)
pGL570	pUT18C containing T18 fused in frame to the 5' end of *S. aureus gpsB*;Amp[R]	(Steele *et al.* 2011)
pGL571	pUT18C containing T18 fused in frame to the 5' end of *S. aureus ypsA*;Amp[R]	(Steele *et al.* 2011)
pGL572	pUT18C containing T18 fused in frame to the 5' end of *S. aureus sepF*;Amp[R]	(Steele *et al.* 2011)
pGL573	pUT18C containing T18 fused in frame to the 5' end of *S. aureus noc*;Amp[R]	(Steele *et al.* 2011)
pGL589	pOB containing upstream of *mreC*, *mreC* and downstream of *mreD* Kan[R]	This study
pGL598 (a&b)	pOB containing upstream of *mreC*, downstream of *mreD* Kan[R]	This study
pGL620	pGL485 containing *mreC* Spec[R] Cat[R]	This study
pGL621	pGL485 containing *mreD* Spec[R] Cat[R]	This study
pGL631	pGL485 containing *mreCD* Spec[R] Cat[R]	This study
pGL632	pKNT25 containing T25 fused in frame to the 3' end of *S. aureus cdsA* Kan[R]	Jorge Garcia-Lara, unpublished
pGL633	pKT25 containing T25 fused in frame to the 5' end of *S. aureus cdsA* Kan[R]	Jorge Garcia-Lara, unpublished

Strain	Relevant genotype/Markers	Source
pGL635	pUT18 containing T18 fused in frame to the 3' end of *S. aureus cdsA*; Amp^R	Jorge Garcia-Lara, unpublished
pALB3	pKT25 containing T25 fused in frame to the 5' end of *S. aureus ftsW* Kan^R	Bottomley, 2012
pALB4	pUT18C containing T18 fused in frame to the 5' end of *S. aureus mreC*;Amp^R	Bottomley, 2012
pALB5	pKT25 containing T25 fused in frame to the 5' end of *S. aureus mreC*; Kan^R	Bottomley, 2012
pALB6	pUT18C containing T18 fused in frame to the 5' end of *S. aureus ftsW*;Amp^R	Bottomley, 2012
pALB7	pKT25 containing T25 fused in frame to the 5' end of *S. aureus mreD*; Kan^R	Bottomley, 2012
pALB8	pKT25 containing T25 fused in frame to the 5' end of *S. aureus rodA*; Kan^R	Bottomley, 2012
pALB9	pKT25 containing T25 fused in frame to the 5' end of *S. aureus zapA*; Kan^R	Bottomley, 2012
pALB10	pUT18C containing T18 fused in frame to the 5' end of *S. aureus zapA*;Amp^R	Bottomley, 2012
pALB11	pUT18C containing T18 fused in frame to the 5' end of *S. aureus mreD*;Amp^R	Bottomley, 2012
pALB12	pUT18C containing T18 fused in frame to the 5' end of *S. aureus pbp2*;Amp^R	Bottomley, 2012
pALB13	pKT25 containing T25 fused in frame to the 5' end of *S. aureus divIB*; Kan^R	Bottomley, 2012
pALB14	pUT18C containing T18 fused in frame to the 5' end of *S. aureus rodA*;Amp^R	Bottomley, 2012
pALB15	pUT18C containing T18 fused in frame to the 5' end of *S. aureus divIB*;Amp^R	Bottomley, 2012
pALB24	pKT25 containing T25 fused in frame to the 5' end of *S. aureus pbp2*; Kan^R	Bottomley, 2012
pALB30	pUT18C containing T18 fused in frame to the 5' end of *S. aureus ltaS*;Amp^R	Bottomley, 2012
pALB31	pUT18C containing T18 fused in frame to the 5' end of *S. aureus pbp4*;Amp^R	Bottomley, 2012

Strain	Relevant genotype/Markers	Source
pALB32	pKT25 containing T25 fused in frame to the 5' end of *S. aureus pbp4*; Kan^R	Bottomley, 2012
pALB33	pKT25 containing T25 fused in frame to the 5' end of *S. aureus ltaS*; Kan^R	Bottomley, 2012
pVF29	pKNT25 containing T25 fused in frame to the 3' end of *S. aureus ftsZ;*Kan^R	(Steele *et al.* 2011)
pVF30	pKNT25 containing T25 fused in frame to the 3' end of *S. aureus ezrA;* Kan^R	(Steele *et al.* 2011)
pVF31	pUT18 containing T18 fused in frame to the 5' end of *S. aureus ftsZ;*Amp^R	(Steele *et al.* 2011)
pVF32	pUT18 containing T18 fused in frame to the 5' end of *S. aureus ezrA;* Amp^R	(Steele *et al.* 2011)
pATL1	pKT25 containing T25 fused in frame to the 5' end of *S. aureus dnaK*; Kan^R	Andrew Liew unpublished
pATL2	pUT18C containing T18 fused in frame to the 5' end of *S. aureus dnaK*;Amp^R	Andrew Liew unpublished
pATL3	pUT18 containing T18 fused in frame to the 3' end of *S. aureus dnaK*;Amp^R	Andrew Liew unpublished

Table 2.4 Plasmids used in this study

2.3   Buffers and solutions

dH$_2$O was used to prepare all buffers and solutions, which were sterilised by autoclaving, if necessary and stored at 4°C or room temperature for immediate use. Sambrook and Russell (2001) was used for all of the methods in this chapter, unless otherwise stated.

2.3.1   Phage Buffer

MgSO$_4$	1 mM
CaCl$_2$	4 mM
Tris-HCl pH 7.8	50 mM
NaCl	0.6 % (w/v)
Gelatin	0.1 % (w/v)

2.3.2 Phosphate buffered saline (PBS)

NaCl	8 g l^{-1}
Na$_2$HPO$_4$	1.4 g l^{-1}
KCl	0.2 g l^{-1}
KH$_2$PO$_4$	0.2 g l^{-1}

The pH was adjusted to 7.4, using NaOH

2.3.3 Tris buffered saline (TBS)

Tris-HCl pH 7.5	50 mM
NaCl	100 mM

2.3.4 TAE (50x)

Trisma base	242 g l^{-1}
Glacial acetic acid	0.57 % (v/v)
Na$_2$EDTA pH8.0	0.05 M

Before use, 50x stock was diluted 1:50 with sdH2O, to produce a working TAE solution.

2.3.5 QIAGEN Buffers

2.3.5.1 QIAGEN Buffer P1

Tris-HCl, pH 8	50 mM
EDTA	10 mM
RNase A	100 μg ml^{-1}

2.3.5.2 QIAGEN Buffer P2

NaOH	200 mM
SDS	1 % (w/v)

2.3.5.2 QIAGEN Buffer P3

C$_2$H$_3$KO$_2$, pH 5.5	3.0 M

2.3.5.3 QIAGEN Buffer EB

Tris-HCl, pH 8.5	10 mM

2.3.5.4   QIAGEN Buffer QBT

NaCl	0.75 M
MOPs	0.05 M

Adjusted to pH 7.0 with NaOH.

Isopropanol	15 % (v/v)
Trition X-100	0.15 % (v/v)

2.3.5.5   QIAGEN Buffer QF

NaCl	1.25 M
Tris	50 mM

Adjusted to pH8.5 with NaOH.

Isopropanol	15 % (v/v)

2.3.5.6   QIAGEN Buffer QG, N3, PB and PE

Supplied in the QIAquick kit, details not provided.

2.3.6   Southern blotting solutions

2.3.6.1   Depurination solution

HCl	20 mM

2.3.6.2   Denaturation solution

NaCl	1.5 M
NaOH	0.5 M

2.3.6.3   Neutralisation solution

NaCl	3 M
Tris-HCl, pH 7.5	0.5 M

2.3.6.4   Saline-sodium citrate (SSC) buffer (20x)

NaCl	3 M
Sodium citrate	300 mM

Adjusted to pH 7 with 1 M NaOH.

2.3.6.5   Prehybridisation solution

SSC	5x
Blocking reagent (Roche)	1 % (w/v)
N-lauroylsarcosine	0.1 % (w/v)
Sodium dodecyl sulphate (SDS)	0.02 % (w/v)

2.3.6.6   Hybridisation solution

Prehybridisation solution with 5-25 ng ml^{-1} labelled DNA probe.

2.3.6.7   Hybridisation wash solution (2x)

SSC	2x
SDS	0.1 % (w/v)

2.3.6.8 Hybridisation wash solution (0.5x)

SSC	0.5x
SDS	0.1 % (w/v)

2.3.6.8   Maleic acid buffer

NaCl	0.15 M
Maleic acid	0.1 M

Adjusted to pH7.5 with NaOH.

2.3.6.9   Detection wash solution

Maleic acid buffer with 3 % (v/v) Tween 20.

2.3.6.10 Blocking solution

Blocking reagent (Roche)	1 % (w/v)

Prepared in maleic acid buffer and gently heated until dissolved. Stored at -20ºC.

2.3.6.11 Antibody solution

Blocking solution, containing 1:5000 dilution of anti-DIG-alkaline phosphatase conjugated antibody stock (Roche).

2.3.6.12 Detection buffer

Tris-HCl (pH 9.5)	100 mM
NaCl	100 mM

2.3.6.13 Colour-substrate solution

Detection buffer containing NBT/BCIP (Roche) 2 % (v/v)

2.3.6.14 TE (10x)

Trisma base	100 mM
Na_2EDTA	10 mM

The pH was adjusted to 7.5 using HCl. The 10x stock was diluted 1:10 to a working solution, with sterile dH_2O.

2.3.7 HiTrap purification buffers

2.3.7.1 0.1M sodium phosphate buffer

1M NaH_2PO_4	31.6 ml
1M Na_2HPO_4	68.4 ml
dH_2O	900 ml

The pH was adjusted to 7.2 and the buffer was autoclaved.

2.3.7.2 START Buffer

0.1M Sodium phosphate buffer	200ml
NaCl	0.5M
dH2O	Up to 1L

8M Urea was added, if required.

2.3.7.3 Elution buffer

Start buffer containing

Imidazole	0.5 M

8M Urea was added, if required.

2.3.8   SDS PAGE solutions

2.3.8.1   SDS PAGE reservoir buffer (10x)

Glycine	144 g l^{-1}
Tris base	30.3 g l^{-1}
SDS	10 g l^{-1}

A 1:10 dilution with sdH$_2$O was made to give a 1x SDS-PAGE working buffer.

2.3.8.2   SDS PAGE loading buffer (2 x)

Tris-HCl pH 6.8	0.62 M
SDS	10% (w/v)
Glycerol	20% (v/v)
Bromophenol blue	0.1% (w/v)

10% (v/v) β-mercaptoethanol was added fresh before each use.

2.3.8.3   Coomassie Blue stain

Coomassie blue	0.1% (w/v)
Methanol	5% (v/v)
Glacial acetic acid	10% (v/v)

2.3.8.4   Coomassie destain

Methanol	5% (v/v)
Glacial acetic acid	10% (v/v)

2.3.9 Western blotting solutions

2.3.8.5   Blotting buffer

Trisma base	2.4 g L^{-1}
Glycine	11.26 g L^{-1}
Methanol	20% (v/v)

2.3.8.6 TBST (20x)

Trisma base	48.4 g l^{-1}
NaCl	120 g l^{-1}
Tween-20	2% (v/v)

2.3.8.7 Blocking Buffer

1x TBST containing:

Dried skimmed milk powder	5% (w/v)

2.3.8.8 Alkaline Phosphatase buffer

Tris-HCL pH 9.5	0.1 M
NaCl	5.8 g l^{-1}
MgCl$_2$.6H$_2$O	10.2 g l^{-1}

2.3.8.9 Detection buffer (ROCHE western blot kit); all solutions supplied by manufacture.

Peroxide solution	25 % (v/v)
Luminol enhancer solution	25 % (v/v)
SuperSignal west Pico stable peroxide solution	25 % (v/v)
SuperSignal west pico Luminol enhancer solution	25 % (v/v)

2.3.9 β-galactosidase liquid assay solutions

2.3.9.1 ABT

NaCl	5.88 g l^{-1}
K$_2$HPO$_4$	10.51 g l^{-1}
KH$_2$PO$_4$	5.44 g l^{-1}
Triton X-100	0.1% (v/v)

2.3.9.2 Stopping Solution

Na$_2$CO$_3$	42.39 g l^{-1}

2.3.9.3 ABTN

ABT	500 ml
Stopping solution	500 ml

2.3.10 GTE Buffer

Glucose	50 mM
EDTA	10 mM
Tris-HCL pH 7.5	20 mM

2.3.11 TBSI

Tris-HCl pH7.5	50 mM
NaCl	0.1 M

Complete mini EDTA-free protease cocktail inhibitor (Roche) was then dissolved in the buffer following manufacturer's instructions.

2.4   Chemicals and enzymes

All chemicals and enzymes used in this study were of analytical grade quality and were purchased from Sigma, Fisher Scientific, MP Biomedicals or Roche unless otherwise stated. All restriction enzymes, T4 ligase and appropriate buffers were purchased from Roche or New England Biolabs. Concentrations of stock solutions and storage conditions are shown in Table 2.5.

Stock solution	Concentration	Dissolved in	Storage
Lysostaphin (Sigma)	5 mg ml^{-1}	20mM sodium acetate	-20°C
Mutanolysin (Sigma)	0.5 mg ml^{-1}	dH2O	-20°C
4-MU (4-methylumbelliferone) (Sigma)	1 mM	DMSO	-20°C
MUG (4-methylumbelliferyl-β-D-galactopyranoside) (Sigma)	4 mg ml^{-1}	DMSO	-20°C
X-Gal (5-bromo-4-chloro-3-indolyl-β-D-galactopyranoside) (Sigma)	80 mg ml^{-1} Or 200 μg ml^{-1}	DMF	Foil wrapped at -20°C
IPTG (isopropyl-β-D-1-thiogalactopyranoside)	1 M	dH2O; filter sterilised (0.2μm pore size)	-20°C
Formaldehyde	16% (w/v)	PBS at 60°C	Short term at 4°C
Glutaraldehyde	25% (w/v)	dH$_2$O	-20°C

Table 2.5 Chemical stock solutions used in this study.

2.5 Centrifugation

A number of different centrifuges were used for harvesting samples. These were:

(2) Eppendorf microfuge 5415D

maximum volume of 2 ml, maximum speed 13,200 rpm (10,000 xg);

(ii) Sigma centrifuge 4K15C

maximum volume of 50 ml, maximum speed of 5,100 rpm (5525 xg)

(iii) Jouan centrifuge JAC50.10

maximum volume of 50 ml, maximum speed 13,000 rpm (10,000 xg);

(iv) Avanti J25I (Beckman)

maximum volumes and speeds dependent on the rotor used:

JA-20: maximum volume of 50 ml, maximum speed 20,000 rpm (48,384 xg)

JA-14: maximum volume of 250 ml, maximum speed 14,000 rpm (30,074 xg)

JA-10.5: maximum volume of 500 ml, maximum speed 10,000 rpm (18,480 xg)

2.6 Determining bacterial cell density

2.6.1 Spectrophotometric measurement (OD$_{600}$)

To quantify the bacterial yield of a culture, spectrophotometric measurements at 600 nm (OD$_{600}$), were performed. These measurements were taken using a Jenway 6100 spectrophotometer. Where necessary, culture samples were diluted 1:10 in sterile culture medium to give a reading below 1.5.

2.6.2 Direct cell counts (cfu ml^{-1})

For quantification of viable cell numbers direct cell counts were performed. Bacterial samples were serially diluted 1:10 in PBS in triplicate. 10 µl samples of each dilution were spotted onto BHI agar plates containing antibiotics and supplements, where necessary. After overnight incubation at 37 °C, the number of colony forming units (cfu) was determined.

2.7 DNA Purification techniques

2.7.1 Genomic DNA preparation

Genomic DNA was isolated and purified from *S. aureus* using a QIAGEN DNeasy^{TM} kit using a method based on the manufacturer's instructions. 200 μl of 5 ml overnight culture was sub-cultured into fresh 5 ml BHI and incubated at 37°C with shaking until OD_{600} 5-6. The cells were recovered by centrifugation in a 25 ml universal bottle at 5,500 rpm, for 5 min at RT. The resulting supernatant was discarded. The cell pellet was washed by resuspension in 1 ml H_2O and centrifugation at 10,000 rpm for 1 min. The pellet was resuspended in 180 μl of H_2O and 5 μl of lysostaphin (5mg/ml), and incubated at 37 °C for up to 1 hour until transparent. After incubation, 200 μl of buffer AL was added, mixed by continuous inversion for 1 min. Then, 200 μl of 100 % (v/v) ethanol was added and mixed thoroughly by inversion. The resulting mixture was pipetted into a DNeasy™ Mini Spin Column and centrifuged at 8,000 rpm for 1 min at RT. The flow-through and collection tube were discarded and the column placed into a new collection tube before 500 μl of buffer AW1 was added. The column was centrifuged at 8,000 rpm for 1 min and again the flow through and collection tube were discarded. 500 ml of buffer AW2 was added and the column was centrifuged at 13,200 rpm for 3 min in order to dry the column. The collection tube was carefully removed so the column did not come into contact with the flow-through. The DNeasy column was then placed into a microfuge tube and the DNA eluted with 100 μl of buffer AE, the column was incubated for 3 min then centrifuged for 1 min at 13,200 rpm.

2.7.2 Small scale plasmid preparation

Small scale plasmid purification from *E. coli* cells was performed using the QIAGEN QIAprep™ Spin column kit. For isolation of plasmids from *S. aureus*, 25μg ml^{-1} lysostaphin was added and the sample incubated at 37°C for 1 hour before the manufacturer's instructions were followed.

2.7.3 Large scale plasmid preparation from *E. coli*

Large scale plasmid preparation from *E. coli* cells was performed using the QIAGEN QIAprep^{TM} HiSpeed Midiprep kit following the manufacturer's instructions.

2.7.4 Gel extraction of DNA using QIAquick Spin Column

DNA was separated in a 1% (w/v) TAE agarose gel and stained with 5 μg ml^{-1} ethidium bromide. The DNA was visualised using a UV trans-illuminator. The required band was excised from the gel using a sterile scalpel blade. Isolation of DNA from the agarose gel slice was then carried out using a QIAGEN QIAquick gel extraction kit following the manufacturer's instructions.

2.7.5 Purification of PCR products using a QIAquick spin column

DNA fragments were purified from PCR reactions using a QIAquick PCR purification kit following manufacturer's instructions.

2.7.6 Ethanol precipitation of DNA

100% (v/v) ethanol corresponding to 2.5x volume of the purified DNA sample, and 0.1x volume of 3 M sodium acetate pH 5.2 were added. Glycogen (Roche) corresponding to 0.05x volume of the purified DNA sample was added to aid visualisation of the DNA pellet. The sample was incubated at -20°C for 30 min to 1 h. Precipitated DNA was recovered by centrifugation at 13,200 rpm for 10 min at RT. The pellet was then washed five times in 70% (v/v) ethanol and centrifuged at 13,200 rpm for 3 min at RT. The pellet was allowed to air dry and then resuspended in an appropriate volume of sdH2O.

2.8 *In vitro* DNA manipulation techniques

2.8.1 Polymerase chain reaction (PCR) techniques

2.8.1.1 Primer design

Primers used for PCR amplification were short synthetic oligonucleotides (20-50 nucleotides) that were based on the DNA sequence of *S. aureus* 8325. Where necessary, suitable restriction sites were introduced at the 5' ends of primers to enable subsequent cloning. An additional 6 bases (A or T) were added to allow efficient restriction digestions at these sites. The predicted annealing temperature and potential dimerisation and cross-dimerisation sites were identified using NetPrimer (www.premierbiosoft.com/netprimer). Primers were synthesised by Sigma or Eurofins MWG Operon and were stored as 100 μM stocks at -20°C. 10 μM working solutions were made with sdH$_2$O before use. Primers used are shown in Table 2.6.

Primer	Sequence (5'-3')	Application	Source
5'GLUSh270A	ATATTT<u>GGATCC</u>TAATGTGGAACTAG	Amplification of upstream of *mreC* Forward primer	This study
3'GLUSh270A	ATATTT<u>GGTACC</u>GTCAGCACGTTTAG	Amplification of downstream of *mreD* Reverse primer	This study
5'GLUSh270B	ATATTT<u>GCGGCCGC</u>CACAAATTTTTTACGGAG	Amplification of *mreC* Forward primer	This study
3'GLUSh270B	ATATTT<u>GCGGCCGC</u>TACTTATAACTACTCAACTATTG	Amplification of *mreD* Reverse primer	This study
5'GLUSh270C	AATATT<u>GCGGCCGC</u>TCTATTATGTCAAAATATTG	Amplification of *mreC* Forward primer	This study
3'GLUSh270C	ATAAAT<u>GCGGCCGC</u>TACATACAACCGCTCAAATATAGGTTC	Amplification of *mreD* Reverse primer	This study
5'GLUSh270D	ATTAT<u>GCGGCCGC</u>TAAAACAATTCCTGATGATG	Amplification of *mreD* Forward primer	This study
3'GLUSh270D	AATTAT<u>GCGGCCGC</u>AAAAAATAATACAGTGTACG	Amplification of *mreC* Reverse primer	This study
5'GLUSh380A	ATAATA<u>GGGCCC</u>TAAGTAAATAATAGAGGTGTTCTGGGTGCTTAAG	Amplification of *mreC* Forward primer	This study
3'GLUSh380A	ATAATA<u>GGATCC</u>TTATTTATCCCTGCTTTCATCATCAG	Amplification of *mreC* Reverse primer	This study
5'GLUSh380B	ATAATA<u>GGGCCC</u>TAAGTAAATAAATGATGAAAGCAGGGATAAATAATG	Amplification of *mreD* Forward primer	This study
3'GLUSh380B	ATAATA<u>GGATCC</u>TTACCATTGACGACGTTTCATGTCAATG	Amplification of *mreD* Reverse primer	This study
5'HXM39B	ATAATA<u>GCGGCCGC</u>ATAAACCCAGCGAACCATTTG	Amplification of *kan^R* cassette Forward primer	This study
3'HXM39B	ATAATA<u>GCGGCCGC</u>ATCGATACAAATTCCTCG	Amplification of *kan^R* cassette Reverse primer	This study
3'HXM39-11A	ATAATAGCAGTAACTGTTCCTTCAAC	Amplification of downstream of *mreD* Forward primer	This study

Primer	Sequence (5'-3')	Application	Source
5'HXM49Aa	ATAATAGGATCCCAGTGCTTAAGTTTTTTAAAAATAAC	Amplification of *mreC* Forward primer	This study
3'HXM46Aa	ATAATAAAGCTTAGTCACTTCTCCTATATATAAATTAC	Amplification of truncated *mreC* Reverse primer	This study
3'HXM46Ab	ATAATAAAGCTTTTTATCCCTGCTTTCATCATC	Amplification of *mreC* Reverse primer	This study
5'HXM49Ba	ATAATAGGATCCCAATGCGTACACTGTATTATTTTTTG	Amplification of *mreD* Forward primer	This study
3'HXM46Ba	ATAATAAAGCTTGAATAACATCGAATGATCTTTG	Amplification of truncated *mreD* Reverse primer	This study
3'HXM46Bb	ATAATAAAGCTTCCATTGACGACGTTTCATG	Amplification of *mreD* Reverse primer	This study
3'HXM67A	ATATTTAGATCTGTCAGCACGTTTAG	downstream of *mreD* Reverse primer	This study
5'HXM130A	ATATTTGGGCCCACAAATTTTTTACGGAG	Amplification of *mreC* Forward primer	This study
3'HXM130A	ATATTTGGATCCGCTACTTATAACTACTCAACTATTG	Amplification of *mreD* Reverse primer	This study
5'HXM159	ATAATAGGATCCAGGAGGGCTAGACATATGCGTTCACAATCTCAATC	Amplification of extracellular domain of *mreC* Forward primer	This study
3'HXM159	ATAATAGAATTCTTATTTATCCCTGCTTTCATCATCAG	Amplification of extracellular domain of *mreC* Reverse primer	This study
5'HXM316A	ATAATACCATGGGTGAACAATATATAGGTGATTCTGTG	Amplification of extracellular domain of *mreC* Forward primer	This study
3'HXM231A	ATAATACTCGAGTTTATCCCTGCTTTCATCATCAG	Amplification of extracellular domain of *mreC* Reverse primer	This study
5'HXM231B	ATAATACCATGGCTTGATGATGAAAGCAGGGATAAATAATGCGTACACTG	Amplification of *mreD* Forward primer	This study

Primer	Sequence (5'-3')	Application	Source
3'HXM231B	ATAATA<u>CTCGAG</u>CCATTGACGACGTTTCATGTCAATGTC	Amplification of *mreD* Reverse primer	This study
O1	GGAAGATCTGTCTAGTTAATGTGTAACGTA	Sequencing of inserts in pMAD Forward primer	(Arnaud *et al.* 2004)
O2	CGCGGATCCGACCTTAATTATATTATAGTCCCAAT	Sequencing of inserts in pMAD Reverse primer	(Arnaud *et al.* 2004)
FWD	TACATGTCAAGAATAAACTGCCAAAGC	Sequencing of inserts in pIMAY Forward primer	(Monk *et al.* 2012)
REV	AATACCTGTGACGGAAGATCACTTCG	Sequencing of inserts in pIMAY Reverse primer	(Monk *et al.* 2012)

Table 2.6 Primers used in this study

Relevant restriction sites are underlined.

2.8.1.2   Standard PCR amplification

PCR amplification reactions were performed using high-fidelity Extensor PCR ReddyMix™ (ThermoScientific). A final reaction volume of 25 μl contains the following:

DNA polymerase   1.25 U
$MgCl_2$ 2.25 mM
dNTPs   0.5 mM (each)
Precipitant and red dye for electrophoresis

The following components were added, on ice, to 0.5 ml thin-walled sterile PCR tubes:

High-fidelity Extensor ReddyMix   12.5 μl
Template DNA   100 ng
Forward and reverse primers   200 nM for each primer
Sterile water to give 1x concentration of PCR ReddyMix.

PCR amplification was carried out using a Techgene PCR machine (Techne). The block was preheated to 95ºC and the following reaction conditions were used:

1 cycle	Initial denaturation	95 ºC	5 min
30 cycles	Denaturation	95 ºC	30 s
	Annealing	49-55 ºC	1 min
	Extension	72 ºC	1min per kb
1 cycle	Final extension	72 ºC	5 min

The reaction products were stored at -20ºC.

2.8.1.3 Colony PCR screening

Primers and sterile water were added to PCR ReddyMix in 0.5 ml thin-walled PCR tubes as described above, without the addition of template DNA. Using a sterile toothpick, a single colony was replicate patched onto a selective agar plate and introduced into the 20 µl sdH$_2$O in PCR reaction tube. For *E. coli*, the PCR reaction was then carried out as described above. For colony PCR of *S. aureus*, the cells were lysed with the following proGram using a Techgene PCR machine (Techne):

37 ºC	15 min
99 ºC	20 min
4 ºC	1 min
99 ºC	2 min
4 ºC	1 min

After PCR, the suspension was mixed by pipetting up and centrifuged down. 8 µl of the supernatant was used as template for 20 µl PCR reaction. The PCR reaction was then carried out as described above.

2.8.2 Restriction endonuclease digestion

Restriction enzymes were purchased from New England Biolabs. Digestion of DNA was performed according to the manufacturer's instructions, with the buffers supplied. The reaction mixture was incubated for 3 h at 37 °C. If digested products were to be used in cloning reactions, restriction enzymes were inactivated by incubation at 65 °C for 20 min,

except for reaction using *Acc*I, which were inactivated at 80°C. Restriction enzymes removed using the QIAquick PCR purification kit (Chapter 2.7.5).

2.8.3   Phosphatase treatment of linearised vector DNA

The treatment of vector DNA with calf intestinal alkaline phosphatase (CIP) significantly reduces self-ligation by removing the 5' PO_4 from the DNA. Phosphatase was directly added to the restriction endonuclease digestion of the vector according to the manufacturer's instructions. The reaction was stopped by incubation at 65°C for 30 min. The CIP phosphatase was then removed using the QIAquick PCR purification kit (Chapter 2.7.5). The dephosphorylated vector was resuspended in sdH_2O and stored at -20 °C.

2.8.4   Ligation of DNA

Insert and vector DNA were prepared by restriction endonuclease digestion. Vector DNA was treated with phosphatase to remove 5' phosphate groups. Each ligation reaction contained approximately a 1:3 molar ratio of vector DNA to insert DNA. The ligations were carried out in a 10 μl volume with 1 μl of 10x T4 DNA ligase buffer and 1 μl of 3 U $μl^{-1}$ T4 DNA ligase (Roche). Reactions were incubated at 16°C overnight. Ligation mixtures were purified by ethanol precipitation (Chapter 2.7.6) and then used to transform competent cells. As a negative control, a ligation reaction was set up as above, except that no insert DNA was added.

2.8.5   Agarose gel electrophoresis

DNA samples were separated in 1% (w/v) agarose gels in 1x TAE Buffer. Horizontally submerged agarose gels were poured and run using various size horizontal electrophoresis tanks (Scie-Plas). 5 μg ml^{-1} ethidium bromide (Sigma) was added to the molten gel to allow the visualisation of DNA.

DNA samples were mixed with 6x DNA loading buffer (ThermoScientific) before loading into the wells of the gel. DNA was resolved for 40 min at 100 V at room temperature. DNA was visualised using an UV transilluminator at 260 nm and photographed using the UVi Tec Digital camera and UVi Doc Gel documentation system. The size and concentration of DNA fragments were estimated by co-electrophoresing 1 μg of 1kb DNA ladder (Table 2.7).

ThermoScientific		New England Biolabs	
Fragment	Size (bp)	Fragment	Size (bp)
1	250	1	500
2	500	2	1 000
3	750	3	1 500
4	1 000	4	2 000
5	1 500	5	3 001
6	2 000	6	4 001
7	2 500	7	5 001
8	3 000	8	6 001
9	4 000	9	8 001
10	5 000	10	10 002
11	6 000		
12	8 000		
13	10 000		

Table 2.7 DNA fragments used as size markers for agarose gel electrophoresis

2.8.6   Plasmid sequencing

1 μg of purified plasmid DNA was sequenced by the Core Genomics Facility (University of Sheffield). Sequencing traces were analysed using Geneious software.

2.9   DNA Hybridisation technique

2.9.1   Preparation of DNA probe

The DNA required for hybridisation was amplified from SH1000 genomic DNA extracted by the GIAGEN DNeasy kit (Chapter 2.7.1) using PCR and the purified using gel extraction (Chapter 2.7.4). The purified probe DNA was denatured immediately prior to digoxigenin labelling, by boiling for 10 min and then chilling on ice for 10 min. The DNA probe was labelled by a random priming method using a commercially available digoxigenin (DIG) DNA labelling and detection kit (Roche). The following components were added to 500 ng probe DNA in a 20 μl volume and incubated at 37 °C, overnight.

Hexanucleotide mixture (vial 5)	2 μl
dNTP labelling mixture (vial 6)	2 μl
Klenow enzyme (vial 7)	1 μl

After incubation the labelled probe was purified using the QIAGEN PCR purification kit (Chapter 2.7.5).

2.9.2 Preparing sample DNA

Genomic DNA was prepared using the QIAGEN DNeasy kit as described in Chapter 2.7.1. 16 µl of genomic DNA was digested with the required restriction enzyme in a total volume of 20 µl at 37 °C overnight.

2.9.3 Southern blotting

6 µl of 1 kb DNA ladder, 20 µl of digested sample DNA (~1µg) and 20 µl (200 ng) of DIG labelled DNA molecular weight marker III (Roche) were resolved on a 1 % (w/v) TAE agarose gel. The gel was photographed using the UVi Tec Digital camera and UVi Doc Gel documentation system. Amersham Life Sciences Hybond-N+ Extra (positively charged nylon membrane) membrane was used for Southern blotting along with a Transblot vacuum system. DNA was transferred from the gel to the nylon membrane using vacuum capillary transfer, set at 70 mbar. Depurination solution was poured onto the surface of the gel and left for 15 min, in order to nick the DNA and aid transfer to the membrane. The procedure was repeated using the denaturation solution, which was then replaced with neutralisation solution and then 10x SSC solution. The latter solution was left over the gel surface for 60 min.

2.9.4 Fixing the DNA to the membrane

The blotted membrane was dried on filter paper for 5 min. DNA was then fixed to the membrane using a UV crosslinker (Amersham Life Sciences RPN 2500), 70 mJ / cm^2; 15 sec and repeated for another 15 sec.

2.9.5 Hybridisation

The membrane was incubated with 20 ml pre-hybridisation solution that had been pre-warmed to 68 °C and incubated rolling in the hybridisation oven at 68 °C for 120 min. Hybridisation solution was prepared by addition of the digoxigenin-labelled DNA probe to 20 ml pre-hybridisation solution followed by incubation in a boiling water bath for 10 min. The pre-hybridisation solution was removed from the membrane, replaced with hybridisation solution and incubated overnight. The hybridisation solution containing the probe was

removed and stored at –20 °C. The membrane was washed well, in the hybridisation oven at 68 °C, with pre-warmed (to 68 °C) 2x hybridisation wash solution for 2 x 5 min, followed by pre-warmed (to 68 °C) 0.5x hybridisation wash solution for 2 x 5 min.

2.9.6   Colourimetric detection

The following steps were performed at room temperature. The membrane was washed in 50 ml detection wash buffer for 1 min then incubated for 30-60 min with gentle agitation in 50 ml blocking solution. The blocking solution was replaced with 50 ml fresh blocking solution containing 10 µl of anti-DIG alkaline phosphatase conjugate antibody (Roche) and incubated for 30 min. The membrane was washed in detection wash buffer for 2x 15 min then washed in detection buffer for 2 min. 400 µl of NBT/BCIP (Roche) was added to 50 ml of fresh detection buffer and the solution poured onto the membrane. The colour was developed in the dark without agitation, washed with TE buffer, dried and scanned. The membrane was then stored in the dark.

2.10   Transformation techniques

2.10.1   Transformation of *E. coli*

2.10.1.1 Preparation of *E. coli* electrocompetent cells

E. coli Top10, BL21, DC10B or BTH101 was streaked for colony isolation on LB agar and incubated overnight at 37°C. A single colony was inoculated into 5 ml LB and incubated overnight at 37°C. Using this overnight culture, 400 ml LB was inoculated to OD_{600} 0.05 and incubated at 37°C, 250 rpm until OD_{600} reached 0.4-0.6. The culture was rapidly chilled on ice slurry for 20 min. Cells were harvested by centrifugation in 4 x 100 ml aliquots at 5500 rpm for 10 min at 4°C. Cell pellets were resuspended in 25 ml ice-cold sdH_2O and the centrifugation step repeated. Pellets were washed twice more in 25 ml ice-cold sdH_2O and the pellets were combined and resuspended in 500 µl sdH_2O. Ice-cold 50% (v/v) glycerol was added to a final concentration of 10% (v/v) and the cells were split into 50 µl aliquots and snap-frozen in liquid nitrogen. Competent cells were stored at -80°C.

2.10.1.2 Transformation of *E. coli* competent cells by electroporation

1 mm electroporation cuvettes (Bio-Rad) were pre-chilled on ice before use. A 50 µl aliquot of *E. coli* competent cells were thawed on ice and 10 µl of ethanol precipitated ligation

reaction was added. Electroporation was carried out using a Gene Pulser system set at 1.75 kV, 25 μF and 200 Ω. *E. coli* cells were recovered by addition of 400 μl LB and incubation statically at 37°C for 15min and then at 250 rpm for 60 minutes. 20 μl, 180 μl and 250 μl cell culture were spread on selective LB agar plates and incubated overnight at 37°C until colonies appeared.

2.10.2 Transformation of *S. aureus*

2.10.2.1 Preparation of *S. aureus* RN4220 electrocompetent cells

S. aureus RN4220 strain was streaked for colony isolation on BHI agar and grown overnight at 37 °C. A single colony was grown in 400 ml BHI at 37 °C with shaking at 250 rpm for 10-12 h. This culture was used to inoculate 400 ml BHI to OD_{600} 0.1 and incubated for 60-90 min at 37°C with shaking at 250 rpm until the OD_{600} had reached 0.4-0.6. Cells were harvested by centrifugation in 4x100 ml aliquots at 5500 rpm at room temperature for 10 min. Cell pellets were washed three times with 25 ml sdH$_2$O by resuspension and centrifugation at 5500 rpm at room temperature for 10 min. Pellets were resuspended in 20 ml 10% (v/v) glycerol and centrifuged at 5100 rpm at room temperature for 10 min. The pellets were then resuspended in 10 ml 10% (v/v) glycerol and incubated at room temperature for 30 min. Cells were harvested by centrifugation at 5500 rpm at room temperature for 10 min and the resulting pellet was resuspended in 500 μl 10% (v/v) glycerol. 50 μl aliquots were used immediately for transformation.

2.10.2.2 Transformation of *S. aureus* RN4220 competent cells by electroporation

Approximately 1 μg plasmid DNA was added to a 50 μl aliquot of *S. aureus* RN4220 electrocompetent cells. The mixture was transferred to a 1 mm electroporation cuvette (Bio-Rad). Electroporation was carried out using a Gene Pulser system set at 1.95 kV, 25 μF and 100 Ω. *S. aureus* cells were recovered by immediate addition of 1 ml BHI and incubation at 37°C, 250 rpm for 3 h or 28°C, 250rpm for 4 hours in a 25 ml universal. 200 μl aliquots were spread on selective BHI agar plates and incubated for 48 h or more at 37°C or 28°C until colonies appeared.

For pIMAY, 200 μl of midi prep was ethanol precipitated and resuspended in 20 μl TAE and 10 μl of the concentrated DNA was used for electroporation. After electroporation cells were recovered in 1ml of TSB+500 mM sucrose for 2h at 28°C (250rpm) and plated on TSA

containing 10 μg/ml of Cat and incubated at 28°C for 48h. Putative positive colonies are streaked out and grown overnight at 28°C on TSA containing Cat (10).

2.10.3 Phage techniques

2.10.3.1 Preparation of phage lysate

The donor strain was grown overnight at 37°C or 28°C in 5 ml BHI containing appropriate antibiotics. Using this overnight culture, 2.5 ml BHI, in a 25 ml universal tube, was inoculated to OD_{600} of 0.2. 2.5 ml of phage buffer and 200 μl of stock phage lysate (Φ11) were added and the sample was incubated at room temperature for 6-8 hours, or until the sample had cleared. Once cleared, 300ul of fresh donor culture was add and incubated at room temperature for overnight. The transparent lysate was then filter sterilised (0.2μm pore size) and stored at 4°C.

2.10.3.2 Phage transduction

The recipient *S. aureus* strain was grown overnight in 50 ml BHI and cells were harvested at 5500 rpm for 10 min. The resulting pellet was resuspended in 1 ml LK. 500 μl of recipient cells were added to 500 μl of phage lysate and 1 ml of LK containing 10 mM $CaCl_2$. The mixture was statically incubated at 37°C for 45 min. 1ml of ice-cold 0.02 M sodium citrate was added and the mixture was placed on ice for 5 min before cells were harvested at 5500 rpm for 10 min. The pellet was resuspended in 1 ml of 0.02 M ice-cold sodium citrate and incubated on ice for 2 hours. 100 μl aliquots were spread onto LK bottom agar plates containing 0.05% (w/v) sodium citrate. Plates were incubated at 37°C for 1.5 hours or for 3 hours for growth impaired mutants or a 28°C growth condition before being overlaid with 5 ml of LK top agar containing 6x normal concentration of selective antibiotic. Plates were incubated at 37°C or 28°C for 24-72 h until colonies appeared. Well isolated colonies were picked and streaked onto BHI agar plates with appropriate antibiotics to ensure they possessed the correct resistance profile.

2.11 Protein analysis

2.11.1 SDS PAGE

Resolving gels were prepared using the following components. APS and TEMED were added immediately before pouring.

12% (w/v) Resolving gel

dH2O	3.5 ml
1.5 M Tris-HCl (pH8.8)	2.5 ml
10% (w/v) SDS	100 μl
30% (w/v) Acrylamide/Bis (37:5:1, BioRad)	4.0 ml
10% (w/v) Ammonium persulphate (APS)	50 μl
TEMED (N,N,N'N'-tetramethyl-ethylenediamine)	5 μl

A layer of isopropanol was applied on top of the gel to isolate it from the air. Once the separating gel had set a stacking gel was applied on top, a comb being placed in the gel immediately to generate loading wells. The components of the stacking gel are:

4% (w/v) Stacking gel

dH2O	2.5 ml
0.5 M Tris-HCl (pH6.8)	0.62 ml
10% (w/v) SDS	50 μl
30% (w/v) Acrylamide/Bis (37:5:1, BioRad)	0.83 ml
10% (w/v) Ammonium persulphate (APS)	25 μl
TEMED (N,N,N'N'-tetramethyl-ethylenediamine)	5 μl

After the stacking gel had solidified, the gel was transferred to a Protean II (BIORAD) gel-running tank and submerged in 1x SDS PAGE reservoir buffer. The comb was removed and appropriate volumes of samples (5-20 μl) were loaded into the wells using a Hamilton syringe. 10 μl of ColorPlus Prestained Protein Ladder, Broad Range (NEB) protein size markers (Table 2.8) were also loaded. Proteins were separated by electrophoresis at 150 V until the blue dye front of the sample buffer was at the base of the gel plate.

Marker	Molecular mass (kDa)
1	230
2	150
3	100
4 (Red)	80
5	60
6	50
7	40
8	30

Marker	Molecular mass (kDa)
9 (Green)	25
10	20
11	15
12	10

Table 2.8 Protein size standards

2.11.2 Coomassie Staining

To visualise proteins, SDS-PAGE gels were submerged in Coomassie blue stain for 40 min. They were then destained in two volumes of Coomassie destain overnight until the background was clear. Molecular masses were determined by comparison to the protein standards of known sizes.

2.11.3 Drying of gels

SDS and native gels were dried between two sheets of DryEase mini Cellophane (Invitrogen) that had been pre-soaked in Gel-Dry™ Drying solution (Invitrogen) using a mini-gel drying frame and base, and left at room temperature for 24 h until completely dry.

2.11.4 Western Blot

Protein samples were separated by SDS-PAGE as described in Chapter 2.11.1. Amersham™Hybond™-ECL membrane (GE Healthcare) was cut to the same size as the SDS PAGE gel. The nitrocellulose membrane was wetted briefly in sdH2O and then equilibrated in blotting buffer for 10 min before use. Proteins were transferred from the gel to the membrane by electroblotting in cold blotting buffer using Mini Trans-Blot apparatus (BIO-RAD) at 60 V for 1.5 h. The membrane was dried on blotting paper for 5 min. The blot was blocked in blocking buffer overnight at 4 °C with gentle agitation. The blot was washed 3 times with TBST for 10 min each time and then incubated with 20 ml blocking solution containing primary antibody at an appropriate dilution for overnight at 4 °C with gentle agitation. The antibody solution was removed and the blot was washed 3 times in TBST for 10 min each time to remove unbound antibody. The blot was incubated in 20 ml blocking solution containing 1:50000 alkaline phosphatase conjugated goat anti-rabbit (Sigma) for 1 h at room temperature with gentle agitation. The secondary antibody solution was removed and the blot was washed 3 times in TBST for 10 min each to remove unbound secondary antibody.

The nitrocellulose membrane was dried on a filter paper for 2 min and submerged in a mixture of equal volumes of enhanced chemiluminescent (ECL) substrate reagent 1 and ECL substrate reagent 2 in the dark room and incubated at room temperature for 5 min. The blot was then dried on a filter paper for 2 min and covered in cling film while ensuring that no air bubbles were trapped between the blot and the cling film. The wrapped blot was fixed in a film cassette, Amersham Hyperfilm™ ECL (GE Healthcare) was cut to the same size as the blot membrane and placed on the top of the wrapped blot for 1 min in the dark. The film was then developed in photographic developing buffer for a few seconds until clear black bands appeared and then rinsed in running dH_2O immediately. The film was then fixed in photographic fixation solution until transparent and rinsed in running dH_2O after. The developed films were air-dried by hanging overnight.

2.11.5 Bradford estimation of protein concentration

The following were added to clean plastic cuvettes:

sdH2O	800 µl
Bio-Rad dye reagent concentrate	200 µl
Protein	10 µl

The cuvettes were sealed with parafilm and mixed carefully by inverting the tube for 30 seconds. The OD_{595} was measured, and the protein concentration should have been between OD_{595} 0.1-0.7. Then the protein concentration was calculated using the following formula:

$$\frac{OD_{595} \times 15}{\text{Volume of protein (µl)}} = \text{Protein concentration (mg/ml)}$$

2.12 Production of recombinant protein

2.12.1 Expression in *E. coli* BL21

A single colony of freshly streaked *E. coli* BL21 containing pET21d with the desired insert was used to inoculate 5 ml LB containing 100 µg ml^{-1} Amp and incubated overnight at 37°C with shaking at 250 rpm. This culture was poured into 1 l autoinduction media and was incubated at 37°C with shaking (250 rpm) for 24 h. Cells were harvested by centrifugation at 5500 rpm for 15 min at 4°C, supernatant discarded, and the resulting pellet stored at -20°C.

2.12.2 Analysis of recombinant protein solubility

During the preparation of cells in Chapter 2.12.1, 1 ml of culture was removed before poured into autoinduction media (uninduced sample), and 2 x 1 ml of culture was removed after 24 h incubation in autoinduction media (induced sample). The cells were harvested by centrifugation at 13200 rpm for 5 min at room temperature, and the supernatant was discarded. The uninduced sample was resuspended in 100 μl SDS loading buffer and one of the induced samples was resuspended in 250 μl SDS loading buffer. The samples were boiled for 5 min and then centrifuged at 13200 rpm for 3 min to pellet any insoluble material. 20 μl of each sample were analysed by SDS-PAGE to confirm overexpression of the recombinant protein. To determine the solubility of the recombinant protein, the second induced sample was resuspended in 250 μl START buffer and lysozyme was added to a final concentration of 1 mg ml^{-1}. The sample was incubated at room temperature for 60 min and then sonicated for 3 x 10 s bursts using a Sanyo soniprep 150. The sample was then centrifuged at 13,200 rpm for 10 min to separate soluble and insoluble material. The supernatant containing soluble proteins was decanted into a fresh microfuge tube and 100 μl SDS loading buffer was added. The pellet containing insoluble material was resuspended fully in 100 μl START buffer containing 8 M urea. 100 μl SDS loading buffer was added and both samples were boiled for 5 min and centrifuged at 13,200rpm for 3 min. 20 μl of each sample was analysed by SDS-PAGE.

2.12.3 Separation of soluble and insoluble material

Cells prepared in Chapter 2.12.1 were thawed and resuspended in 5 ml START buffer without urea. The suspension was then freeze-thawed three times by placing the sample at -80°C for 2 h and then allowing it to thaw completely at 37 °C. The cells were then broken by 10 x 10 s bursts of sonication on ice using a Sanyo soniprep 150. The suspension was centrifuged at 10,000rpm for 25 min at 4°C. The supernatant containing soluble proteins was decanted. The pellet was resuspended thoroughly in 25 ml START buffer containing 8 M urea and incubated overnight at 4°C. The sample was then centrifuged (10,000 rpm, 25 min, 4°C) to remove any unbroken cells and the resulting supernatant containing the solubilised proteins was stored at 4°C.

2.12.4 HiTrap purification

A 5 ml HiTrap column (GE Healthcare) was prepared by washing with 10 ml sterile water, then charged with 10 ml 50 mM NiSO$_4$. Excess NiSO$_4$ was removed by washing with 10 ml sterile water. The BioRad Econo Gradient pump and Fraction Collector was flushed with

START buffer at a flow rate of 1.5 ml min^{-1}. If the proteins were insoluble (Chapter 2.12.3), then 8 M urea was added to both the START and elution buffer. The charged HiTrap column was attached to the BioRad Econo Gradient pump and equilibrated by washing with 5 ml START buffer. The supernatant containing recombinant protein was applied to the column at a flow rate of 1 ml min^{-1} and any non-specific proteins were removed by washing with 5% (v/v) elution buffer until the absorbance returned to zero. The his-tagged proteins were eluted from the column using a gradient of 5-100% (v/v) elution buffer (containing 0.5 M imidazole) at a flow rate of 1 ml min^{-1}, with 1.5 ml fractions being collected. The eluted fractions were then analysed by SDS-PAGE. After elution of the recombinant protein, the HiTrap column was washed with 10 ml 50 mM EDTA to remove NiSO$_4$, followed by 10 ml sterile water. 10 ml 20% (v/v) ethanol was washed through the column before storage at 4°C.

2.12.5 Protein dialysis

2.12.5.1 Preparation of dialysis membrane
Thermo Scientific Slide-A-Lyzer G2 Dialysis Cassette (20K MWCO) was hydrated in PBS and 8 M Urea (dialysis buffer) for 2 minutes by holding the cassette under the surface of dialysis buffer.

2.12.5.2 Dialysis of recombinant protein
The cassette was removed from dialysis buffer and loaded with fractions containing recombinant protein (Chapter 2.12.4) protein sample using pipettes. Excess air in the cassette was removed before floating the cassette in dialysis buffer overnight at 4 ^{o}C. This dialysis step was repeated 3 times more, replacing the dialysis solution with fresh appropriate buffer each time. For insoluble protein, 4 M urea was added to the dialysis solution during the first dialysis. The solution was then replaced by PBS containing 2 M urea followed by PBS containing 1 M and dialysis carried out for overnight at 4°C. The solution was finally resolved in PBS containing 0 M urea. After dialysis, the protein fractions were aspirated from the dialysis cassette and glycerol was added to a final concentration of 10% (v/v). The protein fraction were stored at 4 ^{o}C for short term use and -80°C for long term storage.

2.12.6 Generation of Antibodies
Polyclonal antibodies were raised in rabbits and affinity purified by BioServ (University of Sheffield).

2.13 BACTH analysis

2.13.1 Analysis of β-galactosidase activity on X-Gal plates

β-Galactosidase activity of BACTH strains was measured directly on solid media using the substrate X-Gal. β-Galactosidase hydrolyses X-Gal to produce β-D-galactopyranoside and 5-bromo-4-chloro-3-indole, the latter of which is a visual indicator of β-galactosidase activity due to its blue colouration. To investigate interactions between proteins by detection of β-galactosidase activity, single colonies of BACTH strains were grown overnight in 5 ml TSB containing 100 μg ml^{-1} amp and 50 μg ml^{-1} kan at 37°C, 250 rpm. Cells were harvested from 1 ml culture by centrifugation at 13,200 rpm for 1 min and washed three times by resuspension in 1 ml buffered LB and centrifugation at 13,200 rpm for 1 min. Cells were resuspended in 1 ml buffered LB and a 100-fold dilution was made in sdH$_2$O. 10 μl aliquots of these dilutions were spotted onto freshly-made buffered LB agar. Plates were incubated at 37°C for 12 h. The plates were then incubated at room temperature and the colony colour were detected after 3-4 days.

2.13.2 Analysis of β-galactosidase activity in liquid culture

Liquid culture samples were assayed for β-galactosidase activity with MUG (4-methylumbelliferyl-β-D-galactopyranoside), which is hydrolysed by β-galactosidase into the fluorescent product 4-methylumbelliferone, along with β-D-galactopyranoside. The method used was based on that of Youngman (1990). A single colony of BACTH strains was inoculated into 5 ml of buffered LB containing 100 μg ml^{-1} amp and 50 μg ml^{-1} kan and incubated at 37°C, 250 rpm until OD$_{600}$ reached 0.5. Triplicate samples of 100 μl were collected and cells harvested by centrifugation at 13,200 rpm for 1 min. The supernatant was discarded and the pellets were stored at -80°C. The cell pellets were thawed at RT for 5min and then resuspended in 0.5 ml ABT. 50 μl of freshly prepared MUG was added, tubes mixed and immediately incubated at 25°C for exactly 60 min. The reaction was stopped by addition of 0.5 ml ABTN (Chapter 2.3.10.3).

Aliquots of 250 μl of each sample were pipetted into the top well of a 96-well flat bottom microtitre plate (Nunc). 225 μl of ABTN was added to each of the remaining wells to be used. A 1:10 dilution was made by removing 25 μl sample from the top well and mixing it with 225 μl ABTN. Serial 1:100 and 1:1000 dilutions were also made. 25 μl was removed from the 1:1000 dilution in order to maintain a consistent well volume of 225 μl. The fluorescence of each sample was measured at 355/460 nm, 0.1 s using a Victor^{TM} X3 multilabel reader.

The relationship between the fluorescence and the amount of MU can be determined using a calibration curve. This determines the amount of MU in each 225 µl produced by the β-galactosidase activity of the samples. 1 MUG unit of β-galactosidase activity is defined as the amount of enzyme that catalyses the hydrolysis of 1 pmol of MUG per min, per ml of culture, per unit of optical density at 600nm (OD_{600})

Therefore the following equation was used:

β-galactosidase activity (MUG units) =

$$\frac{\text{Amount MU (pmol) x reaction volume (ml)}}{\text{Incubation time (min) x sample volume (ml) x } OD_{600} \text{ x volume culture (ml)}}$$

Where: reaction volume = 1.05 ml

Incubation time = 60 min

Sample volume = 0.225 ml

Volume of culture = 0.1 ml

2.14 Preparation of samples for microscopy

Samples of appropriate cultures, corresponding to OD_{600} 0.5, were harvested by centrifugation at 13,200 rpm for 1 min. Cells were washed in 1ml sdH2O and harvested by centrifugation. Cells were resuspended in 500 µl PBS and fixed with an equal volume of PBS containing 2.7% (w/v) paraformaldehyde and 0.005% (v/v) gluteraldehyde. Cells were placed on a rotary shaker for 20 min at room temperature followed by 30 min at 4 °C, and then washed 5 times by resuspension in 1 ml dH2O and centrifugation. Cells were resuspended in an appropriate volume of GTE buffer (Chapter 2.3.11) and 5 µl was evenly spread onto a poly-L-Lysine slide (Thermo scientific) and allowed to air dry. Once dry, 10 µl of sdH$_2$O was applied to the slide and a coverslip was then mounted and sealed with DPX mountant (BDH).

2.14.1 Fluorescence microscopy

Fluorescence images were acquired using an Olympus IX70 deconvolution microscope and SoftWoRx 3.5.0 software (Applied Precision). Appropriate filters were used for visualisation of each fluorophore (Table 2.9). Samples were wrapped in foil during fixation and slides were prepared in the dark to prevent fluorophore bleaching.

Filter	Excitation wavelength (nm)	Emission wavelength (nm)	Fluorophore used
DAPI	436/10	457/50	DAPI
FITC-YFP	490/20	528/38	GFP, FITC
mRFP	580/20	630/60	FM4-64, AlexaFluor 594

Table 2.9 Fluorescence filter sets used in this study

2.14.2 *In vitro* staining

Cell membrane and DNA were stained *in vitro* with FM4-64 and DAPI, respectively. 2 μl FM4-64 and 1 μl DAPI were added to 1 ml dH2O and 20 μl of this was evenly applied to fixed cells that had fully dried onto poly-L-lysine slides. Slides were incubated at room temperature for 15 min covered in foil to prevent bleaching. Slides were washed 3 times by application of 100 μl dH2O onto the sample and removal by aspiration. Slides were allowed to dry fully before the coverslip was mounted.

2.14.3 Immunofluorescence

Cells were grown and harvested, and fixed cells were applied to poly-L-lysine slides. Gentle lysis of cells was carried out using lysostaphin at a range of concentrations from 5 ng ml^{-1} for 1 min. Cells were then washed 3 times in sdH$_2$O as described in Chapter 2.14.2 and allowed to air dry. Samples were blocked with 2% (w/v) BSA in PBS for 15 min. Cells were then incubated overnight at 4 $^{\circ}$C with the primary antibody (rabbit anti-*S. aureus* MreC at 1:100) in 2% (w/v) BSA in PBS. Control slides were prepared which had no primary antibody added. The next day samples were washed 8 times with sdH$_2$O before addition of anti-rabbit IgG AlexaFluor 594 conjugate (Invitrogen) at 1:1000 in 2% (w/v) BSA in PBS. Slides were incubated for 2 h in the dark before cells were again washed 8 times with sdH$_2$O. DNA and cell membrane were stained as in Chapter 2.14.2 before addition of a coverslip and sealed with DPX mountant (BDH).

2.15 Cell breakage

Cells were lysed by homogenisation using FastPrep. 1.5 ml of overnight cell culture was added to the glass beads in a 2ml tube and kept on ice. Cells were homogenised in 6 × 30 sec

bursts with cooling on ice between bursts. The cell extract was recovered from the beads by aspiration with a pipette. The extract was clarified by centrifugation at 13,200 rpm for 10 min and supernatant transferred to a fresh eppendorf tube.

2.16 Cell fractionation

Two litres of BHI were inoculated to OD_{600} 0.01 and incubated at 37 $^{\circ}$C, 250 rpm, until cells had reached mid-exponential phase (OD_{600} ~ 0.8). Cells were harvested by centrifugation at 8000 rpm, 10 min, 4 $^{\circ}$C, and the pellet was washed three times by resuspension in dH2O and 85 centrifugation. Cells were then resuspended in 5 ml TBS (Chapter 2.3.12) and transferred to pre-chilled FastPrep tubes containing lysing matrix B (MP Biomedicals). Cells were broken using the FastPrep instrument (MP Biomedicals) set at speed 6 for 40 s for 10 runs, with cooling on ice between runs. The FastPrep beads were allowed to settle before samples were recovered from the tubes and combined in a 50 ml Falcon tube. Beads were washed 3 times with TBS by vigorous shaking, allowing the beads to settle and recovery of the supernatant. Unbroken cells and any remaining beads were removed by centrifugation at 2000 rpm for 5 min. The supernatant was then centrifuged twice at 18000 rpm for 10 min, and the pellets collected represented the cell wall fraction plus any remaining unbroken cells. The supernatant was transferred to ultracentrifuge tubes (Beckman) and cell membranes were harvested by ultracentrifugation at 50000 rpm, 2 h, 4 $^{\circ}$C. The remaining supernatant represented the cytoplasmic fraction. The membrane pellet was washed once by resuspension in TBSI and ultracentrifugation as above. The fractions were resuspended in TBSI and stored at − 20 $^{\circ}$C.

3 Chapter 3 Identification of interactions between MreC, MreD, and other *S. aureus* proteins

3.1 Introduction

Most proteins do not exist as separate entities within a cell but instead form dynamic complexes composed of many components that work cooperatively in a wide range of biological processes, for example the cell division machinery.

A number of *in vitro* techniques have been used to detect protein-protein interactions between cell division components (Rao *et al.* 2014). Affinity chromatography is extensively employed for investigation of interacting partners from *in vitro* mixtures, or potential discovery of novel components from *in vivo* samples using matrix-bound ligands that capture specific bait proteins engineered with an appropriate tag (Urh *et al.* 2009). Following removal of non-specifically bound proteins, interacting proteins are retained on the matrix via specific interactions with the bait protein, and can be eluted from the matrix using competitive molecules such as imidazole or glutathione, and analysed by immunoblotting or mass spectrometry (Urh *et al.* 2009) (Fig. 3.1A).

The widely used tags range from short peptide sequence, including FLAG (A small hydrophilic peptide of eight amino acids), hemagglutinin, myc (derived from the c-myc gene product) and hexa-histidine (his) through to small proteins including green fluorescent protein (GFP), calmodulin-binding protein and glutathione S-transferase (GST). (Chepelev *et al.* 2008). In *E. coli*, his-tagged *E. coli* PBP3 interacts with PBP1B (de Leeuw *et al.* 1999; Bertsche *et al.* 2006). In *C. crescentus*, his-tagged MreC was used as bait to reveal interactions with PBPs in heterogeneous complexes (PBP2, PBP1a, and PBP1b) (Divakaruni *et al.* 2005). GST tags have been used to show that *Helicobacter pylori* MreC co-purifies with PBP2 by glutathione purification (El Ghachi *et al.* 2011). Both his- and GST- tags were combined to show an interaction between FtsW, FtsZ and PBP3 in *Mycobacterium tuberculosis* (Datta *et al.* 2006), and also DivIB and FtsL/DivIC form artificial complex in *S. pneumoniae* (Noirclerc-Savoye *et al.* 2005). A FLAG fusion has also been employed to reveal *E. coli* FLAG-FtsE and FtsZ interaction (Corbin *et al.* 2007). Buddelmeijer and Beckwith (2004) also discovered and FtsL, Myc-tagged FtsQ and FLAG- tagged FtsB interaction. Furthermore, *in vivo* interactions between *E. coli* ParC, ParE and FLAG-tagged FtsK were demonstrated using anti-FLAG antibodies and immunoprecipitation (Espeli *et al.* 2003).

The main limitation of affinity chromatography is that it requires high affinity binding through the washing steps and is therefore unable to identify transient protein interactions.
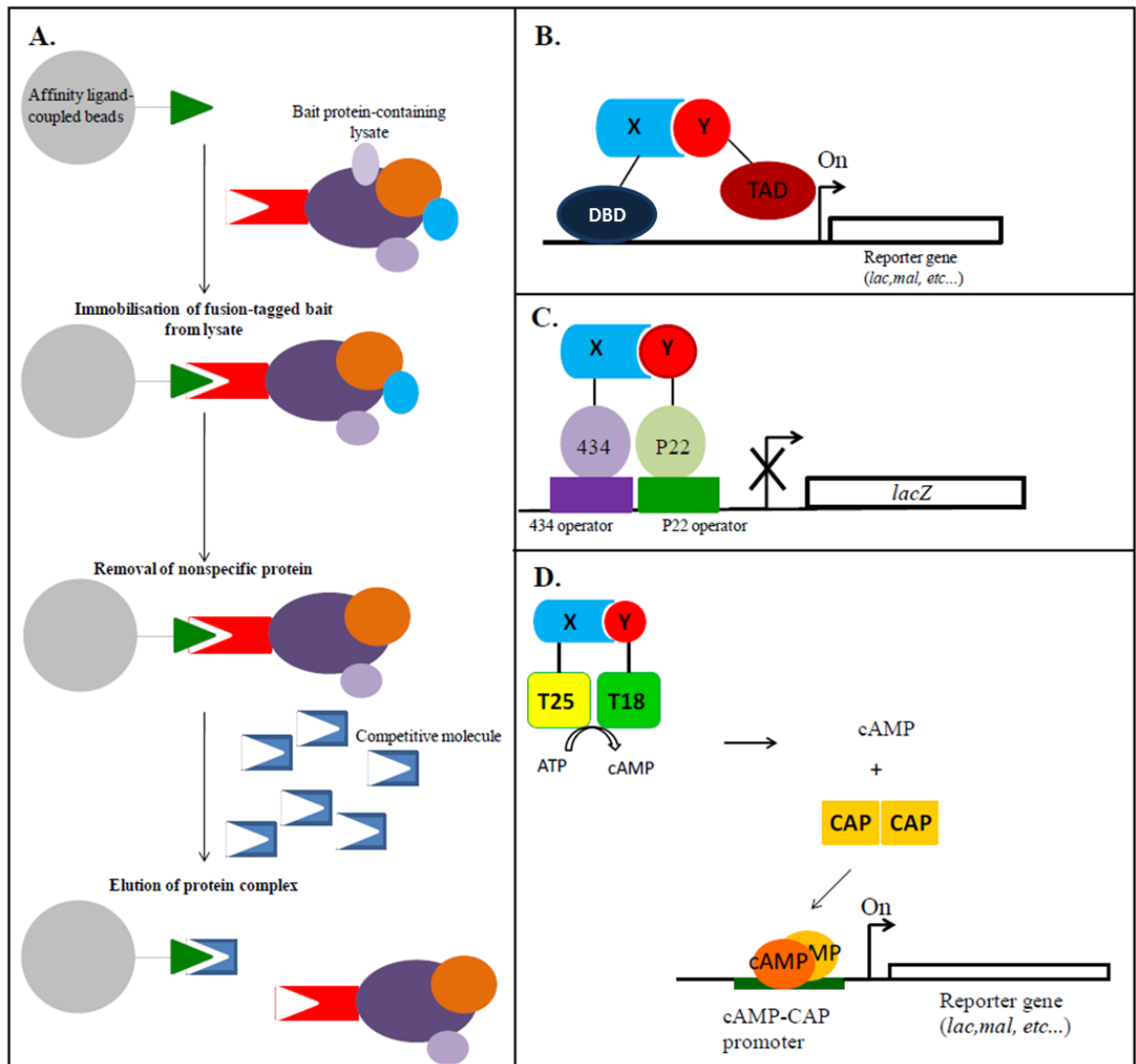
Figure 3-1 Schematics of methods for detection of protein-protein interactions

DiaGrammatic representation of in *vitro* and in *vivo* methods used in the detection of protein-protein interactions.

A.   Affinity purification of a fusion-tagged bait protein and associated proteins using ligand coupled beads.

B.   Yeast two-hybrid system. DBD, DNA binding domain; TAD, transcriptional activation domain.

C.   Bacterial two-hybrid transcriptional repressor system.

D.   Bacterial adenylate cyclase two-hybrid system (BACTH). CAP, Catabolite activator protein.

In panels B, C and D, X and Y represent the 'bait' and 'prey' proteins, respectively. Adapted from Bottomley (2012).

An approach developed to overcome this is to 'fix' the protein interactions with DSP (dithiobis[succinimidyl propionate]) and its water soluble counterpart DTSSP (3,3'–dithiobis[sulfosuccinimidyl propionate]) which form stable bonds between primary amines. Introduction of a reducible disulphate bond allows for the reversal of crosslinking and thus the detection of weak and transient protein interactions. This technique has shown *E. coli* PBP3 and FtsN interaction (Muller *et al.* 2007), and *B. subtilis* FtsZ interaction with both his-tagged and thioredoxin fused EzrA (Chung *et al.* 2004; Haeusser *et al.* 2007) .

Potential protein-protein interactions detected by affinity purification have been combined with other *in vitro* techniques for verification. Surface Plasmon Resonance (SPR) was used to confirm the interactions of FtsN and PBP1B in *E. coli* using immobilised his-FtsN (Muller *et al.* 2007). Also PBP3 and PBP1B using immobilised his-PBP3 in *E. coli* (Bertsche *et al.* 2006). Gel filtration, using size exclusion column has been employed to show EzrA and FtsA interaction and identified SepF as an FtsZ-interacting protein in *B. subtilis* (Singh *et al.* 2007, 2008). Förster resonance energy transfer (FRET) demonstrated homodimerisation of PBP3 and formation of an FtsW-PBP3 complex in *E. coli* (Fraipont *et al.* 2011). Sedimentation assays combined with 90°-angle light scattering analysis have identified ZapC as an FtsZ-interacting protein in *E. coli* (Hale *et al.* 2011). Interactions between MinC, MinD and FtsZ have been verified by sedimentation assays, SPR using biotinylated fusion proteins, gel filtration and FRET (Hu *et al.* 1999; Szeto *et al.* 2001; Okuno *et al.* 2009; Shen & Lutkenhaus 2010). X-ray crystallography and immune-based enzyme assays affirmed ZipA and FtsZ interaction (Mosyak *et al.* 2000; Haney *et al.* 2001). Sucrose gradient ultracentrifugation has shown direct interaction between *E. coli* ZapA and ZapB, and the formation of a complex with FtsZ (Galli & Gerdes 2010). Immunoblotting, where the spotted protein is visualised probing either directly with antibody or with antibodies against the fusion tag of a fused protein on a nitrocellulose memebrane, verified *E. coli* ParC and FtsK interaction (Espeli *et al.* 2003). *M.tuberculosis* FtsZ and FtsW interaction was confirmed using SDS-PAGE separated cell extracts expressing his-tagged FtsW probed with biotinylated FtsZ and streptavidin-alkaline phosphatase (Datta *et al.* 2002). Non-denaturing PAGE and Western blotting detected formation of FtsL and DivIC complex in *B. subtilis* (Sievers & Errington 2000). Mass spectrometry was used to confirm interactions of EzrA, FtsZ, ZapA, FtsA and the novel protein YlmF (SepF) detected by affinity chromatography in *B. subtilis* (Ishikawa *et al.* 2006).

In vivo techniques have allowed the large scale detection of interactions between cell division proteins. Co-immunoprecipitation detected *E. coli* PBP3 and FtsN interaction by *in vivo* crosslinking using DTSSP and co-immunoprecipitation using anti-PBP1B or anti-FtsN

antibodies (Muller *et al.* 2007). The premature targeting technique, based on the ability of ZapA to bind to FtsZ early within the division process and allowing the study of linear protein recruitment, showed recruitment of FtsQ and downstream proteins to the midcell is independent of FtsA (Goehring *et al.* 2005). Strong interactions between *B. subtilis* DivIC and FtsL, and DivIB and PBP2B were demonstrated using *E. coli* artificial septal targeting system, suggesting the interactions were independent of other *B. subtilis* division proteins (Robichon *et al.* 2008).

The advantages of fluorescence labelling have also been used for investigation of protein-protein interactions both *in vitro* and *in vivo*. Immunolocalisation and GFP fusion proteins detected the linearity of protein dependency of FtsZ-(FtsA ZipA)-[FtsE FtsX]-FtsK-FtsQ-[FtsL FtsB]-FtsW-FtsI-FtsN in *E. coli*, in which FtsA and ZipA localisation are independent of each other, whilst FtsE and FtsX, and FtsL and FtsB recruitment are co-dependent (Addinall *et al.* 1996; Addinall & Lutkenhaus 1996a; Addinall *et al.* 1997; Khattar *et al.* 1997; Wang *et al.* 1998; Ghigo *et al.* 1999; Hale & de Boer 1999; Weiss *et al.* 1999; Chen & Beckwith 2001; Mercer & Weiss 2002; Schmidt *et al.* 2004). Thus, FtsZ localisation is independent of other proteins, whereas FtsN depends on all other proteins for midcell recruitment. In *B. subtilis,* depletion or mutation of any one of the division components prevents all others from recruiting to the septum, with the exception of FtsZ (Daniel *et al.* 1998; Daniel & Errington 2000; Katis *et al.* 2000; Feucht *et al.* 2001). This interdependency implies that specific protein-protein interactions are essential to the stabilisation and function of the division machinery.

In 1989, Fields and Song introduced the yeast two-hybrid system (Y2H), which is a sensitive low-tech and scalable technique (Fields & Song 1989). It is based on the fact that yeast transcription factors Gal4 and Gcn4 comprise two functionally distinct domains; A DNA binding (DBD) and a acidic transcription activation domains (TAD) (Hope & Struhl 1986; Keegan *et al.* 1986). Fusion of these domains to proteins of interest (POI) could reconstitute a functional transcriptional activator only if the POI was able to bind to each other. Interactions can be detected by transcriptional activation of an adjacent reporter gene such as *lacZ* (Fig. 3.1B), and many interactions between cell division proteins from different organisms have been detected using Y2H (Sievers & Errington 2000; Espeli *et al.* 2003; Bertsche *et al.* 2006; Hamoen *et al.* 2006; Ishikawa *et al.* 2006; Hale *et al.* 2011). Y2H confirmed that MreC interacts with PBPs in *E. coli* and *H. pylori* (Kruse *et al.* 2005; El Ghachi *et al.* 2011). However, the Y2H system cannot detect interactions involving more than two proteins. The yeast tri-hybrid assay, in which an unfused protein is introduced as a linker between the Y2H separated transcription domains, was developed by Young (1998) and this

method was utilised to confirm *B. subtilis* DivIB, DivIC and FtsL interaction (Young 1998; Daniel *et al.* 2006). The main drawback of Y2H system is that the interactions detected are restrained to the nucleus making it unsuitable for the investigation of large proteins, membrane bound proteins or those requiring post-translational modifications. False positive interactions could also be resulted from non-specific binding of the separated domains (Deane *et al.* 2002).

Nearly a decade later, the bacteria two-hybrid system based on the reconstitution of adenylate cyclase activity in *E. coli* (BATCH) was developed to overcome some of the limitations seen within Y2H (Karimova *et al.* 1998). The catalytic domain of the *Bordetella pertussis* adenylate cyclase consists of two sub-domains: a 25 kDa fragment (T25) that contains the catalytic site and an 18 kDa fragment (T18) that contains the main calmodulin binding site (Ladant 1988). POI can be fused to these two sub-domains respectively, and thus if the proteins interact, the hybrid protein brings the two sub-domains together. In the presence of calmodulin, the catalytic activities will then be restored resulting synthesis of cyclic adenosine 3', 5'-monophosphate (cAMP) from ATP within the cytosol. cAMP in turn can bind the transcriptional activator catabolite activator protein (CAP) and form a cAMP/CAP complex, which is a promiscuous regulator and drives the expression of a large number of genes including those involved in the catabolism of lactose and maltose (Fig. 3.1D). By using lactose or maltose as the unique carbon source, interactions can be easily distinguished under certain selective conditions in *E. coli*. The BACTH system has been effectively utilised for the study of division proteins and it has been used to establish division networks in a number of organisms (Mazouni *et al.* 2004; Karimova *et al.* 2005; Daniel *et al.* 2006; Datta *et al.* 2006; Muller *et al.* 2007; Claessen *et al.* 2008; Ebersbach *et al.* 2008; Patrick & Kearns 2008; Marbouty *et al.* 2009; Galli & Gerdes 2010; Fraipont *et al.* 2011; Steele *et al.* 2011).

Investigation of division networks in a range of phylogenetically distant microorganisms displayed a conservation of a core complex of proteins involved in the division process, implying that assembly of the divisome may be conserved across species. Indeed, cross-interactions has been discovered between division proteins from *E. coli* and *S. pneumoniae*, indicating their importance for the division process (Maggi *et al.* 2008). The BACTH system is a simple and rapid technique which may help the detection of membrane protein interactions and therefore understanding the establishment of cell division networks in different species.

Other bacteria two-hybrid (B2H) systems are also available based on transcriptional activation. For example, in 2001, Di Lallo and co-workers introduced a technique based on the dimerisation of bacteriophage λ repressor protein, in which phage P22 and phage 434

operators together forms a chimeric repressor that can be recognised and bound by a hybrid P22 and 434 repressors (Fig. 3.1C). Interaction of POI fused to each phage repressor leads to formation of hybrid repressor which can then bind to the hybrid operator and blocks the transcription of downstream reporter genes, such as *lacZ* (Di Lallo *et al.* 2001). This method has been used to reveal large networks of interactions for division proteins in *E. coli* and *S.pneumoniae* (Di Lallo *et al.* 2003; Fadda *et al.* 2007; Maggi *et al.* 2008).

3.2 Aims of this chapter

- Bioinformatic identification of putative *S. aureus* cell division genes.
- Analysis of protein-protein interactions between MreC, MreD and other putative cell division components of *S. aureus.*
- Analysis of protein-protein interactions between MreC, MreD and two essential proteins involved in lipid metabolism (PlsY and CdsA) in *S. aureus.*

3.3 Results

3.3.1 Genes selected for investigation

Cell division genes highly conserved between *B. subtilis* and *S. aureus* are shown in Table 3.1. Homologues of *B. subtilis* division components proved to be important for growth in *S. aureus*, for example FtsZ and EzrA (Beall & Lutkenhaus 1991; Pinho & Errington 2003; Steele *et al.* 2011), suggesting certain conservation of the physiological roles of these divisome components. Some division genes in *B. subtilis* have been reported not to be essential in *S. aureus*, such as *divIVA* (Pinho & Errington 2004), or not conserved, such as *minCD*. This alludes to many similarities between the division proteins in both species, but also differences perhaps explained by the shape and modes of cell wall synthesis in two organisms. Other essential genes important in major cellular process are also shown in Table 3.1 as there is potential that these components may interact with cell division proteins.

To determine direct protein-protein interactions between putative growth and division components, 22 *S. aureus* proteins were chosen in respect to their homology to cell division proteins of *B. subtilis*. Proteins selected covered all aspects of the growth and division process, from DNA segregation and correct septum placement, through to late division proteins involved in septum biosynthesis and synthesis of major macromolecules (Table 3.1). Homologues of proteins involved in *B. subtilis* elongation were also included, since *S. aureus* does not undergo cell elongation and these proteins may play an alternative role in division of cocci.

B. subtilis gene	Essentiality in *B. subtilis* (E: Essential, N: Not essential)	*S. aureus* homologue (strain NCTC 8325)	Essentiality in *S. aureus* (E: Essential, N: Not essential)	Gene product Identity/ Similarity (%)	*S. aureus* gene product size (kDa)
Chromosome segregation					
parC	E (Huang *et al.* 1998)	SAOUHSC_01352	N (Bottomley *et al.* 2014)	59/76	90.9
parE	E (Huang *et al.* 1998)	SAOUHSC_01351	E (Chaudhuri *et al.* 2009)	71/85	74.4
Septum placement					
noc	N (Wu & Errington 2004)	SAOUHSC_03049	E (Chaudhuri *et al.* 2009)	48/65	32.2
Z-ring formation					
ftsZ	E (Beall & Lutkenhaus 1991)	*ftsZ*	E (Pinho & Errington 2003)	63/76	41.0
ftsA	E* (Beall & Lutkenhaus 1992)	*ftsA*	E (Chaudhuri *et al.* 2009)	32/55	52.9
zapA	N (Gueiros-Filho & Losick 2002)	SAOUHSC_01096	N (Chaudhuri *et al.* 2009)	49/68	9.6
ezrA	N (Levin *et al.* 1999)	SAOUHSC_01827	E (Steele *et al.* 2011)	22/51	66.2
sepF	E (Hamoen *et al.* 2006)	SAOUHSC_01154	E (Chaudhuri *et al.* 2009)	70/86	21.0
Late division proteins					
ftsL	E (Daniel *et al.* 1998)	SAOUHSC_01144	E (Chaudhuri *et al.* 2009)	23/42	15.3
divIC	E (Levin & Losick 1994)	SAOUHSC_00482	E (Chaudhuri *et al.* 2009)	23/41	15.3
divIB	E** (Beall & Lutkenhaus 1989)	SAOUHSC_01148	E (Bottomley *et al.* 2014)	28/52	50.2
ftsW	E (Kobayashi *et al.* 2003)	SAOUHSC_01063	E (Chaudhuri *et al.* 2009)	28/45	44.8
gpsB	N (Claessen *et al.* 2008)	SAOUHSC_01462	E (Chaudhuri *et al.* 2009)	63/81	13.1
Penicillin bind proteins					
ponA	N (Murray *et al.* 1998)	*pbpB*	E (Pinho *et al.* 2001)	37/56	80.4
pbpB	E (Daniel *et al.* 1996)	*pbpA*	E (Chaudhuri *et al.* 2009)	40/60	82.7
pbpA	N (Murray *et al.* 1997)	*pbpC*	N (Pinho *et al.* 2000)	44/63	77.2
Teichoic acid synthesis					
ltaS	N (Kobayashi *et al.* 2003)	*ltaS*	E (Grundling & Schneewind 2007a)	57/73	74.4
Elongation					
rodA	E (Henriques *et al.* 1998)	SAOUHSC_02319	N (Chaudhuri *et al.* 2009)	31/51	44.6
mreC	E (Leaver & Errington 2005)	SAOUHSC_01759	N (Chaudhuri *et al.* 2009)	36/58	31.0

B. subtilis gene	Essentiality in *B. subtilis* (E: Essential, N: Not essential)	*S. aureus* homologue (strain NCTC 8325)	Essentiality in *S. aureus* (E: Essential, N: Not essential)	Gene product Identity/ Similarity (%)	*S. aureus* gene product size (kDa)
mreD	E (Leaver & Errington 2005)	SAOUHSC_01758	N (Chaudhuri *et al.* 2009)	29/54	20.8
Lipid membrane synthesis					
plsY	E (Hunt *et al.* 2006)	SAOUHSC_01350	E (Chaudhuri *et al.* 2009)	46/66	22.2
cdsA	E (Kobayashi *et al.* 2003)	SAOUHSC_01238	E (Chaudhuri *et al.* 2009)	47/63	28.9
Unknown function					
ypsA	unknown	SAOUHSC_01463	unknown	43/61	22.1

Table 3.1 Conservation of cell growth and division genes between *B. subtilis* and *S. aureus*

The gene product identity/similarity and *S. aureus* gene product size were analysised using https://blast.ncbi.nlm.nih.gov/Blast.cgi

* *B. subtilis* mutants in *ftsA* are viable but show severe defects in division and growth, and therefore the gene is classed as essential.

** *B. subtilis divIB* is essential only at elevated temperatures.

3.3.2 Construction of BACTH plasmids

3.3.2.1 C-terminal fusions

To investigate interactions between proteins these were tested systematically for pairwise interactions using the bacterial two-hybrid system (BACTH). Genes of interest were amplified by PCR and cloned into pKT25 or pUT18C to create in-frame protein fusions to the C-terminus of either T25 or T18, in collaboration with Jagath Kasturiarachchi and Martin Larke (University of Sheffield) (Fig. 3.2). Ligation products were used to transform electrocompetent *E. coli* TOP10 with selection on TSB kan 50 μg ml^{-1} or amp 100 μg ml^{-1}. Construction of PBP1, ParE and PBP3 fused to the C-terminus of T18 was not successful, although fusion to T25 was achieved. It is likely that overproduction of these genes from the high copy-number plasmid pUT18C is toxic to *E. coli*. Positive clones were identified by colony PCR using the same primers used to amplify the genes of interest (Chapter 2.8.1, data not shown), and by plasmid extraction, restriction digestion with *EcoR*I and *Hind*III, and electrophoresis on a 1% (w/v) agarose gel. Plasmids were sequenced by the University of Sheffield Core Genomics Facility to check for the introduction of errors during PCR (data

not shown). Three constructs were found to contain amino acid substitutions; T18-DivIC contained leucine to serine substitution at position 116, an I127T substitution had occurred in T18-PlsY, and T18-SepF had an asparagine to tyrosine substitution at position 92. These fusion proteins may be non-functional, resulting in false negative interactions. However, T25 fusions for these proteins showed 100% identity to the predicted amino acid sequences and so results for interactions with both fusions are presented here.
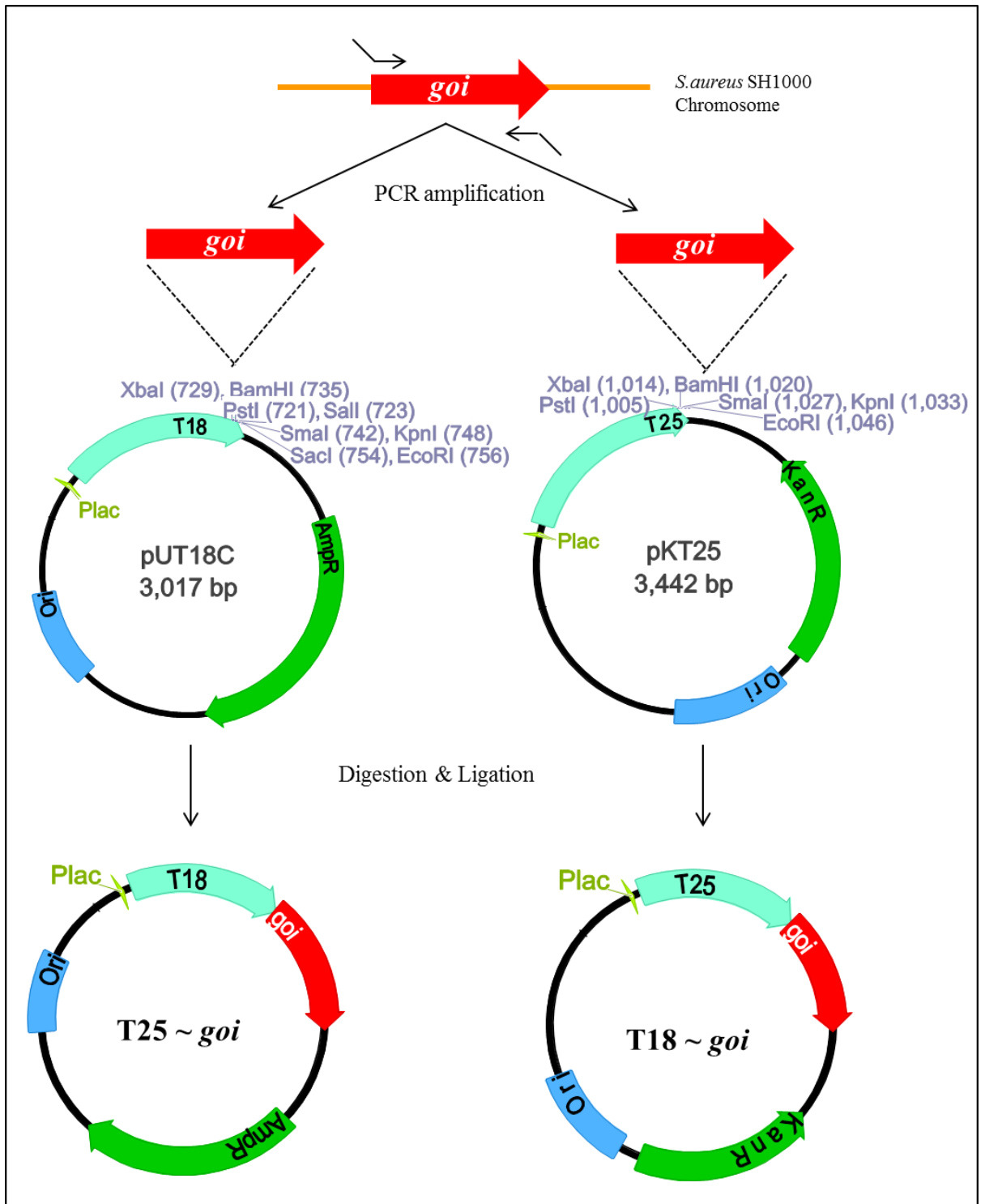
FFigure 3-2 Construction of BACTH plasmids carrying C-terminal fusions

DiaGrammatic representation of gene fusions of the encoding regions for the C-terminus of T18 and T25 fragments to the N-terminus of genes of interest (*goi*). This work was carried out in collaboration with Jagath Kasturiarachchi (University of Sheffield).

3.3.2.2 N-terminal fusions

Fusion of *S. aureus* FtsZ and EzrA to the C-terminus of T18 or T25 did not show self-interactions or interactions with any other protein fusion used in this study (results not shown). A fusion of *E. coli* FtsZ to the N-terminus of T25 showed a positive interaction with T18-FtsA (Karimova *et al.* 2005; Shiomi & Margolin 2007) and an *M.tuberculosis* FtsZ-T25 fusion showed interaction of FtsZ with FtsW (Datta *et al.* 2006). Thus, fusion of T18 or T25 to the C-terminus of FtsZ may result in misfolding of the protein, or block potential interaction sites. *S. aureus* EzrA is predicted to have a single N-terminal transmembrane helix with a N_{out}-C_{in} topology in the cell membrane. N-terminal fusions of T18 and T25 to EzrA are therefore necessary to position the adenylate cyclase fragments in the cytosol. Plasmids carrying N-terminal fusions of T25 and T18 to *S. aureus* FtsZ and EzrA were constructed by Victoria Fairclough (University of Sheffield) (Fig. 3.3). *ftsZ* and *ezrA* were amplified by PCR and cloned into pKNT25 (Claessen *et al.* 2008) or pUT18 and sequenced (University of Sheffield Core Genomics Facility). The translated plasmid sequences showed 100% identity to predicted amino acid sequences (data not shown).

Construction of plasmids carrying N-terminal fusions of T25 and T18 to *S. aureus* *mreC* or *mreD* were attempted using pKNT25 and pUT18, respectively (Fig. 3.3). The experiment was attempted three times by digestion of *Pst*I and then *Kpn*I, *Kpn*I and then *Pst*I, or double digestion. Unfortunately, no positive clones were identified from *E. coli* Top 10 transformants. Fusions of *S. aureus* MreC and MreD to the C-terminus of T18 and T25 were constructed by Jagath Kasturiarachchi, and the resulting plasmids showed 100% identity to predicted amino acid sequences by DNA sequencing (University of Sheffield Core Genomics Facility, data not shown) and were used for this study.
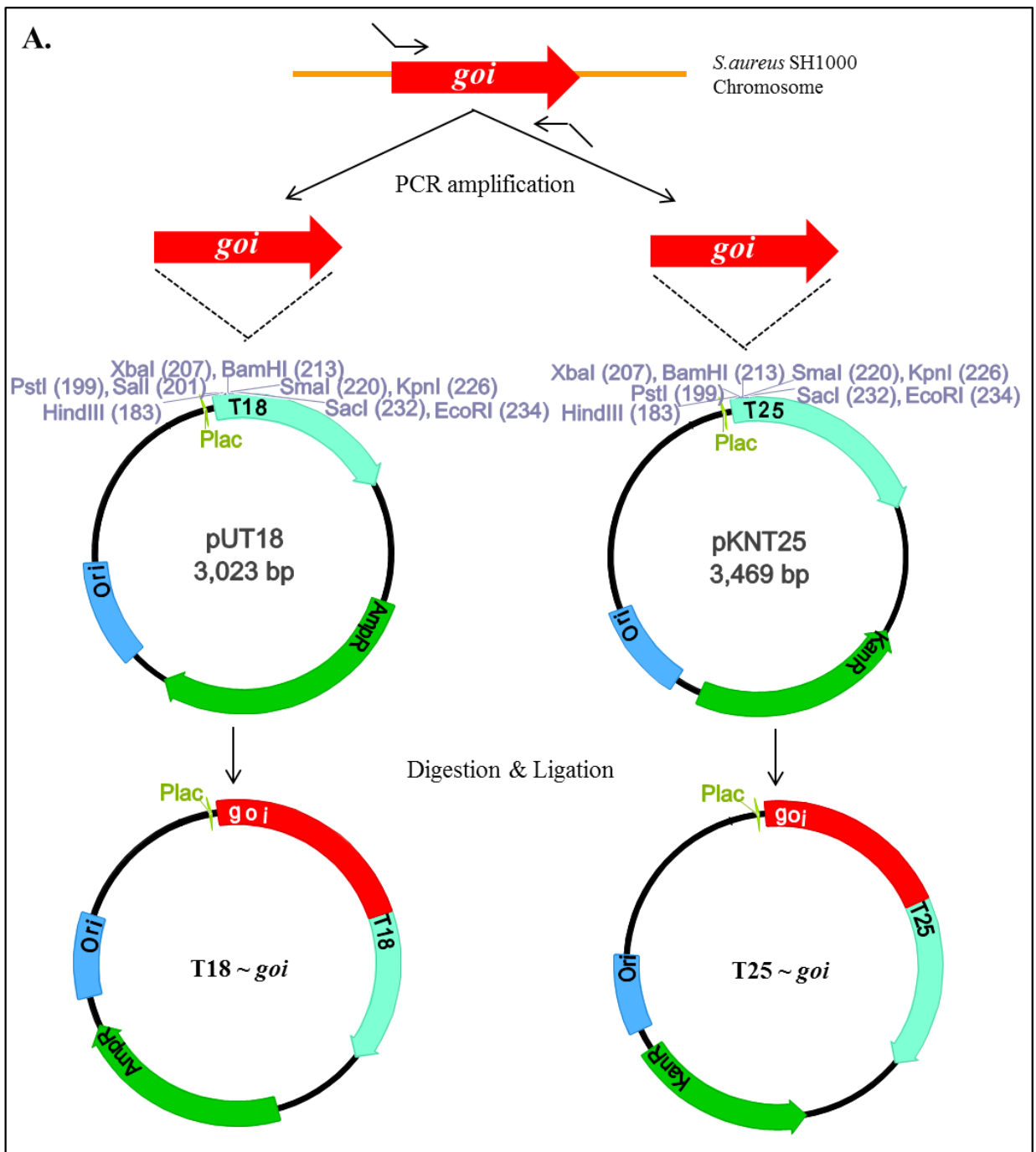
Figure 3-3 Construction of BACTH plasmids carrying N-terminal fusions

DiaGrammatic representation of gene fusions of the encoding regions for the N-terminus of T18 and T25 fragments to the C-terminus of *genes of interest* (*goi*).

3.4 Transformation of BACTH plasmids into *E. coli* BTH101

Two common reporter strains were evaluated, *E. coli* DHM1 and BTH101. DHM1 showed slower growth and weaker interaction signals than BTH101 or even no signal was detected using DHM1, when BTH101 gave a positive signal (data not shown). This concurs with a previous report (Battesti & Bouveret 2012). Therefore, BTH101 was chosen as the reporter strain for this study. BTH101 is a non-reverting adenylate cyclase deficient reporter strain with high complementation efficiency. The frequency of spontaneous Lac$^+$ revertants due to cAMP/CAP independent promoter mutations is 10^{-8}, making BTH101 a suitable strain for detection of protein-protein interactions due to reconstitution of adenylate cyclase (Karimova *et al.* 1998). *E. coli* BTH101 was transformed with *mreC* or *mreD* constructed T18- or T25-fusions and made electrocompetent. Plasmids carrying fusions of T25 or T18 to a number of *S. aureus* cell division and other proteins (as seen in Fig.3.5) were then transformed into the electrocompetent BTH101 containing one of the T18- or T25- constructed plasmids. Transformation of pGL566 (pUT18C-ParC) into BTH101 was not successful despite repeated attempts, probably due to the high level of fusion protein being toxic for *E. coli*.

3.4.1 Optimisation of detection conditions for BACTH assay

To test for the best detection conditions, the same cell cultures were spotted on two buffered LB plates containing 100 μg ml^{-1} amp, 50 μg ml^{-1} kan and 200 μg ml^{-1} X-gal (Chapter 2.13.1). The two plates were incubated simultaneously at 37°C for 12 hrs followed by ~3 days at RT, or 30°C (Steele *et al.* 2011) up to 72 hrs. Interestingly, colonies of experimental clones turned blue before the negative control (~72hrs) at 30°C, whereas, the positive clones that were incubated at 37°C prior to the RT incubation showed interactions after 48 hrs compared to the negative control (-ve; pUT18~pKT25) (Fig. 3.4).

Two different pH (7.5 and 8), in combination with two different solvents for X-gal, DMF and DMSO, were compared to detect the best discrimination between positive and negative interactions when samples were spotted on solid media. It was found that the combination of pH7.5 and DMF delivered the best contrast (Fig. 3.5). To maintain the fixed pH at 7.5, LB broth and agar were buffered with phosphates (Chapter 2.1.1.3).
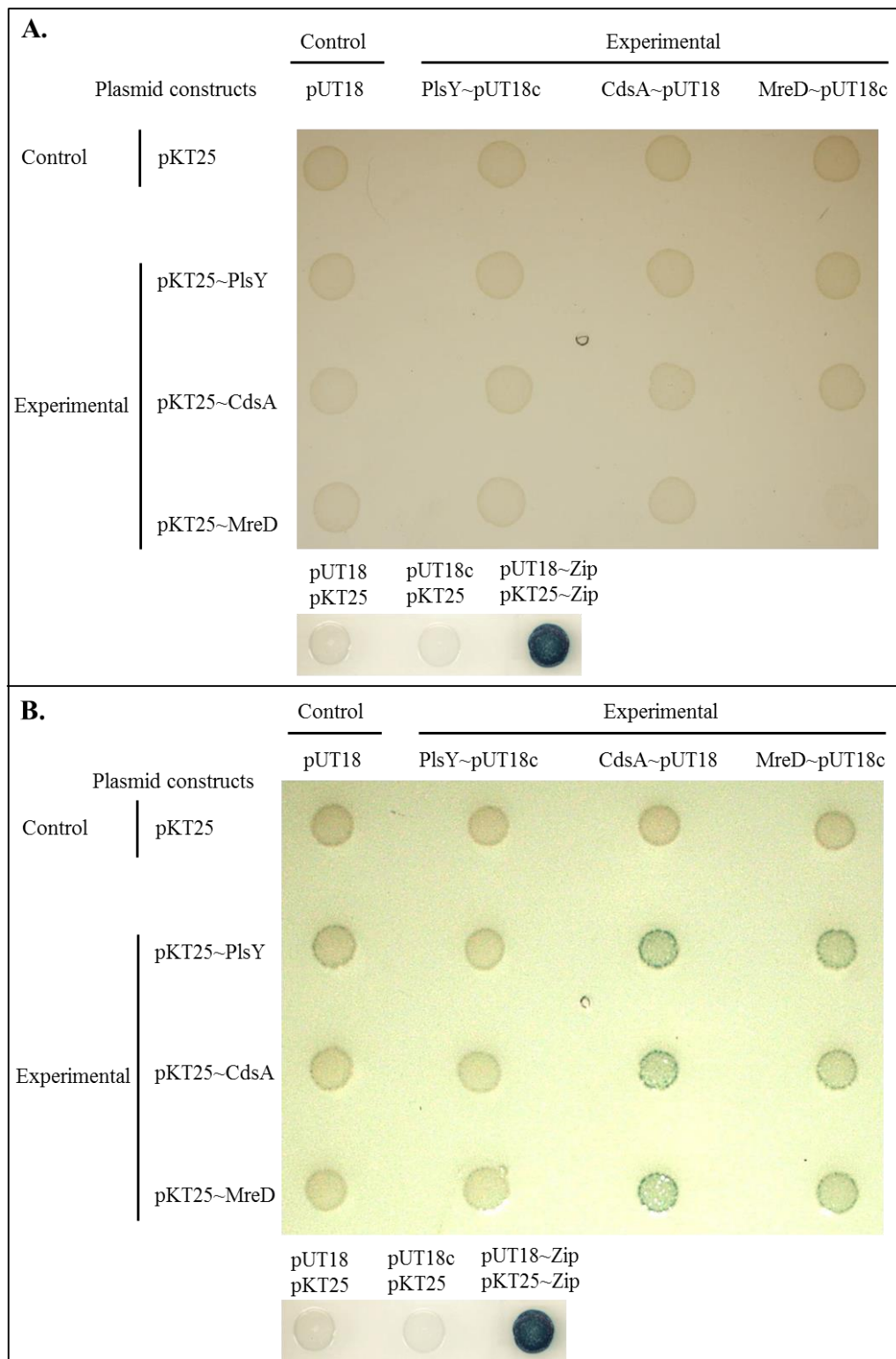
Figure 3-4 BATCH analysis of *S. aureus* division components on solid medium

Interactions of MreD, CdsA and PlsY –T18 with T25 fusions to the same proteins. 10 μl cell culture at exponential growth phase were spotted onto buffered LB containing amp (100), kan (50) and X-gal (200) at pH7.5, incubated at 30°C for 72hrs (A) or 37°C for 12hrs followed by 3 days at RT (B). The positive control (+ve; T25-zip~T18-zip) is taken from a separate plate, in which negative controls were included.
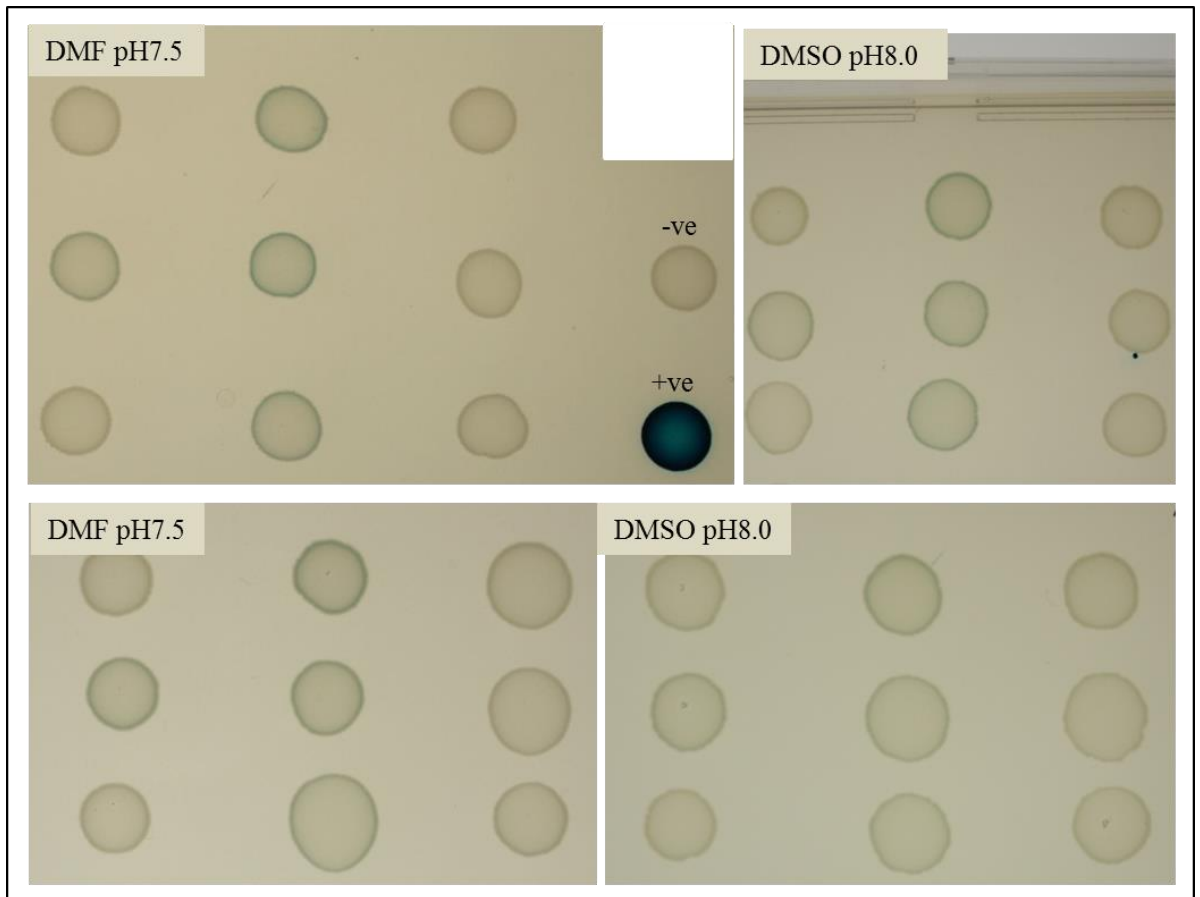
Figure 3-5 Determination of optimum pH level and dissolvent for X-gal for BACTH analysis

T25-PlsY~T18-MreD cultures were used for this testing. 9 colonies were randomly selected from transformation plates and allowed to grow at 30°C for 2 hours. Each culture was plated on buffered LB containing different pH at values, and X-gal was prepared in different solvents, DMF/pH7.5, DMF/pH8, DMSO/pH7.5 and DMSO/pH8. The plates were incubated at 37°C for 12hrs followed by 2-3 overnight at RT simultaneously. BTH101 pKT25~zip pUT18c~Zip (+ve) and BTH101 pKT25 pUT18C (-ve) were only plated on the DMF pH7.5 plate. Cultures spotted at the same position on each plate were from the same inoculant.

3.4.2 Investigating physical interactions of *S. aureus* MreCD with cell division proteins

3.4.2.1 Solid assay

To investigate positive interactions between the POI, co-transformed strains were selectively grown overnight in TSB broth with both ampicillin and kanamycin at 37°C. The cells were then sub-cultured in buffered LB at an OD_{600} 0.01, and incubated with shaking at 250rpm until OD_{600} ~0.5. The cells were harvested and washed three times in buffered LB and resuspended in 5ml buffered LB before 10µl aliquots of 1:1000 diluted cell culture were spotted onto buffered LB containing 200 µg ml^{-1} X-Gal, 100 µg ml^{-1} amp and 50 µg ml^{-1} kan. The plates were allowed to dry and incubated at 37°C for 12 hrs followed by 3 days incubation at RT. The positive control strain carrying plasmids encoding T25 and T18 fused to the leucine zipper domain of GCN4 (pKT25-leucine zip or pUT18c-leucine zip) (Karimova *et al.* 1998) and the negative control strain carrying unfused T18 and T25 fragments (pKT25 or pUT18C) were also spotted onto plates. As a further negative control fusion proteins were also co-transformed with the opposing unfused adenylate cyclase fragment. If either negative control gave a positive result the experiment was discarded.

MreC and MreD were constructed as C-terminal fusion of both T18 and T25 (Jagath Kasturiarachchi, University of Sheffield). Positive interactions of MreC with cell division proteins, EzrA, FtsA, FtsL, FtsW, DivIB, DivIC, PBP1, PBP3, GpsB, RodA and MreC, were observed (Fig. 3.6). MreD also showed an interaction signal with cell division components, EzrA, FtsZ, FtsA, FtsL, FtsW, DivIB, DivIC, PBP2, PBP3, ZapA, GpsB, ParC, MreC and MreD, but at a very low level. However, no interactions were detected between T25-LtaS and the T18 fusions of the same proteins, suggesting that fusion to either T18 or T25 could result in a non-functional, or only partially functional, hybrid protein. Of the proteins that showed interactions, results could be detected with both T18 and T25 fusions (where available) in almost all MreC constructs (FtsA, FtsL, FtsW, DivIC, RodA and GpsB). However, there were some interactions that were detected in one orientation of fusion proteins but not with the reciprocal co-transformation: T18-MreC~T25-CdsA showed a positive signal where T25-MreC~T18-CdsA did not; in contrast, T25-MreD interacts with T18-MreC but no interaction occurs with the T25-MreC~T18-MreD construct; T25-MreC interacts with T18-EzrA but T18-MreC~T25-EzrA is negative. In addition MreD is highly interactive with an EzrA N-terminal fusion of T18 but not C-terminal fusion of T18. Some positive interactions showed strong interaction signals, but weaker in the other orientation, such as T18-MreC~T25-FtsA vs. T18-FtsA~T25-MreC and T18-MreD~T25-DivIC vs. T18-DivIC~T25-MreD. These results show that the MreC and MreD do interact with divisome components and that fusion to T18 and T25 may result in only a partially functional hybrid protein.

3.4.2.2 Liquid assay

To further quantify the observed protein-protein interactions, the efficiencies of functional complementation between fusion proteins in liquid culture was examined by measuring β-galactosidase activity using MUG as a substrate. Strains displaying positive interaction on solid assay together with other fusions of specific genes, including those will be discussed in Chapter 5 were selected and grown to mid-exponential phase (OD_{600} ~0.5) in buffered LB at $37^{\circ}C$ in the presence of IPTG to induce expression of fusion proteins. The fresh cells were used for testing in two attempts. Surprisingly, the β-galactosidase activities of all samples tested were very similar to the negative control, including the positive control. The fresh mid-exponentially growth cells were then frozen at $-80^{\circ}C$ prior to the testing as described in Chapter 2.13.2. Freezing resulted in observed positive activity. This suggests the freezing step to be crucial.

Statistical analysis of the β-galactosidase activity between MreC or MreD and other proteins using one-way ANOVA showed the interaction of MreC with DivIB, PBP1, GpsB, PBP3, MreC, FtsL, LtaS and DnaK to be significantly different from the negative control, (SJF3624 (pUT18c~pKT25)). Statistically, T18-MreD~T25-YpsA was the only one that showed higher signal in liquid assay when compared to the negative controls, (SJF3624 (pUT18c~pKT25) and SJF3697 (pUT18~pKT25)). The intensity of blue colour was visually much stronger for the interaction of T25-MreD to T18 fused proteins; DivIB, DivIC, PBP2, MreC, EzrA and LtaS when compared to T18-MreD~T25-YpsA in the presence of X-Gal on solid medium, however did not show interaction in liquid medium. Those showing less intensity of blue colour could still clearly be discriminated from the negative controls from solid assay (Fig. 3.7 B) were all considered as positive interactions.

All the interactions on both solid and liquid assays are summarised in table 3.2.
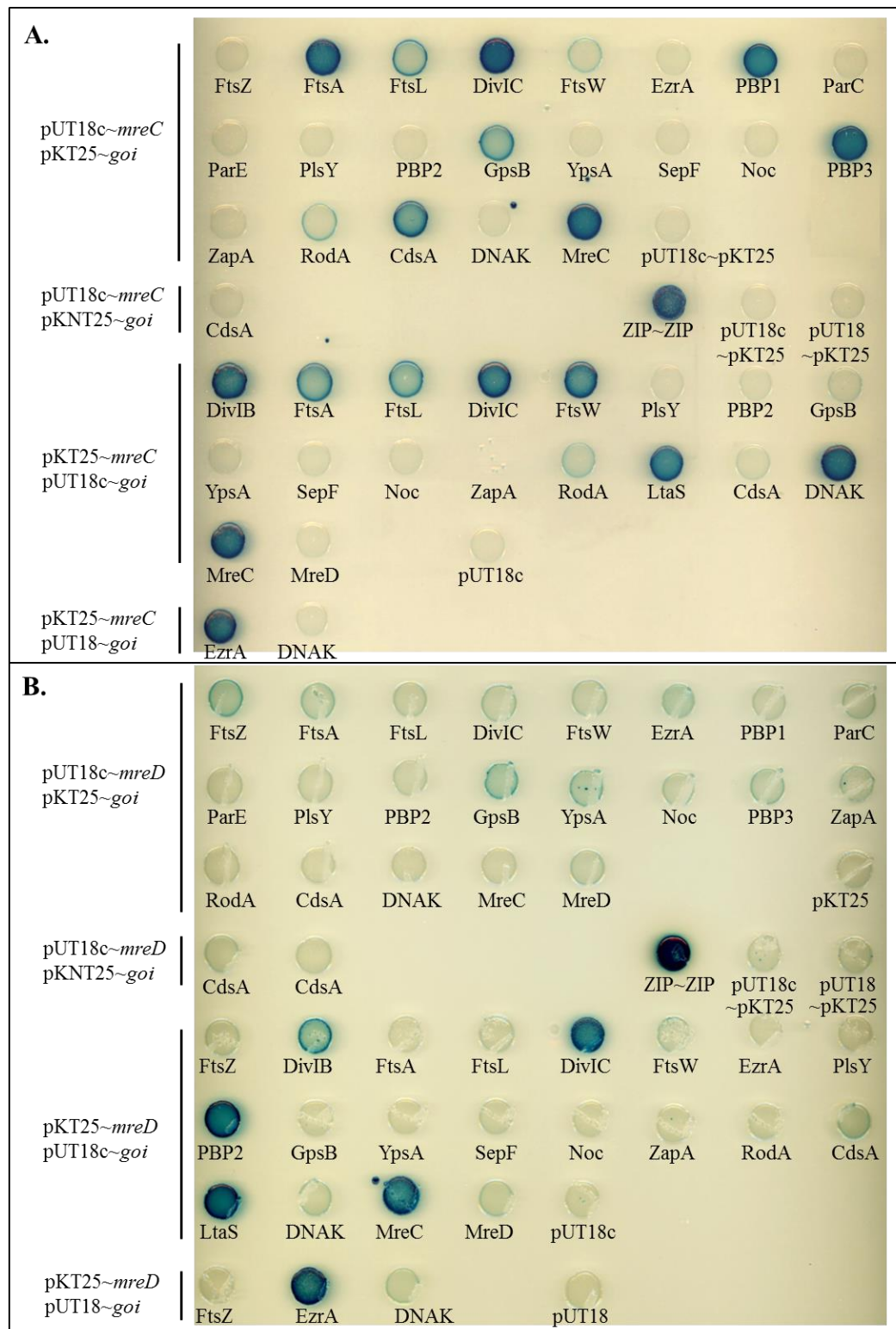
Figure 3-6 BATCH analysis of growth and divisome components on solid medium

Two hybrid clones were plated on buffered LB plates at 37ºC in the dark for 12 hrs. followed by incubation at room temperature for 3 days before photographing.

A. MreC interactions

B. MreD interactions
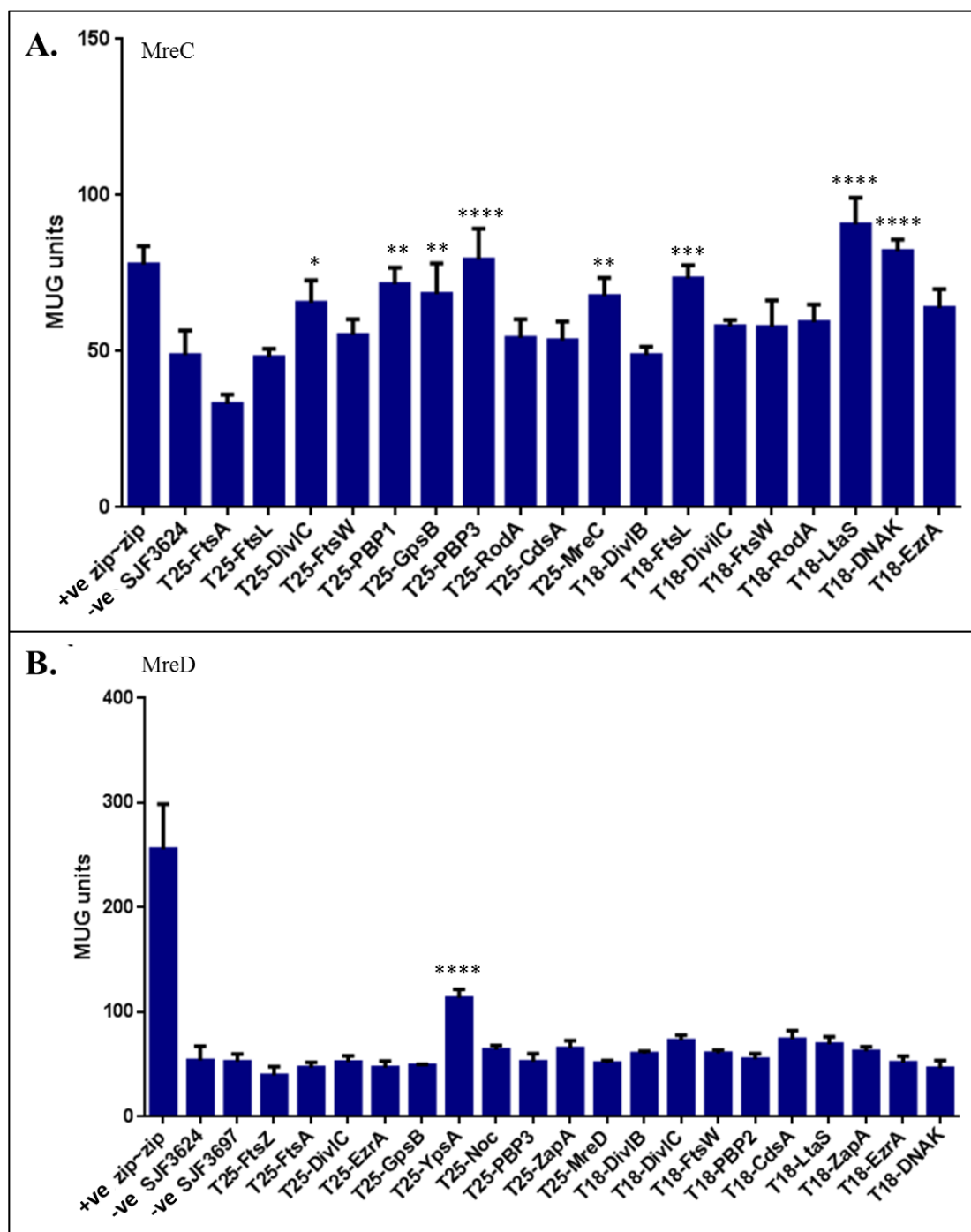
Figure 3-7 β-galactosidase activity of T25 fused POI with T18 proteins

Interactions of the POI fused to T25 were quantified by measuring β-galactosidase activity of *E. coli* BTH101 cells expressing complementary fusions. A. MreC interaction. B. MreD interactions. Activity is displayed as the mean of three independent measurements of β-galactosidase activity for each co-transformant. Error bars represent the standard deviation. Values that are significantly different from the negative control, as determined by one way ANOVA, are indicated by asterisks. * denotes p< 0.05, ** denotes p< 0.001, *** denotes p< 0.005 & **** denotes p< 0.0001.

MreC interactions							MreD interactions					
T18~ goi	T25~ goi	goi~ T18	goi~ T25	Solid Assay	Liquid Assay		T18~ goi	T25~ goi	goi~ T18	goi~ T25	Solid Assay	Liquid Assay
cdsA	mreC			-			cdsA	mreD			+	
divIB	mreC			+++			divIB	mreD			++	
divIC	mreC			+++			divIC	mreD			+++	
dnaK	mreC			+++	++++		dnaK	mreD			-	
ftsA	mreC			++			ezrA	mreD			-	
ftsL	mreC			++	+++		ftsA	mreD			-	
ftsW	mreC			+++			ftsL	mreD			-	
gpsB	mreC			-			ftsW	mreD			-	
ltaS	mreC			+++	++++		ftsZ	mreD			-	
mreC	ftsZ			-			gpsB	mreD			-	
mreC	ezrA			-			ltaS	mreD			+++	
mreC	parC			-			mreC	mreD			+++	
mreC	parE			-			mreD	ftsZ			++	
mreC	plsY			-			mreD	ftsA			++	
mreC	pbp2			-			mreD	ftsL			-	
mreC	ypsA			-			mreD	divIC			+	
mreC	sepF			-			mreD	ftsW			-	
mreC	noc			-			mreD	ezrA			+	
mreC	zapA			-			mreD	pbp1			-	
mreC	dnaK			-			mreD	parC			+	
mreC		cdsA		-			mreD	parE			-	
mreC	ftsW			+			mreD	plsY			+	
mreC	rodA			+			mreD	pfp2				
mreC	ftsL			++			mreD	gpsB			++	
mreC	gpsB			++	++		mreD	ypsA			++	++++
mreC	ftsA			+++			mreD	noc			+	
mreC	divIC			+++	+		mreD	pbp3			+	
mreC	pbp1			+++	++		mreD	zapA			+	
mreC	pbp3			+++	++++		mreD	rodA			-	
mreC	cdsA			+++			mreD	cdsA			+	
mreC	mreC			+++	++		mreD	dnaK			-	
mreC	mreC			+++			mreD	mreD			+	
mreD	mreC			-			mreD			cdsA	+	
noc	mreC			-			mreD	mreD			+	
pbp2	mreC			-			noc	mreD			-	
plsY	mreC			-			pbp2	mreD			+++	
rodA	mreC			+			plsY	mreD			-	
sepF	mreC			-			RodA	mreD			-	
ypsA	mreC			-			SepF	mreD			-	
zapA	mreC			-			ypsA	mreD			-	
	mreC	dnaK		-			zapA	mreD			-	
	mreC	ezrA		+++				mreD	ftsZ		-	
	pKT25	pUT18		-				mreD	ezrA		+++	
pUT18c	pKT25			-				mreD	dnaK		-	

Table 3.2 Summary of all MreC and MreD BATCH constructs

3.4.3 Investigation of physical interactions of *S. aureus* MreCD with phospholipid biosynthesis components

The bacterial cell wall is essential for the temporal and spatial management of cell morphology as discussed in Chapter 1. Surprisingly, wall-less bacteria are capable of dividing by scission after blebbing, tubulation or vesiculation dependent upon an altered rate of membrane biosynthesis (Mercier *et al.* 2014). This implies that the membrane phospholipid layer also plays a critical role in the adaptation to the environment (Yao & Rock 2013). Membrane curvature can act as a cue for localisation of components, including division proteins (Strahl & Hamoen 2012). Both MreC and MreD are transmembrane proteins that interact with many division proteins as described above. Hence the question arises as to whether these two shape determining proteins influence the phospholipid biosynthesis pathway? Here I investigate the positive protein-protein interactions between MreC, MreD and two essential proteins involved in lipid metabolism, PlsY and CdsA, in *S. aureus*.

3.4.4 Solid assay

To investigate interactions between the POI and phospholipid biosynthesis components, PlsY and CdsA were selected for this investigation. Approximately 150 single colonies of co-transformants of each combination were randomly selected and streaked on buffered LB plates containing 200 μg ml^{-1} X-Gal, 100 μg ml^{-1} amp and 50 μg ml^{-1} kan. Positive colonies were grown overnight in TSB broth with both ampicillin and kanamycin at 37°C. The co-transformants were sub-cultured in buffered LB at an OD$_{600}$ 0.01, and incubated with shaking at 250rpm until OD$_{600}$ reached ~0.5. The cells were harvested and washed three times in buffered LB and resuspended in 5ml buffered LB before 10μl aliquots of 1:1000 diluted cell culture were spotted onto buffered LB containing 200 μg ml-1 X-Gal, 100 μg ml^{-1} amp and 50 μg ml^{-1} kan. The plates were allowed to dry and incubated at 37°C for 12 hrs followed by 3 days incubation at RT. The positive control strain carrying plasmids encoding T25 and T18 fused to the leucine zipper domain of GCN4 (pKT25-leucine zip or pUT18c-leucine zip) (Karimova et al. 1998) and the negative control strain carrying unfused T18 and T25 fragments (pKT25 or pUT18) were also spotted. As a further negative control fusion proteins were also co-transformed with the opposing unfused adenylate cyclase fragment. If either negative control gave a positive result the experiment was discarded and repeated.

MreD and PlsY were fused to the C- termini of T18 and T25, whereas, CdsA was fused to the N-terminus of T18 and C-terminus of T25 (Jagath Kasturiarachchi, University of Sheffield). T18-CdsA and T18-MreD positively interacts with the other T25 fused proteins, including themselves, when compared to the negative control on the same plate (Fig. 3.4 B). MreD interacts with CdsA in both orientations. PlsY fused to the C-terminus of T18 maybe

non-functional, as it does not interact with any protein, however, the interaction was detected with the reciprocal co-transformation. All the negative controls co-transformed with fusion proteins and the opposing unfused adenylate cyclase fragment remained negative, implying that the interactions are real. These results suggested that *S. aureus* MreD interacts with phospholipid biosynthesis components PlsY and CdsA, which also interact with each other, in the BATCH system.

MreC was fused to the C-terminus of T18. A strong positive interaction was seen with CdsA C-terminal fusion of T25 (SJF3992 (pKT25-CdsA~pUT18c-MreC)), However, not with CdsA N-terminal fusion of T25 (SJF3988 (pKNT25-CdsA~pUT18c-MreC)) and the reciprocal co-transformation (Fig. 3.6 A). This finding may suggest that MreC is also involved in phospholipid biosynthesis.

Due to time constraints, the interactions detected by solid assay were not further confirmed by liquid assay.

3.5   Discussion

Bacterial two-hybrid analysis of protein-protein interactions has provided a powerful tool in exploring the physiological role of proteins. It has been extensively used in investigation of a wide range of cell processes, including transcriptional regulation (Domain & Levy 2010), molybdenum cofactor biosynthesis (Magalon et al. 2002), cell wall synthesis (White et al. 2010) and virulence factors involved in invasion of eukaryotic cells (Darwin et al. 2001). BACTH has also been useful for the investigation of protein-protein interactions in a wide variety of organisms; such as *Pseudomonas* (Goodman et al. 2009), *Bacillus* (Szurmant et al. 2007), *Streptomyces* (Hudson & Nodwell 2004), *Mycobacteria* (Pearce et al. 2008), human cells (Yamada et al. 2003) and viruses (Dautin et al. 2003).

Within *S. aureus*, a complex interaction map of cell division proteins has been established (Steele et al. 2011). 22 proteins believed to be involved in *S. aureus* cell growth and division were screened and 29 interactions which had been previously identified in *E. coli*, *S. pneumoniae* and *B. subtilis* were detected in *S. aureus* and also several novel interactions leading to the proposal of a core of 16 proteins as members of the division complex. These proteins are involved at each step of the division process, ranging from chromosome segregation and septum placement to peptidoglycan and other macromolecular synthesis (Table 3.1).

Results from this study identified that both MreC and MreD interact with multiple partners, suggesting a presence in the division complex (Fig. 3.8). MreC showed interactions at all stages of the growth and division cycle, from Z-ring formation to late division, and lipid synthesis. Notably, MreC and MreD do not directly interact with chromosomal segregation proteins, ParC & ParE and the septum placement protein, Noc.

3.5.1   MreC and MreD are involved in cell wall synthesis

Many of these interactions detected in *S. aureus* have previously been seen in other organisms with BACTH system as well as other methods. MreC dimerisation was consistently seen in many species, such as *E. coli* (Kruse *et al.* 2005), *B. subtilis* (van den Ent *et al.* 2006), and *S. coelicolor* (Kleinschnitz *et al.* 2011). Interaction of MreC with MreD has been shown by BATCH in *E. coli* (Kruse *et al.* 2005) and *B. subtilis* (van den Ent *et al.* 2006). MreC was found to directly interact with PBPs in *E. coli* and *H. pylori* by Y2H (Kruse *et al.* 2005; El Ghachi *et al.* 2011), in *B. subtilis* and *S. coelicolor* by BACTH (van den Ent *et al.* 2006; Kleinschnitz *et al.* 2011), in *C. crescentus* by affinity chromatography (Divakaruni *et al.* 2005) and BATCH (White *et al.* 2010), and in .*S. pneumoniae* D39 by a mutagenesis study (Land & Winkler 2011). The observation of MreC interaction with both high and low molecular weight PBPs might suggest that MreC is likely to be involved in peptidoglycan synthesis (Holtje 1998; Popham & Young 2003). The interactions of MreC with GpsB and EzrA concurs with previous findings in *B. subtilis* (Claessen *et al.* 2008), which suggested that MreC is involved in the shuttling of PBPs between each division cycle. MreC was also found to interact with other Z-ring associated proteins other than EzrA, including FtsA, FtsL and FtsW. Since MreC has the ability to interact with cytoplasmic proteins as well as those with extracytoplasmic domains, it may provide a link between early and late division processes. It was surprising to detect interactions in *S. aureus* for MreC and the RodA protein, which in *B. subtilis* is elongation specific (Henriques *et al.* 1998; Leaver & Errington 2005). My investigation using BACTH system suggests that the cell shape proteins, MreC and MreD together with RodA form a large network of interactions with each other and enzymes involved in peptidoglycan precursor synthesis (Fig. 3.9).

Like MreC, MreD also interacts with LtaS, suggesting that MreC and MreD might play a role in synthesis of polyglycerol phosphate, which is a cell membrane anchored cell wall component and required for accurate positioning of septa and cell division processes (Grundling & Schneewind 2007a). V. Kent (2013) discovered that MreD interacts with LytR-CpsA-Psr (LCP) proteins which are involved in WTA sythesis via transformation of the cell wall polymer from its lipid-linker precursor to the peptidoglycan (unpublished data). This

result implies that MreCD, LtaS, PBPs and other enzymes involved in cell wall synthesis form a multi-enzyme complex which integrates biosynthetic processes. Interestingly, MreD interacts with FtsZ, however, it still remains unknown whether MreD guides FtsZ to the proper division site or vice versa. Linking these results to previous studies on *S. aureus*, an interaction map between the Mre and cell division proteins can be established (Fig. 3.9).

In *E. coli* and *B. subtilis*, MreC is predicted to have a single transmembrane span N_{in}-C_{out} topology, and the MreD protein is predominantly hydrophobic with four or six transmembrane spans and both termini inside the cytoplasm (Kruse *et al.* 2005; Leaver & Errington 2005). Here, we also propose that the N-terminus of MreC is inside of the cell, since the N-terminal fusion of MreC interacts with cytoplasmic proteins GpsB, probably on the cytosolic face of the membrane via the extreme N-terminus of MreC. We therefore propose that the N-terminus of *S. aureus* MreD is inside the cell and surface-exposed loops of MreD could contact the extracellular cell wall synthetic machinery.

3.5.2   MreC and MreD may influence lipid metabolism

MreC and MreD both interact with essential membrane phospholipid synthesis protein, CdsA. MreD also interacts with another essential protein, PlsY, which in turn interacts with CdsA (Fig. 3.4). PlsY is a transmembrane acyltransferase that catalyses the first acylation step of phosphatidic acid biosynthesis in *B. subtilis* and *S. pneumoniae* (Paoletti *et al.* 2007). CdsA is responsible for conversion of phosphatidic acid to CDP-diacylglycerol in a later step (Dowhan 1997). These results suggest that MreC and MreD are in contact with lipid metabolism pathway proteins and may influence membrane formation.

Both *B. subtilis* and *S. pneumoniae* PlsY are predicted to consist of five membrane-spanning domains with a N_{out}-C_{in} topology (Hunt *et al.* 2006; Lu *et al.* 2007). The *S. aureus* homologue is also predicted to have a similar membrane topology. If this topology prediction is correct for *S. aureus* PlsY, detection of protein interactions using C-terminal BACTH fusions will not give any positive results since the T18 and T25 fragments will be physically separated from its complementary fragment by the cell membrane. Interestingly, N-terminal MreD and PlsY interact with each other on solid medium, which further consolidates the predicted topology.
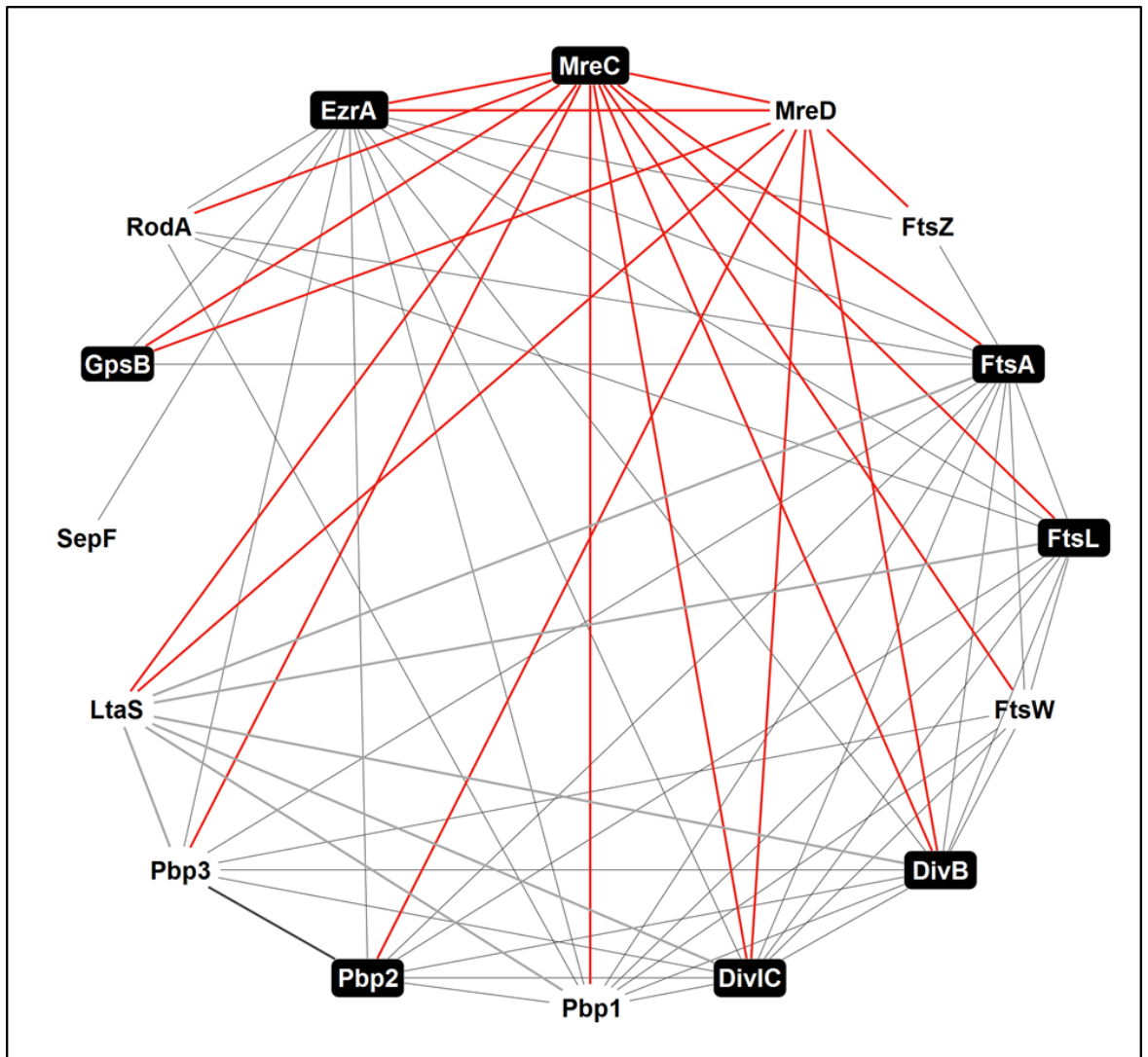
Figure 3-8 Interaction map of *S. aureus* cell division proteins

Interactions between *S. aureus* cell division proteins as determined by BACTH are displayed. Self-interacting proteins are in black boxes. Grey lines represent interactions that have been observed previously and red lines represent novel interactions of MreC and MreD in *S. aureus* observed in this study. The interaction map was concluded from both solid assays and liquid assays. This work was carried out in collaboration with Amy Bottomley (University of Sheffield).

3.5.3 Future directions

This comprehensive investigation of interactions between *S. aureus* cell division proteins using the BACTH system has helped the further understanding of a model of the *S. aureus* divisome machinery, which is composed of a core set of components that are conserved across many species of different architectures (Fig. 3.9). However, the BACTH liquid assay is not without its caveats, and some protein-protein interactions may not have been detected using intact cells. Gene fusions of the encoding regions for the C-terminus of T18 and T25 fragments to the N-terminus of MreC and MreD may reveal novel components of the divisome including those not selected for investigation using the BACTH assay, such as ParC and ParE.

The plasmids pKT25 and pKNT25 are low copy vectors, in contrast, pUT18 and pUT18c are high copy vectors. Previous studies using the BACTH system have found expression levels of hybrid *E. coli* proteins to be up to several thousand copies per cell (Karimova et al. 2005), whereas, *S. aureus* PBP1 is present at ~150 copies per cell (Pucci and Dougherty 2002). This may enhance the chance to detect many weak interactions that would not necessarily be seen at lower protein concentrations. The local concentration of proteins at the division site is likely to be higher which may also facilitate weak and transient interactions.

BACTH only proposes possible interactions, therefore alternative methods to detect interactions, such as immunoprecipitation using an affinity-tagged protein, will help verify interactions detected in this study.
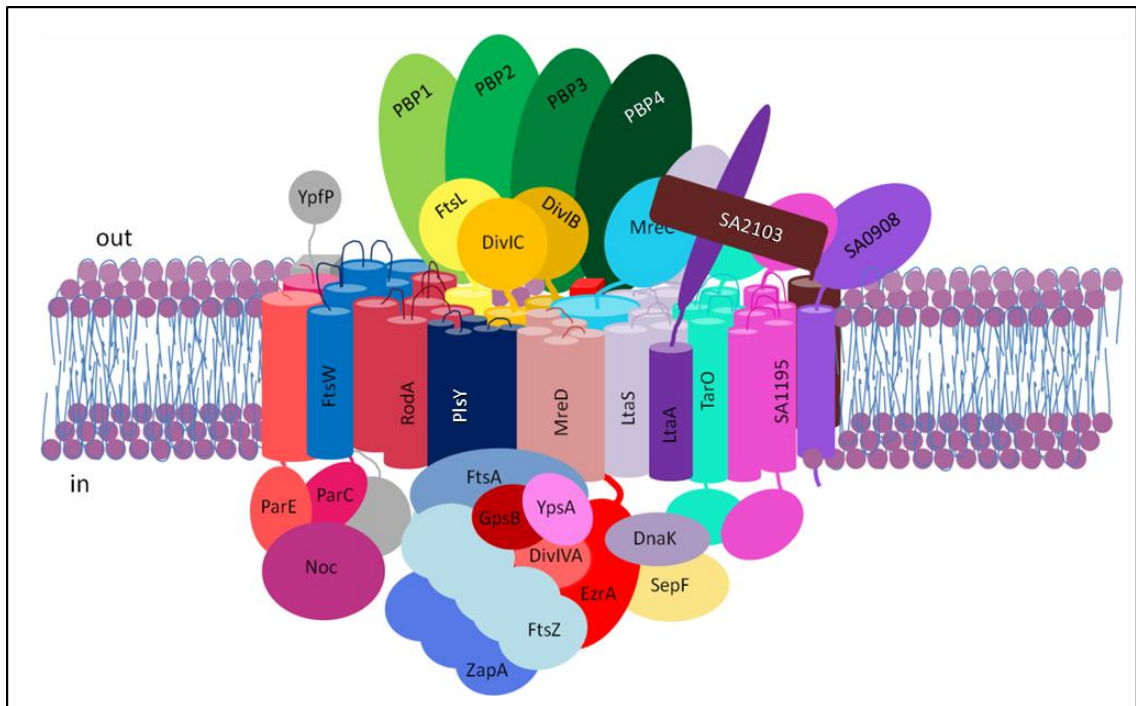
Figure 3-9 Schematic representation of the *S. aureus* divisome

Interacting components of the *S. aureus* divisome were identified using the BACTH assay, both previously (Steele *et al.* 2011) and within this study. This complex is dynamic thus not all divisome interactions are represented and not all will be concurrent.

4   Chapter 4 Cellular localisation of MreCD

4.1   Introduction

Many division proteins have been shown to localise to the midcell in *S. aureus*. FtsZ has been localised by immunofluorescence and both green fluorescent protein (GFP) and cyan fluorescent protein (CFP) fusions (Pinho & Errington 2005; Liew *et al.* 2011; Veiga *et al.* 2011); PBP1 has been localised by immunofluorescence (Pereira *et al.* 2007b, 2009); and PBP2 by green fluorescent protein fusion (Pinho & Errington 2003, 2005); EzrA localisation has been determined by CFP and GFP fusions (Pereira *et al.* 2010; Steele *et al.* 2011), and EzrA-mCherry with FtsZ-CFP co-localisation has also been reported (Veiga et al. 2011).

BACTH analysis indicated that MreC and MreD interact with many putative *S. aureus* cell division components including, FtsA, FtsL, DivIB, DivIC, FtsW, EzrA, PBP1, PBP2, PBP3, GpsB, RodA and LtaS respectively (Chapter 3). Protein-protein interactions may be indicative of co-localisation of MreCD at the midcell with many division proteins.

In *B. subtilis*, several essential membrane phospholipid biosynthesis proteins have been also found to localise to the midcell. For instance, CdsA, encoding cytidine 5'-diphosphate (CDP)-diacylglycerol synthase, has been localised using a GFP fusion (Nishibori *et al.* 2005). PlsY (YneS) is predicted to be a transmembrane protein with five transmembrane domains and has been detected at the cell periphery using a GFP fusion (Hunt *et al.* 2006). Work in *S. aureus* has also found that CdsA-GFP and PlsY-GFP are predominantly localised at the midcell with multiple foci around the cell periphery of (Garcia-Lara *et al.* 2015). In Chapter 3, BACTH studies have shown that both MreC and MreD interact with CdsA, also MreD interacts with PlsY on solid medium. Thus, this evidence may imply co-localisation of partners at the mid-cells and/or cell periphery with phospholipid biosynthesis proteins.

In rod shaped organisms, MreC and MreD are predicted to be cell membrane associated proteins. In *B. subtilis* and *E. coli*, the N-terminus of MreC is anchored to the cell membrane and the major C-terminal domain is located outside the cytoplasmic membrane, whereas, MreC was found to be a periplasmic protein in *C. crescentus* (Lee & Stewart 2003; Divakaruni *et al.* 2005; Kruse *et al.* 2005). The polytopic membrane protein MreD is highly hydrophobic embedded in the membrane with five transmembrane α-helices (Kruse *et al.* 2005). A prior study in *E. coli* has shown that MreC and MreD localise at the cell periphery using a GFP fusions (Kruse *et al.* 2005). In *B. subtilis*, MreC-GFP and MreD-GFP appear as a pattern of oblique bands reminiscent of a helical organisation (Leaver & Errington 2005). In *C. crescentus*, MreC was also found to localise spirally by immunofluorescence

microscopy and an mCherry fusion (Divakaruni *et al.* 2005; Dye *et al.* 2005), whereas, MreD localises to the midcell and pole (White *et al.* 2010).

In ovococcal bacteria, MreC and MreD localise to the equators and septa of dividing *S. pneumoniae* cells shown by immunofluorescence microscopy, furthermore, MreD also localises to other regions in the cell, suggesting that MreD travels around the cell during different stage of cell division (Land & Winkler 2011). However, localisation of MreC and MreD in *S. aureus* has never been shown. SOSUI predicted that MreC has a single transmembrane span with its major hydrophilic C-terminal domain in cytoplasm and MreD was predominantly hydrophobic with five transmembrane spans and N_{out}-C_{in} topology (Fig. 4.1). Here, localisation of the MreC and MreD proteins in *S. aureus* is determined. Also evidence is presented that MreD co-localises with essential membrane phospholipid biosynthesis proteins.

4.2 Aims

- Study of the subcellular localisation of MreC and MreD in *S. aureus*.

4.3 Results

4.3.1 Bioinformatic analysis of MreC and MreD

Previous bioinformatic analysis of an *mreC* and *mreD* orthologues in *S. aureus* identified SAOUHSC_01759 and SAOUHSC_01758 as likely candidates, respectively (Table 3.1). In *S. aureus*, *mreD* is located directly downstream of *mreC* in the same operon, which is similar to *B.subtilis mreCD*, in which *mreC* and *mreD* are co-transcribed with *mreB*, suggesting that SAOUHSC_01759 and SAOUHSC_01758 are the *S. aureus* orthologues of *B. subtilis mreCD*. This is similar to *S. pneumoniae mreCD*, which also lacks an *mreB* homologue.

S. pneumoniae MreC consists of 273 amino acids and has a predicted molecular weight of 29.7 kDa and a pI of 6.2. *S. aureus* MreC is a protein of 281 amino acids with a predicted molecular weight of 30.9 kDa and a pI of 8.2. Alignment of *S. pneumoniae* and *S. aureus* MreC showed the proteins have 30% identity and 50% positive alignment (Fig. 4.2 A). Hydropathy plots using SOSUI (Hirokawa et al. 1998) predict that both *S. pneumoniae* and *S. aureus* MreC contain a single transmembrane domain near the N terminus (Fig. 4.2 B). *S. pneumoniae* MreC has previously been shown to be associated with the membrane (Land & Winkler 2011), suggesting that MreC does contain a transmembrane domain. From Figure

4.2 it can be seen that *S. aureus* MreC has an extra amino acid at the N terminus, and also 12 extra residues at the extreme C terminus that are not found in the *S. pneumoniae* homologue.

B. subtilis MreD consists of 173 amino acids and with a predicted molecular weight of 19.8 kDa and a pI of 8.2. *S. aureus* MreD is a protein of 177 amino acids with a predicted molecular weight of 20.8 kDa and a pI of 9.5. Alignment of *B.subtilis* and *S. aureus* MreD showed the proteins have 18.5% identity and 42% positive alignment (Fig. 4.3 A). Hydropathy plots using SOSUI (Hirokawa et al. 1998) predict that both *B. subtilis* and *S. aureus* MreD contain 5 transmembrane domains (Fig. 4.3 B). From Figure 4.2 it can be seen that *S. aureus* MreD has four extra amino acids at the extreme C terminus that are not found in the *B. subtilis* orthologue.

4.3.2   Production of recombinant MreC and MreD

In *C. crescentus*, the periplasmic domain of MreC interacts with cell wall assembly complexes (Divakaruni *et al.* 2005). The C terminal domain of *B. subtilis* MreC is also required for the interaction with the majority of high-molecular-weight penicillin binding proteins shown by BACTH (van den Ent *et al.* 2006), suggesting an importance of the C terminal domain of MreC for proper function. Thus, the C terminal domain of MreC from *S. aureus* was expressed as a recombinant his-tagged protein for the production of antibodies and for use in biochemical assays.

There is a proline-proline bond at the initial part of the C terminal domain of *S. aureus* MreC, cMreC ((Fig 4.1), Proline exists in the both *cis-* and *trans-* configuration in peptides and the *cis/trans* isomerisation may impede the progression of protein folding (Wedemeyer *et al.* 2002), in particular when the native protein requires the *cis* isomer. To avoid the potential risk of improper folding of the cMreC, it was decided to start the recombinant protein from a glutamic acid at position 37 of the predicted C terminal domain. The cloned *S. aureus* cMreC consists of 245 amino acids and has a predicted molecular weight of 27 kDa and a pI of 8.7. The entire MreD was also attempted to be produced.
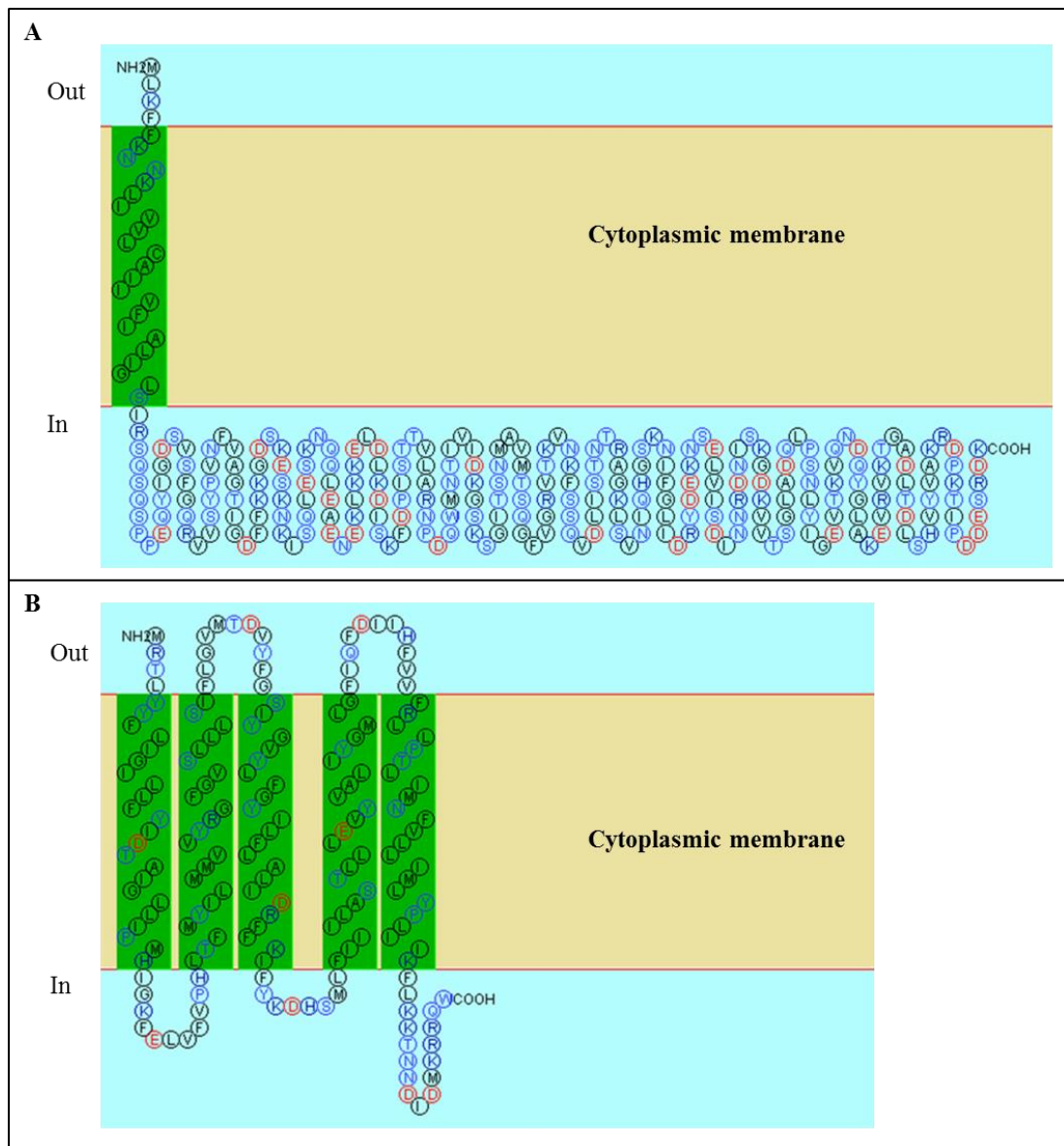
Figure 4-1 Schematic topological diaGram of *S. aureus* MreC and MreD using SOSUI

A. MreC is a membrane protein with 1 transmembrane helix. Its predicted molecular weight is 30.9kDa.

B. MreD is a membrane protein with 5 transmembrane helices. Its predicted molecular weight is 20.8kDa.
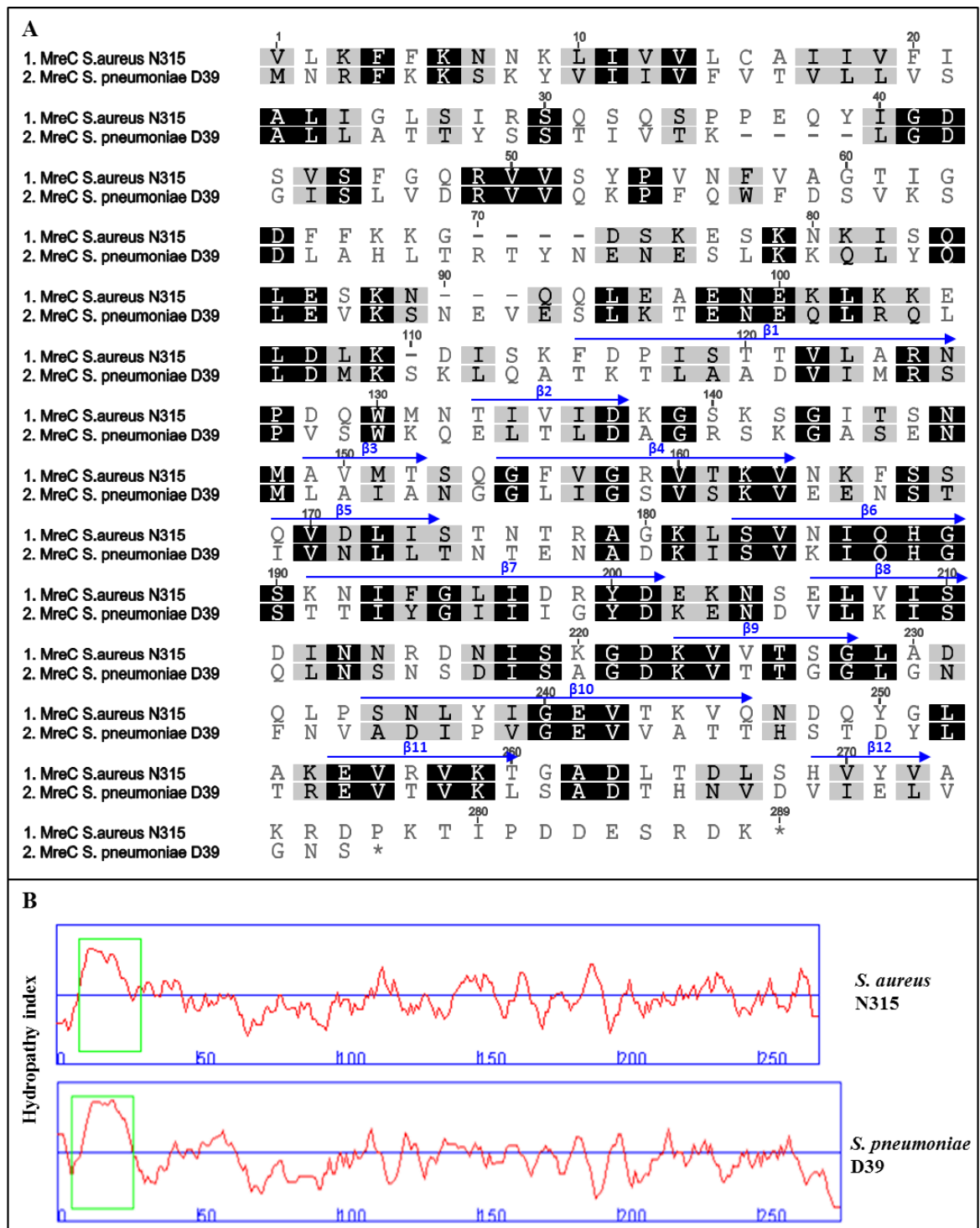
Figure 4-2 Sequence alignment of MreC from *S. aureus* and *S. pneumoniae*

A. Alignment of MreC protein sequences from *S. aureus* and *S. pneumoniae* with ClustalW using the Geneious software. Residues blocked in black boxes are conserved; grey boxes indicate semi-conserved substitutions. β strands are indicated by blue arrows.

B. Hydropathy plots of *S. aureus* and *S. pneumoniae* MreC produced using SOSUI. The transmembrane domains are highlighted in green.
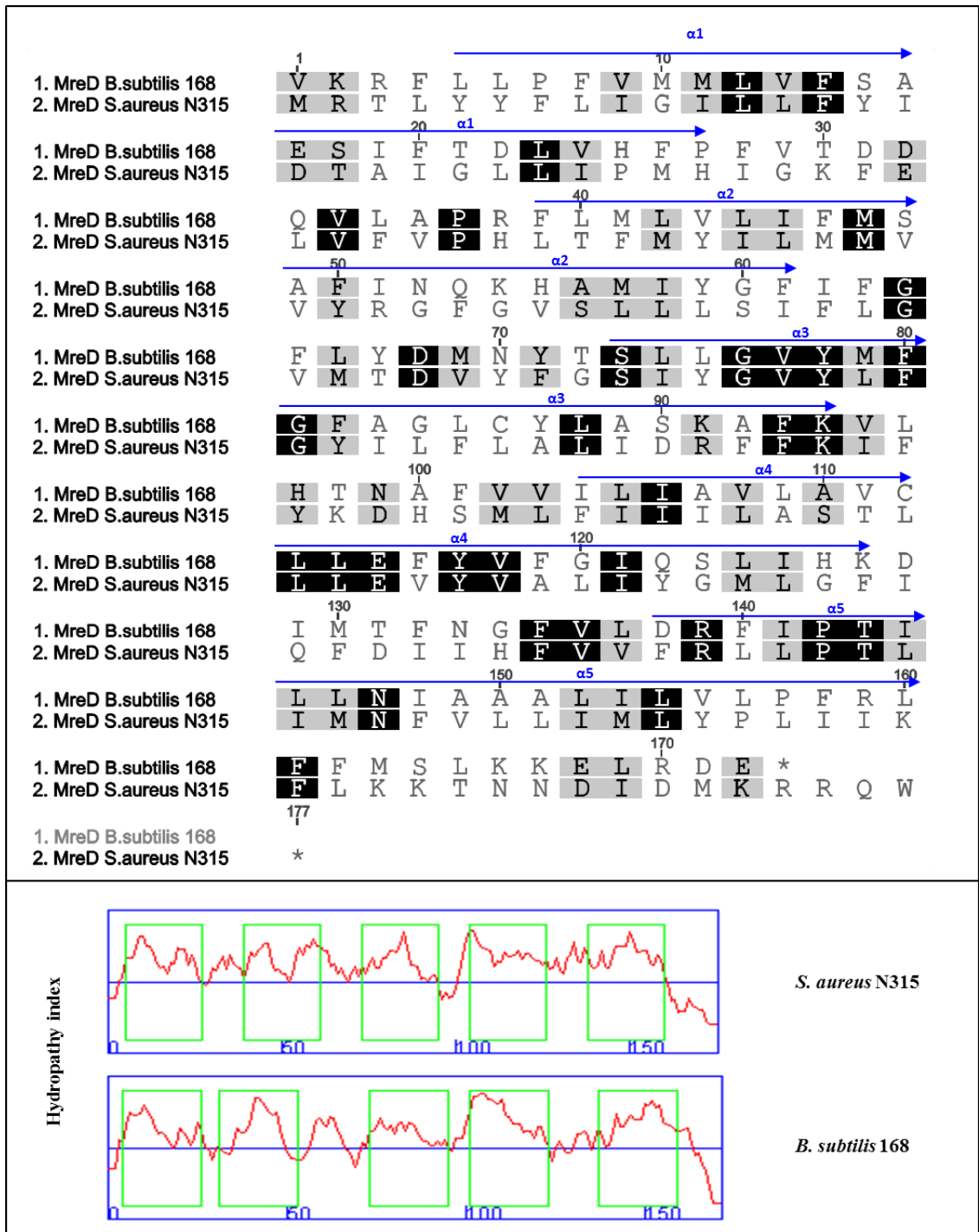
Figure 4-3 Sequence alignment of MreD from *S. aureus* and *B. subtilis*

A.   Alignment of MreD protein sequences from *S. aureus* and *B.subtilis* with ClustalW using the Geneious software. Residues blocked in black boxes are conserved; grey boxes indicate semi-conserved substitutions. α helixes are indicated by blue arrows.

B.   Hydropathy plots of *S. aureus* and *B. subtilis* MreD produced using SOSUI. The transmembrane domains are highlighted in green.

4.3.2.1 Construction of *S.aureus* MreC and MreD expression plasmids

4.3.2.1.1 Construction of *S.aureus* MreC and MreD expression plasmids using pET21d

The pET system was chosen since it can result in the desired protein constituting over 50% of the total cell proteins after just a few hours of induction in *E.coli*. The target gene is cloned under the control of a strong bacteriophage T7 promoter downstream of a *lac* operator. The target gene is not transcribed unless T7 RNA polymerase is present since the T7 promoter is not recognised by bacterial RNA polymerase. Using an expression host containing a chromosomal copy of the T7 RNA polymerase under control of *lacUV5* allows for transcription of the T7 RNA polymerase to be regulated by the presence or absence of different carbon sources (Novagen, Gibbstown, NJ, USA).

The pET21d vector, which carries a C terminal His$_6$ tag, was chosen for expression of cMreC which was identified based on topology predictions (Fig. 4.1). The primers were designed to keep the C terminal *mreC* sequence in frame by introducing a single G residue due to the *Nco*I restriction site, and to allow read-through to the his-tag at the 3' end of the gene. The *C-mreC* and entire *mreD* were amplified from *S.aureus* SH1000 genomic DNA using primers 5HXM316A and 3HXM231A, and 5HXM231B and 3HXM231B, respectively (Table 2.6). Purified PCR products were digested with *Nco*I and *Xho*I and ligated into pET21d which had been digested with the same restriction enzymes (Fig. 4.4 A ii-iii B & C). Ligation products were used to transform electrocompetent *E.coli* TOP10 with selection on LB Amp 100 μg ml^{-1}. Positive clones encoding cMreC were identified by PCR using primers 5HXM316A and 3HXM231A (Fig. 4.4 D). The clones, which gave an expected band on 1% (w/v) agarose gel were sequenced by the University of Sheffield Core Genomics Facility to check for the introduction of substitutions or frame shift mutations during PCR. 100% identity was seen for cMreC sequences compared to N315 in database (data not shown). No positive clones for MreD were found and the construction of the MreD expression plasmid was aborted due to time constraints and the challenges to be faced during the purification stage of the hydrophobic protein MreD.
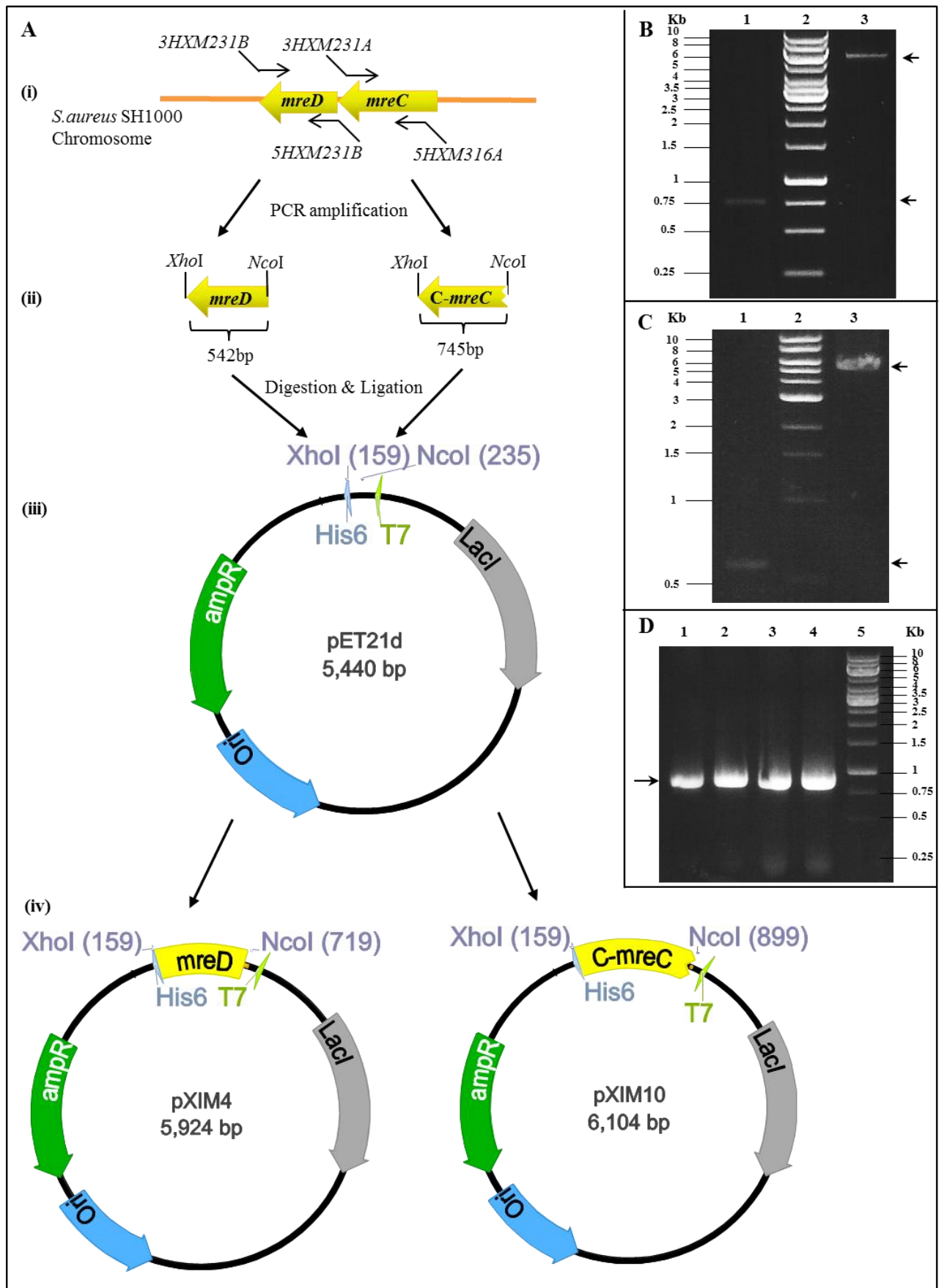
Figure 4-4 Construction of MreC expression plasmid with pET21d

A.   DiaGrammatic representation of the construction of pXIM4 (*mreD*) and pXIM10 (*mreC*) in *E.coli.* Primer binding sites for 5HXM316A, 3HXM231A, 5HXM231B and 3HXM231B, and relevant restriction sites used are shown. i) *S.aureus* chromosomal DNA; ii) PCR fragments to be cloned into pET21d; iii) Digestion of PCR fragments with *Xho*I and *Nco*I and ligation into plasmid pET21d at the same sites. iv) Resulting pXIM4 and pXIM10.

B.   1% (w/v) TAE agarose gel showing *Xho*I and *Nco*I restriction digested PCR products of the C-terminal *mreC* region with primers 5HXM316A and 3HXM231A (lane 1) and pET21d vector digested with the same enzymes (lane 3). Arrows indicate the expected sizes of 745bp and ~5.3bp respectively. Fragments correspond to those in panel A (ii-iii). Lane 2 contains a 1kb DNA ladder used as a marker (Fermentas).

C.   1% (w/v) TAE agarose gel showing *Xho*I and *Nco*I restriction digested PCR products of the entire *mreD* with primers 5HXM231B and 3HXM231B (lane 1) and pET21d vector digested with the same enzymes (lane 3). Arrows indicate the expected sizes of 542bp and ~5.3bp respectively. Fragments correspond to those in panel A (ii-iii). Lane 2 contains a 1kb DNA ladder used as a marker (NEB).

D.   1 % (w/v) TAE agarose gel showing products of PCR amplification of *mreC* from pXIM10 with primers 5HXM316A and 3HXM231A using QIAGEN mini prep DNA extracted from 4 randomly selected *E.coli* BL21 transformants (lane 1-4).   Arrow marks the expected size of 745bp. Lane 5 contains a 1kb DNA ladder used as a marker (NEB).

4.3.2.2 Production and purification of recombinant *S. aureus* C-terminal domain of MreC

pXIM10 (containing *S. aureus* C terminal domain of MreC) was transformed into a strain that can recognise the T7 promoter. BL21 was used which is a *lacZY* deletion mutant. The strain carries a chromosomal copy of the T7 RNA polymerase gene under the control of the *lacUV5* promoter. *E.coli* BL21 is also deficient in Lon and OmpT proteases, reducing the risk of degradation of proteins produced from cloned genes.

Auto-induction broth was used instead of IPTG (Chapter 2.1.1.6), where a small concentrated glucose is added, which restrains uptake of lactose until the glucose is depleted (Studier 2005). As the glucose is depleted, usually at mid or late log phase, lactose can then be utilised and converted by β-galactosidase to the inducer allolactose which in turn leads to release of *lac* repressor from its specific binding site in the DNA and thereby induces T7 RNA polymerase expression from the *lacUV5* promoter and unblocks the T7lac promoter, allowing expression of target proteins by T7 RNA polymerase. This allows automatic induction from the *lac* promoter at a high density cell growth without checking optical density and adding inducer.

To produce recombinant protein, the cMreC was overexpressed from pXIM10 using auto-induction broth Chapter 2.1.1.6. To determine the induction of protein expression, a sample of freshly uninduced cells, before the subculture into auto-induction broth, was taken, and again after overnight auto-induction. To determine the solubility of the recombinant proteins, a sample of induced cells were lysed and separated into soluble and insoluble fractions (Chapter 2.12.2). Whole cell lysates for each sample were run on a 12% (w/v) SDS-PAGE gel and stained with Coomassie blue (Fig. 4.5). A band of ~ 28 kDa for *S. aureus* cMreC was seen in the induced samples (+), which is the expected size. Investigation of solubility showed that cMreC appeared to be predominantly insoluble (Fig. 4.5A I). To purify the protein, cells were grown and expression of recombinant protein was induced (Chapter 2.12.1). The insoluble fraction of cMreC was resuspended in 8 M urea to solubilise protein, and then purified using an affinity column charged with Ni^{2+}, to which the his_6 tag binds. The column was washed with 5% (w/v) imidazole buffer (Chapter 2.3.7.3) to remove any non-specifically bound material and recombinant protein were eluted from the column using an increasing concentration of imidazole (Chapter 2.12.4). The resulting protein fractions were separated on 12% (w/v) SDS-PAGE gel, showing a single major band corresponding to the expected size of the cMreC (Fig. 4.5 B-E). To remove the imidazole and urea, fractions containing recombinant proteins were dialysed in an excess of PBS containing a series of dilutions of Urea from 8 M to 0M (Chapter 2.12.5.2). However, after one dialysis step it was found that the cMreC protein precipitated out in two independent preparations. 1 µl of a total sample

(~20 ml) from both preps was separated on a 12% (w/v) SDS-PAGE gel compared to different concentrations of BSA (NEB). Some other faint bands not corresponding to the expected size of the cMreC were also present in the final purified protein (Fig. 4.5F, marked with asterisks). The lower two bands may correspond to degradation of the recombinant protein.

4.3.3 Generation of anti-MreC antibodies

Rabbit α-C-MreC polyclonal antibodies were raised against purified recombinant cMreC by BioServ (University of Sheffield) (Chapter 2.12.5).

Reactivity and specificity of the antibodies against recombinant cMreC were assessed. Whole cell lysates of cMreC expression strain SJF3850 were analysed by Western blot (Chapter 2.3.9). Blots were probed with polyclonal α-cMreC serum at a range of dilutions from 1:5000 to 1:100000. A strong band of reactivity was detected at ~28 kDa for recombinant cMreC (Fig. 4.6 A). Several bands with lower molecular mass were also seen, probably due to cMreC degradation. Polyclonal α-cMreC reacted with several *S. aureus* proteins, with the most reactive band seen at about 28 kDa in all samples, a possible doublet of reactive bands of ~ 56 kDa was also observed at all dilutions tested (Fig. 4.6 A & B), which due to the presence of coiled coil region, which may mediate MreC self-interaction (van den Ent *et al.* 2006; Lovering & Strynadka 2007).

Cross-reactivity of the antiserum against native *Enterococcus faecalis* proteins was completely absent, a native extract of *S. aureus* SH1000 gave a very strong signal at 28kDa corresponding to c-MreC (Fig. 4.6 C), showing the apparent specificity of the antiserum for *S.aureus* cMreC (Fig. 4.6 C) This antibody solution was used for all subsequent Western blots at a concentration of 1:5000.
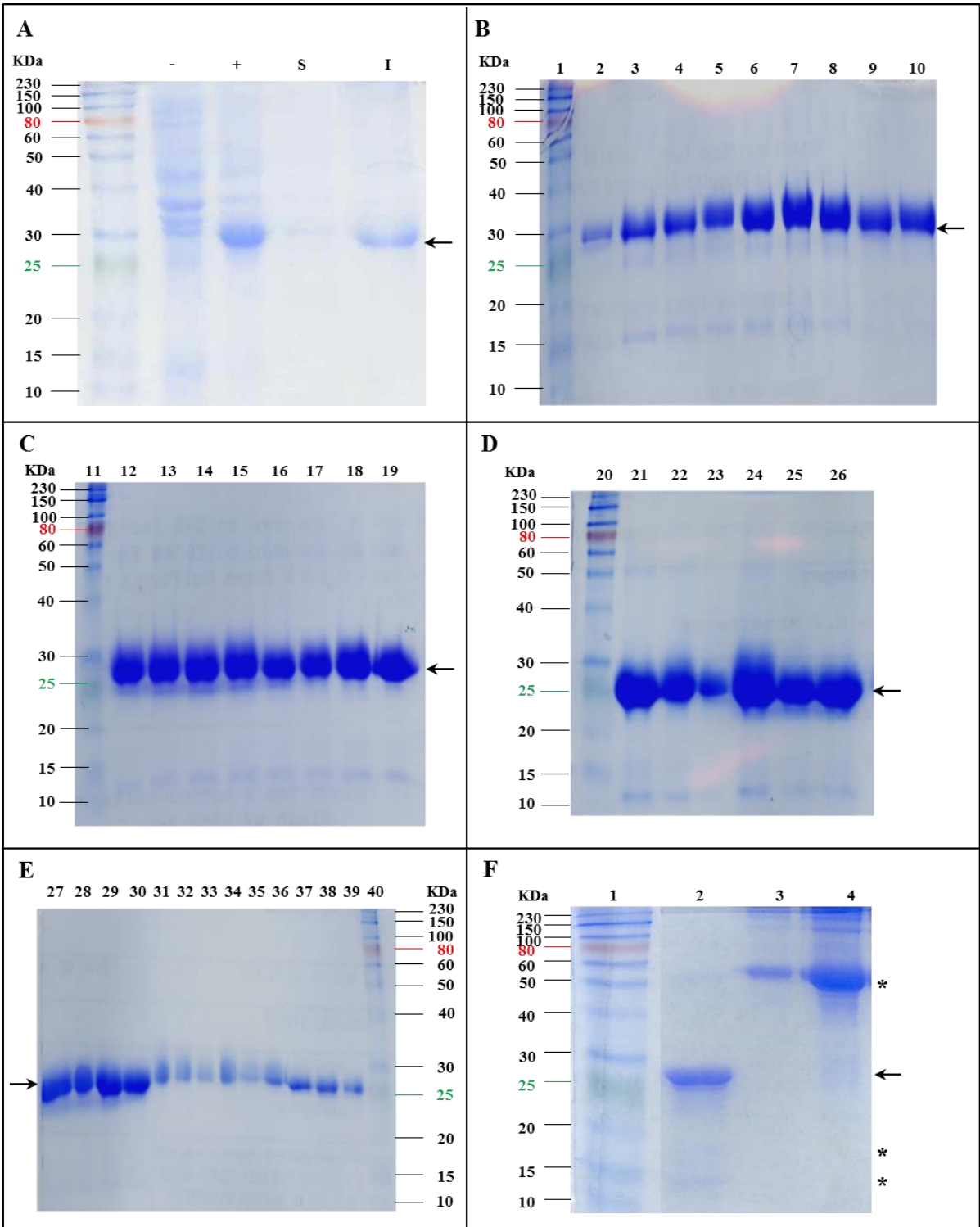
Figure 4-5 Production of recombinant cMreC in *E. coli* BL21

E. coli BL21 (DE3) containing pXIM10 was grown overnight in auto-induction medium (Chapter 2.1.1.6).

A.   Expression of *S. aureus* cMreC. Black arrows indicate the protein band of expected size of ~ 28 KDa. Samples was taken before transferring to auto-induction medium (-) and after overnight induction (+). An induced sample was also separated into soluble (S) and insoluble (I) proteins. Whole cell lysates of all samples were separated on a 12% (w/v) SDS-PAGE gel (Chapter 2.11.1). 1ml of each sample culture was loaded. Lane 1 contains ColorPlus™ Prestained Protein Ladder (NEB).

B-E.   10 µl of 1.5 ml fractions eluted from a nickel affinity column were resolved on a 12% (w/v) SDSPAGE gel. Fractions 6-41 are shown here as examples. Lane 1, 11, 20 and 40 contains ColorPlus™ Prestained Protein Ladder (NEB). A linear gradient of 5-100% elution buffer B was used over 75ml, a total of 50 x 1.5 ml fractions were collected.

F.   Purified recombinant protein. 3 µl of purified c-MreC protein sample (lane 2) was tested. Lane 3 contains 1µl BSA at a concentration of 0.5µg/µl. Lane 4 contains 1µl BSA at a concentration of 1µg/µl. Lane 1 ColorPlus™ Prestained Protein Ladder (NEB).

4.3.4 Subcellular localisation of MreC

Determination of the subcellular localisation of uncharacterised proteins can provide functional information. A combination of techniques was therefore used to study the localisation of MreC within *S. aureus*.

4.3.4.1 Western blot analysis of subcellular fractions

Bioinformatic analysis indicates that MreC carries a putative N-terminal transmembrane domain (Fig. 4.1 A & 4.2 B), similar to those found in *E. coli*, *B. subtilis*, *L. monocytogenes* and *S. pneumoniae* (Lee & Stewart 2003; Kruse *et al.* 2005; van den Ent *et al.* 2006; Land & Winkler 2011). The localisation of *S.aureus* MreC was therefore determined by Western blot analysis of cellular fractions.

Cellular fractions of LC102 (*spa::tet*) were prepared as described in Chapter 2.18 and a crude extract of WT *S. aureus* and an *mreC* deletion mutant (Chapter 5.2.1) were prepared according to Chapter 2.17. Samples corresponding to an equal number of cells were analysed by SDS-PAGE and Western blot, probing with α-MreC. A strong band of ~ 28 kDa, corresponding to MreC, was found in the cell wall fraction, *S. aureus* SH1000 crude extract and positive control, cMreC protein (Fig 4.7). No reactive protein was present in membrane or cytoplasmic fractions and a crude extract of the *mreC* deletion mutant (SJF2625). This confirms that the cMreC is likely in the periplasm associated with the cell wall in *S. aureus*.
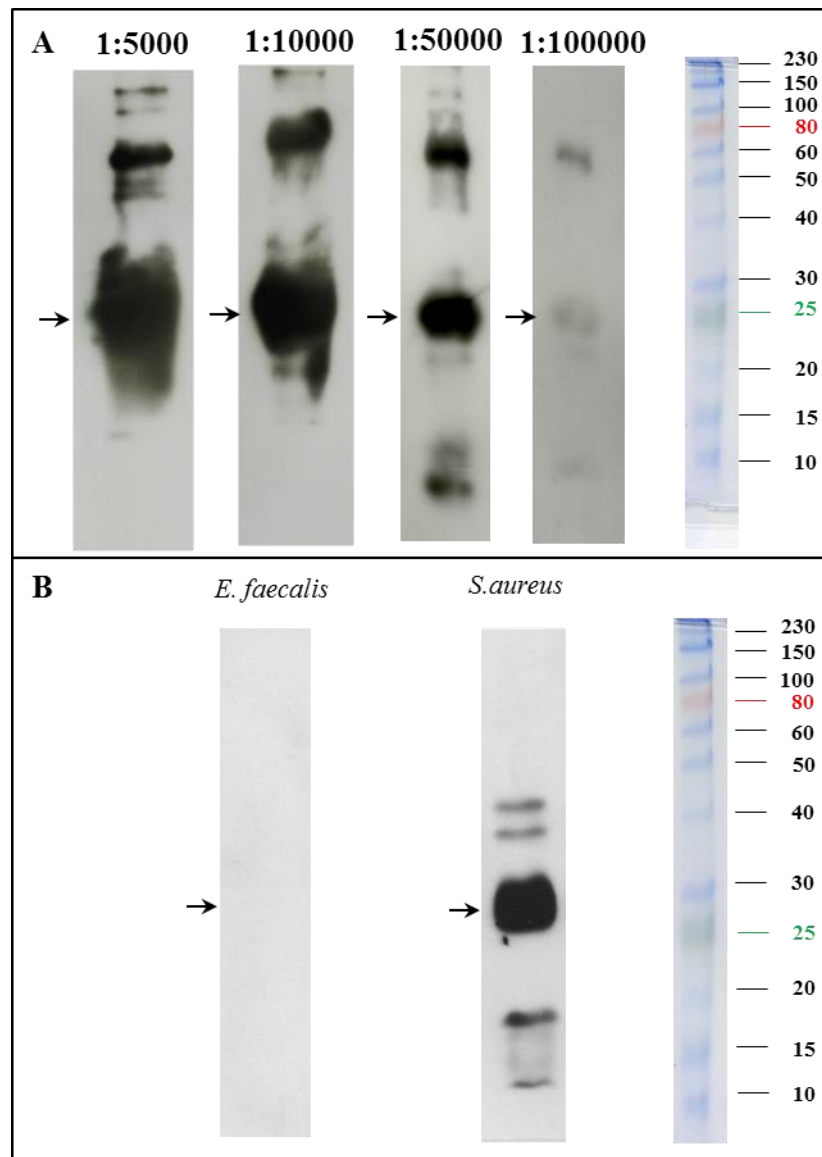
Figure 4-6 Reactivity of polyclonal α-MreC antibodies

A.   100 ng of recombinant MreC was separated by 12% (w/v) SDS-PAGE and Western blotted. Blots were probed with rabbit polyclonal α-MreC antibodies at 1:5000 to 1:100 000. Black arrows indicate bands detected at ~28 kDa. ColorPlus™ Prestained Protein Ladder (NEB) was used.

B.   Whole cell lysates 15 µl of *S. aureus* LC102 (*spa::tet*) and *E. faecalis.* ColorPlus™ Prestained Protein Ladder (NEB) was used.
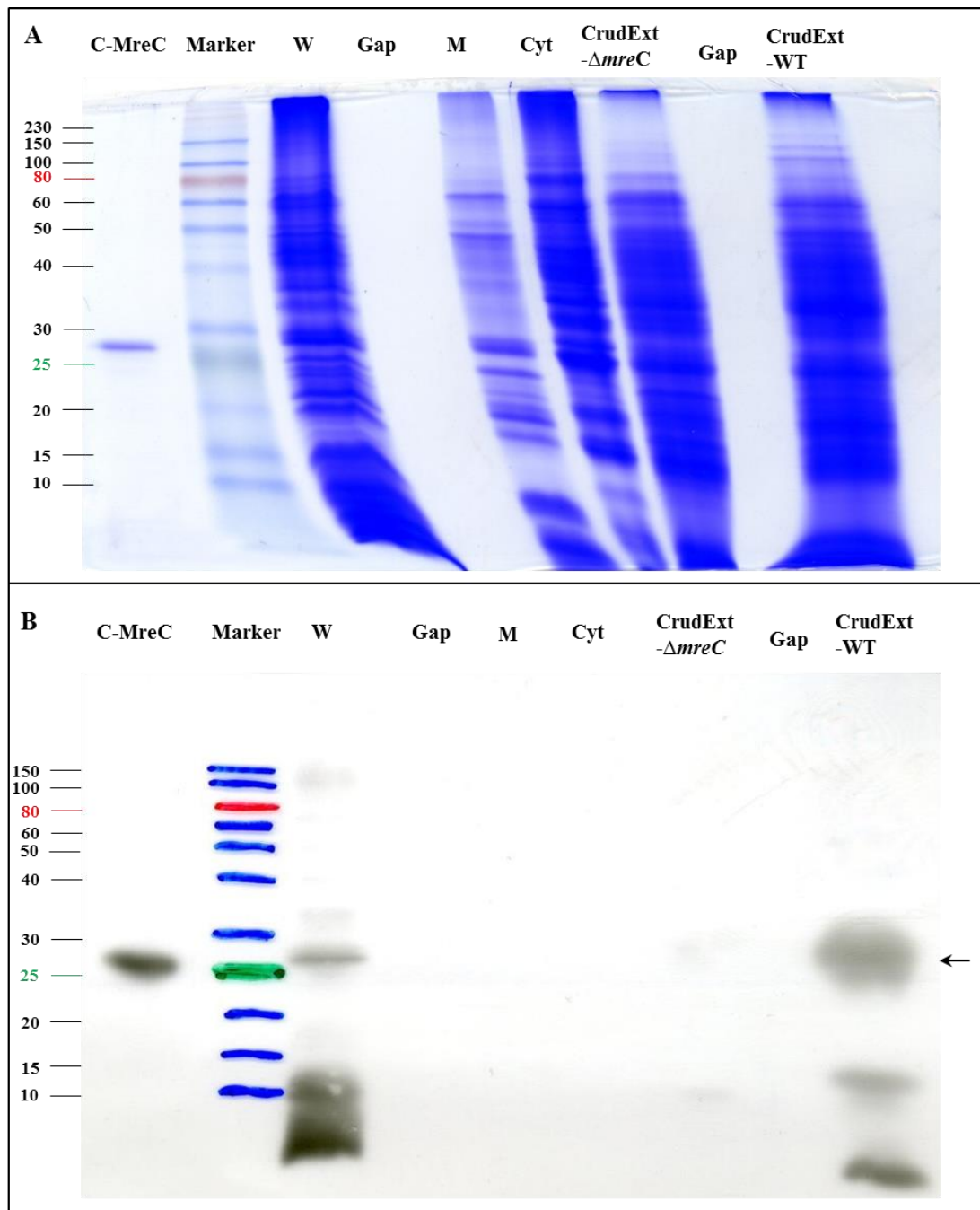
Figure 4-7 Subcellular localisation of cMreC in *S. aureus*

A.   Exponentially growing LC102 (*spa::tet*) and *mreC* deletion mutant (SJF2625) were broken and 15 µl equal proportions of fractions were loaded onto 12% (w/v) SDS-PAGE. Pre-stained molecular markers (NEB) are indicated in kDa. W, cell walls; M, membrane; Cyt, cytoplasm; CrudExt-MreC: Crude extract of *mreC* mutant; CrudExt-WT, Crude extract of ST SH1000. ColorPlus™ Prestained Protein Ladder (NEB) was used.

B.   Western Blot with polyclonal α-MreC antibodies at 1:5000. The position of MreC is indicated by a black arrow. ColorPlus™ Prestained Protein Ladder (NEB) was used.

4.3.5 Construction of MreCD GFP fusion strains

4.1.1.1 C-terminal fusions

Fluorescent protein fusions have been extensively used to show cellular localisation to specific structures or complexes within a cell and therefore suggest cellular roles. A C-terminal fusion of MreC to red fluorescent protein fusion (mRFP1) in *Caulobacter* lies spirally in the periplasm (Dye *et al.* 2005).

S. aureus MreC and MreD were predicted to possess cytoplasmic C termini domains by SOSUI (Fig. 4.1). However, my data suggests that the cMreC may be periplasmic (Chapter 4.2.4). Green fluorescent protein (GFP) is thought not generally functional when fused to an extracellular domain of a protein (Feilmeier *et al.* 2000). In order to determine the localisation of MreC and MreD within *S. aureus*, C-terminal GFP fusions of *S. aureus* MreC and MreD were constructed by Jagath Kasturiarachchi (University of Sheffield) using the vector pMUTIN-Gfp$^+$ (Kaltwasser *et al.* 2002).

The ribosome binding site and coding sequence of *S. aureus mreC* or *mreD* were cloned into pMUTIN-GFP$^+$ to create an in-frame fusions of *mreC* or *mreD* to *gfp$^+$*. The resulting plasmids, pJGL229 (*mreC::gfp*) and pJGL230 (*mreD::gfp*), were transformed into electrocompetent *S. aureus* RN4220. A single crossover event results in integration of the plasmid into the chromosome, with a *mreC-gfp+* or *mreD-gfp+* fusions under the control of the their native promoters, and a native copy of *mreC* or *mreD* under the control of IPTG inducible promoter P$_{Spac}$ (Fig. 5.4). The chromosomal region, including the plasmid insertion, was transferred to SH1000 via transduction using φ11, generating strains SJF2100 (*mreC::gfp*) and SJF2101 (*mreD::gfp*) as listed in Table 2.2.

Fusion of GFP to a protein of interest can result in misfolding, loss of activity and/or incorrect targeting. No difference was seen in growth between SH1000, SJF2100 (*mreC::gfp*) and SJF2101 (*mreD::gfp*) (data not shown). Due to time constraints, the functionality of MreC-GFP$^+$ and MreD-GFP$^+$ fusion proteins were not further tested, where a multi-*lacI* repressor plasmid could be introduced in order to reduce basal expression of the native protein from P$_{Spac}$ in the absence of IPTG. The subcellular localisation of MreC and MreD in *S. aureus* were visualised by fluorescence microscopy of SJF2100 (*mreC::gfp*) and SJF2101 (*mreD::gfp*) (Chapter 4.3.5.3).
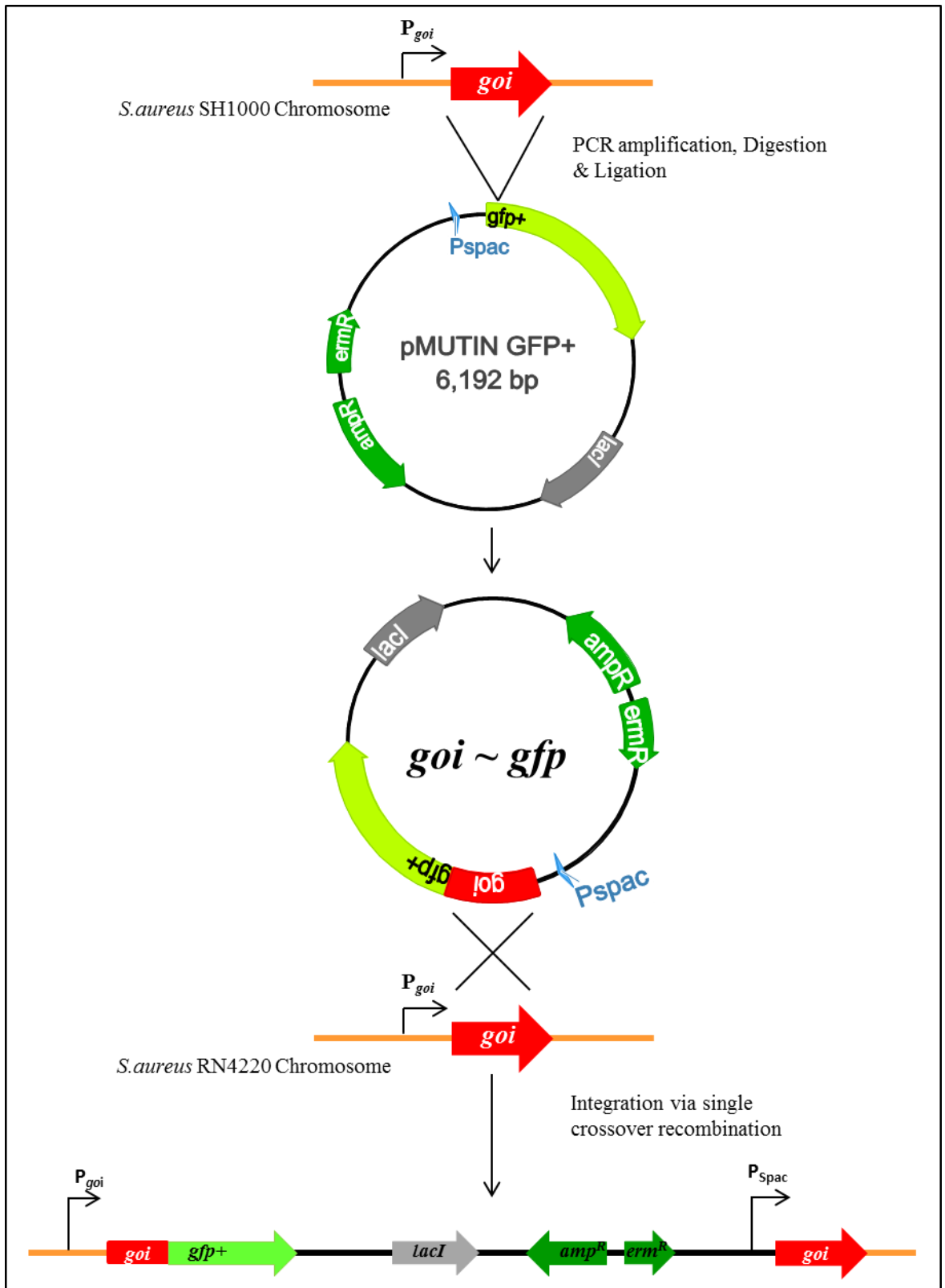
Figure 4-8 Construction of an *S. aureus mreC-gfp+* or *mreD-gfp+* strains

DiaGrammatic representation of construction of pJGL229 or pJGL230 and insertion of the plasmids into *S. aureus* RN4220. This work was carried out by Jagath Kasturiarachchi (University of Sheffield). *goi*, gene of interesting, represents *mreC* or *mreD*.

4.3.5.1   N-terminal fusions

GFP fusions to the N termini of MreC and MreD have been extensively studied. In, *E. coli*, fusions to MreC and MreD gave a peripheral GFP signal (Kruse *et al.* 2005). In *B. subtilis*, N-terminal fusions to GFP exhibited membrane and septal localisation (Leaver & Errington 2005). Since the C-terminal GFP fusion of *S. aureus* MreC might be periplasmic and for confirmation of localisation pattern, N-terminal GFP fusions of *S. aureus* MreC and MreD were constructed (Fig. 4.9 & 4.10) using the vector pSG1729 (Lewis & Marston 1999).

To make sure there is only one functional copy of the gene of interest after the plasmid integration into the chromosome via single crossover, the truncated *mreC* and *mreD* were amplified as well as entire *mreC* and *mreD* by primers 5HXM49Aa, 5HXM49Ab, 5HXM49Ba, 5HXM49Bb, 3HXM46Aa, 3HXM46Ab, 3HXM46Ba and 3HXM46Bb, respectively (Fig. 4.9 i & ii). Products consistent with the expected sizes of 729bp, 867bp, 318bp and 542bp were obtained, respectively. The purified products were digested with *BamH*I/*Hind*III and separated on a 1 % (w/v) agarose gel along with vector pSG1729 (Lewis & Marston 1999) restricted with the same enzymes (Fig 4.10 A). Ligations were carried out at 16°C in a PCR machine overnight (Chapter 2.8.4), and the ligation products were used for transformation of electrocompetent *E. coli* TOP10 with selection on LB Amp 100 μg ml^{-1} plates, generating pGL605a, pGL605b, pGL606a and pGL606b (Fig. 4.9 iv). Positive clones were verified by plasmid purification, PCR amplification of cloned regions (Fig. 4.10 B) and restriction digestion with either *BamH*I/*Hind*III or *Xho*I/*Hind*III and electrophoresis in a 1 % (w/v) agarose gel (Fig. 4.10 D). Electroporation of resulting plasmids pGL605a and pGL606a was not successful. The electroporation was not repeated due to the time constraints and potential challenges where the truncated *mreC* and *mreD* maybe not sufficient for recombination into *S. aureus*.

The resulting plasmids, pGL605b and pGL606b, were introduced into *S. aureus* RN4220 by electroporation, followed by selection on BHI spectinomycin (Spec) 50 μg ml^{-1} plates. Plasmids pGL605b and pGL606b have no origin for replication in *S. aureus* and therefore integrate into the chromosome via homologous recombination (Fig. 4.11 i & ii). This results in the *mreC*-GFP^{+} or *mreD*-GFP^{+} gene under the control of P$_{xyl}$ and a native *mreC* or *mreD* gene under the control of the native *mreC* or *mreD* promoter (Fig. 4.11 ii & iv). Unexpectedly, all the Spec 50 μg ml^{-1} plates were covered by a lawn of bacteria, except negative controls. The experiment was repeated with fresh Spec (Sigma), still a lawn of bacteria appeared on the plates.
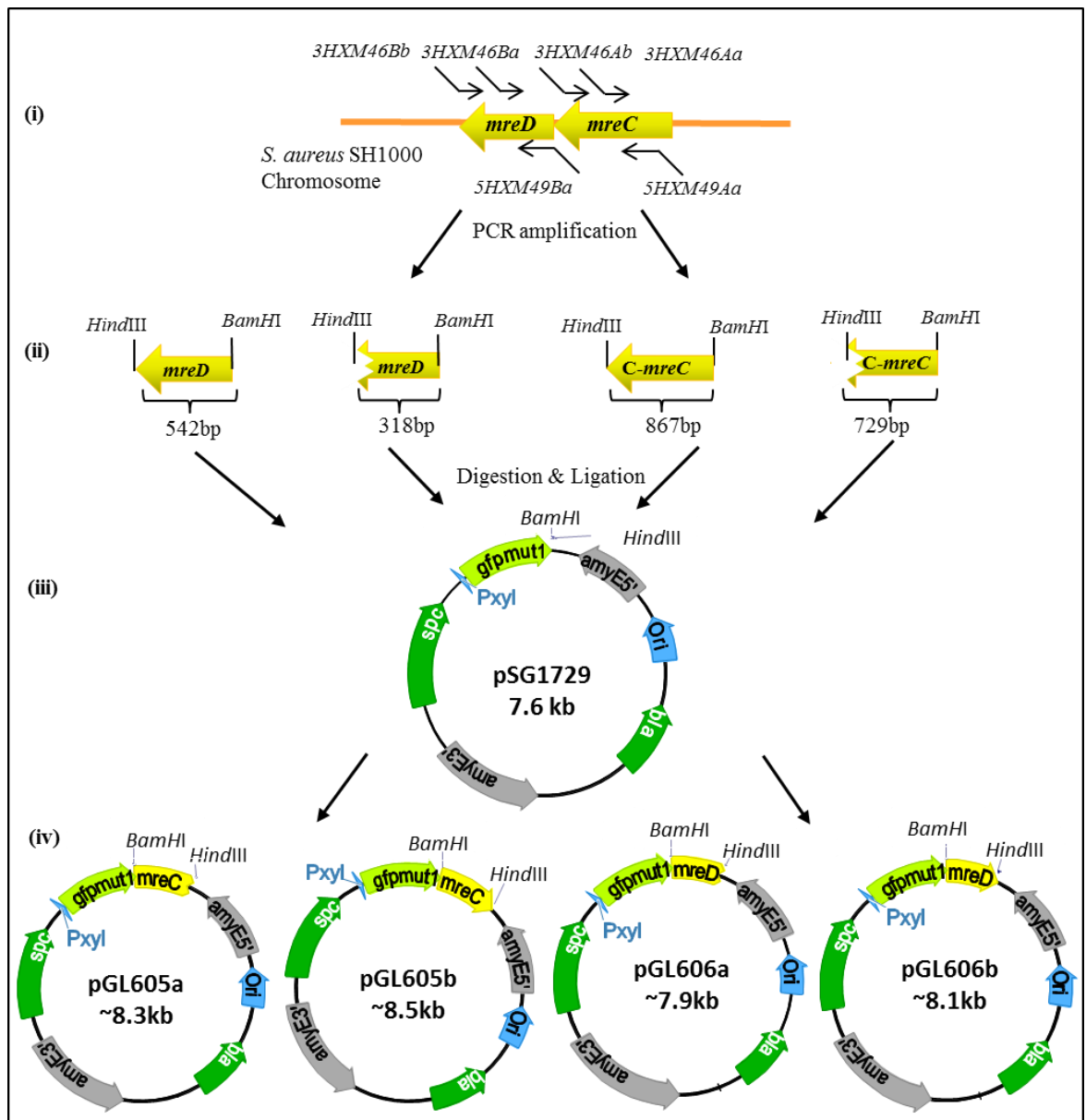
Figure 4-9 Construction of *S. aureus mreC-gfp+* and *mreD-gfp+* plasmids

DiaGrammatic representation of the construction of pGL605a, pGL605b, pGL606a and pGL606b, in *E. coli*. Primer binding sites for 5HXM49Aa, 5HXM49Ba, 3HXM46Aa, 3HXM46Ab, 3HXM46Ba and 3HXM46Bb, and relevant restriction sites used are shown.

i)   *S. aureus* chromosomal DNA

ii)   PCR amplification of whole *mreC* and *mreD* and the truncated versions of both genes, which were cloned into pSG1729

iii)   Digestion of PCR fragments with *BamH*I and *Hind*III and ligation into plasmid pET21d at the same sites.

iv)   Resulting plasmids pGL605a (truncated *mreC*), pGL605b (whole *mreC*), pGL606a (truncated *mreD*) and pGL606b (whole *mreD*).
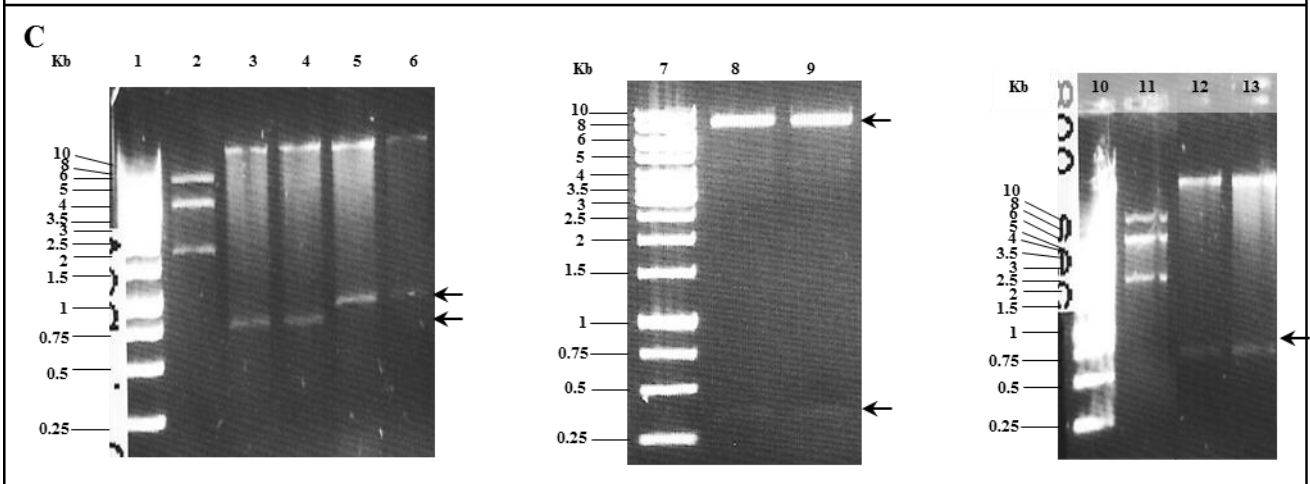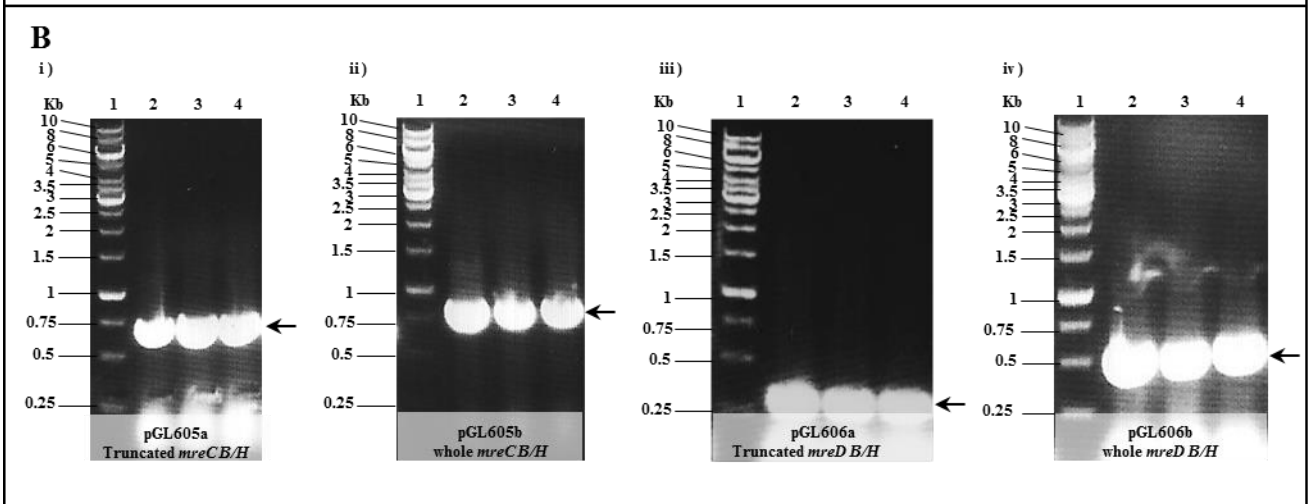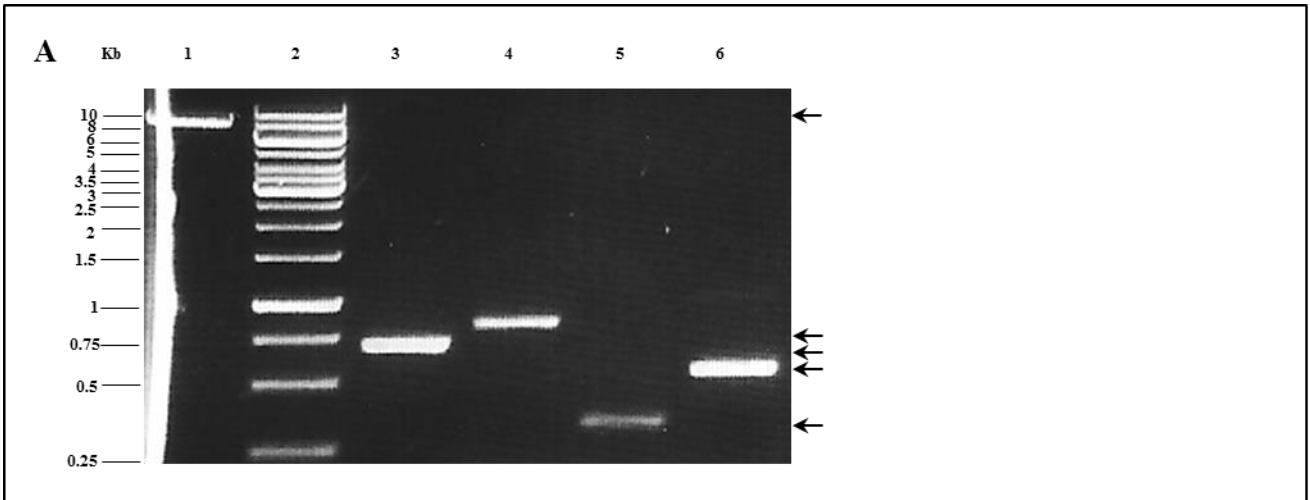
Figure 4-10 Construction of an *S.aureus mreC-gfp+* and *mreD-gfp+* plasmids

1% (w/v) TAE agarose gels were used.

A.	1% (w/v) TAE agarose gel showing *BamH*I and *Hind*III restriction digested pSG1729 (lane 1), PCR products of truncated *mreC* with primers 5HXM49Aa and 3HXM46Aa (lane 3), entire *mreC* with primers 5HXM49Aa and 3HXM46Ab (lane 4), truncated *mreD* with primers 5HXM49Ba and 3HXM46Ba (lane 5) and entire *mreD* with primers 5HXM49Ba and 3HXM46Bb (lane 6). Arrows indicate the expected sizes of 318bp, 542bp, 729bp, 867bp and ~7.6kb respectively. Fragments correspond to those in Fig. 4.9 (ii-iii). Lane 2 contains 1kb DNA ladder used as a marker (Fermentas).

B.	1% (w/v) TAE agarose gel showing PCR amplification of truncated *mreC*, *mreC*, truncated *mreD* and *mreD* using correspondence primers as described in Fig. 4.10A using pGL605a, pGL605b, pGL606a and pGL606b DNA extracted from 3 (of each) randomly selected *E.coli* transformants. i) amplification of truncated *mreC* from pGL605a, ii) amplification of whole *mreC* from pGL605b, iii) amplification of truncated *mreD* from pGL606a and iv) amplification of whole *mreD* from pGL606b. Arrows indicate the expected sizes of 318bp, 542bp, 729bp, 867bp and ~7.6kb respectively. Fragments and plasmids correspond to those in Fig. 4.9 (ii). Lane 1 contains 1kb DNA ladder used as a marker (Fermentas).

C.	1% (w/v) TAE agarose gel showing *BamH*I and *Hind*III restriction digested pGL605a (lane 3 & 4), pGL605b (lane 5 & 6), pGL606a (lane 8 & 9) and pGL606b (lane 12 & 13). 2 clones, which gave positive PCR bands, of each constructs were selected for this testing. Arrows indicate the expected sizes of 318bp, 542bp, 729bp and 867bp respectively. Fragments correspond to those in Fig. 4.9 (ii-iii). Lane 2 and 8 contains pSG1729 digested with the same enzymes by double digestion. Lane 1, 7 and 11 contains 1kb DNA ladder used as a marker (Fermentas).
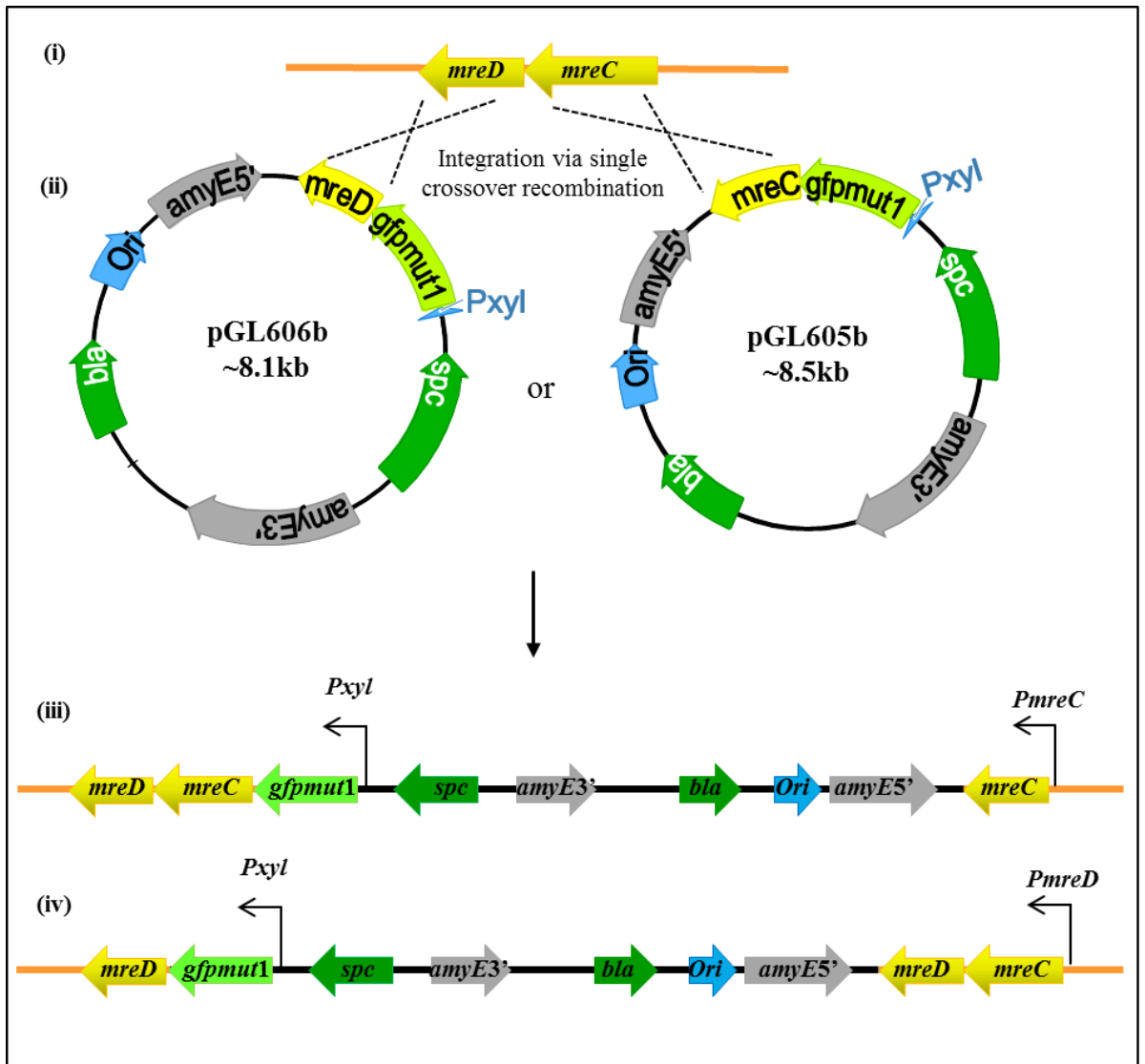
Figure 4-11 Homologous recombination of pGL605b and pGL606b into the *S. aureus* chromosome

DiaGrammatic representation of the outcomes of recombination of pGL605b or pGL606b into the *S. aureus* RN4220 chromosome.

i)   *S. aureus* chromosomal DNA

ii)   Integration of plasmid pGL605b or pGL606b into the *S. aureus* RN4220 chromosome via single crossover.

iii)   Physical map of resulting integration of pGL605b to give strain SJF2688

iv)   Physical map of resulting integration of pGL606b to give strain SJF2692
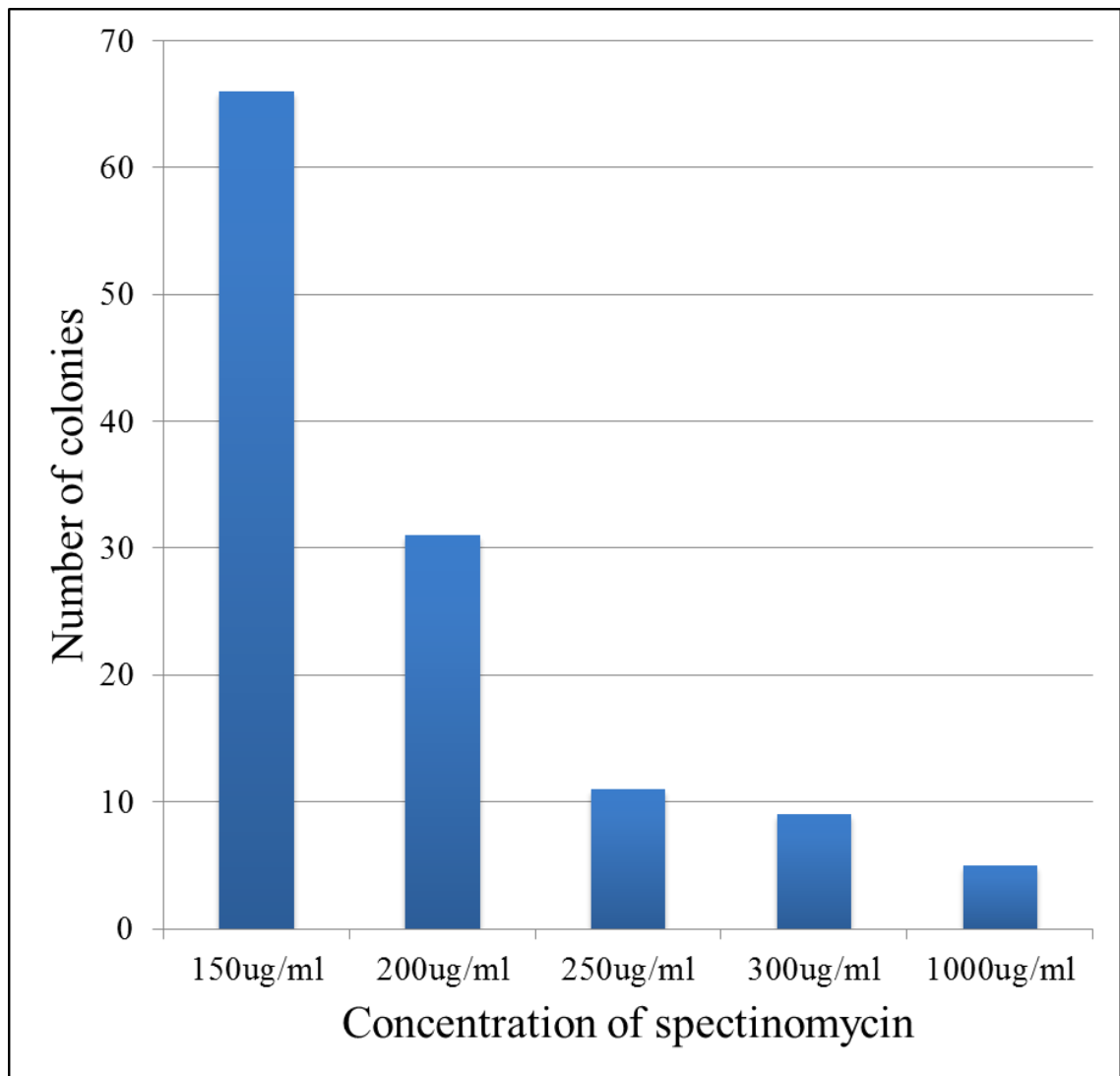
Figure 4-12 Determination of minimal inhibitory concentration for spectinomycin selective marker of pSG1729

100 µl of 10^{-5} dilution of exponentially grows *S. aureus* cells (OD_{600}= ~0.5) were spread on TSB agar containing different concentrations of spectinomycin (Spec). 66 colonies appeared on plates containing 150 µg/ml spectinomycin, 31 colonies appeared on plates containing 200 µg/ml spectinomycin, 11 colonies appeared on plates containing 250 µg/ml spectinomycin, 9 colonies appeared on plates containing 300 µg/ml spectinomycin, and 5 colonies appeared on plates containing 1000 µg/ml spectinomycin. Colonies appeared of different sizes. A lawn of bacteria appeared on the control plate, which does not contain Spec.

Therefore, a minimal inhibitory concentration test was carried out. A series of concentrations of Spec, from 30 µg/ml to 1000 µg/ml, were added to BHI agar just before pouring. 100 µl of a 10^{-5} dilution of exponentially grown RN4220 (OD$_{600}$ = ~0.5) with recombination plasmid pSG1729 was spread on BHI spec plates. A lawn of bacteria appeared on plates containing 30 µg/ml, 50 µg/ml, 80 µg/ml and 100µg/ml spec. Many colonies appeared on plates containing 150 µg/ml, 200 µg/ml and 250 µg/ml (Fig. 4.12). At very high concentration of Spec^R, colonies still appeared. A selection at 300 µg/ml for the 3rd attempt of transformation into *S. aureus* RN4220. 8 colonies of each constructs were grown in the presence of 1 % (w/v) xylose and screened for green fluorescence by microscopy. The resulting strains, SJF2687 (*mreC*~GFP$^+$ *mreC*$^-$), SJF2688 (*mreC*~GFP$^+$ *mreC*$^+$), SJF2691 (*mreD*~GFP$^+$ *mreD*$^+$), and SJF2692 (*mreD*~GFP$^+$ *mreD*$^+$) were used for transduction into *S. aureus* SH1000. Unfortunately, no transductants were green viewed via fluorescence microscopy when approximately 18 colonies of each construct were screened from 3 different transductions. Due to the time constraints, the experiment was not continued.

4.3.5.2 Localisation of *S.aureus* MreC-GFP$^+$ and MreD-GFP$^+$

The subcellular localisation of MreC and MreD in *S.aureus* was visualised by fluorescence microscopy of C-terminal fusions, SJF2100 (*mreC-gfp*$^+$) and SJF2101 (*mreD-gfp*$^+$). Cells were grown to mid-exponential phase (OD$_{600}$ 0.5) before fixation with formaldehyde/gluteraldehyde and staining with vancomycin for peptidoglycan staining. Cells were viewed by fluorescence microscopy using a deconvolution microscope.

MreC showed very weak fluorescence and no obvious localisation pattern (Fig. 4.12 A-D). MreD displayed a distinct localisation patterns (Fig. 4.12 E-H). MreD was predominantly localised at midcell with regular discrete peripheral foci on each cell, or each hemisphere of dividing cells. Independent of the division stage, septal localisation was seen in the majority of the cells (62%). At the early division cycle, MreD was already present at midcell prior to septation (Fig. 4.12 G & Fig. 4.13 A i & ii). When the septa starts invagination (Class II) or is completely closed (Class III), only one localisation pattern was observed, MreD overlaid with septa and also was distributed to the cell periphery. Notably, by the late cell division phase, daughter cells showed equatorial localisation or a distinct regular dotty pattern around the cell periphery and perpendicularly to the current division plane of dividing cells but not at septa. Concomitant labelling with vancomycin further confirmed this apparent cell equatorial or peripheral labelling.

4.3.5.3 Immunolocalisation of MreC

Immunolocalisation of *B. subtilis* MreC showed a diffused staining along the cell periphery with higher intensity at midcell (Lee *et al.* 2003). In *S. pneumoniae*, MreC was also specifically localised to the midcell shown by immunolocalisation (Land & Winkler 2011). The localization of MreC-GFP$^+$ in *S aureus* failed to yield an indicative signal (Fig. 4.12 A-D). Therefore, the subcellular immunolocalisation of MreC in *S.aureus* was carried out. In order to prevent non-specific binding of α-MreC antibodies to *S.aureus* Protein A, immunolocalisation was performed in LC102 (*spa::tet*) (Cooper *et al.* 2009), in which the Protein A encoding gene (*spa*) was replaced with a tetracycline resistance cassette (Hartleib *et al.* 2000). Immunolocalisation was performed as previously described by Pinho and Errington (2005; Section 2.14.3), except that the secondary antibody used was AlexaFluor594-conjugated α-rabbit IgG (Invitrogen) at a dilution of 1:1000, to allow co-localisation studies with GFP-tagged proteins if required.

A range of α-MreC concentrations from 1:100 to 1:1600 were tested, with optimum results observed for 1:100 dilution of the primary antibody (data not shown). Gentle lysis of cells using lysostaphin was carried out to permeabilise the cell wall to allow α-MreC to bind its target. Cells were incubated with lysostaphin at concentrations of 0-12 ng ml^{-1}, since it has previously found that a concentration range up to 15 ng ml^{-1} gives enough permeability without cell lysis (Bottomley, 2011). No fluorescence was observed in controls without primary antibody (Fig. 4.14 A-C). Unexpectedly, MreC is found around the periphery of each cell, or each hemisphere of dividing cells but not at midcell (Fig.4.14 D-F).
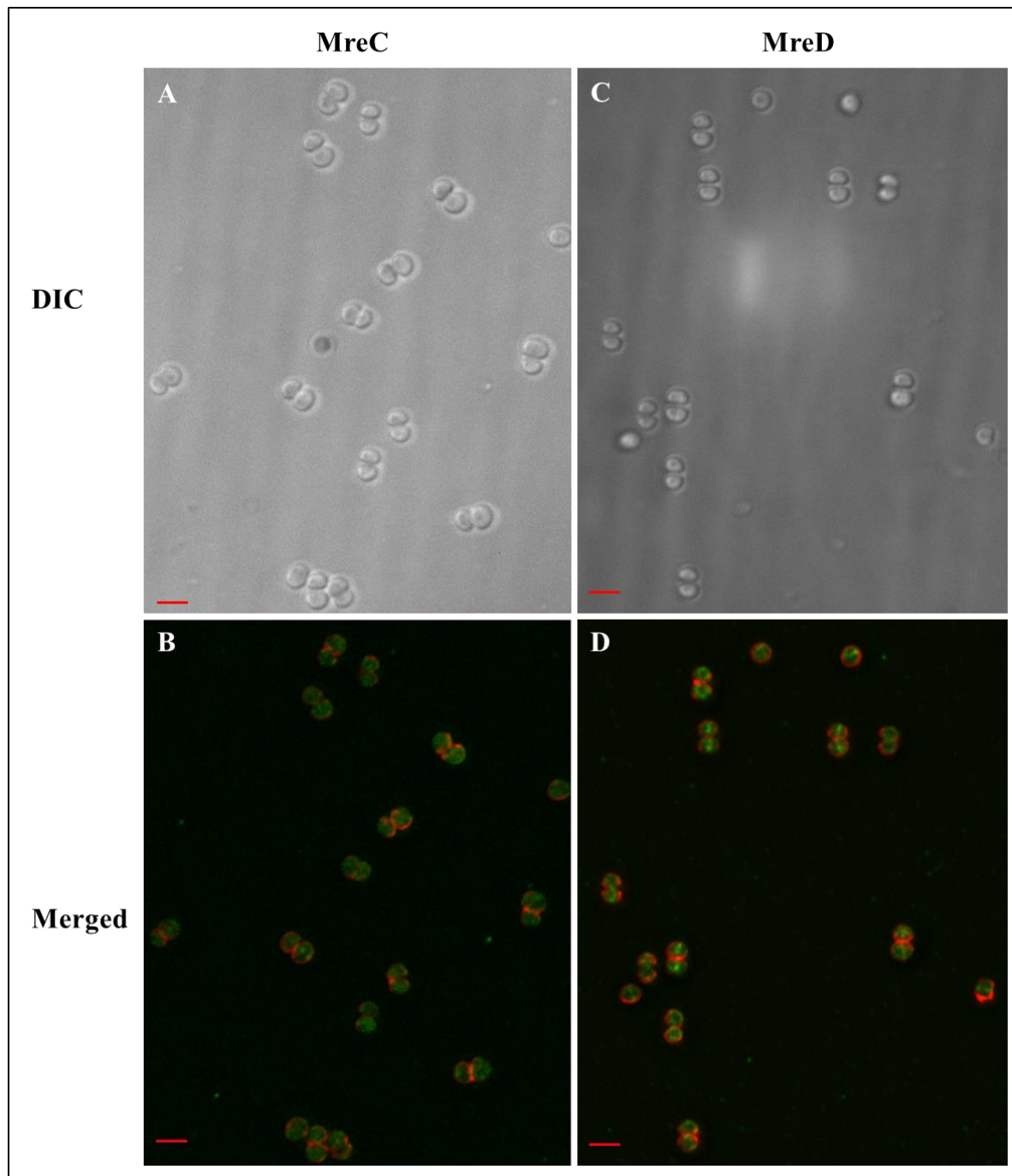
Figure 4-13 Localisation of MreC-GFP+ and MreD-GFP+ *S. aureus* SH1000

Fluorescence images and phase contrast images of SJF2100 (*mreC-gfp*[+]) (A&B) and SJF2101 (*mreD-gfp*[+]) (C&D), which were freshly sub-cultured and grown to mid-exponential phase (OD_{600} 0.5). The localisation of MreC-GFP[+] and MreD-GFP[+] were determined by fluorescent microscopy of fixed cells. All images are to the scale shown by the bar. The MreC-GFP[+] and MreD-GFP[+] signal is shown in green in the images (B&D). peptidoglycan is labelled in red with vancomycin (B&D). Images were acquired using an Olympus IX70 microscope and SoftWoRx 3.5.0 software (Applied Precision). Scale bars represent 2 μm.
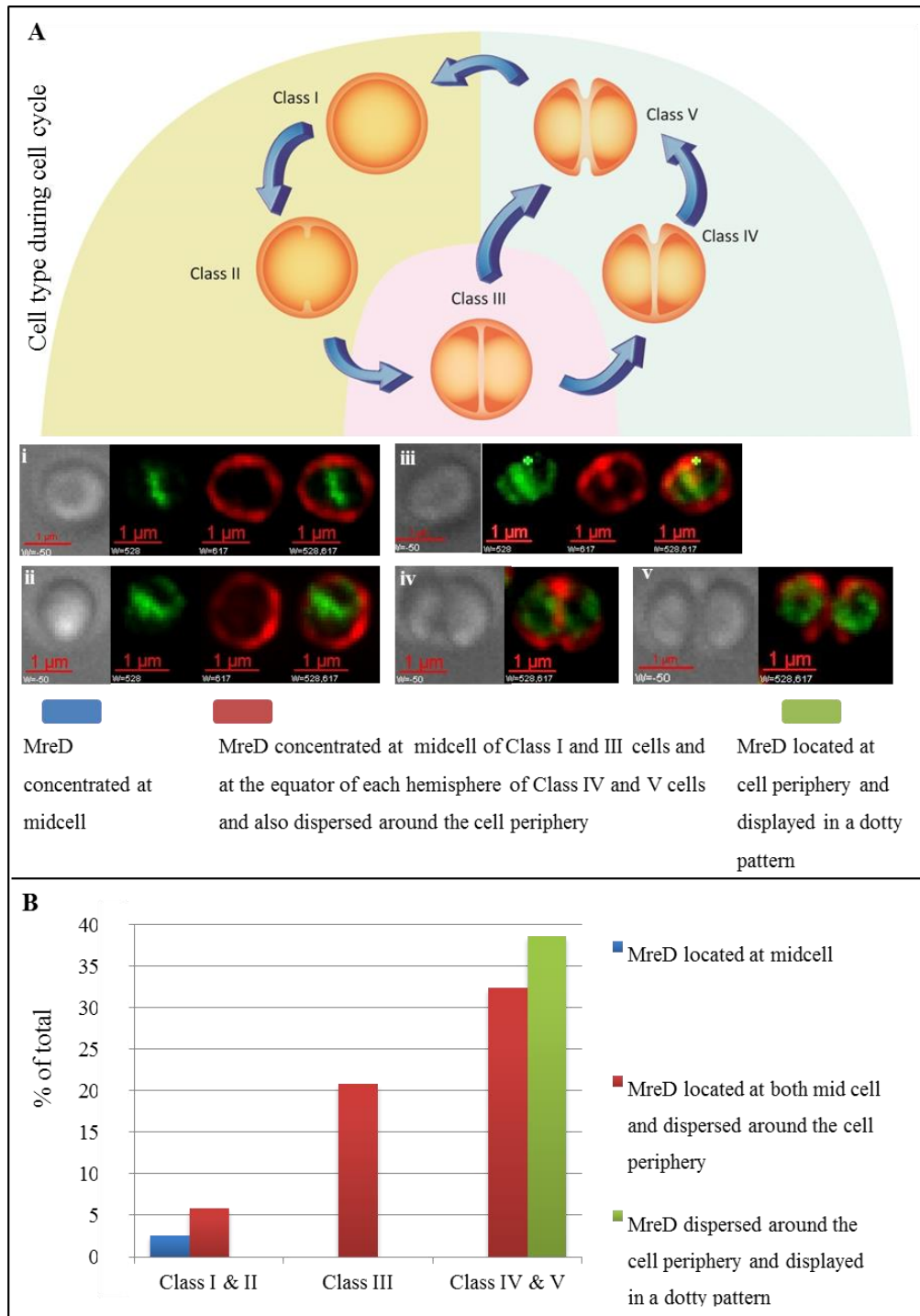
Figure 4-14 Frequency of phenotypes of localisation of MreD-GFP+ in *S. aureus* SH1000

Fresh cells were inoculated into BHI and allowed to grow to an OD_{600} 0.5. The localisation of MreD-GFP+ was determined by fluorescence microscopy. Cells were given one of three phenotypes on the basis of cell division stages and MreD-GFP+ distribution. Examples of the three phenotypes are shown above with MreD-GFP shown in green (A i-v) and vancomycin in red. The frequency of phenotypes of SJF2101 (*mreD-gfp*[+]) is shown. The number of cells measured was 274. Cell measurements were made using SoftWoRx software. Scale bars represent 1 μm.
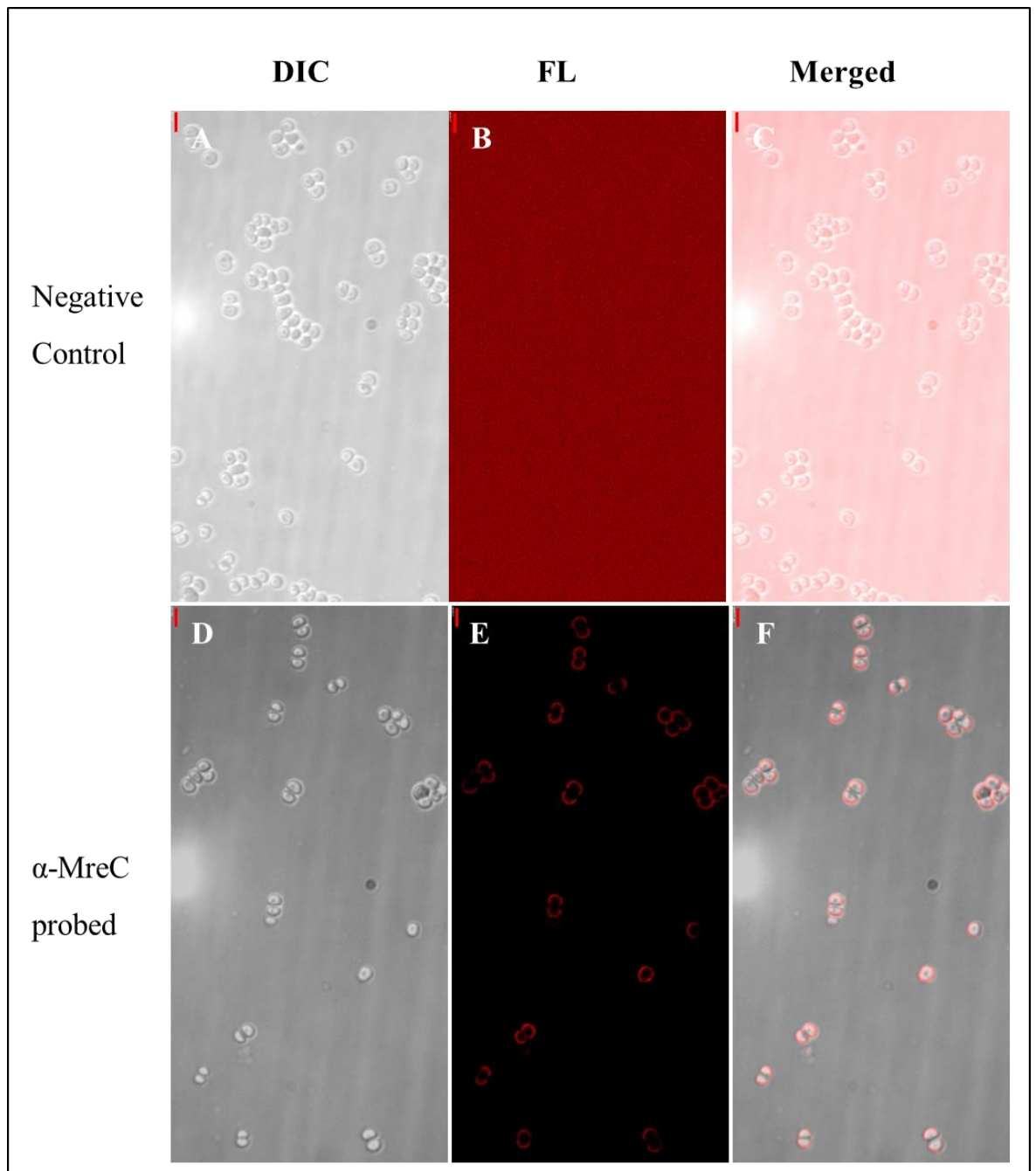
Figure 4-15 Immunolocalisation of MreC in *S. aureus*

A-C, Phase contrast, fluorescence (red 617nm) and the merged images of a negative control without primary antibody.

D-F, phase contrast, fluorescence (red 617nm) and the merged images of *S. aureus spa::tet* probed with α-MreC at 1:100 and detected with AlexaFluor594-conjugated α-rabbit IgG.

Images were acquired using an Olympus IX70 microscope and SoftWoRx 3.5.0 software (Applied Precision). Scale bars represent 2 μm.

155

4.4   Discussion

4.4.1   Localisation of *S. aureus* MreC and MreD

The cMreC has been reported to be present in the periplasmic domain in rod shaped bacteria and an ovococcus (Lee *et al.* 2003; Divakaruni *et al.* 2005; Kruse *et al.* 2005; Lovering & Strynadka 2007). Surprisingly, *S. aureus* MreC was predicted to have an N_{out}-C_{in} membrane topology (SOSUI). However, immunoblot analysis of native *S. aureus* MreC found the protein to be associated with the cell wall not cytosol, as expected, suggesting that like its homologs in other species, the major domain of MreC is also present outside the cell membrane. The C-terminal GFP fusion of MreC did not give enough fluorescence to enable a distinct MreC-GFP localisation confirming that the C-terminal domain is probably on the outside of the membrane, as GFP was thought not normally functional when fused to an extracellular domain of a protein (Feilmeier *et al.* 2000). I propose that *S. aureus* MreC has a single transmembrane spanning helix with a short cytoplasmic N-terminal domain and a large periplasmic C-terminal domain. This topology could be confirmed by protein cleavage of periplasmic proteins (Tjalsma & van Dijl 2005).

Immunofluorescence microscopy showed that MreC did not localise to midcell in *S. aureus*. Previous localisation studies in *B. subtilis* have shown that many divisome components localise to midcell during the division process (Levin & Losick 1996; Edwards & Pojeto 1997; Raskin & deBoer 1997; Levin *et al.* 1999; Daniel & Errington 2000; Daniel *et al.* 2000; Katis *et al.* 2000; Feucht *et al.* 2001; Gueiros-Filho & Losick 2002; Hamoen *et al.* 2006). Some division proteins are localised not only at the midcell but also newly formed cell poles, like DivIVA in *S. pneumoniae* (Fadda *et al.* 2007), PBP3(FtsI) in *M. smegmatis* (Datta *et al.* 2006) and *E. coli* (Weiss *et al.* 1997). Other division proteins (MinD and DivIVA) do not localise to midcell, but along the cell periphery and at newly formed poles in *B.subtilis* and *E.coli* (Cha & Stewart 1997; Edwards & Errington 1997; Raskin & de Boer 1999b, a; Wu *et al.* 2009); whilst localisation of FtsL and DivIB on cell hemispheres persists throughout the division process in *S. aureus*, with midcell localisation only observed during Z ring constriction (Noirclerc-Savoye *et al.* 2005; Bottomley *et al.* 2014).

In *B. subtilis*, MreC is present predominantly at the septum and cell membrane showing a helical pattern (Leaver & Errington 2005). Cell wall synthesis is directed by apparent helical incorporation of new peptidoglycan in the side wall and MreC is thought to play a key role in connecting the intracellular cytoskeleton and the extracellular cell wall synthetic machinery (Leaver & Errington 2005). *S. aureus*, only carries out major cell wall synthesis at the septum, the absence localisation of *S.aureus* MreC at the midcell observed by this study suggests MreC is unlikely to participate in cell division. Indeed, we found that inframe

deletion of *mreC* does not affect cell growth compared to SH1000 and no apparent morphological changes were observed by TEM (Chapter 5). This may further indicate that MreC is not essential for cell division. BACTH showed that MreC interacts with division machinery, including DivIB which is suggested to be required for a molecular checkpoint during cell division to ensure the appropriate assembly of the division machinery at midcell and to prohibit hydrolytic growth of the cell lacking a completed septum (Bottomley *et al.* 2014). In addition, the peripheral localisation of MreC raises the possibility that MreC may play a different role in cell growth in the outer wall, which is not essential for *S. aureus*.

In *S. pneumoniae*, immunolocalisation of MreD showed that MreD localised to the same division sites as MreC, and also cycles to other sites during different phases (Land & Winkler 2011). *S. aureus* MreD was predicted to have an intracellular C terminus, which was fused to GFP. Concomitant labelling of MreD with peptidoglycan synthesis using fluorescent vancomycin showed that MreD is localised to the midcell before septum formation in single cells and is mainly retained at midcell during peptidoglycan synthesis. By the late cell division stage, MreD is seen mainly distributed in the middle of daughter cells or around the cell periphery showing a clear dotty pattern reminiscent of GpsB localisation pattern in *S. pneumoniae* (Land *et al.* 2013). MreD may localise to the new division plane prior to Z-ring formation at the midcell. This seems against the previous finding that FtsZ ring formation is thought to represent the first stage in bacterial cell division, with all other division proteins requiring FtsZ for correct localisation (Errington *et al.* 2003). Since MreD has the ability to interact with FtsZ and late cell division proteins (Chapter 3), it may provide a guidance between late and early division processes. Like *C. crescentus* MreD (White *et al.* 2010), *S.aureus* MreD may be also play a key role in determining the localisation of cell wall synthetic complexes.

Localisation of the cell division protein DipM of *C. crescentus* has been shown to depend on the distinction between septal and non-septal peptidoglycan (Poggio *et al.* 2010). Previous labelling of *S. aureus* and *S. pneumoniae* with fluorescent vancomycin showed that peptidoglycan synthesis occurs primarily at midcell (Pinho & Errington 2003; Ng *et al.* 2004). Despite the Z-plane sectioning angle, MreD predominantly present at the middle of single cells prior to apparent septum formation (Fig. 4.13 Class I & II) and the equator of daughter cells by late division phase (Fig. 4.13 Class IV & V) before peptidoglycan synthesis at the new septum. Atomic force microscopy (AFM) of *S. aureus* peptidoglycan revealed a thickening of peptidoglycan, described as a 'piecrust', midcell at the site of the presumptive septum (Turner *et al.* 2010). After division, this structure remains as orthogonal 'ribs' (quarter, half and whole), marking the location of previous division planes, and allowing conservation

of division of *S.aureus* in sequentially orthogonal planes. A quarter rib determines a new piecrust formation plane. Like DivIB, MreD may also recognise the specific peptidoglycan architecture and/or structure of the quarter rib and therefore directing the divisome to the correct future division site. Simultaneous AFM and fluorescence imaging of MreD in *S. aureus* would show direct localisation of the protein to specific peptidoglycan structures.

4.4.2   The cell wall binding properties of MreCD in *S. aureus*

Previous studies found that the cell shape proteins MreC and MreD were involved in positioning of the peptidoglycan synthesis machinery and ultimately direct incorporation of new cell wall material in rod shaped cells (Lovering & Strynadka 2007; White *et al.* 2010). MreC colocalises with PBP2 in *Rhodobacter sphaeroides* (Slovak *et al.* 2006). *S. aureus* MreCD interacts with PBPs shown by BACTH assay (Chapter 3). Immunoblot analysis of native *S.aureus* MreC found the protein to be associated with the cell wall, indicating *in vivo* binding of MreC to peptidoglycan and suggesting the function of *S. aureus* MreC as a peptidoglycan-binding protein. The peptidoglycan binding property should be further investigated *in vitro* by sedimentation analysis to help understanding the role of *in vivo* peptidoglycan binding by MreC in cell division.

4.4.3   Future directions

The construction of the MreD expression strain was terminated, since MreD is a very hydrophobic polytopic membrane protein which may potentially lead to difficulties in expression and purification. However, generation of recombinant MreD protein will help further understanding the localisation and function of MreD in cell division.

Construction of an N-terminal GFP fusion of MreC is required to confirm the peripheral localisation detected by immunfluorescence microscopy. MreC and MreD interact with many essential cell division proteins. Co-labelling studies of MreC and interacting proteins detected by BACTH in *S. aureus* would be useful to determine if MreC or MreD co-localise with division proteins. The localisation of MreC and MreD could also be shown in strains depleted for essential division components in order to investigate the dependence of MreC and MreD localisation on other facters.

Wall teichoic acids (WTAs) have been shown to effect cell wall protein localisation (Schlag *et al.* 2010). The role of WTAs, if any, in regulating MreC or MreD localisation will also provide insights into the involvement of WTAs in cell division. Construction of an *S. aureus*

tagO mutation expressing MreC-GFP$^+$ or MreD-GFP$^+$ from the chromosome may allow the affect of WTAs on the localisation of MreCD to be fully investigated.

Finally, it is important to further establish the putative nature of binding of cMreC to the cell wall by sedimentation or more quantitative assays, such as surface plasmon resonance.

5 Chapter 5 Functional Analysis of MreC and MreD

5.1 Introduction

The *mreCD* genes are conserved throughout Gram-negative species and a large proportion of low GC Gram-positive bacteria, including *S. aureus, B. subtilis* and *S. pneumoniae* (Fig. 5.1 & 5.2). In many organisms, *mreC* and *mreD* are co-transcribed with *mreB*, which is a putative cytoskeletal element. It was previously thought that the actin homologue MreB forms helices lying just beneath the cell membrane (Kruse *et al.* 2005), but later studies suggest that it forms dynamic patches that circulate around the cell in *E. coli* (van Teeffelen *et al.* 2011), *C. crescentus* (Kim *et al.* 2006; Biteen *et al.* 2008) and *B. subtilis* (Dominguez-Escobar *et al.* 2011; Garner *et al.* 2011). Very recently, a co-crystallisation study of *C. crescentus* MreB shows that MreB appears to form pairs of straight protofilaments that adopt an antiparallel arrangement rather than a helical pattern *in vitro* and *in vivo* (van den Ent *et al.* 2014). MreB interacts with the elongasome, including MreC and MreD (van den Ent *et al.* 2014). Interestingly, cocci lack MreB homologues, but have MreC and MreD homologues as shown in Fig. 1.1 (Margolin 2009). Previous chapters have shown that *S. aureus* MreC and MreD interact with a lot cell division proteins and seem to co-localise with them.

In rod-shaped bacteria, MreC and MreD, along with MreB, are essential cell shape-determining morphogenetic proteins (Land & Winkler 2011). In *E. coli*, the MreBCD complex was suggested to direct longitudinal cell wall synthesis in a mechanism critical to maintain cell morphology (Kruse *et al.* 2005). Depletion of MreC or MreD produces spherical cells with apparent loss of cell wall integrity (Wachi *et al.* 1987; Kruse *et al.* 2005). In *B. subtilis*, low levels of cellular MreC leads to bent cell formation showing a "shepherd's crook" appearance, which can be twisted into irregular shapes by further reduction of the MreC level (Lee & Stewart 2003). MreC-depleted *B. subtilis* appear to have weakened cell wall structure, which is prone to lysis caused by osmotic pressure, indicating a role of MreC in peptidoglycan synthesis (Lee & Stewart 2003). Depletion of MreC and/or MreD results in an inability of cells to elongate and production of irregular shaped ghost cells. Interestingly, those swollen cells were still able to generate division septa with asymmetric multi-septa, presumably due to the loss of localisation of elongasome and PBPs (Lee & Stewart 2003; Leaver & Errington 2005). An *mreC* null mutant can be successfully constructed, However, construction of an *mreD* mutant in *B. subtilis* failed, suggesting that the requirement for MreD may be more stringent than for MreC in *B. subtilis* (Leaver & Errington 2005). *C. crescentus* *mreC* mutants are able to expand, however appear to arrest in expansion along the long axis

of the cell probably due to loss of spatial localisation of PBPs and consequently reduced peptidoglycan synthetic activity (Divakaruni *et al.* 2007).

In *H. pylori,* deletion of *mreC* gene is not achievable, indicating it is essential for cell viability (El Ghachi *et al.* 2011). Conditional mutational analysis of *H. pylori mreC* showed enlarged spherical cells, subsequent to division arrest and eventually lysis due to disruption of the PBP2/MreC complex formation (El Ghachi *et al.* 2011). Overproduction of MreC results in long *H. pylori* cells, suggesting that the sustained expression of *mreC* may prevent the assembly of the divisome (El Ghachi *et al.* 2011). In *S. coelicolor,* absence of MreC or MreD does not affect viability, however, leads to germination of enlarged spores with a diffused cell wall and the spores appear to be irregular in shape, suggesting that peptidoglycan synthesis is influenced by MreCD depletion (Kleinschnitz *et al.* 2011).

In the ovococcus bacterium *S. pneumoniae*, deletion of *mreC* and/or *mreD* genes results in cell rounding, chain formation and rapid lysis in strain D39 (Land & Winkler 2011). *S. pneumoniae* D39 MreC and MreD are only essential for growth in the presence of functional PBP1a and depletion of MreCD results in aberrant PBP1a localization, suggesting MreCD cooperates with PBP1a in peripheral PG synthesis (Land & Winkler 2011).

In *S. aureus*, a close relative to *B. subtilis* (Fig. 5.1 & 5.2), the role of MreCD remains unknown, they have been suggested not to be essential (Chaudhuri *et al.* 2009). To understand the function of the *mreC* and *mreD* genes of *S. aureus*, non-polar replacement mutants of *mreD* and *mreCD*, and an in-frame *mreC* deletion were constructed in this study. The results implied that the proteins have different roles in cell division of *S. aureus* and MreD may have a crucial role in initialisation of the precise septum formation at mid-cell.
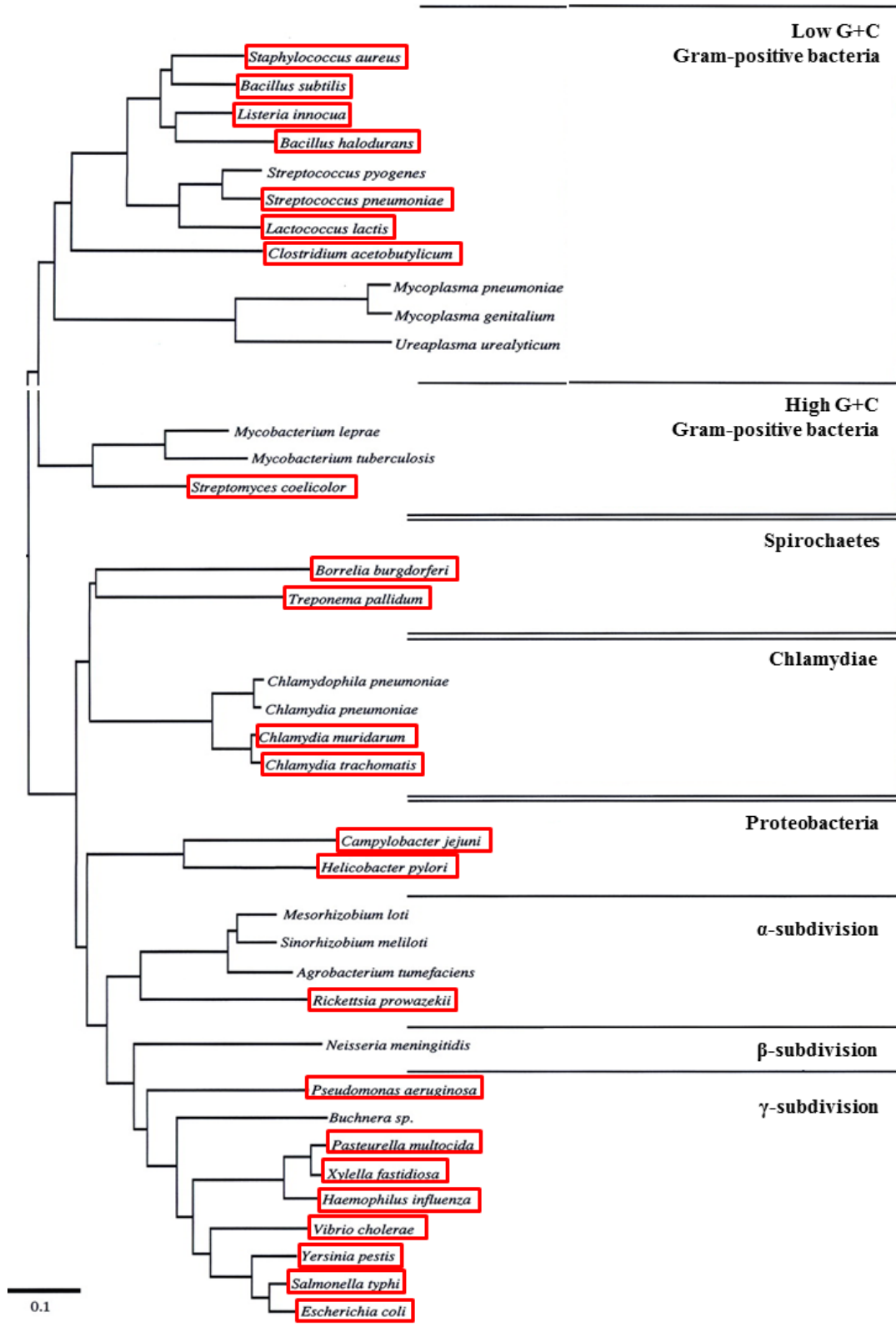
Figure 5-1 Phylogenetic distribution of *mreC* in selected bacteria. The phylogenetic relationship between organisms is based on 16S sequences. (Adapted from Condon & Putzer, 2002). Red boxes indicate organisms possessing apparent *mreC* homologues, based on BlastP probability ($P < 10^{-15}$).
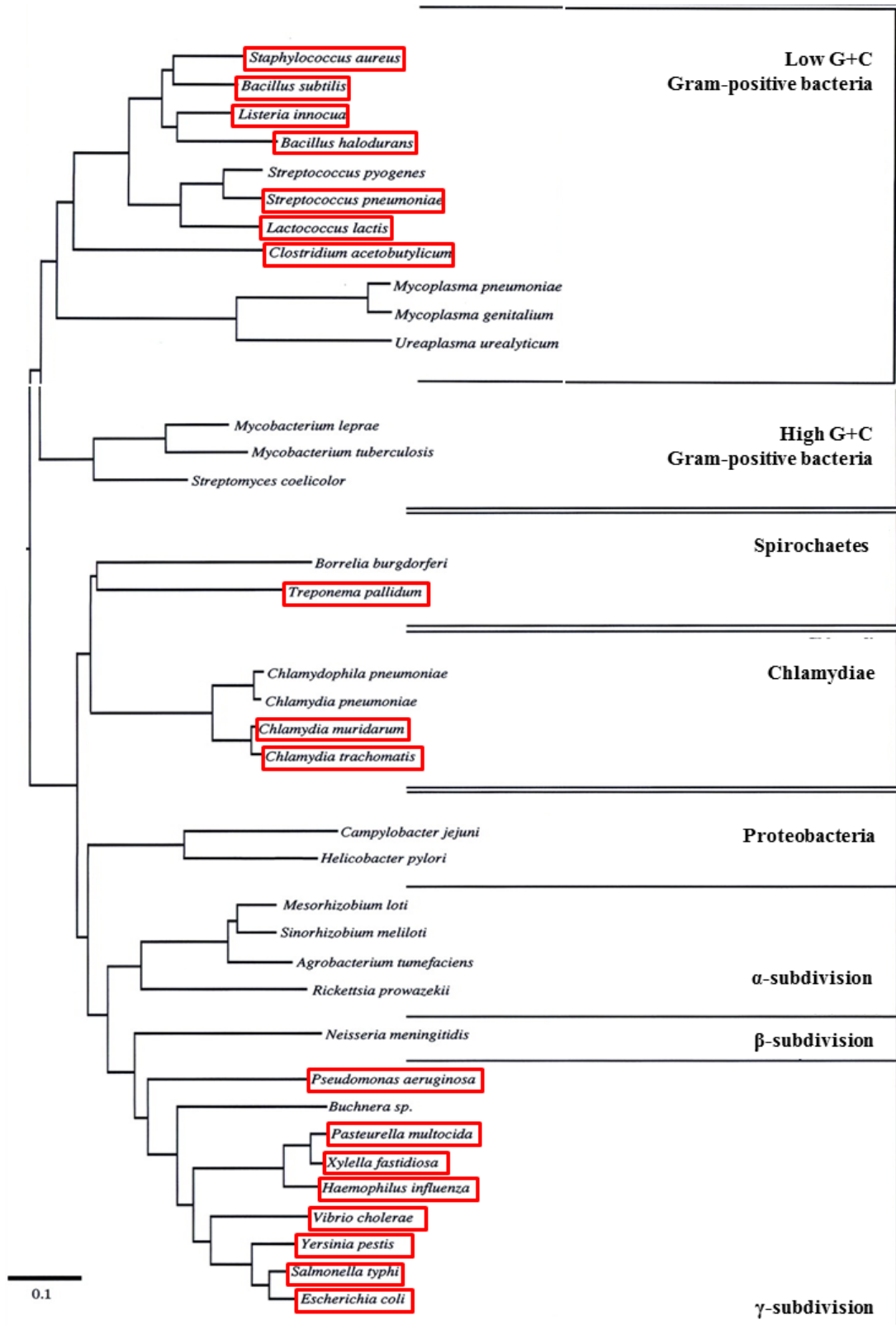
Figure 5-2 Phylogenetic distribution of *mreD* in selected bacteria. The phylogenetic relationship between organisms is based on 16S sequences. (Adapted from Condon & Putzer, 2002). Red boxes indicate organisms possessing apparent *mreD* homologues, based on BlastP probability ($P < 10^{-15}$).

163

5.2   Aim of this chapter

- Construction of *mreC* and *mreD* null mutants
- Investigate the role of MreC and MreD in *S. aureus*

5.3   Results

5.3.1   Construction of an *S. aureus mreC* deletion mutant

In order to determine the role of *mreC* in *S. aureus*, an inframe deletion mutant was constructed. As *mreC* and *mreD* are present on the same operon, there could be polar effects upon inactivation of *mreC*. The construction of an unmarked inframe deletion of *mreC* was therefore carried out to prevent downstream effects on *mreD* (Fig 5.3 - 5.6).

The vector pIMAY was constructed to allow mutagenesis of genes in non-naturally transformable Gram positive bacteria, including *S. aureus* (Monk *et al.* 2012). Construction of deletion mutants using pIMAY is performed via a two-step strategy; initially homologous recombination occurs between the target sequence in the chromosome and a homologous sequence on the temperature-sensitive plasmid. Integration of the plasmid into the chromosome by a single crossover event is selected for by growth at a non-permissive temperature in the presence of selective pressure. After integration, growth under selective conditions leads to a second recombination event that results in resolution of the plasmid and potential excision of the gene of interest from the chromosome. pIMAY is an *E. coli-S. aureus* shuttle vector, containing a low copy number *E. coli* origin of replication (*p15A*), a highly thermosensitive replicon (*repA^{TS}*) for Gram-positive bacteria (Maguin *et al.* 1992). Also it encodes a highly expressed chloramphenicol resistance marker (*cat^R*) for selection in both Gram-positive and Gram-negative bacteria and a tetracycline-inducible antisense *secY* region (*anti-secY*) which upon induction inhibits bacterial growth (Ji *et al.* 2001), thus giving a positive selection for plasmid excision from the chromosome. Unmarked deletion mutations of the *S. aureus hsdR* and *sauUSI* genes, thought to be involved in restriction modification, was successfully achieved with pIMAY (Monk *et al.* 2012). Thus, pIMAY is a suitable system for constructing an unmarked in frame deletion of *mreC* in *S. aureus*.

Regions upstream and downstream of the *mreC* gene were amplified by PCR using *S. aureus* SH1000 genomic DNA as template and primer pairs 5HXM292/5GLUSh270C and 5GLUSh270D/3GLUSh270A respectively (Table 2.6). *Sac*I and a *Kpn*I restriction enzyme sites were introduced to the 5' and 3' end of upstream and downstream arms, respectively, to allow ligation into pIMAY. Products of sizes consistent with the expected 1289 bp and 1570

bp were obtained (Fig. 5.3 B). The upstream arm carries the native promoter of the *mreC* gene; the downstream arm encodes residues 807-843 of *mreC*, corresponding to the extreme C terminus of MreC subdomain, which carries the ribosome binding site of the *mreD* gene and the entire *mreD* gene. The resulting PCR products were purified from a 1% (w/v) agarose gel using a QIAquick gel extraction kit (Chapter 2.7.4) and restriction digested with *Not*I/*Sac*I and *Not*I/*Kpn*I respectively. The recipient plasmid pIMAY vector was also restricted with *Sac*I/*Kpn*I resulting in the expected size of 5743 bp (Fig. 5.3 C) followed by dephosphorylation using alkaline phosphatase (Chapter 2.8.3). All three digested DNA fragments were purified by QIAquick gel extraction and mixed at approximately a 1:3 molar ratio of vector DNA to insert DNA in a three-way ligation reaction (Fig 5.3 A ii-iv). The ligation mixture was ethanol precipitated and transformed into *E. coli* TOP10 electrocompetent cells (Invitrogen) and selected on LB 15µg ml^{-1} chloramphenicol (Cat) at 37°C. 14 colonies out of 92 were randomly selected and the insertion of the downstream *mreC* fragment was screened for the presence of the *mreD* gene by colony PCR with the primer pair 5GLUSh270D/3GLUSh270B (Fig 5.3 D). Four positive clones were verified by plasmid purification, restriction digestion with *Nco*I (Fig 5.3 E) and with *Sac*I/*Kpn*I (Fig 5.3 F), which cut the insert back out, and separation by 1% (w/v) agarose gel electrophoresis. A positive clone, named pXIM5, was further confirmed by DNA sequencing (Chapter 2.8.10).

The resulting plasmid was then purified using a QIAprep^{TM} Miniprep kit (Chapter 2.7.2) and ethanol precipitation (Chapter 2.7.6). The plasmid was dissolved 10 µl of sdH$_2$O the concentrated pXIM5 DNA (~ 1 µg) was transformed into electrocompetent *E. coli* DC10B (DH10BΔ*dcm*) (Monk & Foster 2012). DC10B, a mutant with the *dcm* gene deleted, allows direct transformation into Gram-positive strain *S. aureus*. Selection was on LB 15 µg ml^{-1} cat and thousands of colonies were produced after 18h at 37°C. 4 clones of pXIM5 were verified by PCR of *mreD* gene and *Sac*I/*Kpn*I or *Nco*I restriction digestion (data not shown). 2 clones were further confirmed by DNA sequencing.

The resulting plasmid was purified using QIAprep^{TM} Midiprep kit from *E. coli* DC10B and ethanol precipitation. 10 µg of the concentrated pXIM5 DNA in sdH$_2$O was transformed into electrocompetent *S. aureus* RN4220 (Chapter 2.10.2.2). Selection was on TSB 10 µg ml^{-1} cat and 334 colonies were produced after 2 O/N at 28°C. 16 colonies were streaked on TSB 10 µg ml^{-1} cat again at 28°C to obtain pure isolated colonies. 4 clones from a streaking where all colonies showed a uniformed size, were tested for the presence of the plasmid pXIM5 by colony PCR using forward primers within upstream region of *mreC* and backward primers annealing to the downstream region of *mreD*, the primer pair 5GLUSh270B/3GLUSh270B. 1 clone yielded a product consistent with the expected size of 743 bp (results not shown).
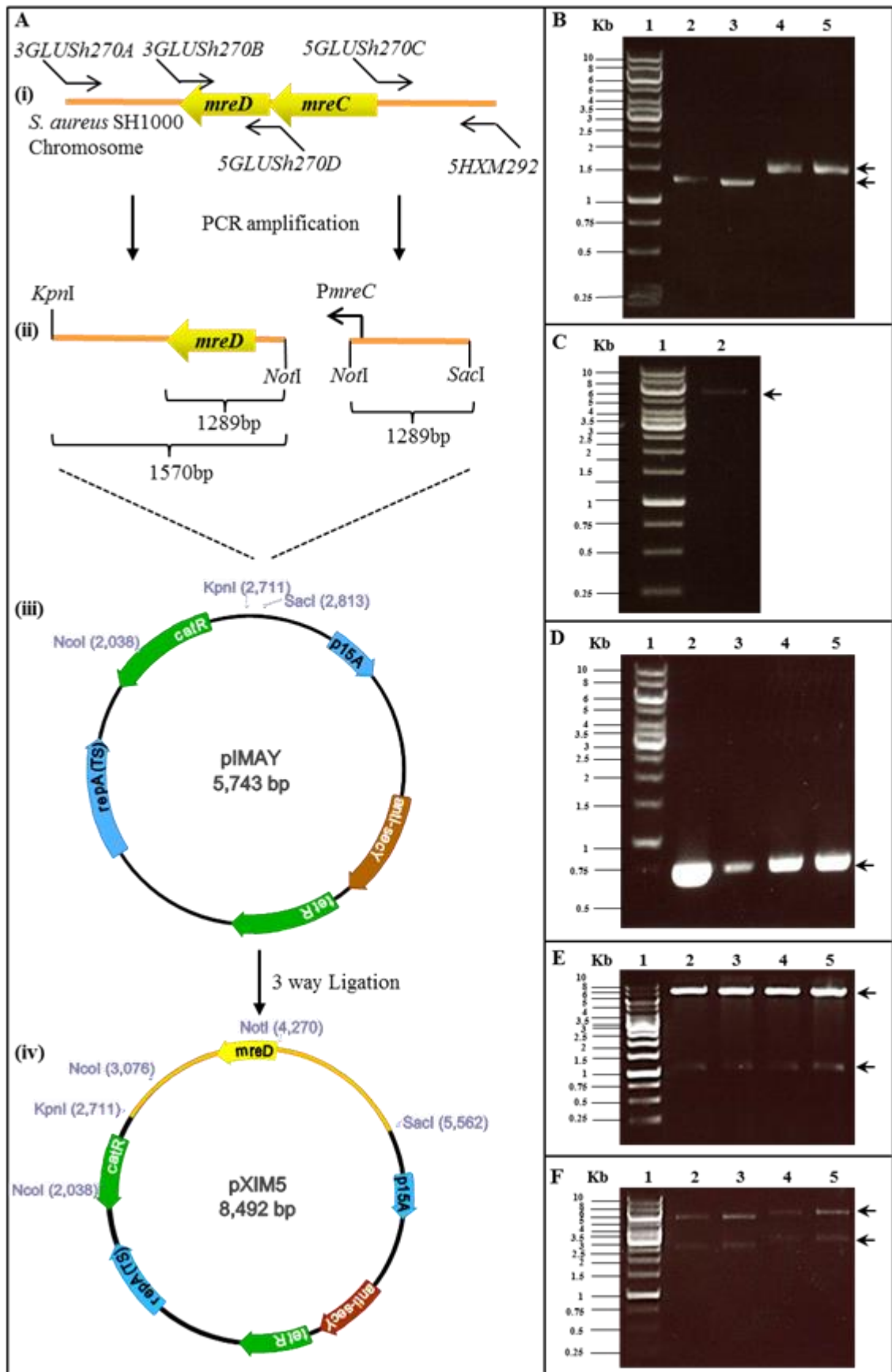
Figure 5-3 Construction of plasmid pXIM5 for deletion of *mreC*

A.   DiaGrammatic representation of the construction of pXIM5 (*mreC::tet::cat*) in *E. coli*. Primer binding sites for 3GLUSh270A, 3GLUSh270B, 5GLUSh270C, 5GLUSh270D and 5HXM292 and relevant restriction sites used are shown. i) *S. aureus* chromosomal DNA; ii) PCR fragments to be cloned into pIMAY (iii); iv) Resulting pXIM5.

B.   1% (w/v) TAE agarose gel showing products of PCR amplification of the *mreC* upstream region with primers 5HXM292 and 5GLUSh270C (lane 2 and 3) and *mreC* downstream region with primers 5GLUSh270D and 3GLUSh270A (lane 4 and 5) using SH1000 genomic DNA as template corresponding to those in panel A(i). Arrows indicate the expected sizes of 1289bp and 1570bp respectively. Fragments correspond to those in panel A(ii). Lane 1 contains 1kb DNA ladder used as a marker.

C.   1% (w/v) TAE agarose gel showing a *NotI* restriction digestion of the pIMAY shuttle vector. An arrow indicates a band at the expected size of 5740bp (lane 2) and corresponds to the restriction map shown in panel A (iii). Lane 1, 1kb DNA ladder used as a marker.

D.   1% (w/v) TAE agarose gel showing PCR amplification *mreD* region with primers 5GLUSh270D and GLUSh270B and using pXIM5 DNA extracted from 4 randomly selected *E. coli* transformants, termed pXIM5.1-4 (lane 2-4). An arrow indicates bands at the expected size of 630bp. Fragments correspond to those in panel A(ii). Lane 1 contains 1kb DNA ladder used as a marker.

E.   pXIM5.1-4 showing the presence of the *mreD* gene in Panel D were then restriction digested with *Nco*I and analysed by electrophoresis on a 1% (w/v) TAE agarose gel. Products of the expected 2232 and 6260 bp were obtained (indicated by arrows) as shown by the restriction map in panel A(iv). Lane 1, 1kb DNA ladder used as a marker.

F.   pXIM5.1-4 were restriction digested with *Kpn*I and *Sac*I and analysed by electrophoresis on a 1% (w/v) TAE agarose gel. Products of the expected 2851 and 5641 bp corresponding to upstream region and downstream region of *mreC* insert (indicated by arrow), as shown by the restriction map displayed in panel A(iv). Lane 1 contains 1kb DNA ladder used as a marker.

The positive clone was lysed with Φ11 and plasmid transferred to SH1000 via transduction at 28°C. 6 clones were tested for the presence of the plasmid pXIM5 (Fig. 5.4 B). Integration of the plasmid into the chromosome was achieved by successive plating the resulting strain (7) at the non-replicating temperature of either 37°C or 39°C on TSB 10 µg ml⁻¹ cat (Fig. 5.4 A). Growth of clones at 37°C showed heterogeneous colony size, therefore discarded. 16 well isolated colonies were picked up from 39°C incubated plates where only one size of colonies was visible. The upstream arm single cross-over construct (Fig. 5.4 A iii) was confirmed by genomic DNA extraction and PCR amplification with primer pair 5GLUSh270B/ FWD (Fig. 5.4 C). After integration, an isolate was inoculated in TSB at 39°C, a serial dilution of the cell culture was plated on BHI in the presence of 1 µg ml⁻¹ anhydrotetracycline (ATc), which induces the expression of *secY* antisense RNA therefore prevents growth of merodiploids that possess the integrated plasmid and selects for cells that have lost the plasmid insertion (Bae & Schneewind 2006), for 5 O/N at 28°C. This leads to a second recombination event that result in resolution of the plasmid and potential excision of the gene of interest from the chromosome (Fig. 5.4 A i) (Monk *et al.* 2012). Positive clones were patched onto BHI 10 µg ml⁻¹ cat and then BHI 1 µg ml⁻¹ ATc for 24h at 37°C (Fig. 5.5). 6 cat sensitive ATc resistant clones were obtained.

In the presence of ATc, the merodiploids may undergo two types of excision: single cross-over at the upstream region of *mreC*, in which generates wild type clones; single cross-over at the downstream region of *mreC*, in which generates a *ΔmreC* mutant. The inframe deletion of *mreC* was screened for by genomic DNA extraction (Chapter 2.7.1) and PCR with primer pair 5GLUSh270B/3GLUSh270D and 5GLUSh270B/3GLUSh270B (Fig. 5.6 A ii). 2 out of 6 clones yielded products consistent with the expected sizes of 282 bp and 743 bp respectively (Fig. 5.6 B). The resulting mutant (SJF4098) was further verified by Southern blot. Genomic DNA from SH1000 and SJF4098 (*ΔmreC*) were digested with *BspH*I overnight. A DIG-labelled probe, consisting of a 387bp region downstream of *mreCD*, was prepared using primers 3HXM39-11A and 3GLUSh270C (Table 2.6). The hybridizing bands for *BspH*I digestion of SH1000 genomic DNA and SJF4098 were consistent with the expected of 2949bp and 2139 bp respectively (Fig. 5.6 C). The downstream sequence of *mreC* gene was also confirmed to be identical to *mreD* gene by DNA sequencing.

Thus, *mreC* can be deleted and it is not essential for the growth of *S. aureus*.

A

(i)

mreD *mreC* *S. aureus* SH1000 Chromosome

or

NotI (4,270)

mreD

KpnI (2,711)

SacI (5,562)

catR

pXIM5
8,492 bp

p15A

repA(TS)

anti-secY

tetR

Integration via single crossover recombination

(ii) *3GLUSh270B* *FWD* *3GLUSh270B*

mreD P₁₅ₐ anti-secY tet^R repA^TS cat^R *mreD* *mreC*

or *5GLUSh270B* *REV* *5GLUSh270B*

(iii) *3GLUSh270B* *FWD* *3GLUSh270B*

mreD *mreC* P₁₅ₐ anti-secY tet^R repA^TS cat^R *mreD*

5GLUSh270B *REV* *5GLUSh270B*

B kb 1 2 3 4 5 6 7

10
8
6
5
4
3.5
3
2.5
2

1.5

1

0.75

0.5

C Kb 1 2 3 4 5 6 7 8

10
8
6
5
4
3.5
3
2.5

2

1.5

1

0.75

0.5

0.25

Figure 5-4 Homologous recombination of pXIM5 into *S. aureus* SH1000

A.   DiaGrammatic representation of the outcome of recombination of pXIM5 into the *S. aureus* SH1000 chromosome by single crossover. Primer binding sites for 5GLUSh270B, 3GLUSh270B, FWD and REV and the *Kpn*I, *Sac*I and *Not*I restriction sites used in ligation into pIMAY are shown. Downstream arm single crossover events would lead to outcome shown in (ii) and upstream arm single crossover events would lead to outcome shown in (iii).

B.   1% (w/v) TAE agarose gel showing products of PCR of *mreD* gene with primers 5GLUSh270B and 3GLUSh270B using chromosomal DNA extracted from 6 *S. aureus* SH1000 transformants, termed pXIM5.1.4.6.7, pXIM5.1.4.6.9-11, pXIM5.1.4.6.14 and pXIM5.1.4.6.16 (lane 2-7). Arrow marks the expected sizes of 743bp. Lane 1 contains 1kb DNA ladder used as a marker.

C.   1 % (w/v) TAE agarose gel showing products of PCR amplification of downstream sequences of *mreC* gene with primers 5GLUSh270B and FWD using chromosomal DNA extracted from 7 *S. aureus* SH1000 transductants, listed above (lane 2-8).   Arrow marks the expected sizes of 1763bp. Lane 1 contains 1kb DNA ladder used as a marker.
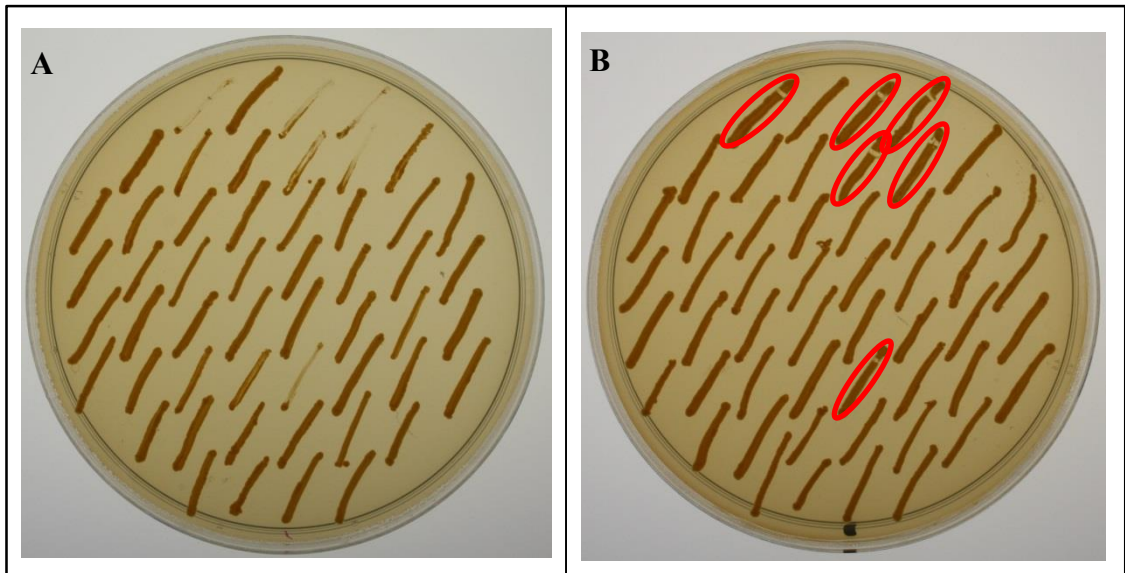
Figure 5-5 Drug sensitivity test of the plasmid pXIM5 excision in *S. aureus* SH1000

A.   Colonies appearing on the ATc plates were firstly patched onto BHI 10 µg ml^{-1} cat.

B.   The same colonies were then secondly patched onto BHI µg ml^{-1} ATc at 37°C. The red circle indicates the selected clones for further confirmation.

A

(i) mreD mreC P15A anti-secY tetR repATS catR mreD

REV

Excision

(ii) 3GLUSh270B 3GLUSh270D
BspHI PmreC BspHI
mreD
PROBE
5GLUSh270B
S. aureus mreC deleted SH1000 Chromosome
2139bp

or

(iii) 3GLUSh270B 3GLUSh270D
BspHI BspHI
mreD mreC
PROBE
5GLUSh270B
S. aureus SH1000 Chromosome
2949bp

B

C
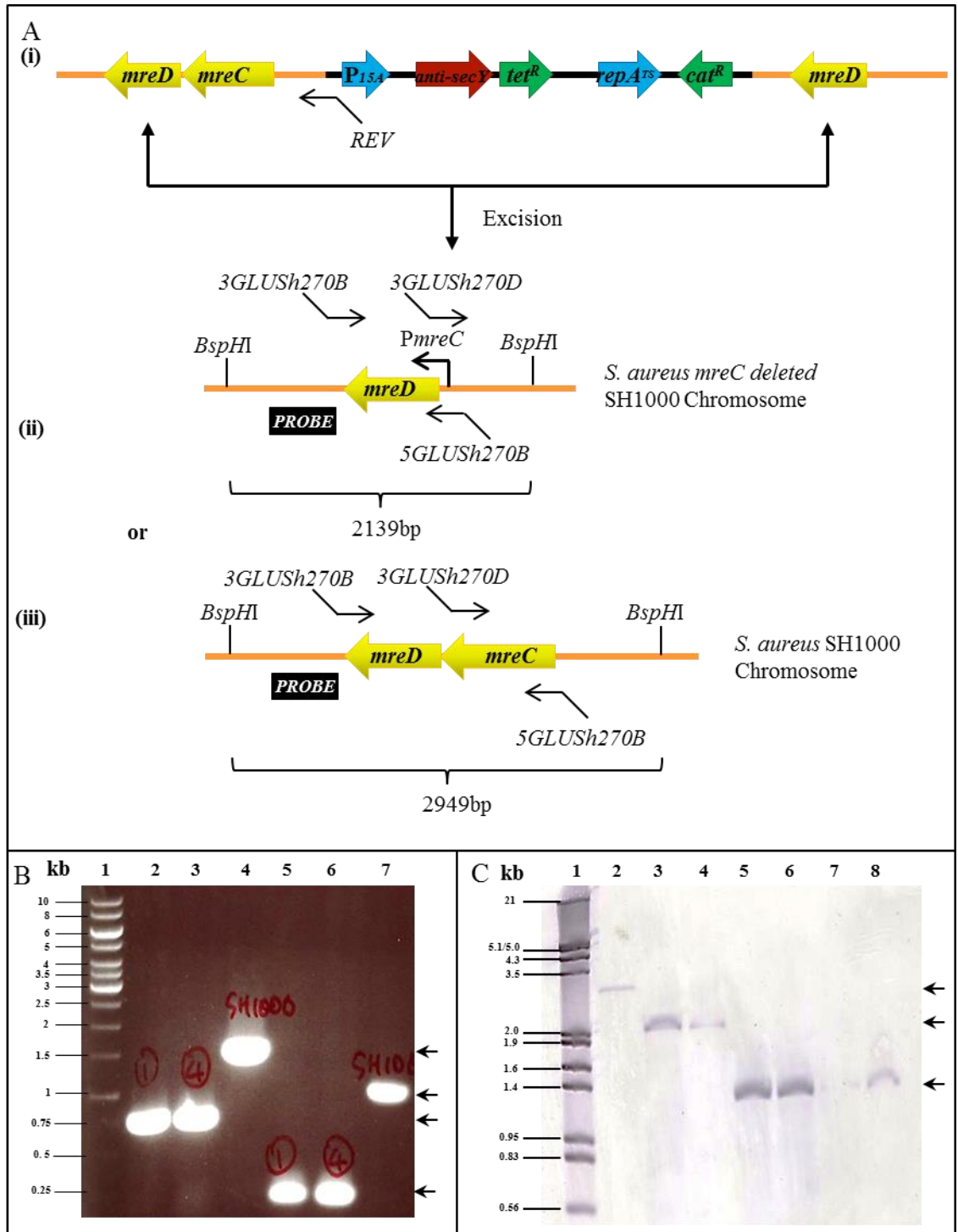
Figure 5-6 Deletion of *mreC* in *S. aureus* SH1000

A.   DiaGrammatic representation of the excision of pXIM5 from the *S. aureus* chromosome (i-iii). Primer binding sites for 5GLUSh270B, 3GLUSh270B and 3GLUSh270D and the *BspH*I restriction sites used in Southern blot analysis are shown. Black boxes indicate the binding sites of the DIG-labelled probe. The two different excision possibilities are shown (ii & iii).Genomic DNA extracted from *S. aureus* SH1000 was applied as a control, which has the same physical map as (iii).

B.   1% (w/v) TAE agarose gel showing products of PCR amplification of the *mreCD* region with primers 5GLUSh270B and 3GLUSh270B (lane 2 and 3) and *mreC* region with primers 5GLUSh270B and 3GLUSh270D (lane 5 and 6) using a potential *mreC* deletion mutant genomic DNA as a template corresponding to that in panel A (ii) and SH1000 genomic DNA was applied as a control. Arrows indicate the expected sizes of 743bp, 282bp, 1.56kb and 1.02kb respectively. Lane 1 contains 1kb DNA ladder used as a marker.

C.   Southern blot showing hybridising bands of *BspH*I digested genomic DNA from strains SH1000 (Lane 2), SJF4098 (*mreC⁻*) (Lane 3 & 4) SJF2625 (*mreCD::kan*) (Lane 5) and SJF2976 (*mreD::kan*) (Lane 6). Lane 7 and 8 contains Newman based *mreCD* deletion mutant, SJF3729 and *mreD* deletion mutant, SJF3731, respectively. Lane 1 contains DIG-labelled DNA molecular weight marker. Arrows mark the expected sizes of 2949bp, 2139 bp and 1312 bp respectively.

5.3.2 Construction of a *S. aureus mreD* deletion mutant

In order to analyse the role of *mreD* in *S. aureus*, an insertion deletion mutation was constructed.

The deletion of *mreD* in *S. aureus* was achieved by exchanging the entire open reading frame with a kanamycin resistance cassette via pMAD (Arnaud *et al.* 2004). pMAD is an *E. coli-S. aureus* shuttle vector, with a *E. coli* replication origin from pBR322 (Bolivar *et al.* 1977) and a *S. aureus* thermosensitive origin of replication from pE194[ts] (Villafane *et al.* 1987). This allows efficient transformation of plasmid into *S. aureus* RN4220 at low permissive temperatures (30°C), and loss of the plasmid at higher, non-permissive temperatures (45°C). The vector also confers ampicillin resistance in Gram-negative bacteria, erythromycin resistance in Gram-positive bacteria and carries a constitutively expressed transcriptional fusion with the *bgaB* gene encoding a thermostable β-galactosidase, allowing blue/white selection on X-Gal plates (Chapter 2.13.1).

DNA fragments corresponding to the upstream region and the downstream region of *mreD* were amplified with the primer pairs 5GLUSh270A/3GLUSh270D and 3GLUSh270C/3GLUSh270A respectively (Table 2.6), and chromosomal DNA from strain *S. aureus* SH1000 as template. *BamH*I and *Kpn*I restriction enzyme sites were engineered at the 5' and 3' end of upstream and downstream arms, respectively, to allow ligation into vector pOB (Horsburgh *et al.* 2002) as an intermediate step in construction of the *mreD* deletion mutation. The upstream arm contains the upstream region of *mreC* and the entire *mreC* open reading frame. Products of sizes consistent with the expected 2177 bp and 983 bp were obtained and treated with *Not*I/*BamH*I and *Not*I/*Kpn*I restriction enzymes, respectively. The digested PCR purified from a 1% (w/v) agarose gel and ligated together at a 1:1 molar ratio. The ligation mixture was then used as a template for PCR amplification of a 3160 bp bipartite DNA fragment using primers 5GLUSh270A/3GLUSh270A. A product consistent with the expected size was obtained and gel purified followed by *BamH*I and *Kpn*I restriction enzyme digestion (Fig. 5.7 B). The digested fragment was ligated into *BamH*I/*Kpn*I cut pOB (Chapter 2.8.4) and the ligation products were transformed into electrocompetent *E. coli* Top10 cells (Invitrogen) followed by selection on BHI 100 µg ml⁻¹ amp at 37°C. 7 colonies were randomly selected and screened for the presence of the region including upstream of *mreC*, *mreC* and downstream of *mreD* by colony PCR with the primer pair 5GLUSh270A/3GLUSh270A (data not shown). One positive clone was verified by plasmid purification, restriction digestion with *EcoR*I (Fig 5.7 D), which cuts once in the insert and once on the backbone of pOB vector, and *Cla*I (Fig 5.7 D), which cuts twice in the insert. The positive clone, called pGL589 (Fig 5.4 A v) was further confirmed by DNA sequencing (Chapter 2.8.10).

A

(i) 3GLUSh270A   3GLUSh270D   *S. aureus* SH1000 Chromosome

mreD mreC

3GLUSh270C   5GLUSh270A

PCR amplification

(ii) KpnI   NotI   NotI   BamHI

mreC

983bp   2177bp

Ligation & PCR

(iii) KpnI   BamHI

mreC

NotI

KpnI (17), BamHI (22)

(iv) pOB 4,464 bp

ermR   ampR

Digestion & Ligation

(v) ampR   ermR

BamHI (3,135)   pGL589 7,577 bp

EcoRI (2,081)   EcoRI (1)
ClaI (2,029)   KpnI (17)
mreC   ClaI (477)
NotI (977)

(vii) HindIII (2,334), HindIII (2,347)
ClaI (2,467)

kanR   mreC

ClaI (3,525)

ClaI (477)   pGL607b 9,073 bp   HindIII (4,661)

ermR   ampR

(vi) 3HXM39B

kanR   PCR   kanR

pGL433   NotI   NotI

5HXM39B

B 1 2 3

C 1 2 3

D 1 2 3 4

E 1 2 3 4 5 6 7 8 9 10 11 12 13

F 1 2 3 4 5

175

Figure 5-7 Construction of plasmid pGL607b for deletion of *mreD*

A.   DiaGrammatic representation of construction of pGL607b (*mreD::kan*) in *E. coli*. Primer binding sites for 5GLUSh270A, 3GLUSh270A, 3GLUSh270C, 3GLUSh270D, 5HXM39B and 3HXM39B and relevant restriction sites used are shown. i) *S. aureus* chromosomal DNA map; ii) PCR amplification of upstream and down stream of *mreD*; iii) Ligation of the PCR products generated from ii); iv) Plasmid pOB map; v) Resulting in pGL589; vi) PCR amplification of *kan^R* cassette; vii) Insertion of *kan^R* cassette into pGL589 resulting pGL607b.

B.   1% (w/v) TAE agarose gel showing *BamH*I/*Kpn*I digested products of PCR amplification of the bipartite DNA fragment including upstream *mreC* and downstream *mreC* with primers 5GLUSh270A/3GLUSh270A (lane 2) and pOB vector (lane 3). Arrows indicate the expected sizes of 3160 bp and 4464 bp respectively. Fragments correspond to those in panel A (iii & iv). Lane 1, 1kb DNA ladder used as a marker.

C.   1% (w/v) TAE agarose gel showing *Not*I digested PCR products of amplification of the *kan^R* cassette with primers 5HXM39B/3HXM39B (lane 3) and pGL589 plasmid (lane 1). Arrows indicate the expected sizes of 1550 bp and 7577 bp respectively. Theses products correspond to that shown in panel A (v & vi). Lane 2, 1kb DNA ladder used as a marker.

D.   pGL589 were restriction digested with *EcoR*I or *Cla*I and analysed by electrophoresis on a 1% (w/v) TAE agarose gel. Lane 2, pOB (4464 bp). *EcoR*I cut pGL589 shows the expected size of 2080 bp and 5497 bp (lane 3), *Cla*I cut pGL589 shows the expected size of 1552 bp and 6025 bp (lane 4) and correspond fragments shown by the restriction map in panel A (v). Lane 1, 1kb DNA ladder used as a marker.

E.   1% (w/v) TAE agarose gel showing products of PCR amplification of the *kan^R* cassette with primers 5HXM39B/3HXM39B. 12 colonies (lane 2-13) were screened and showed bands at the expected size of 1550 bp corresponding to those in panel A (vi). Lane 1 contains 1kb DNA ladder used as a marker.

F.   pGL607b from two isolates was restriction digested with *Cla*I or *Hind*III and analysed by electrophoresis on a 1% (w/v) TAE agarose gel. *Cla*I cut pGL589 shows the expected size of 1058 bp, 1990 bp and 6025 bp (lane 3&5), *Hind*III cut pGL589 shows the expected size of 13 bp, 2326 bp and 6746 bp (lane 2&4) as shown by the restriction map in panel A (vii). Lane 1 contains 1kb DNA ladder used as a marker.

A kanamycin resistance (kan^R) cassette including its native promoter was amplified from pGL433b (Table 2.4) with the primer pair 5HXM39B/3HXM39B (Table 2.6). A *Not*I restriction enzyme site was engineered at the both end of the Kan^R cassette to allow insertion into pGL589. Products of sizes consistent with the expected 1550 bp were obtained (Fig 5.7 A vi). The resulting PCR products were purified from a 1% (w/v) agarose gel and restricted with *Not*I (Fig 5.7 C). The recipient plasmid pGL589 vector was also restricted with *Not*I resulting in the expected size of 7577bp (Fig 5.7 C), followed by dephosphorylation using alkaline phosphatase (Chapter 2.8.3). Both digested kan^R cassette and pGL589 vector were purified by QIAquick gel extraction and mixed at approximately a 1:3 molar ratio of vector DNA to insert DNA in a ligation reaction (Fig 5.7 A v-vii). The ligation mixture was ethanol precipitated and transformed into *E. coli* Top10 electrocompetent cells (Invitrogen) and selected on BHI 50 μg ml^{-1} Kanamycin (Kan) at 37°C for O/N. 12 colonies were randomly picked and screened for the insertion of the kan^R cassette by colony PCR with the primer pair 5HXM39B/3HXM39B (Fig 5.7 E). All of them displayed the expected 1550 bp band. Clones 1 to 4 were further confirmed by QIAprep^{TM} Miniprep and restricted with *Cla*I and *Hind*III, the positive clones 1 and 2, containing pGL607b (Fig 5.7 F), were selected for the strain collection, named SJF2673 and SJF2674 respectively (Table 2.2).

The fragment containing the upstream region of *mreC*, *mreC* gene, kan^R cassette and downstream region of *mreD* was amplified by PCR using pGL607b plasmid DNA as template and primer pair 5GLUSh270A/3HXM67A (Table 2.6). *BamH*I and *Bgl*II restriction enzyme sites were introduced to the 5' and 3' end of upstream region and downstream region, respectively, to allow ligation into pMAD. Products of a size consistent with the expected 4624 bp were obtained (Fig. 5.8 A i-ii). The resulting PCR product was purified from a 1 % (w/v) agarose gel using QIAquick gel extraction kit and restriction digested with *BamH*I/*Bgl*II (Fig. 5.8 B). The recipient plasmid pMAD vector was also restricted with the same enzymes resulting in the expected size of 9666 bp (Fig. 5.8 B) followed by dephosphorylation using alkaline phosphatase. The insert containing upstream region of *mreC*, kan^R cassette and downstream region of *mreC* was ligated into the vector pMAD at *BamH*I and *Bgl*II sites. The ligation mixture was ethanol precipitated and transformed into *E. coli* TOP10 electrocompetent cells (Invitrogen) and selected on LB 50 μg ml^{-1} Kan at 30 °C for 48hrs. 6 well isolated colonies out of 201 were selected and the plasmids were extracted for screening by restriction digestion with *Cla*I (Fig. 5.8 C), which cuts three times in the insert and five times on the backbone of pMAD, or *BamH*I/*Bgl*II (Fig. 5.8 D), which cut the insert back out, and separation by 1 % (w/v) agarose gel electrophoresis. Two positive clones, called pGL613, was further confirmed by DNA sequencing and stored in the SJF strain collection termed SJF2923 and SJF2924 (Table 2.2).

177

A

(i)

pGL607b
9,073 bp

kanR mreC

3HXM67A

5GLUSh270A

emR ampR

(ii) PCR amplification

*Bg*II

kanR mreC

*BamH*I

4624bp

(iii)

BgIII (6,193)
BamHI (6,267)

bgaB

pBR322

bla

pMAD
9,666 bp

emC

pE194 (TS)

Digestion & Ligation

(iv)

ClaI (8,647)

kanR mreC

ClaI (6,657)

ClaI (9,705)

BgIII (6,193)
ClaI (6,057)

ClaI (5,697)
ClaI (5,460)

bgaB

BamHI (10,811)

pGL613
14,210 bp

pBR322

bla

ClaI (3,760)

pE194 (TS)

emC

ClaI (32)

B

1 2 3 4

kb

10
8
6
5
4
3.5
3
2.5
2

1.5

1

0.75

0.5

0.25

C

kb 1 2 3

10
8
6
5
4
3.5
3
2.5

2

1.5

1

0.75

0.5

0.25

D

kb 1 2 3 4

10
8
6
5
4
3.5
3
2.5
2

1.5

1

0.75

0.5

0.25

178

Figure 5-8 Construction of plasmid pGL613 for deletion of *mreD*

A.   DiaGrammatic representation of construction of pGL613 (*mreD::kan*) in *E. coli*. Primer binding sites for 5GLUSh270A and 3HXM67A and relevant restriction sites used are shown. i) plasmid pGL607b map; ii) PCR amplification of the tripartite *mreD::kan* fragment; iii) Insertion of the PCR products generated from ii) into pMAD and plasmid pMAD map; iv) Resultant plasmid pGL613.

B.   1% (w/v) TAE agarose gel showing purified restriction digestion of the 4624 bp PCR product (upstream *mreC*, *mreC*, *kan*[R] and downstream *mreD*) with *Bgl*II or *Bam*HI (lane 4). pMAD and pGL471b were also digested with the same enzymes resulting linearised vector at the expected sizes of 9666 bp and 6732 bp, shown in lane 2 and 3 respectively (indicated by arrows) and corresponding fragments and vector digestion map shown in panel A (ii & iii). Lane 1, 1kb DNA ladder used as a marker.

C.   1% (w/v) TAE agarose gel showing restriction digestion of pGL613 with *Cla*I restriction enzyme. Products of the expected 237, 450, 520, 2252, 2540 and 3728 bp were shown (indicated by arrows) and as shown by the restriction map in panel A (iv). Clones correspond to lane 1 and 2 were selected for SJF strain collection, named SJF2923 and SJF2924, and SJF2924 was used for the subsequent experiments. Lane 1, 1kb DNA ladder used as a marker.

D.   1% (w/v) TAE agarose gel showing restriction digestion of pGL613 extracted from three isolated *S. aureus* RN4220 with *Bgl*II and *Bam*HI restriction enzyme (lane 2-4). All three tested clones generated the linearised pMAD vector and the tripartite *mreD::kan* insert at the expected size of ~10 kb and 4624 bp respectively. This product corresponds to the restriction map shown in panel A (iv). Lane 1, 1kb DNA ladder used as a marker.

The resulting plasmid, pGL613, was purified using a QIAprep™ Miniprep kit and ethanol precipitation. The plasmid was dissolved in 30 μl of sdH$_2$O. 10 μl of the concentrated pGL613 DNA (~ 10 μg) was transformed into electrocompetent *S. aureus* RN4220. With selection on BHI 50 μg ml^{-1}, Kan 50 μg ml^{-1} Neomycin (Neo) and 80 μg ml^{-1} X-Gal, 6 blue colonies were randomly selected and screened for the presence of *kan*^{R} cassette by colony PCR with primer pair 5HXM39B/3HXM39B (data not shown). All 6 clones were positive. 1 single blue colony was selected and streaked on BHI 50 μg ml^{-1} Kan, 50 μg ml^{-1} Neo and 80 μg ml^{-1} X-Gal at 30°C overnight. 1 single blue colony was inoculated into BHI without antibiotic at an OD$_{600}$ = 0.01 and incubated with shaking for 2 h at 30°C followed by 6 h at non-permissive temperature of 42°C. A dilution of 10^{-5} of this culture was plated on BHI 50 μg ml^{-1} Kan, 50 μg ml^{-1} Neo and 80 μg ml^{-1} X-Gal and incubated at 42°C overnight.

One light blue clone, which possessed the integrated plasmid via a single cross over event (Arnaud *et al.* 2004), was randomly selected amongst thousands of intensive blue colonies, which possess several copies of free plasmid (Fig. 5.10 A-B). It was lysed with Φ11 and the plasmid transferred to SH1000 via transduction at 42°C until colonies appeared on BHI 50 μg ml^{-1} Kan, 50 μg ml^{-1} Neo and 80 μg ml^{-1} X-Gal. Transductants were subjected to successive plating at 42°C on BHI 50 μg ml^{-1} Kan, 50 μg ml^{-1} Neo and 80 μg ml^{-1} X-Gal, to potentiate second recombination event that results in resolution of the plasmid and a potential excision of the gene of interest from the chromosome (Fig 5.9 A iii) (Arnaud *et al.* 2004). Following 4 rounds of plating at 42°C for 48 h, 6 clones were found, where all the colonies on the streaking appeared yellow indicating complete excision of the plasmid (Fig. 5.10 B), and were confirmed for the absence of *mreD* gene by genomic DNA extraction and PCR amplification with primer pair 5GLUSh270B/3GLUSh270A (data not shown). Clones were tested for the presence of the *kan*^{R} cassette by colony PCR with primer pair 5HXM39B/3HXM39B and yielded products consistent with the expected sizes of 1550 bp (data not shown).

Replacement of *mreD* with the *kan*^{R} cassette was confirmed by PCR amplification using genomic DNA with the primer pair 5GLUSh270B /3HXM67A and 2 clones generated product consistent with the expected size of ~ 3500 bp (Fig. 5.9 B only shown 1). The resulting *mreD* insertion mutant was further verified by Southern blot. Genomic DNA from SH1000, SJF2976 *(mreD::kan)* was digested with *BspH*I overnight. A DIG-labelled probe, consisting of a 387bp region downstream of *mreCD*, was prepared using primers 3HXM39-11A and 3GLUSh270C. The hybridizing bands for *BspH*I digestion of SH1000 genomic DNA, SJF2976 was consistent with the expected 2949 bp and 1312 bp respectively (Fig. 5.9 C). The sequence of the mutation was alto confirmed by DNA sequencing (data not shown).
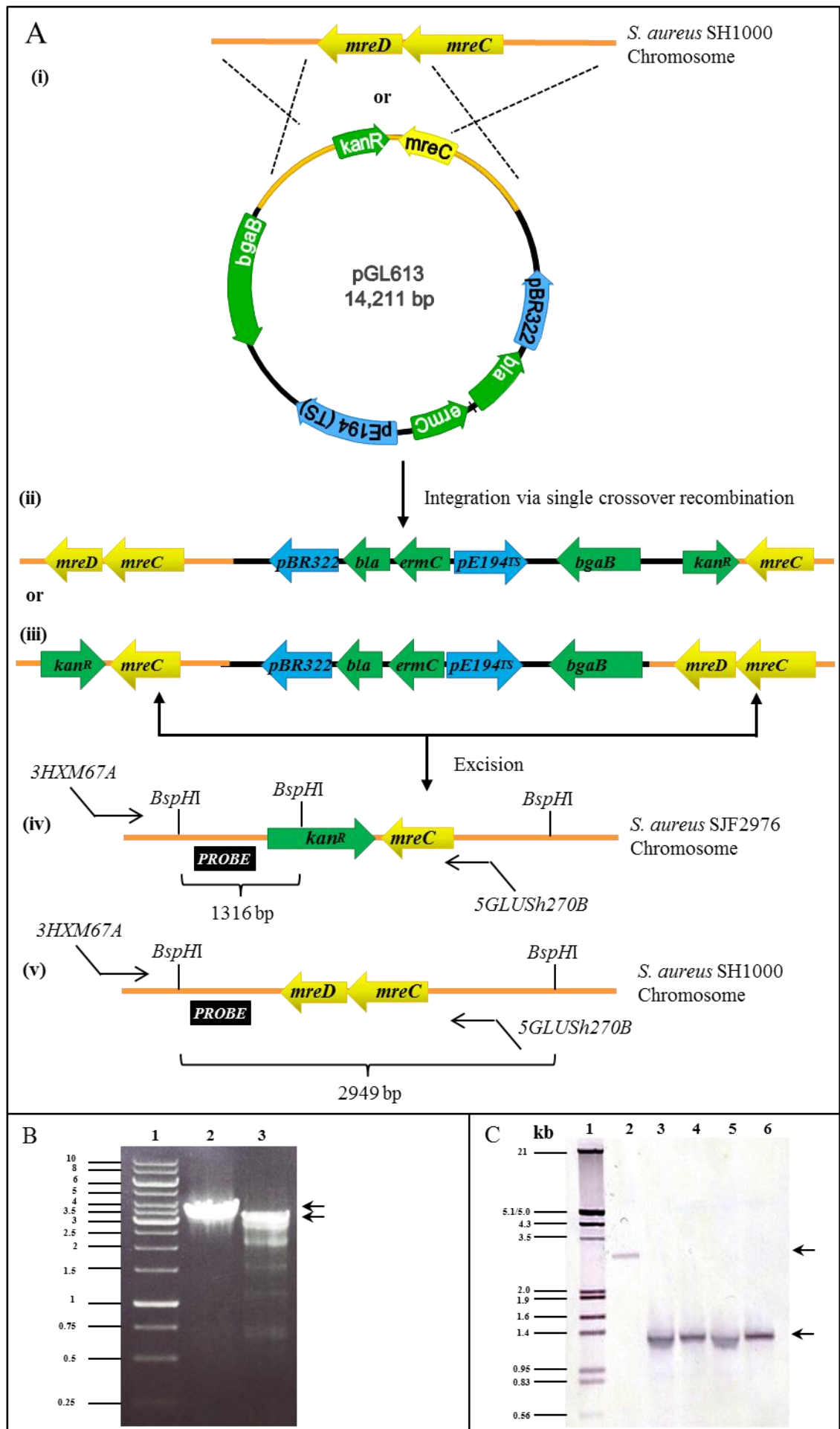
Figure 5-9 Deletion of *mreD* in *S. aureus* SH1000

A.   DiaGrammatic representation of integration of pGL613 into the *S. aureus* chromosome. Primer binding sites for 5GLUSh270B /3HXM67A and the *BspH*I and restriction sites used for Southern blot analysis are shown. Black box indicates the binding site of the DIG-labelled probe.

B.   1 % (w/v) TAE agarose gel showing products of PCR amplification with primers 5GLUSh270B /3HXM67A using genomic DNA extracted from SJF2976 (*mreD::kan*) (lane 2) and SH1000 (lane 3). Arrows mark the expected sizes of ~ 3500 bp (Lane 2) and ~ 2500 bp (Lane 3) respectively, corresponding to integration via double crossover recombination. Lane 1, 1kb DNA ladder used as a marker.

C.   Southern blot showing hybridising bands of *BspH*I digested genomic DNA from strains SH1000, SJF2625/SJF2626 (*mreCD::kan*) (lane 3 & 4), SJF2976/SJF2977 (*mreD::kan*) (lane 5 & 6) The black box in panel A indicate the binding sites of the DIG-labelled probe. DIG-labelled markers are also shown in lane 1. Arrows mark the expected bands of 2949 bp for the wild type SH1000 and 1316 bp for the mutants.
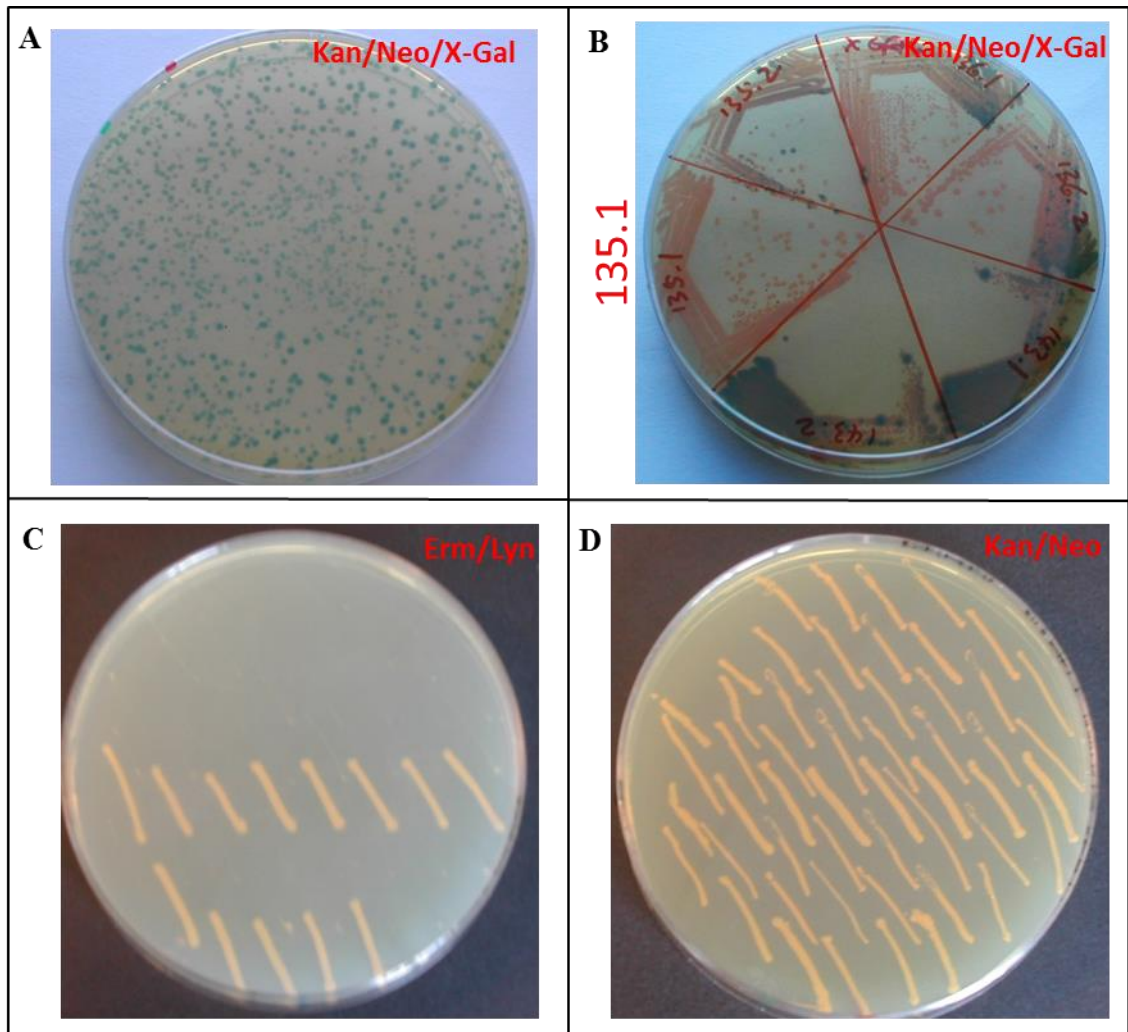
Figure 5-10 Colour selection and drug sensitivity test of the plasmid pGL613 excision in *S. aureus* SH1000

A.   One light blue transductant was grown at 42°C and 100 µl of 10^{-5} diluted cell culture were plated on BHI 50 µg ml^{-1} Kan, 50 µg ml^{-1} Neo and 80 µg ml^{-1} X-Gal.

B.   Streaking of 18 yellow transductants on BHI 50 µg ml^{-1} Kan, 50 µg ml^{-1} Neo and 80 µg ml^{-1} X-Gal at 42°C. 6 out of 18 producing yellow isolates, for example 135.1, consistently were chosen for drug sensitivity test shown in C and D.

C.   Colonies appearing in yellow on X-Gal plates from B were firstly patched onto BHI 5 µg ml^{-1} Erm and 25 µg ml^{-1} Lin.

D.   The same colonies were then secondly patched onto BHI 50 µg ml^{-1} Kan, 50 µg ml^{-1} Neo and 80 µg ml^{-1} X-Gal at 42°C.

Thus, absence of *mreD* gene is not lethal for *S. aureus*, implying that *mreD* is not essential for the growth of *S. aureus.*

5.3.3 Construction of an *mreCD* double deletion mutant

Previous experiments implied that separate deletion of *mreC* and *mreD* gene is not lethal for *S. aureus*. It was important to determine the combined role of the genes, and so an inframe *mreCD* double deletion mutant was constructed for this purpose.

The vector pOB (Horsburgh et al. 2002) was employed for construction of deletion mutation of *mreCD* in *S. aureus* via allelic replacement with a *kan^R*, thereby deleting the chromosomal copy. pOB is a suicide vector in Gram-positive bacteria, with a *E. coli* replication origin from pGEM3Zf(+) (Horsburgh *et al.* 2002). The vector also confers ampicillin resistance to Gram-negative bacteria and erythromycin resistance to Gram-positive bacteria. A two-step strategy is required; initially homologous recombination occurs between the target sequence in the chromosome and a homologous sequence carried on the suicide plasmid. Integration of the plasmid into the chromosome by a single crossover event is selected in the presence of selective pressure. The *mreCD::kan^R* was introduced into the chromosome of *S. aureus* SH1000 by transductional outcross.

DNA fragments corresponding to the upstream region and the downstream region of *mreCD* were amplified with the primer pairs 5GLUSh270A/5GLUSh270C and 3GLUSh270C/3GLUSh270A respectively (Table 2.6), and using chromosomal DNA from strain *S. aureus* SH1000 as a template (Fig. 5.11A i). *BamH*I and *Kpn*I restriction enzyme sites were engineered at the 5' and 3' end of upstream and downstream arms, respectively, to allow ligation into vector pOB (Fig. 5.11A ii). Products of sizes consistent with the expected 1288 bp and 983 bp (Fig. 5.11B) were obtained and treated with *Not*I/*BamH*I and NotI/KpnI restriction enzymes, respectively. The digested PCR products were purified from a 1% (w/v) agarose gel and ligated together at 1:1 molar ratio. The ligation mixture was then used as a template for PCR amplification of a 2271 bp bipartite DNA fragment using primers 5GLUSh270A and 3GLUSh270A (Fig. 5.11C). Products of sizes consistent with the expected size were obtained and gel purified followed by *BamH*I and *Kpn*I restriction enzyme digestion as well as pOB vector, which was then treated with CIP (Chapter 2.8.3). The digested bipartite fragment was ligated into pOB at *BamH*I and *Kpn*I sites (Chapter 2.8.4) and the ligation products were ethanol precipitated and transformed into electrocompetent *E. coli* Top10 cells (Invitrogen) followed by selection on BHI 100 μg ml-1 amp at 37°C. 4 colonies out of thousands were randomly selected and the insertion was verified by plasmid purification, restriction digestion with *EcoR*I (Fig 5.11D), which cuts once in the insert and once on the backbone of pOB vector. The positive clone, called pGL590 (Fig 5.11A iv) was further confirmed by DNA sequencing (Chapter 2.8.10).
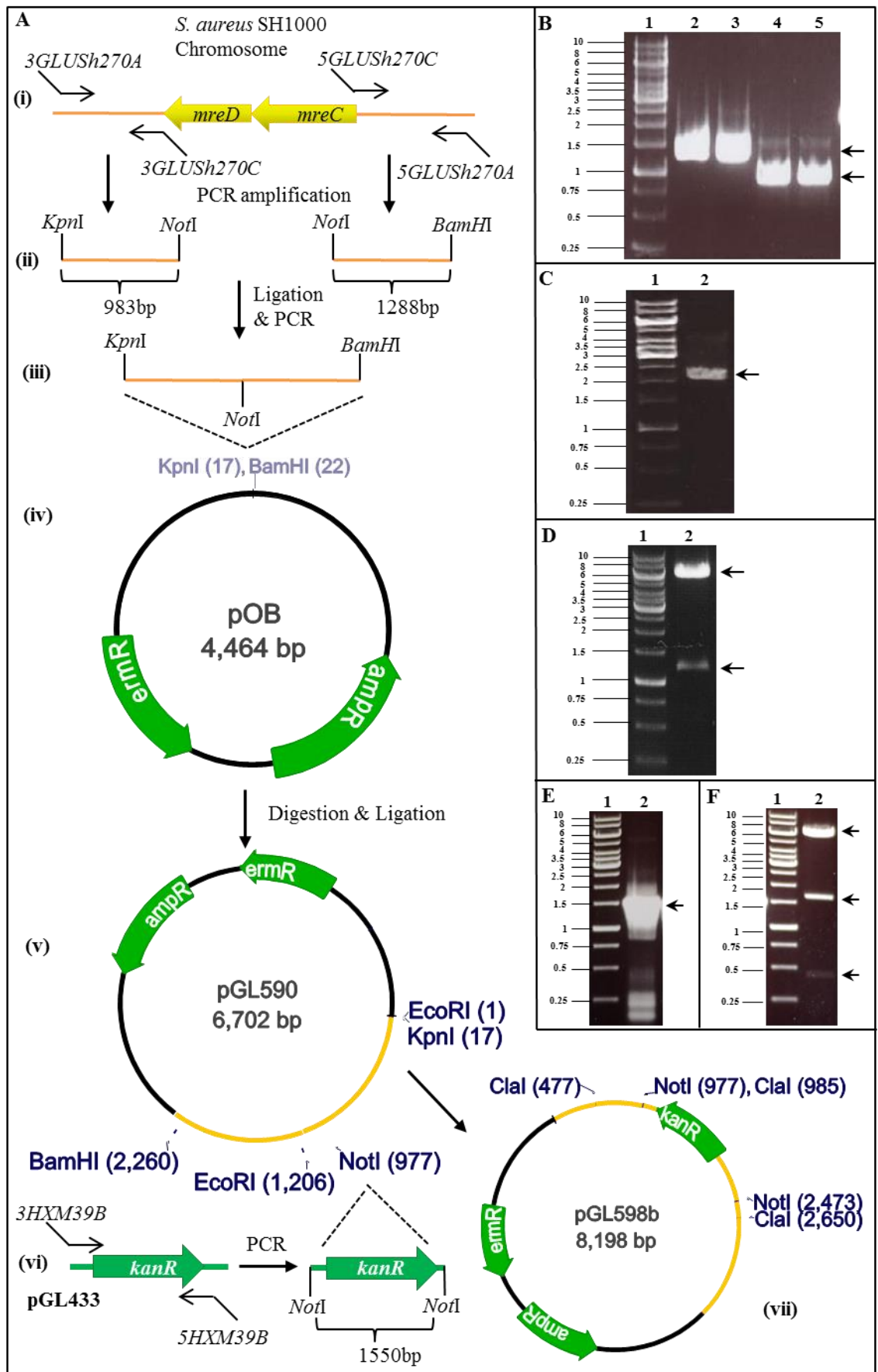
Figure 5-11 Construction of plasmid pGL598b for deletion of *mreCD*

A. DiaGrammatic representation of construction of pGL598b (*mreCD::kan*) in *E. coli*. Primer binding sites for 5GLUSh270A, 3GLUSh270A, 5GLUSh270C, 3GLUSh270C, 5HXM39B and 3HXM39B and relevant restriction sites used are shown. i) *S. aureus* chromosomal DNA map; ii) PCR amplification of upstream of *mreC* and downstream of *mreD*; iii) Ligation of the PCR products generated from ii); iv) Plasmid pOB map; v) Resulting in pGL590; vi) PCR amplification of *kan^R* cassette; vii) Insertion of *kan^R* cassette into pGL590 resulting pGL598b.

B. 1% (w/v) TAE agarose gel showing products of PCR amplification of including upstream *mreCD* and downstream *mreCD* with primers 5GLUSh270A/3GLUSh270C (lane 2 & 3) and 3GLUSh 270C/3GLUSh270A (lane 4 & 5) respectively. Arrows indicate the expected sizes of 1288 bp and 983 bp respectively. Fragments correspond to those in panel A (ii & iii). Lane 1, 1kb DNA ladder used as a marker.

C. 1% (w/v) TAE agarose gel showing the PCR amplification of the bipartite DNA, upstream *mreC* and downstream *mreD* (lane 2). Arrows indicate the expected sizes of 2271 bp. The PCR reaction was run in duplicates for higher PCR products yield. This product corresponds to that shown in panel A (iii). Lane 1, 1kb DNA ladder used as a marker.

D. pGL590 were restriction digested with *EcoR*I and analysed by electrophoresis on a 1% (w/v) TAE agarose gel. *EcoR*I cut pGL590 shows the expected sizes of 1205bp and 5497 bp (lane 2) and correspond to the fragment shown by the restriction map in panel A (v). 4 different clones were tested on this gel. Lane 1, 1kb DNA ladder used as a marker.

E. 1% (w/v) TAE agarose gel showing products of PCR amplification of the *kan^R* cassette with primers 5HXM39B/3HXM39B. Colony showed bands at the expected size of 1550 bp (lane 2) corresponding to that in panel A (vi). Lane 1 contains 1kb DNA ladder used as a marker.

F. pGL598b was restriction digested with *Cla*I and analysed by electrophoresis on a 1% (w/v) TAE agarose gel. *Cla*I cut pGL598b shows the expected sizes of 508 bp, 1665 bp and 6025 bp (lane 2) as shown by the restriction map in panel A (vii). Lane 1 contains 1kb DNA ladder used as a marker.

A *kan^R* cassette including its native promoter was amplified from pGL433b (Table 2.4) with the primer pair 5HXM39B/3HXM39B (Table 2.6). A NotI restriction enzyme site was engineered at the both end of the *kan^R* cassette to allow insertion into pGL590. The resulting PCR products of sizes consistent with the expected 1550 bp were purified from a 1% (w/v) agarose gel and restricted with *Not*I. The recipient plasmid pGL590 vector was also restricted with *Not*I resulting in the expected size of 6702 bp followed by dephosphorylation using alkaline phosphatase (Chapter 2.8.3). Both digested *kan^R* cassette and pGL590 vector were purified by QIAquick gel extraction and mixed at approximately a 1:3 molar ratio of vector DNA to insert DNA in a ligation reaction (Fig 5.11A iv-vi). The ligation mixture was ethanol precipitated and transformed into *E. coli* Top10 electrocompetent cells (Invitrogen) and selected on BHI 50 µg ml^{-1} kanamycin (Kan) at 37°C for O/N. 2 colonies out of thousands were randomly picked and screened for the insertion of *kan^R* cassette by PCR with the primer pair 5HXM39B/3HXM39B using QIAprepTM Miniprep DNA. Both of them displayed the expected 1550 bp band (Fig 5.11E) and the insertion was confirmed by *Cla*I restriction enzyme digestion (Fig 5.11F). The clones 1 and 2 were called pGL598a and pGL598b respectively (Fig 5.11vi), (Table 2.2). Plasmid pGL598b was successfully integrated into chromosomal DNA by single cross-over and generated *mreCD* double deletion mutant in SH1000, which will be illustrated below.

The resulting plasmid was purified using QIAprepTM Midiprep kit from *E. coli* TOP10 and ethanol precipitation. 10 µg of the concentrated pGL598b DNA in sdH$_2$O was transformed into electrocompetent *S. aureus* RN4220 (Chapter 2.10.2.2). Selection was on BHI 50 µg ml^{-1} Kan/Neo. A single cross-over recombinant of pGL598b was confirmed by QIAGEN DNeasyTM genomic DNA extraction and PCR amplification for the presence of *mreC*, *mreD* genes and *kan^R* cassette with primer pairs 5GLUSh270A/3GLUSh270D, 5GLUSh270D/3GLUSh270A, 5/3GLUSh270B and 5GLUSh27B/3GLUSh27B (Fig 5.12 B).

A clone was lysed with Φ11 and plasmid transferred to SH1000 via transduction at 37°C. Transductants were streaked onto BHI 5 µg ml^{-1} Erm and 25 µg ml^{-1} Lin and also BHI 50 µg ml^{-1} Kan, 50 µg ml^{-1} Neo. pGL598b transductant number 4 (B4) (Fig 5.13 A-B), appeared to be Erm/Lin sensitive (E/L^S) and Kan/Neo resistance (K/N^R), was further verified by genomic DNA extraction and PCR amplification of the region containing upstream *mreC*, allelic replacement *kan^R* cassette, and downstream *mreD* gene. Clone B4 produced a band consistent with expected size of 3821 bp and a 1550bp *kan^R* cassette band (Fig 5.12 C).

A
(i)

Downstream — mreD ← mreC ← *Upstream*

S.aureus SH1000 Chromosome

or

kanR

pGL598b 8,198 bp

KpnI (17)

BamHI (3,756)

ermR

ampR

Integration via single crossover recombination

(ii)

3HXM39B

3GLUSh270A 3GLUSh270B 3GLUSh270D

kanR — ampR ermR — mreD mreC

5HXM39B

5GLUSh270D 5GLUSh270B 5GLUSh270A

(iii)

3GLUSh270A 3GLUSh270B 3GLUSh270D

3GLUSh27B

mreD mreC — ampR ermR — kanR

5GLUSh270D 5GLUSh270B 5GLUSh270A

5GLUSh27B

Transduction

(iv)

3GLUSh270A   BspHI   BspHI   BspHI

S.aureus SH1000 Chromosome

PROBE   kanR

5GLUSh270A

1316bp

3821bp

B Kb 1 2 3 4 5 6

10
8
6
5
4
3.5
3
2.5
2
1.5
1
0.75
0.5
0.25

C Kb 1 2 3

10
8
6
5
4
3.5
3
2.5
2
1.5
1
0.75
0.5
0.25

189

Figure 5-12 Deletion of *mreCD* in *S. aureus* SH1000

A. DiaGrammatic representation of integration of pGL598b into the *S. aureus* chromosome. Primer binding sites for 5/3GLUSh270A, 5/3GLUSh270B, 5/3GLUSh270D and 5/3HXM39B and the *BspH*I and restriction site used in Southern blot analysis (Fig 5.7 C) are shown. Black box indicates the binding site of the DIG-labelled probe. (i) Chromosomal DNA and pGL598b DNA map; (ii) Downstream region single cross over; (iii) Upstream region single cross over; (iv) Excision of plasmid DNA via second single cross over.

B. 1 % (w/v) TAE agarose gel showing products of PCR amplification with primer pairs 5GLUSh270A/3GLUSh270D, 5/3GLUSh270B, 5GLUSh270D/3GLUSh270A and 5/3HXM39B using genomic DNA extracted from one clone containing pGL598b. Arrows mark the expected sizes of ~ 2.2 kb (Lane 3 & 5), ~ 1.5 kb (lane 2), ~1.6 kb (lane 4) bp and 1550 bp (Lane 6) respectively, corresponding to integration via single crossover recombination. Lane 1, 1kb DNA ladder used as a marker.

C. 1 % (w/v) TAE agarose gel showing products of PCR amplification of the tripartite and Kan^R cassettes with primer pairs 5GLUSh270A/3GLUSh270D and 5/3HXM39B. Arrows mark the expected sizes of ~3.8 kb and 1550 bp. Lane 2 and 3 represent the PCR amplification products of B4 (pGL598b colony number 4), respectively. Clone B4 was further confirmed by Southern Blot shown in Fig. 5.9 C. Lane 1, 1kb DNA ladder used as a marker.
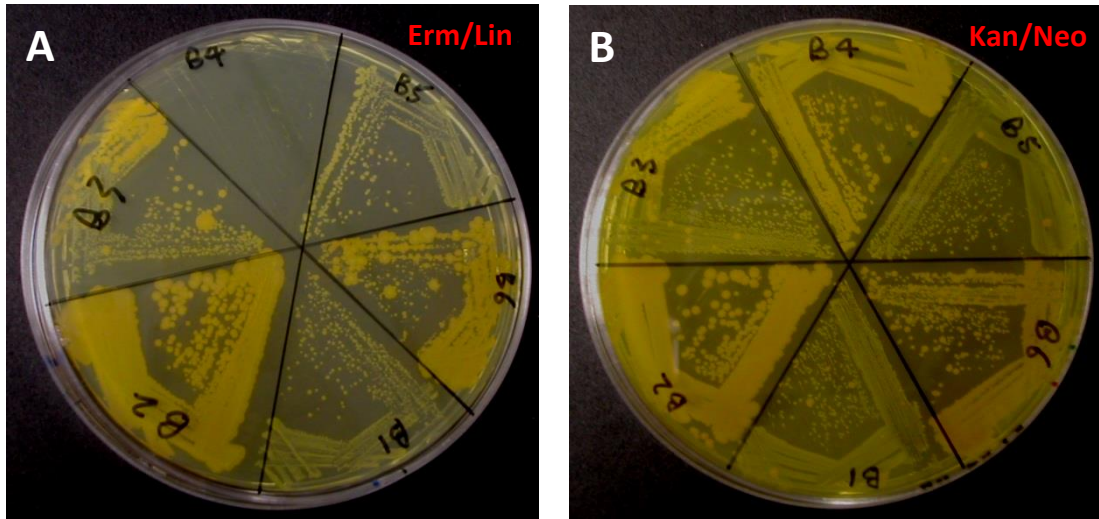
Figure 5-13 Drug sensitivity test of the plasmid pGL598b excision in *S. aureus* SH1000

A. Colonies appearing on the Kan/Neo plates were firstly patched onto BHI 5 µg ml^{-1} Erm and 25 µg ml^{-1} Lin.

B. The same colonies were then secondly patched onto BHI 50 µg ml^{-1} Kan, 50 µg ml^{-1} Neo µg ml^{-1} at 37°C. Two colonies from B4 were selected for Southern Blot (Fig. 5.7 C lane 3 & 4).

Two isolated colonies from the putative clone (B4) was further verified by Southern Blot and named SJF2624 (*ΔmreCD*) and SJF2625 (*ΔmreCD*). Genomic DNA from SH1000, SJF2624 (*ΔmreCD*) and SJF2625 (*ΔmreCD*) were digested with *BspH*I overnight. A DIG-labelled probe, consisting of a 387bp region downstream of *mreCD*, was prepared using primers 3HXM39-11A and 3GLUSh270C (Table 2.6). The hybridizing bands for *BspH*I digestion of SH1000 genomic DNA and SJF4098 were consistent with the expected of 2949bp and 2139 bp respectively (Fig. 5.4 C).

Thus, *mreCD* can be deleted and the genes are not essential for the viability of *S. aureus*.

5.3.4 Effects of *mreC* and *mreD* deletion on growth

In order to verify the role of *mreC* or *mreD* gene in *S. aureus* on growth, SJF2625 (*mreCD::kan*), SJF2976 (*mreD::kan*) and SJF4098 (*ΔmreC*) were grown under normal growth conditions. Growth in both solid and liquid culture was compared to WT SH1000. A single colony of SJF2625 (*mreCD::kan*), SJF2976 (*mreD::kan*) and SJF4098 (*ΔmreC*) from BHI plates containing 50 µg ml^{-1} Kan and 50 µg ml^{-1} Neo were streaked on a BHI plate without drugs, a single colony of SH1000 from BHI containing no drugs were also streaked on the same plate. The plate was incubated at 37°C and monitored over 2 days. After 24 hours, there were no single visible colonies produced by *mreD* and *mreCD* mutants, whereas, SH1000 showed a very strong growth and a lot good sized isolates were appeared on the plate (Fig 5.12 A). After 48 hours incubation, SH1000 has over grown (Fig 5.12 B). In comparison, visible isolates were appeared by *mreD* and *mreCD* mutants.

Strains SJF2625 (*mreCD::kan*), SJF2976 (*mreD::kan*) and SJF4098 (*ΔmreC*) were also grown in liquid BHI. Overnight cultures were inoculated into 50ml BHI broth without drugs in 250ml conical flasks and incubated at 37°C with shaking at 250rpm for 15 hrs. Cells were sub-cultured into fresh BHI to an OD$_{600}$ = 0.05 and incubated at 37°C with shaking at 250rpm for 2 hrs to exponential phase. The cells were sub-cultured again at OD$_{600}$ = 0.05 and incubated at 37°C with shaking at 250rpm.

Growth of SJF2625 (*mreCD::kan*) and SJF2976 (*mreD::kan*) compared to the parental strain SH1000 revealed a severe defect for all strains carrying the *mreD* mutation, but not for *mreC* alone. This suggests that MreD is involved in cell growth. The growth of SJF4098 (*ΔmreC*) was comparable to that of the wild-type strain SH1000 on both solid medium (data not shown) and liquid culture (Fig. 5.14). This implies that MreC is unlikely involved in the cell growth process.
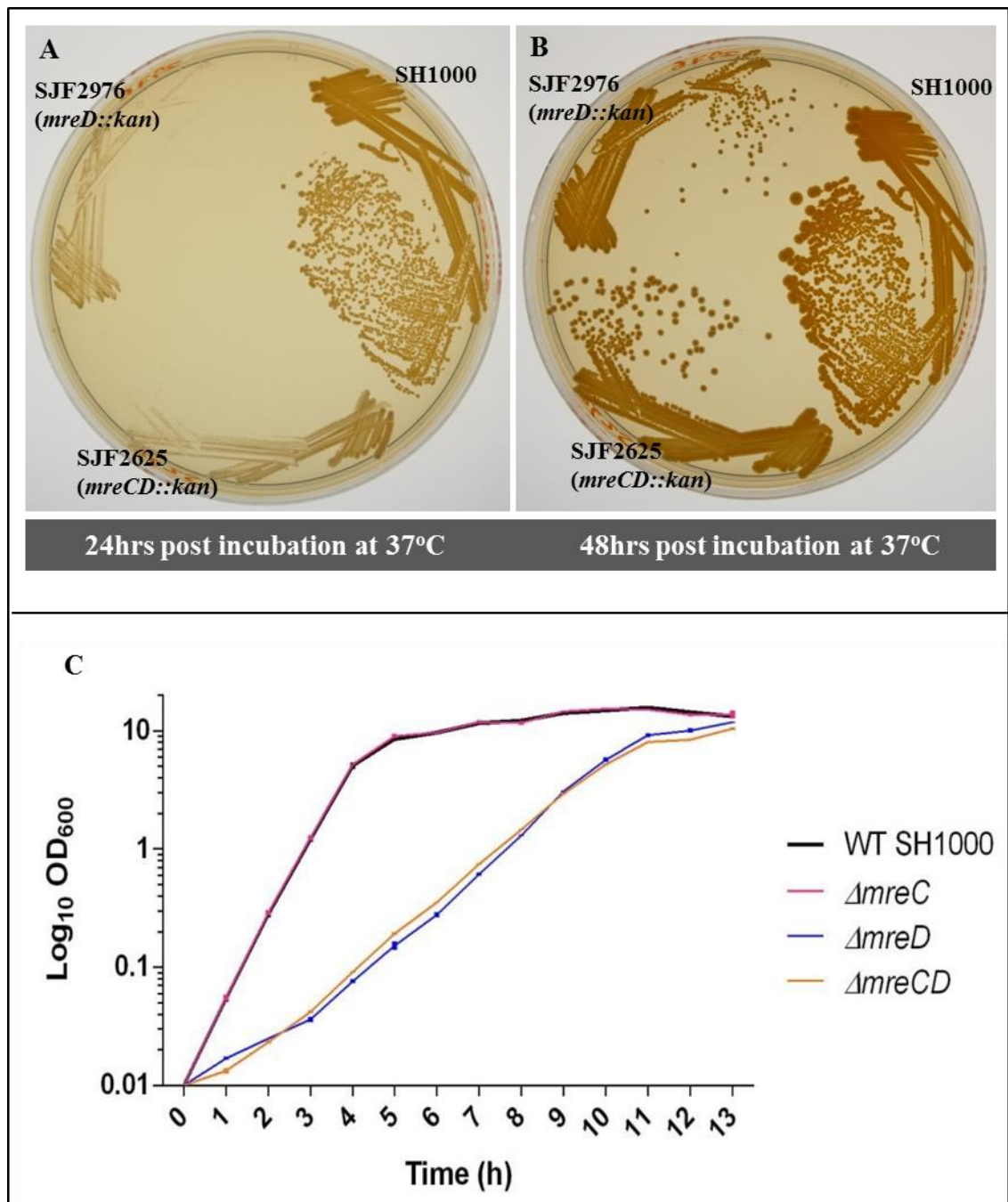
Figure 5-14 The effect of the deletion of *mreC, mreD* or *mreCD* on growth rate.

A.   Strains SJF2625 (*mreCD::kan*), SJF2976 (*mreD::kan*) and WT SH1000 were grown on BHI agar plates at 37ºC for 24 hr. SJF4098 (*ΔmreC*) is not shown.

B.   Strains SJF2625 (*mreCD::kan*), SJF2976 (*mreD::kan*) and WT SH1000 were grown on BHI agar plates at 37ºC after 48 hr. SJF4098 (*ΔmreC*) is not shown.

C.   Growth curves of Strains SJF2625 (*mreCD::kan*), SJF2976 (*mreD::kan*), SJF4098 (*ΔmreC*) and WT SH1000. Cells were grown in in triplicates in BHI broth with no drug at 37ºC with shaking at 250 rpm. Error bars representing the standard deviation are shown.

5.3.5   Construction of complementation strains of *mreCD* in *S. aureus*

In order to confirm that the observed growth defect of SJF2976 (*mreD*::kan) and SJF2625 (*mreCD*::kan) at 37 °C is due to the absence of *mreD* gene, complementation plasmids were constructed (Fig. 5.15 iv). A wild-type copy of the *mreC* and/or *mreD* gene (s) with their native promoter was cloned into the *E. coli-S. aureus* shuttle vector pGL485 (Cooper et al. 2009) (Fig. 5.15 i - iii), a chloramphenicol resistant (Cat^R) derivative of pMJ8426 (Jana et al. 2000).

The *mreC*, *mreD* and *mreCD* genes, with native promoters, were amplified by PCR using SH1000 genomic DNA as a template with primer pairs 5/3GLUSh380A, 5/3GLUSh380B, and 5/3HXM130A respectively. Products consistent with the expected ~ 880 bp, ~ 530 bp and ~1.4 kb corresponding to *mreC*, *mreD* and *mreCD* genes were obtained. The DNA fragments were restricted with *Apa*I and *BamH*I and cloned into pGL485 vector, which was treated with *Apa*I/*BamH*I restriction enzymes and alkaline phosphatase (Fig. 5.15 B C D). The ligation products were transformed into *E. coli* electrocompetent TOP10 with selection on 100 μg ml^{-1} spec. Transformants were screened for the presence of the insert by plasmid purification and restriction digestion giving sizes of ~880 bp, ~530 bp and ~1.4 kb for *mreC*, *mreD* and *mreCD* respectively (Fig 5.3 E-G). All the resultant plasmids were confirmed by DNA sequencing.

The plasmid, pGL620 (carrying *mreC*), pGL621 (carrying *mreD*) and pGL631 (carrying *mreCD*) were introduced into RN4220 individually using selection with 15 μg ml^{-1} chloramphenicol. Φ11 lysates of the resultant strains were prepared and used to transduce plasmids pGL620, pGL621 and pGL631 into SJF2625, SJF2976 and SH1000. To obtain a control strain, pGL485 was also transduced into SJF2625, SJF2976 and SH1000.
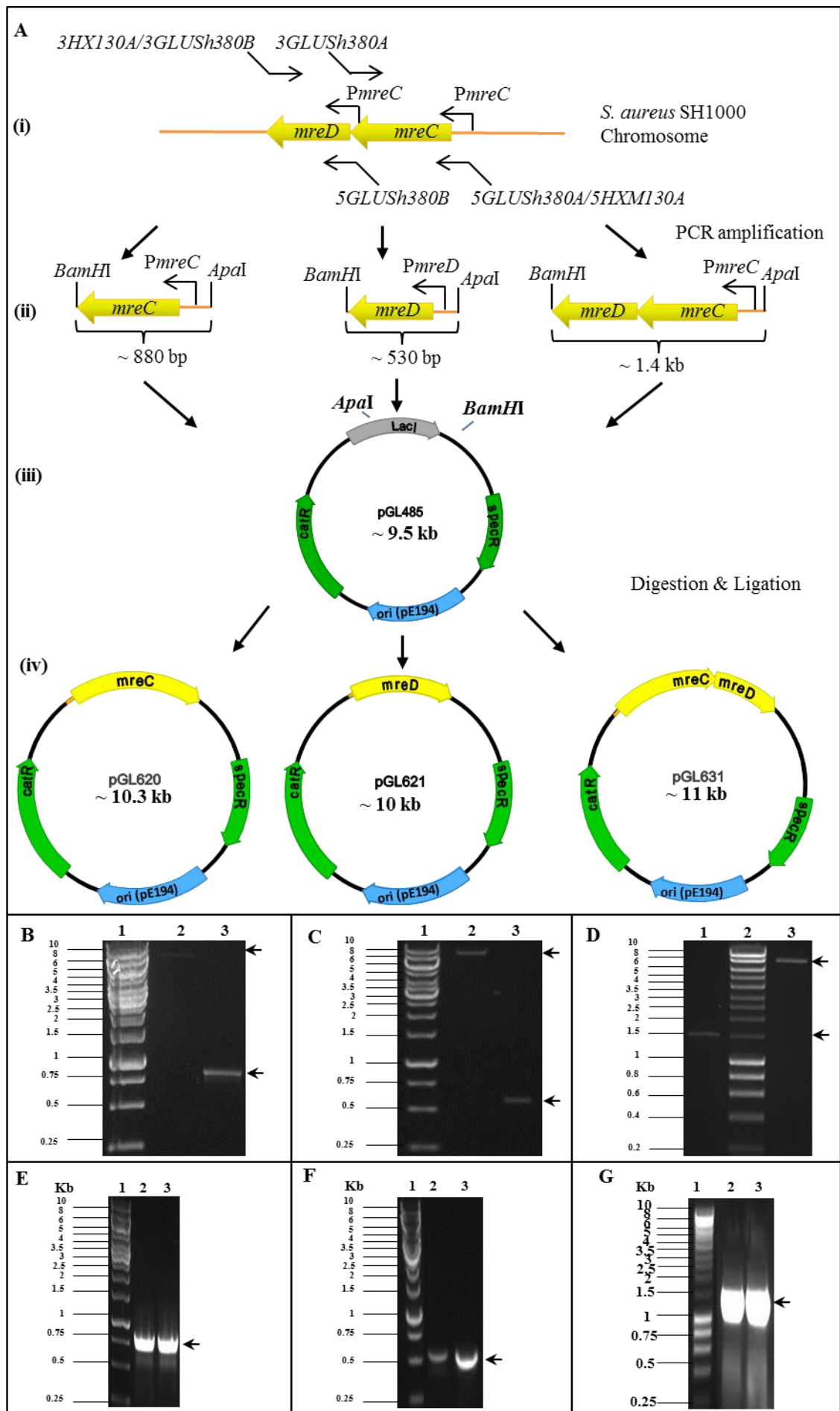
Figure 5-15 Construction of *mreC, mreD* and *mreCD* complementation plasmids pGL620, pGL621 and pGL631

A.   DiaGrammatic representation of strategy used for construction of *mreC*, *mreD* and *mreCD* complementation plasmids, pGL620, pGL621 and pGL631 in *E. coli*. Primer binding sites of 5/3GLUSh380A, 5/3GLUSh380A, and 5/3HXM130A (i) and the restriction sites used are shown. (ii) PCR products of (i). (iii) Map of pGL485 vector. (iv) Maps of pGL620, pGL621 and pGL631.

B.   1% (w/v) TAE agarose gel showing *Apa*I/*BamH*I digested pGL485 vector (lane 2) and PCR products of *mreC* gene (lane 3). Arrow marks the expected sizes of 880 bp and 9.5 kb. Lane 1 contains 1kb DNA ladder used as a marker.

C.   1% (w/v) TAE agarose gel showing *Apa*I/*BamH*I digested pGL485 vector (lane 2) and PCR products of *mreD* gene (lane 3). Arrow marks the expected sizes of 530 bp and 9.5 kb. Lane 1 contains 1kb DNA ladder used as a marker.

D.   1% (w/v) TAE agarose gel showing *Apa*I/*BamH*I digested PCR products of *mreCD* gene (lane 1) and pGL485 vector (lane 3). Arrow marks the expected sizes of 1.4 kb and 9.5 kb. Lane 2 contains hyper ladder I DNA ladder used as a marker.

E.   1% (w/v) TAE agarose gel showing PCR products of *mreC* gene (lane 2 & 3) using primer pair 5/3GLUSh380A. 14 colonies were screened and were all positive. Two isolates were selected and stored in the strain collection named SJF2927 and SJF2928 (Table 2.3). Arrow marks the expected sizes of 880 bp. Lane 1 contains 1kb DNA ladder used as a marker.

F.   1% (w/v) TAE agarose gel showing PCR products of *mreD* gene (lane 2 & 3) using primer pair 5/3GLUSh380B. 6 out of 14 colonies were screened positive. Two isolates were selected and stored in the strain collection named SJF2933 and SJF2934 (Table 2.3). Arrow marks the expected sizes of 530 bp. Lane 1 contains 1kb DNA ladder used as a marker.

G.   1% (w/v) TAE agarose gel showing PCR products of *mreCD* gene (lane 2 & 3) using primer pair 5/3HXM130A. The two isolates were selected and stored in the strain collection named SJF3187 and SJF3188 (Table 2.3). Arrow marks the expected sizes of 1.4 kb. Lane 1 contains hyper ladder I DNA used as a marker.

5.3.6   Complementation *mreD* and *mreCD* mutants

The growth rate of complemented strains was tested in BHI broth containing 15 µg ml^{-1} Cat (Fig. 5.14).   Strains SJF3189 (SH1000 pGL485), SJF3191 (SH1000 pGL620 (*mreC*)), SJF3193 (SH1000 pGL621 (*mreD*)), SJF3195 (SH1000 pGL631 (*mreCD*)), SJF3200 (*mreCD::kan* pGL620 (*mreC*)), SJF3202 (*mreCD::kan* pGL621 (*mreD*)), SJF3205 (*mreCD::kan* pGL631 (*mreCD*)), SJF3207 (*mreCD::kan* pGL485), SJF3208 (*mreD::kan* pGL621 (*mreD*)) and SJF3210 (*mreD::kan* pGL485) were inoculated into BHI (15µg ml^{-1} Cat) to an OD$_{600}$ = 0.05 and incubated at 37$^{\text{o}}$C with shaking at 250rpm for 2 h to exponential phase. The cells were sub-cultured again at OD$_{600}$ = 0.01 and incubated at 37$^{\text{o}}$C with shaking at 250rpm. OD$_{600}$ of all cultures was measured hourly.

The growth rate of the *mreCD* deletion mutant was partially restored by addition of ectopic *mreCD* (Fig. 5.16 C) and *mreD* (Fig. 5.16 B) expressed from the pGL485 vector, however not *mreC* alone (Fig. 5.16A). The successful complementation of the *mreCD* mutant confirms that it is absence of *mreD* that confers the growth defect. Complementation of *mreD* in the *mreD* background did not restore the growth defect of the mutant, this maybe due to problems with expression of *mreD*, but complements *mreCD*.
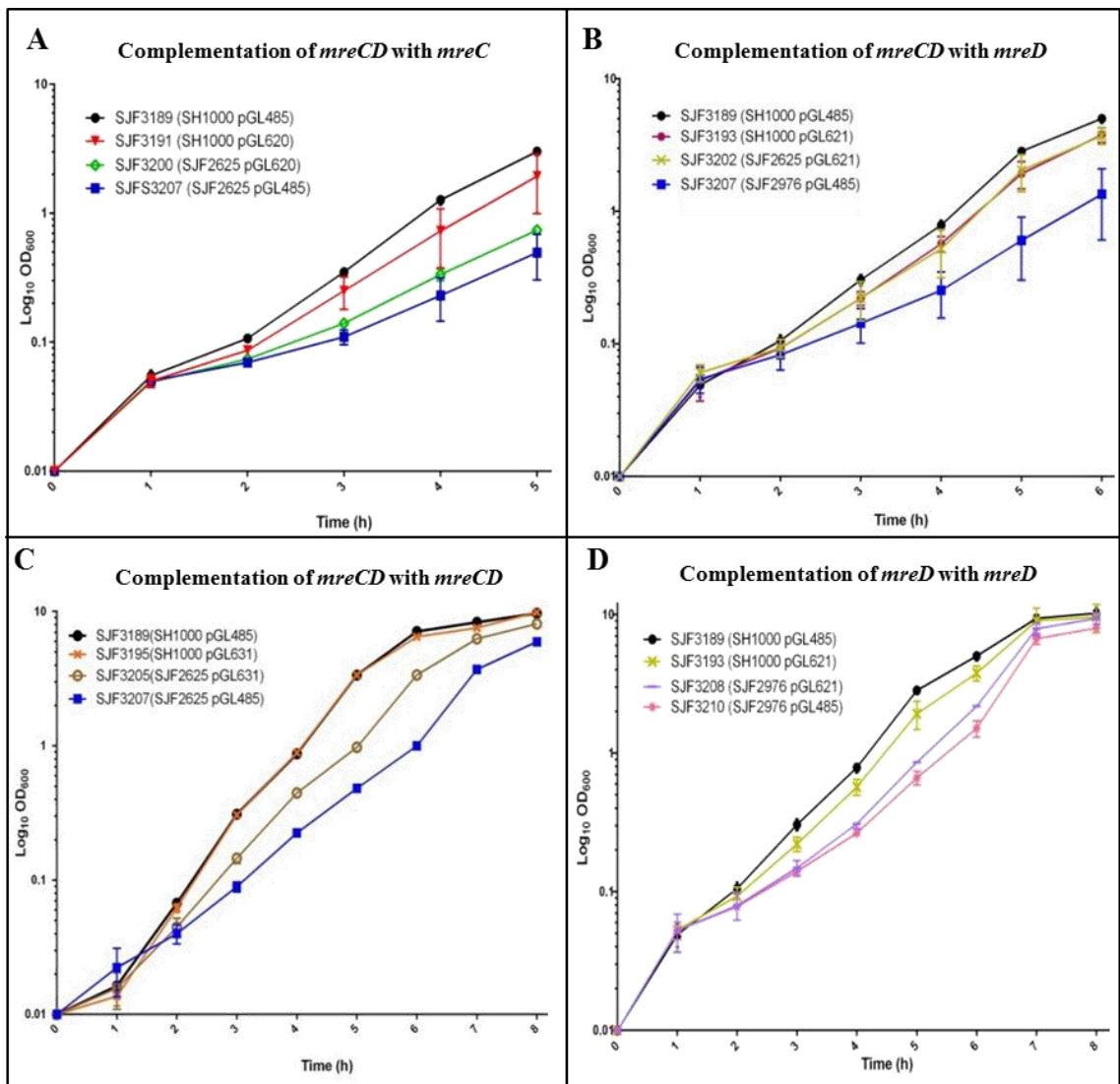
Figure 5-16 Growth of *mreC, mreD* or *mreCD* complemented strains

Cells were grown in BHI broth containing 15 μg ml^{-1} Cat at 37°C with shaking at 250 rpm. Growth was measured as OD$_{600}$ plotted as Log$_{10}$ OD$_{600}$. Mean values for 3 independent experiments are plotted and error bars represent the standard deviation.

A.   Growth curves of strains SJF3189 (SH1000 pGL485), SJF3191 (SH1000 pGL631 (*mreCD*)), SJF3205 (*mreCD::kan* pGL631 (*mreCD*)) and SJF3207 (*mreCD::kan* pGL485).

B.   Growth curves of strains SJF3189 (SH1000 pGL485), SJF3193 (SH1000 pGL621 (*mreD*)), SJF3202 (*mreCD::kan* pGL621 (*mreD*)) and SJF3207 (*mreCD::kan* pGL485).

C.   Growth curves of strains SJF3189 (SH1000 pGL485), SJF3195 (SH1000 pGL631 (*mreCD*), SJF3205 (*mreCD::kan* pGL631 (*mreCD*)) and SJF3207 (*mreCD::kan* pGL485).

D.   Growth curves of strains SJF3189 (SH1000 pGL485), SJF3193 (SH1000 pGL621 (*mreD*)), SJF3208 (*mreD::kan* pGL621 (*mreD*)) and SJF3210 (*mreD::kan* pGL485).

199

5.3.7 Effect of *mreCD* deletion on cell morphology

To determine the effect of *mreC*, *mreD* and *mreCD* deletion on cell morphology, strain SJF2625 (*mreCD::kan*), SJF2967 (*mreD::kan*), SJF4098 (*ΔmreC*) and SH1000 WT were inoculated in 1ml of BHI without drugs. Cells were grown at 37°C to exponential phase (OD$_{600}$=0.3). The cells were then fixed and examined via light and electron microscopy (Chapter 2.14).

Morphology of SJF4098 (*ΔmreC*) appeared similar to wild type SH1000. In the absence of MreD or MreCD a variety of phenotypes were observed: some wild type cells were present, most cells appeared slightly enlarged compared to SH1000 WT, and a few greatly enlarged cells were seen as well as mini sized cells (Fig. 5.17). Some of these enlarged cells were attached to a minicell, suggested that deletion of *mreD* or *mreCD* effects *S. aureus* cell division.

The cell diameter was measured after using Van-FL labelled cells, which will be further discussed in Chapter 5.3.8.6, shown in Figure 5.18. Only single cells that were visually spherical in phase contrast image were measured using Van-FL. The cell diameter of SJF4098 (*ΔmreC*) showed an increased proportion of enlarged cells with a mean diameter of 1.273 ± 0.168 comparing to a mean diameter of 1.198 ± 0.178 of WT, which is statistically significant ($p<0.05$) (Fig. 5.18). The growth of *mreD* deficient cells was significantly enlarged compared to WT: mean diameters was 1.352 ± 0.209 (P<0.0001), and more than 70% of SJF2976 (*mreD::kan*) has an diameter greater than 1.25 μm. Compared to SH1000 WT, a double deletion of *mreCD* showed different distribution patterns, in which the sizes are widely distributed ranging from 0.75 to 2.3 μm. The majority of the SJF2625 (*mreCD::kan*) cells have a diameter greater than 1.25 μm (87%), with nearly 15% cells over 1.75 μm, Whereas, there were no WT cells larger than 1.75 μm in diameter observed by this study. Interestingly, a higher frequency of enlarged cells (greater than 1.75 μm) was observed in SJF2625 (*mreCD::kan*) when compared to SJF4098 (*ΔmreC*) (20% more) and SJF2976 (*mreD::kan*) (17% more).

To further investigate the phenotype of SJF4098 (*ΔmreC*), SJF2976 (*mreD::kan*) and SJF2625 (*mreCD::kan*), transmission electron microscopy (TEM) was used to examine any morphological changes. Examples of typical *mreC, mreD* and *mreCD* deleted cells are shown in Figure 5.19. All the MreD deficient cells have a furry cell wall and a thicker septum (Fig. 5.19 C & D). Nearly half of SJF2976 (*mreD::kan*) (42%) and the majority of SJF2625 (*mreCD::kan*) (63%) lost spherical shape but were still capable of forming septa, though these septa were often asymmetric and resulted in the formation of multiple compartments (Fig.

5.19). This could be an indirect effect due to incorrect positioning of the division machinery in abnormally shaped cells.
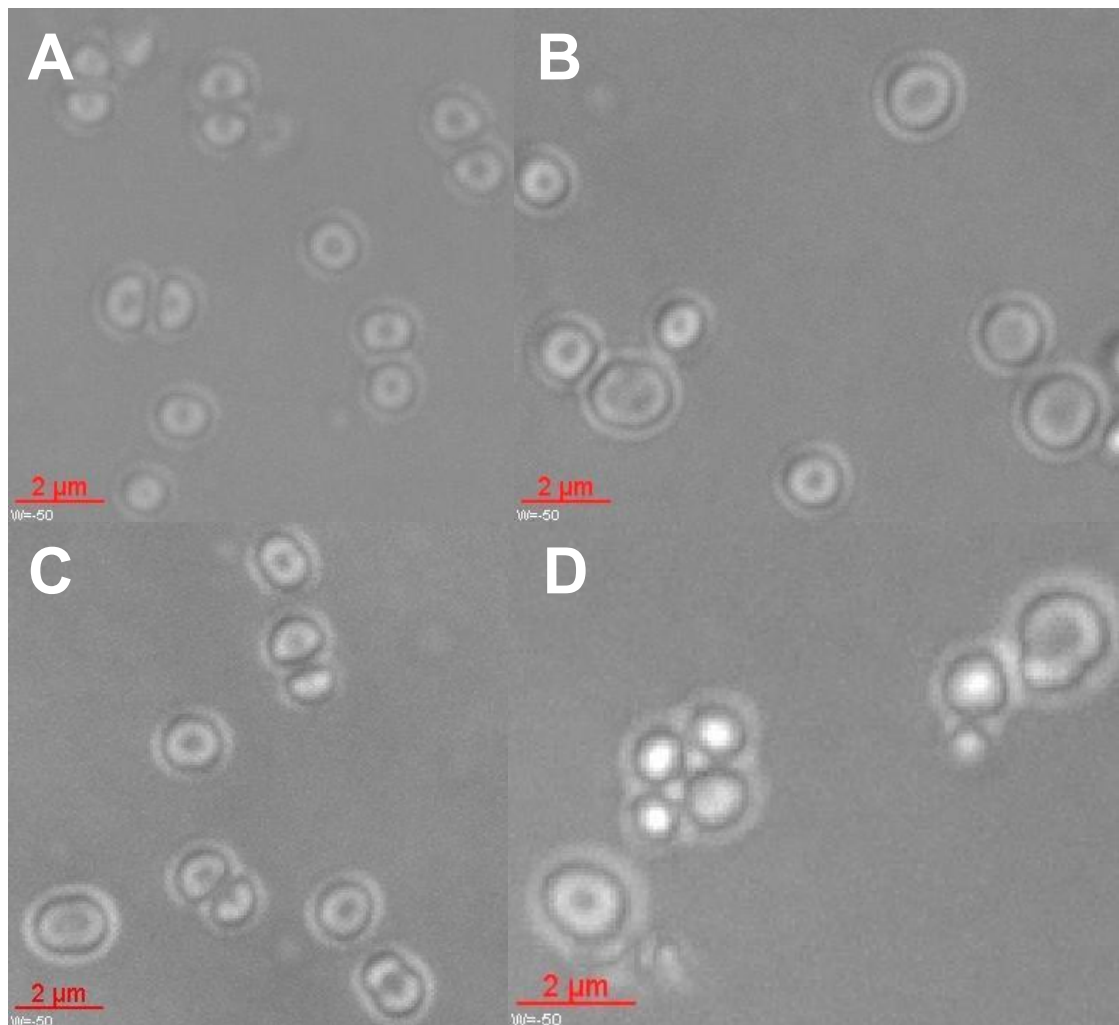
Figure 5-17 The effect of *mreC, mreD or mreCD* deletion on cell morphology

Phase contrast images of strain SH1000 (panel A), SJF2967 (*mreD::kan*) (panel B), SJF4098 (*ΔmreC*) (panel C) and SJF2625 (*mreCD::kan*) (panel D) grown in BHI without drugs to exponential phase (OD$_{600}$=0.3). Scale bar: 2µm.

SH1000 WT — Mean = 1.198μm, SDV = 0.178

SJF4098 (ΔmreC) — Mean = 1.273μm, SDV = 0.168

SJF2976 (ΔmreD) — Mean = 1.352μm, SDV = 0.209

SJF2625 (ΔmreCD) — Mean = 1.501μm, SDV = 0.243
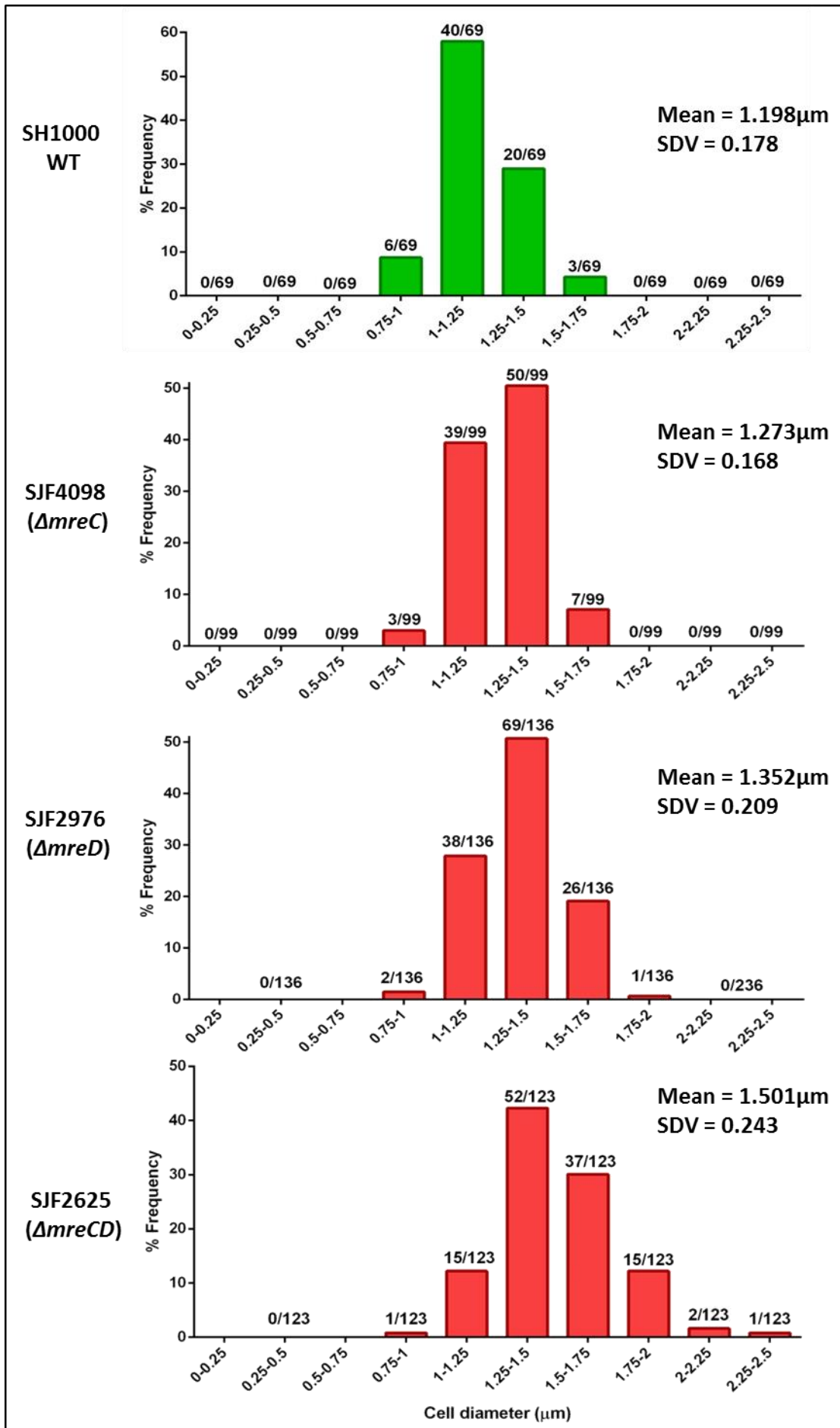
Figure 5-18 Role of MreC, MreD and MreCD in cell diameter determination

HistoGrams showing the distribution of cell diameters of SH1000 WT (green), SJF4098 (*ΔmreC*), SJF2976 (*mreD::kan*) and SJF2625 (*mreCD::kan*) grown in BHI with no drugs until OD$_{600}$=0.3. Statistically, the diameter of SJF4098 (*ΔmreC*) was significantly larger than SH1000 WT. SJF2976 (*mreD::kan*) and SJF2625 (*mreCD::kan*) showed significant increase in the number of enlarged cells. Measurements were made using softWoRx image analysis software. The numbers of each diameter category (x) are shown against the total number (y) of cells measured (x/y).
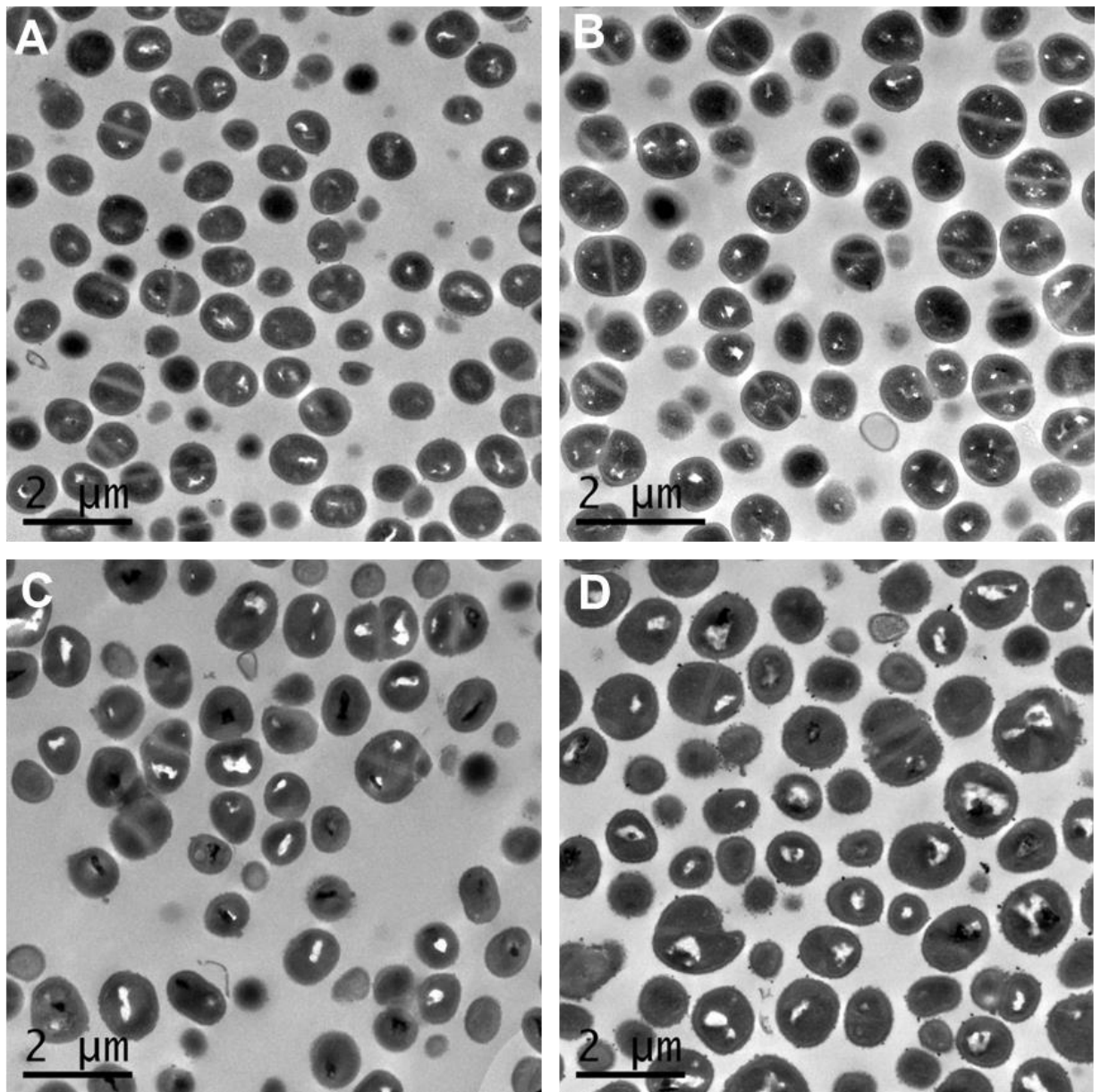
Figure 5-19 The role of MreC and MreD in cell morphology

TEM images of strain SH1000 (panel A), SJF4098 (*ΔmreC*) (panel B), SJF2967 (*mreD::kan*) (panel C) and SJF2625 (*mreCD::kan*) (panel D) grown in BHI without drugs until $OD_{600}=0.3$. Scale bar: 2μm.
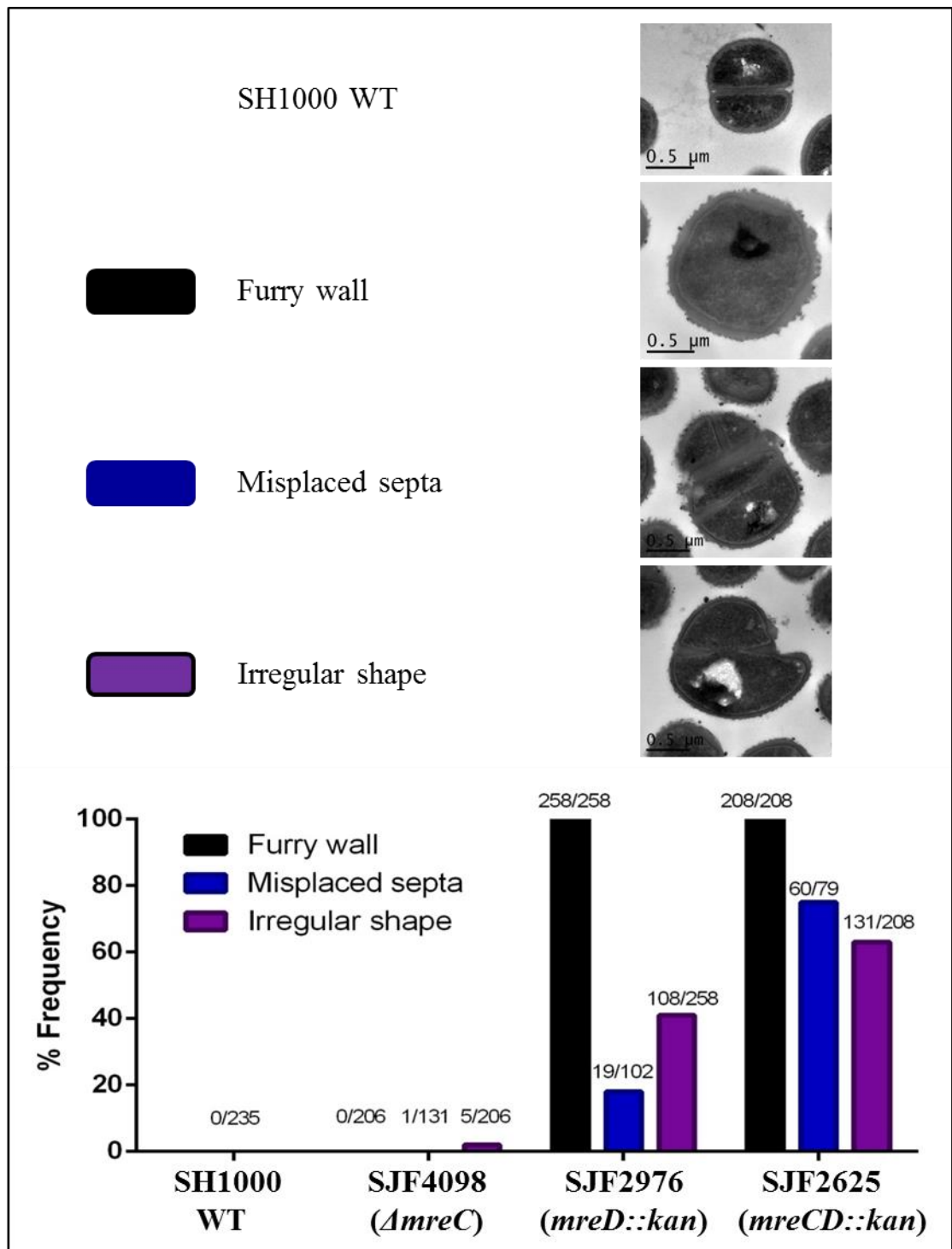
Figure 5-20 Frequency of morphological phenotypes in *mreC*, *mreD* or *mreCD* deleted *S. aureus*

HistoGrams showing the frequency of different cell morphologies of SH1000 WT, SJF4098 (*ΔmreC*), SJF2976 (*mreD::kan*) and SJF2625 (*mreCD::kan*) grown in BHI with no drugs until OD_{600}=0.3.

5.3.8 Role of *mreC*, *mreD* and *mreCD* deletion in localisation of cell division components

In order to further elucidate the roles of MreC and MreD during *S. aureus* cell division, and the order and hierarchy of division complex assembly, the localisation of other cell division components was performed in the mutant background.

5.3.8.1 Effect of MreC, MreD and MreCD-deletion on Noc localisation

In the rod-shaped organism *B. subtilis*, Noc is a non-sequence specific DNA-binding protein that recruits the nucleoid to membrane and therefore blocks cell division at these site (Wu & Errington 2012). A *S. aureus* Noc-GFP$^+$ fusion strain was constructed by Jagath Kasturiarachchi (University of Sheffield) using the same strategy as used to construct JGL229 (*mreC-gfp*). The ribosome binding site and coding sequence of *S. aureus noc* were cloned into pMUTIN-GFP+ to create an in-frame fusion of *noc* to *gfp*. The resulting plasmid was transformed into *S. aureus* RN4220 by electroporation. Integration of the plasmid into the chromosome results in a *noc-gfp* fusion under the control of the *noc* promoter, and a native copy of *noc* under the control of P$_{Spac}$. The plasmid insertion was transferred into the SH1000 background by phage transduction using Φ11.

The *noc-gfp* gene was transduced into SJF4098 (*ΔmreC*), SJF2976 (*mreD::kan*) and SJF2625 (*mreCD::kan*) using a Φ11 lysate of JGL220 (*noc-gfp$^+$*; P$_{Spac}$-*noc*). Due to insufficient time, construction of an alternative Noc-GFP$^+$ strain via allelic replacement was not attempted. Therefore in order to verify that native Noc is not required for localisation of Noc-GFP+, and that alterations of Noc-GFP+ localisation are due to levels of MreD and not levels of Noc, a control strain was made by Φ11 transduction of pGL485 into JGL228 (*noc-gfp*; P$_{Spac}$-*noc*) resulting in VF95 (*noc-gfp$^+$*; P$_{Spac}$-*noc* pGL485) (Steele *et al.* 2011). Both JGL220 (*noc-gfp$^+$*; P$_{Spac}$-*noc*) and VF95 (*noc-gfp$^+$*; P$_{Spac}$-*noc* pGL485) showed similar *noc*-GFP localisation.

In order to determine the effect of MreC and MreD on Noc localisation, the subcellular localisation of Noc in SJF4116 (*ΔmreC*; *noc*-gfp; P$_{Spac}$-*noc*), SJF4117 (*mreD::kan*; *noc-gfp*; P$_{Spac}$-*noc*) and SJF4114 (*mreCD::kan; noc-gfp*; P$_{Spac}$-*noc)* was examined.

Fluorescence microscopy of JGL220 (*noc-gfp$^+$*; P$_{Spac}$-*noc*) showed that in *S. aureus* Noc is predominantly in 2 foci away from developing septum (76.5%) (Fig. 5.21 A - C), suggesting that it could have a role in nucleoid occlusion. JGL220 (*noc-gfp$^+$*; P$_{Spac}$-*noc*) also displayed the same localisation pattern as VF95 (*noc-gfp$^+$*; PSpac-*noc* pGL485) (Steele *et al.* 2011), suggesting that native Noc is not required for localisation of Noc-GFP$^+$, and that alterations of Noc-GFP$^+$ localisation in JGL220 (*noc-gfp$^+$*; P$_{Spac}$-*noc*) is not due to the level of Noc.

	DIC	FL	Merged

WT

A | B | C

ΔmreC

D | E | F

ΔmreD

G | H | I

ΔmreCD

J | K | L
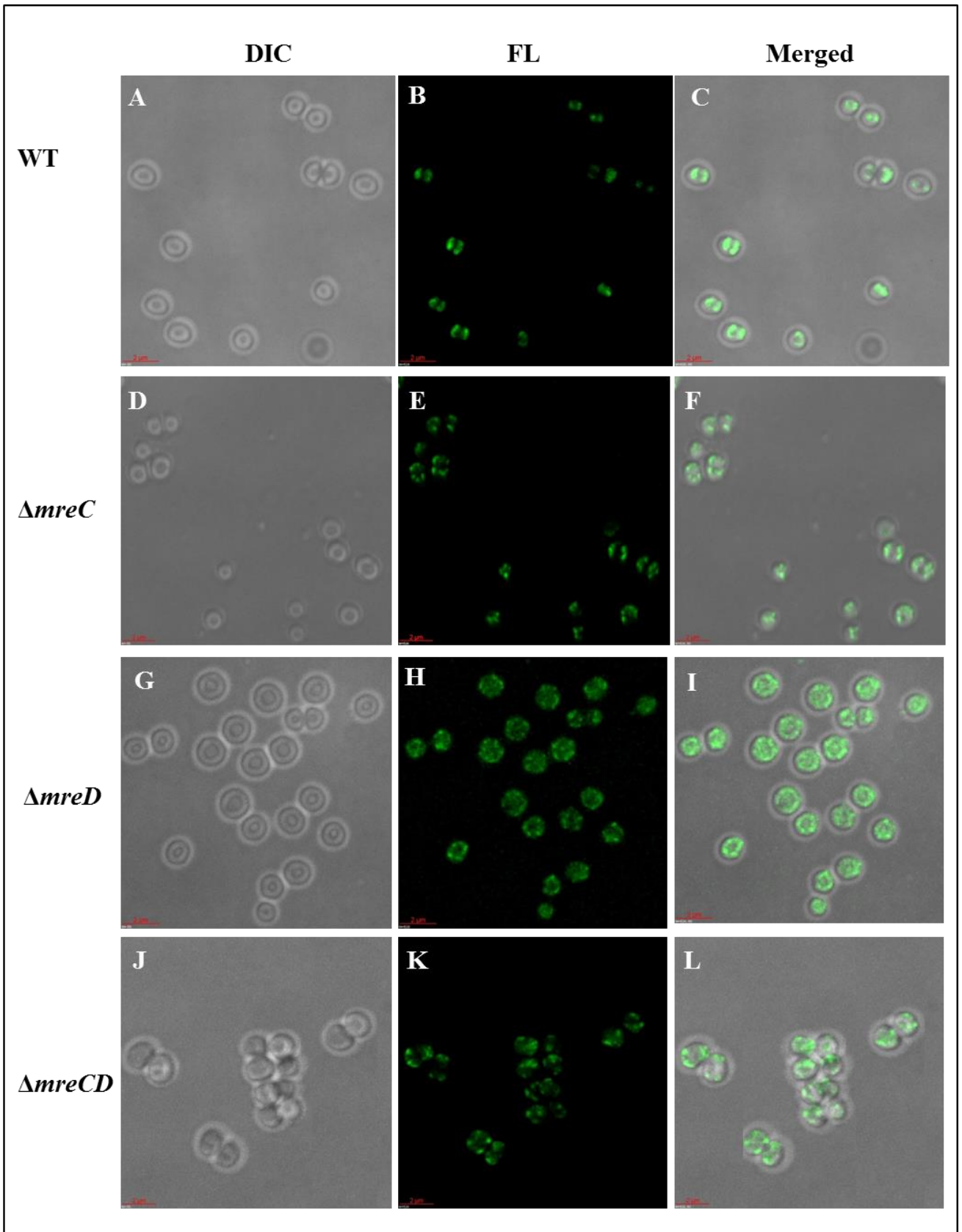
Figure 5-21 Localisation of Noc-GFP+ in MreC, MreD or MreCD-depleted *S. aureus*

Fluorescence and phase contrast images of JGL220 (*noc-gfp*$^+$; P$_{Spac}$-*noc*) (Panel A-C), SJF4116 (*ΔmreC*; *noc-gfp*; P$_{Spac}$-*noc*) (Panel D-F), SJF4117 (*mreD::kan*; *noc-gfp*$^+$; P$_{Spac}$-*noc*) (Panel G-I) and SJF4114 (*mreCD::kan; noc-gfp*$^+$; P$_{Spac}$-*noc)* (Panel J-L). The localisation of Noc was determined by fluorescent microscopy of fixed cells. All images are to the scale shown by the bar. The Noc-GFP$^+$ signal is shown in green in the merged image. Images were acquired using an Olympus IX70 microscope and SoftWoRx 3.5.0 software (Applied Precision). Scale bar: 2µm.

Previous results showed that the average cell diameter of the MreD deficient and MreCD deficient *S. aureus* was larger than wild-type (Chapter 5.2.7). The measurement of Noc-GFP+ distribution within a cell, as well as its diameter, allowed classification altered phenotypes. The cell populations were categorised into four types: small cells (diameter (D) <1.25 µm) with 2-foci, large cells (D > 1.25 µm) with 2 foci, small cells (D < 1.25 µm) with Noc dispersed all over the cells and large cells (D > 1.25 µm) with Noc dispersed all over the cells.

SJF4116 (*ΔmreC*; *noc-gfp*; P$_{Spac}$-*noc*), showed 17% less 2 foci Noc localisation than JGL220 (*noc-gfp*; P$_{Spac}$-*noc)*. Noc localisation was diffused (Fig. 5.22 G - I) in almost all cells (98%) of the enlarged SJF4117 (*mreD::kan*; *noc-gfp*; P$_{Spac}$-*noc*) (Fig. 5.22), indicating that septum formation does not occur in enlarged cells. Localisation of Noc-GFP+ in SJF4114 (*mreCD::kan; noc-gfp*; P$_{Spac}$-*noc*) (Fig. 5.19 J - L) showed different localisation pattern to all the other strains. No small cells were observed containing 2 foci Noc-GFP+ localisation comparing to 42% of that in wild type cell. 95% cells were enlarged and of which 74% contains 2 foci Noc-GFP+, and 26% enlarged cells contain dispersed Noc-GFP+. This observation implies loss of MreD significantly impacted on the Noc-GFP+ localisation.

Small cell (D<1.25 µm) with 2 foci Noc-GFP+

Small cell (D<1.25 µm) with Noc-GFP+ dispersed all over the cell
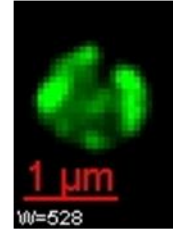
Big cell (D>1.25 µm) with 2 foci Noc-GFP+

Big cell (D>1.25 µm) with Noc-GFP+ dispersed all over the cell

Legend (chart):
- Big cell (D>1.25) with Noc-GFP+ present in the mid-cell
- Big cell (D>1.25) with two foci Noc-GFP+
- Small cell (D<1.25) with Noc-GFP+ present in the mid-cell
- Small cell (D<1.25) with two foci Noc-GFP+

Chart x-axis: SH1000 WT, SJF4098 (ΔmreC), SJF2976 (mreD::kan), SJF2625 (mreCD::kan)

n=85   n=65   n=63   n=41

Y-axis: %
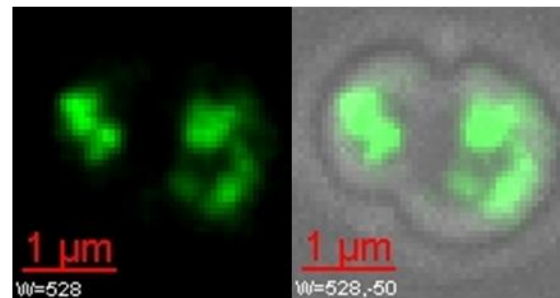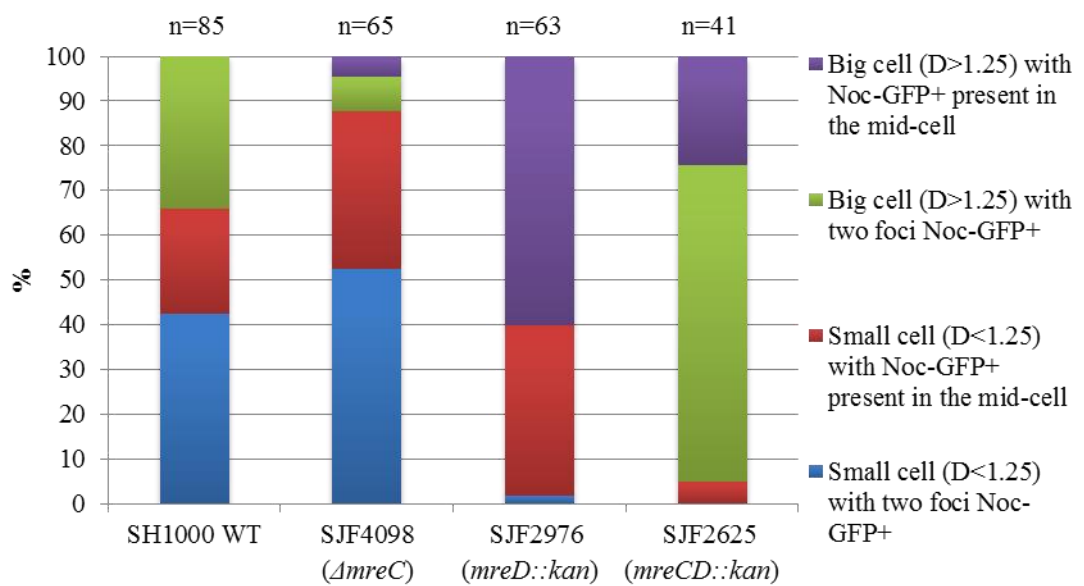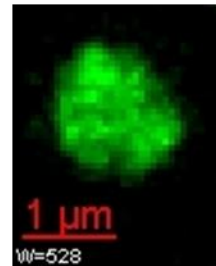
Figure 5-22 Frequency of phenotypes of Noc-GFP+ in MreC, MreD or MreCD-deleted
S. aureus

The localisation of Noc-GFP$^+$ was determined by fluorescence microscopy. Cells were given one of four phenotypes on the basis of their diameter (D) and Noc-GFP$^+$ distribution. Examples of the four phenotypes are shown above with Noc-GFP$^+$ shown in green. The frequency of phenotypes of JGL220 (*noc-gfp$^+$*; P$_{Spac}$-*noc*), SJF4116 (*ΔmreC*; *noc-gfp$^+$*; P$_{Spac}$-*noc*), SJF4117 (*mreD::kan*; *noc-gfp$^+$*; P$_{Spac}$-*noc*) and SJF4114 (*mreCD::kan; noc-gfp$^+$*; P$_{Spac}$-*noc*) is shown. The number of cells measured was 85, 65, 63 and 41 respectively. Cell measurements were made using SoftWoRx software. Scale bar: 1µm.

5.3.8.2   Role of MreC, MreD and MreCD in EzrA localisation

In *S. aureus*, EzrA is essential for growth and is required for assembly of the divisome at midcell (Steele *et al.* 2011). *S. aureus* EzrA has also been shown to interact with cytoplasmic, integral membrane and bitopic proteins and is required for peptidoglycan synthesis (Steele *et al.* 2011). Thus, EzrA may act as a scaffold protein for the recruitment of division proteins and formation of the divisome at midcell, and is required for correct PBP2 activity.

A *S. aureus* EzrA-GFP$^+$ fusion strain was constructed by Jagath Kasturiarachchi (University of Sheffield). The ribosome binding site and coding sequence of *S. aureus* *ezrA* were cloned into pMUTIN-GFP+ to create an in-frame fusion of *ezrA* to *gfp*. The resulting plasmid, pGL514, was transformed into *S. aureus* RN4220 by electroporation. Integration of the plasmid into the chromosome results in an *ezrA-gfp* fusion under the control of the *ezrA* promoter, and a native copy of *ezrA* under the control of P$_{Spac}$. The plasmid insertion was transferred into an SH1000 background by phage transduction using Φ11 generating JGL227 (*ezrA-gfp$^+$*; P$_{Spac}$-*ezrA*).

The EzrA-GFP+ construct was transduced into SJF4098 (*ΔmreC*), SJF2976 (*mreD::kan*) and SJF2625 (*mreCD::kan*) using a Φ11 lysate of JGL227 (*ezrA-gfp$^+$*; P$_{Spac}$-*ezrA*). Due to insufficient time, construction of an alternative EzrA-GFP+ strain via allelic replacement was not attempted. Therefore in order to verify that native EzrA is not required for localisation of EzrA-GFP+, and that alterations of EzrA-GFP+ localisation in JGL227 (*ezrA-gfp*; P$_{Spac}$-*ezrA*) is not due to the level of EzrA, a control strain was made by Φ11 transduction of pGL485 into JGL227 (*ezrA-gfp$^+$*; P$_{Spac}$-*ezrA*) resulting VF85 (*ezrA-gfp*; P$_{Spac}$-*ezrA* pGL485) (Steele *et al.* 2011). Both JGL227 (*ezrA-gfp*; P$_{Spac}$-*ezrA* and VF85 (*ezrA-gfp$^+$*; P$_{Spac}$-*ezrA* pGL485) showed identical *ezrA*-GFP localisation (Fig. 5.23 A-C).

	DIC	FL	Merged

WT

A B C

ΔmreC

D E F

ΔmreD

G H I

ΔmreCD

J K L
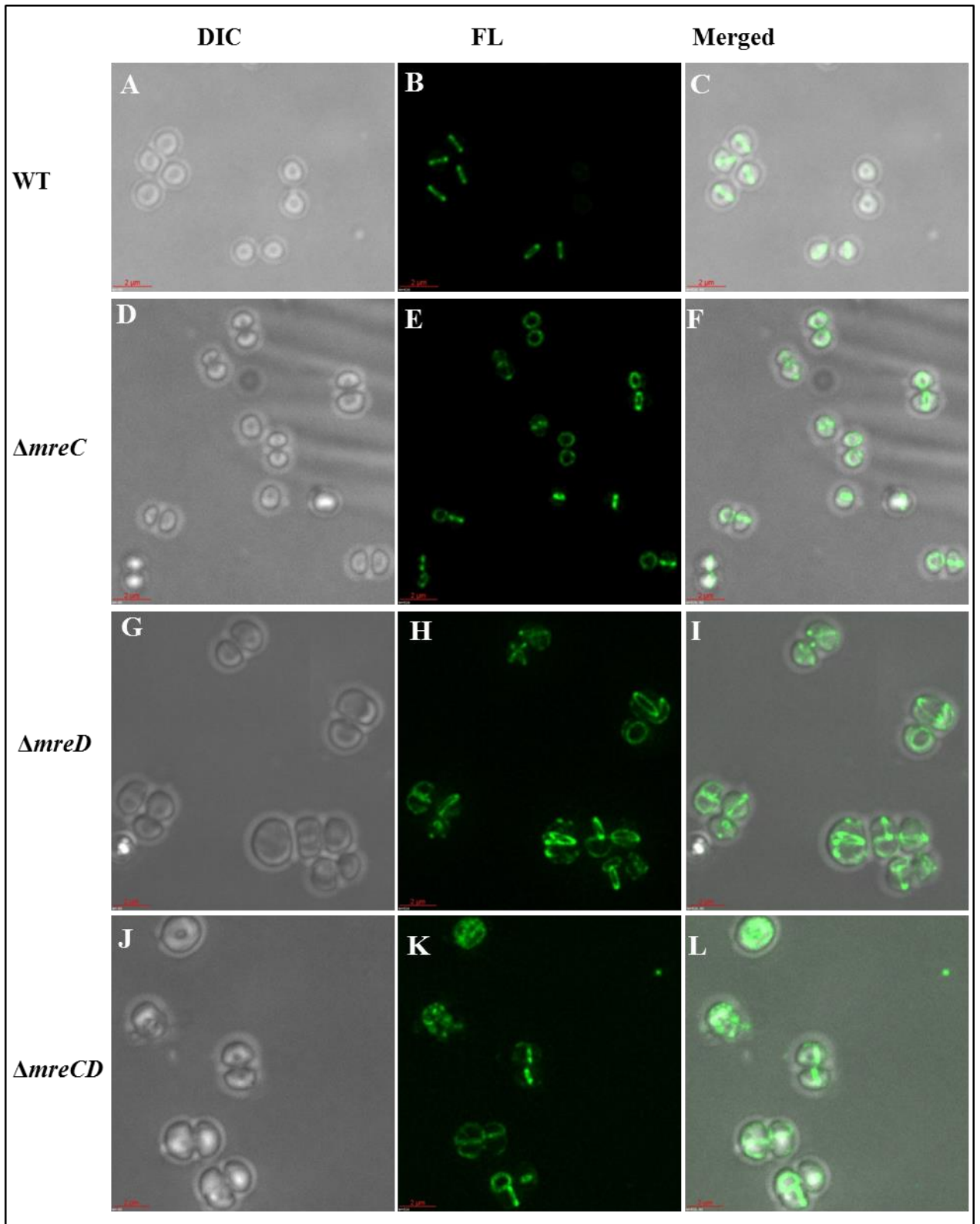
Figure 5-23 Localisation of EzrA-GFP+ in MreC, MreD or MreCD depleted *S. aureus*

Fluorescence and phase contrast images of JGL227 (*ezrA-gfp*$^+$; P$_{Spac}$-*ezrA*). (Panel A-C), SJF4103 (*ΔmreC*; *ezrA-gfp*$^+$; P$_{Spac}$-*ezrA*) (Panel D-F), SJF3286 (*mreD::kan*; *ezrA-gfp*$^+$; P$_{Spac}$-*ezrA*) (Panel G-I) and SJF3285 (*mreCD::kan; ezrA-gfp*$^+$; P$_{Spac}$-*ezrA)* (Panel J-L). The localisation of EzrA was determined by fluorescent microscopy of fixed cells.

SJF4103 (*ΔmreC*; *ezrA-gfp*; P$_{Spac}$-*ezrA*) showed similar localisation pattern of EzrA as control JGL227 *(ezrA-gfp*; P$_{Spac}$-*ezrA*), SJF3286 (*mreD::kan*; *ezrA-gfp*$^+$; P$_{Spac}$-*ezrA*) and SJF3285 (*mreCD::kan; ezrA-gfp*$^+$; P$_{Spac}$-*ezrA)* showed irregular EzrA localisation, including a spiral shape (H) and misplaced septa (K). Scale bar: 2μm. The EzrA-GFP+ signal is shown in green in the merged image. Images were acquired using an Olympus IX70 microscope and SoftWoRx 3.5.0 software (Applied Precision).

Fluorescence microscopy of JGL227 (*ezrA-gfp$^+$*; P$_{Spac}$-*ezrA*) showed that in *S. aureus* SH1000, EzrA is localised as a ring to the division site in nearly all cells, consistent with a role in cell division in this organism (Fig. 5.23 A - C). In MreC deficient cells (Fig. 5.23 D - F), EzrA-GFP+ was observed as a ring at the division septum in half of the cells (96%), However, slightly less than WT cells (94%) (Fig. 5.24), which is statistically significant (P value = 0.0048). The majority of SJF3286 (*mreD::kan*; *ezrA-gfp$^+$*; P$_{Spac}$-*ezrA*) (68%) showed misplaced septal localisation of EzrA (Fig. 5.24). Those cells were still capable of forming septa, though these septa were often asymmetric resulting in the formation of multiple compartments (Fig. 5.23 G-L), whereas, this was not observed in WT cells and *mreC* cells. As predicted SJF3285 (*mreCD::kan; ezrA-gfp$^+$*; P$_{Spac}$-*ezrA)* displayed a more severe defect with an increased number of mutant cells showing an irregular septum formation and again there was an increased proportion of enlarged cells (Fig. 5.24). Notably, punctate EzrA-GFP$^+$ was localised around the cell periphery (Fig. 5.24).

This observation showed that the localisation of EzrA-GFP$^+$ was affected by deletion of *mreC*, *mreD* or *mreCD*, suggesting that MreCD is required for recruitment of EzrA to the correct division septum.

Small cell (D<1.25 μm)
with a ring of EzrA-GFP+
at midcell
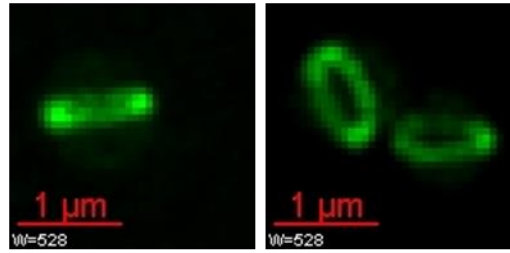
Big cell (D>1.25 μm)
with ring of EzrA-GFP +
at midcell
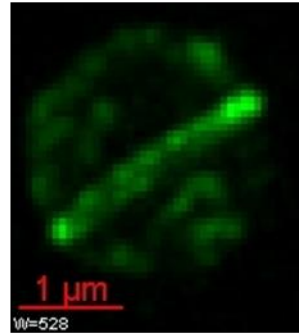
Big cell (D>1.25 μm)
with EzrA-GFP + dispersed
around cell periphery

Big cell (D>1.25) with
EzrA-GFP+ dipersed
around the cell periphery
or misplace multi-ring

Big cell (D>1.25) with
ring of EzrA-GFP+ at
midcell

Small cell (D<1.25) with
ring of EzrA-GFP+ at
midcell
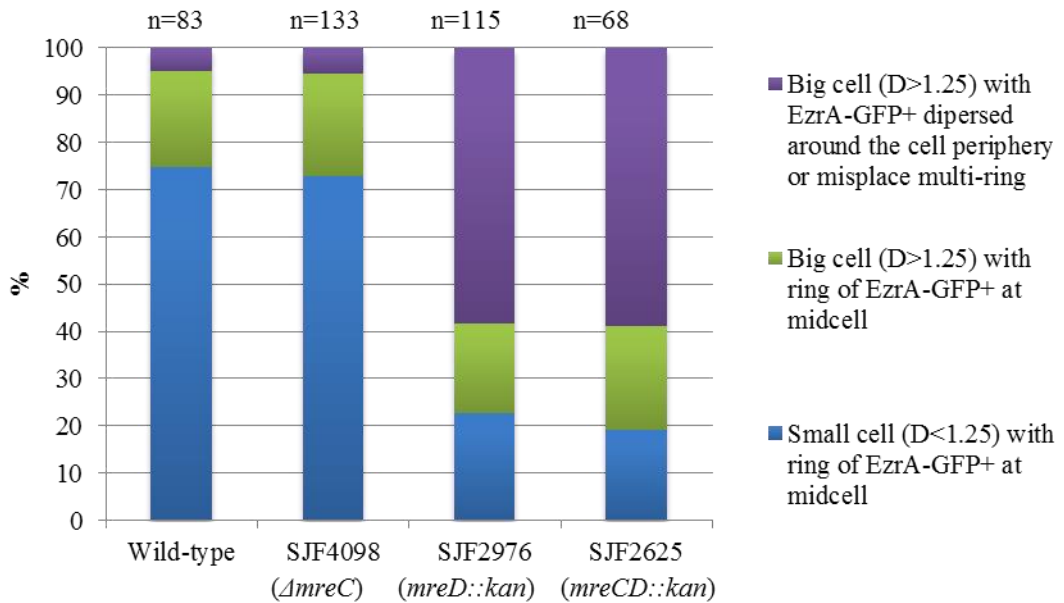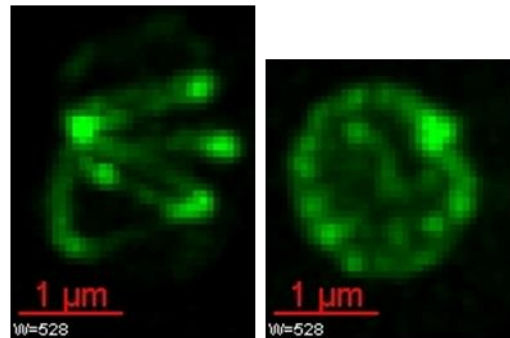
Figure 5-24 Frequency of phenotypes of EzrA-GFP+ in MreC, MreD or MreCD depleted *S. aureus*

The localisation of EzrA was determined by fluorescence microscopy. Cells were given one of three phenotypes on the basis of their diameter (D) and EzrA distribution. Examples of the three phenotypes are shown above with EzrA-GFP+ shown in green. The frequency of phenotypes of JGL227 (*ezrA-gfp*; P$_{Spac}$-*ezrA*), SJF4103 (*ΔmreC*; *ezrA-gfp*; P$_{Spac}$-*ezrA*), SJF3286 (*mreD::kan*; *ezrA-gfp*; P$_{Spac}$-*ezrA*) and SJF3285 (*mreCD::kan; ezrA-gfp*; P$_{Spac}$-*ezrA*) is shown. The number of cells measured was 83, 133, 115 and 68 respectively. Cell measurements were made using SoftWoRx software. Scale bar: 1µm.

5.3.8.3 Role of MreC, MreD and MreCD in GpsB localisation

In *B. subtilis*, an *ezrA/gpsB* double mutant is synthetically lethal, with defects in both cell division and cell elongation. It has been suggested that GspB and EzrA act together to orchestrate the shift in localization of PBP1 between elongation and division sites (Claessen *et al.* 2008). In *B. subtilis*, time-lapse microscopy of a GpsB-GFP$^+$ fusion has shown GpsB to localise to the lateral cell wall during elongation and to the septum during division. In *S. aureus*, GpsB localises to the division septum (Steele *et al.* 2011). BACTH analysis has shown both MreC and MreD interact with GpsB in *S. aureus* (Fig. 3.6).

A *S. aureus* GpsB-GFP$^+$ fusion strain was constructed by Jagath Kasturiarachchi (University of Sheffield) using the same strategy as used to construct JGL229 (*mreC-gfp$^+$*). The ribosome binding site and coding sequence of *S. aureus gpsB* were cloned into pMUTIN-GFP+ to create an in-frame fusion of *gpsB* to GFP+. The resulting plasmid was introduced into *S. aureus* RN4220 by electroporation. Integration of the plasmid into the chromosome results in a *gpsB-gfp$^+$* fusion under the control of the *gpsB* promoter, and a native copy of *gpsB* under the control of P$_{Spac}$. The plasmid insertion was transduced into an SH1000 background by phage transduction using Φ11.

The *gpsB*-GFP gene was transduced into SJF4098 (*ΔmreC*), SJF2976 (*mreD::kan*) and SJF2625 (*mreCD::kan*) using a Φ11 lysate of JGL228 (*gpsB-gfp$^+$*; P$_{Spac}$-*gpsB*). In order to determine the effect of MreC and MreD on GpsB localisation, the subcellular localisation of GpsB in SJF4109 (*mreC*; *gpsB-gfp$^+$*; P$_{Spac}$-*gpsB*), SJF4120 (*mreD::kan*; *gpsB-gfp$^+$*; P$_{Spac}$-*gpsB*) and SJF4121 (*mreCD::kan; gpsB-gfp$^+$*; P$_{Spac}$-*gpsB)* was analysed by fluorescent microscopy of fixed cells. Due to insufficient time, construction of an alternative GspB-GFP+ strain via allelic replacement was not attempted. Steel verified that native GpsB is not required for localisation of GpsB-GFP+, and that alterations of GpsB-GFP+ localisation in JGL228 *gpsB-gfp$^+$*; P$_{Spac}$-*gpsB*) are not due to the level of GpsB, (Steele *et al.* 2011). Therefore, JGL228 *(gpsB-gfp*; P$_{Spac}$-*gpsB*) was considered as a control.

Fluorescence microscopy of JGL228 (*gpsB-gfp*; P$_{Spac}$-*gpsB*) showed that in *S. aureus* SH1000, GpsB was localised to the division site in nearly all cells, consistent with a role in cell division in this organism (Fig. 5.25 A - C). In MreC deficient cells, localisation of GpsB-GFP+ was similar to SH1000 WT (Fig. 5.25 D - F), although most (85%) had multi focus of GpsB-GFP+ (Fig. 5.26). In SJF4120 (*mreD::kan*; *gpsB-gfp$^+$*; P$_{Spac}$-*gpsB*) and SJF4121 (*mreCD::kan; gpsB-gfp$^+$*; P$_{Spac}$-*gpsB)*, many large cells (D> 1.25 μm) were observed, as seen previously for *mreC* and *mreCD* (Chapter 5.3.7), the localisation of GpsB-GFP+ in *mreD* was not statistically significant comparing to WT (P value = 0.1177), despite the size differences.
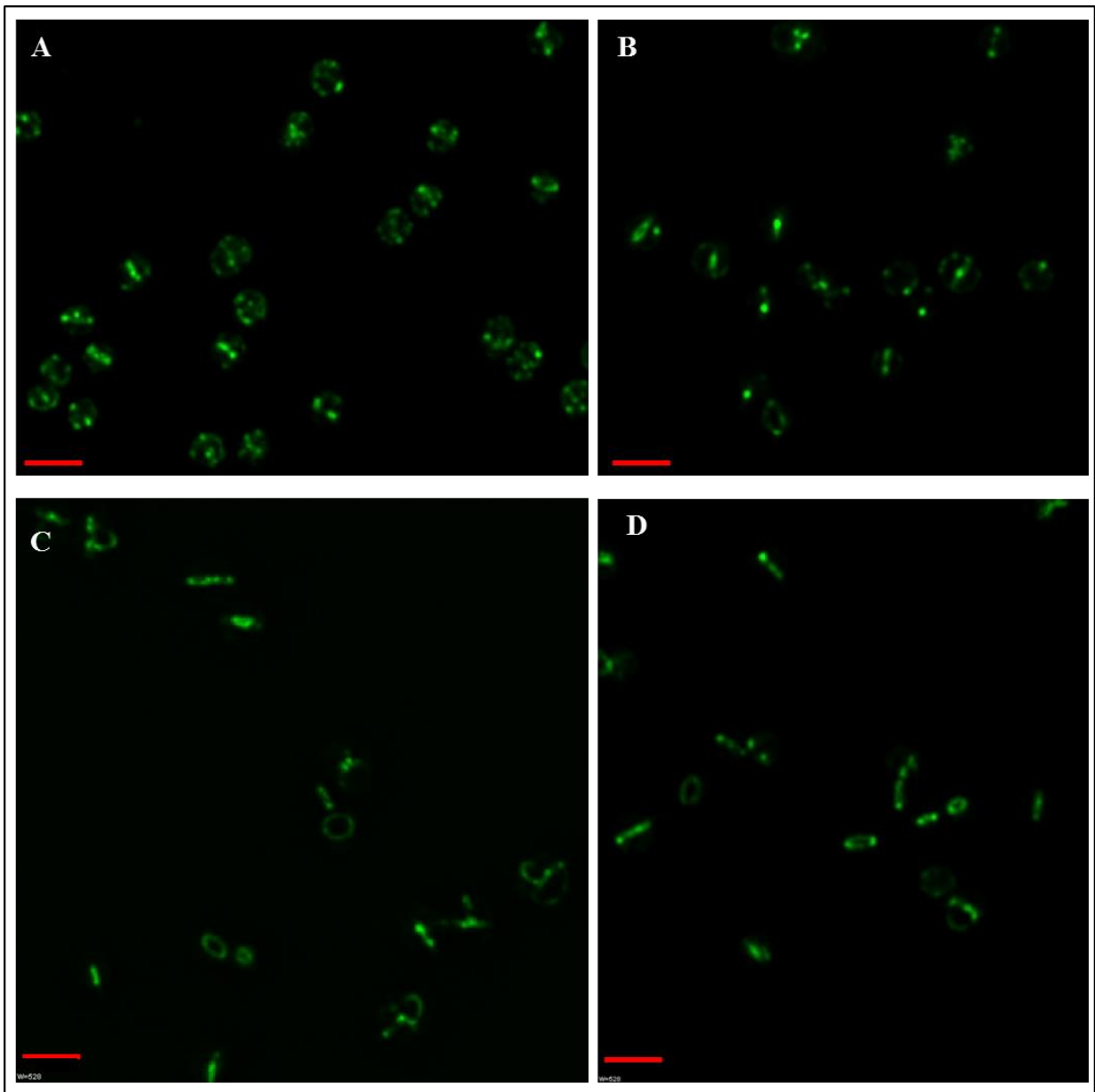
Figure 5-25 Localisation of GpsB-GFP+ in *mreC*, *mreD* and *mreCD S. aureus*

Fluorescence images of JGL228 (*gpsB-gfp$^+$*; P$_{Spac}$-*gpsB*) (Panel B), SJF4109 (*ΔmreC*; *gpsB-gfp*; P$_{Spac}$-*gpsB*) (Panel A), SJF4120 (*mreD::kan*; *gpsB-gfp*; P$_{Spac}$-*gpsB*) (Panel C) and SJF4121 (*mreCD::kan; gpsB-gfp$^+$*; P$_{Spac}$-*gpsB)* (Panel D), which were grown for 1.5h and 3 h in BHI to allow three doublings. The localisation of GpsB was determined by fluorescent microscopy of fixed cells. All mutant strains showed similar localisation of GpsB as control JGL228 (*gpsB-gfp$^+$*; P$_{Spac}$-*gpsB*), which displayed the same GpsB distribution pattern as VF94 (*gpsB-gfp$^+$*; P$_{Spac}$-*gpsB* pGL485) (Steele *et al.* 2011). All images are to the scale shown by the bar. The GpsB-GFP+ signal is shown in green in the merged image. Images were acquired using an Olympus IX70 microscope and SoftWoRx 3.5.0 software (Applied Precision). Scale bar, 2μm.

Notably, deletion of both *mreD* and *mreCD* genes resulting accumulation of GpsB-GPF+ to the septal, nearly 23% (*mreD*) and 25% (*mreCD*) more cells showed mid-cell localisation than that in the wild-type cells.

This observations implied localisation of GpsB-GFP+ was affected by deletion of MreC, and MreCD, suggesting that MreC or MreCD may paly a role in affecting the temporal localisation of GpsB to the division septum in *S. aureus*.

Small cell (D<1.25 μm)
with ring of GpsB-GFP+
at midcell
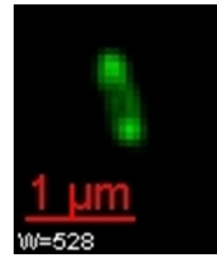
Small cell (D<1.25 μm)
with multi foci GpsB-GFP+
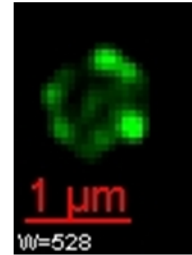
Big cell (D>1.25 μm)
with ring of GpsB-GFP+
at midcell
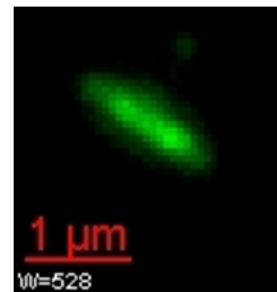
Big cell (D>1.25 μm)
with multi foci GpsB-GFP+
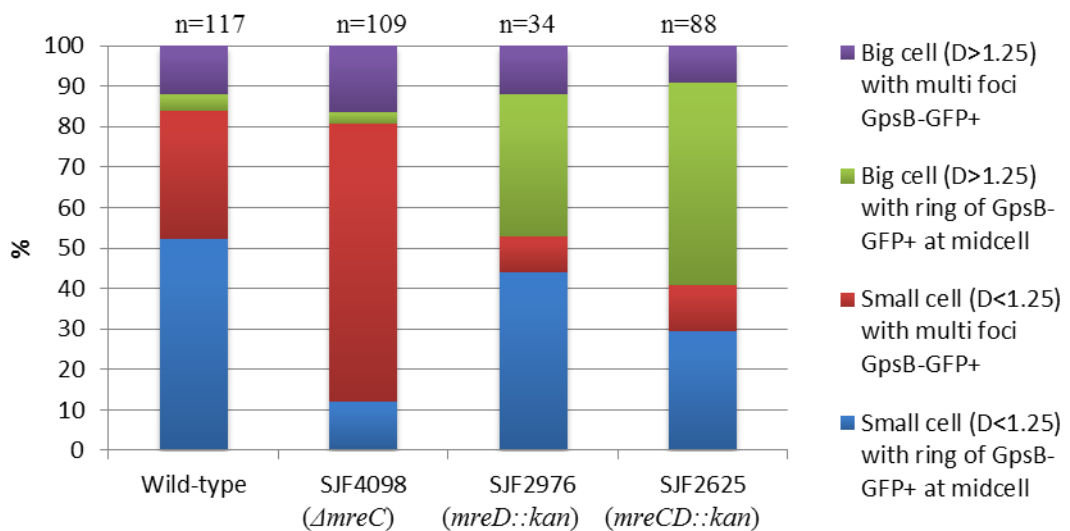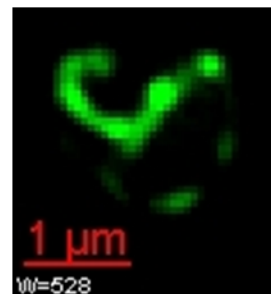
Figure 5-26 Frequency of phenotypes of GpsB-GFP+ in *mreC*, *mreD* and *mreCD* deleted *S. aureus*

Fresh cells were inoculated in BHI and allowed to grow for three doubling time. The localisation of GpsB-GFP+ was determined by fluorescence microscopy. Cells were given one of four phenotypes on the basis of their diameter (D) and GpsB-GFP+ distribution. Examples of the four phenotypes are shown above with GpsB-GFP+ shown in green. The frequency of phenotypes of JGL228 (*gpsB-gfp$^+$*; P$_{Spac}$-*gpsB*), SJF4109 (*ΔmreC*; *gpsB-gfp$^+$*; P$_{Spac}$-*gpsB*), SJF4120 (*mreD::kan*; *gpsB-gfp$^+$*; P$_{Spac}$-*gpsB*) and SJF4121 (*mreCD::kan; gpsB-gfp$^+$*; P$_{Spac}$-*gpsB*) are shown. The number of cells measured was 117, 109, 34 and 88 respectively. Cell measurements were made using SoftWoRx software. Scale bar: 1μm.

5.3.8.4 Role of MreC, MreD and MreCD in PlsY localisation

In *B. subtilis,* PlsY is an essential membrane-bound acyltransferase that catalyses the first acylation step of glycerol-P of phosphatidic acid biosynthesis (Kobayashi *et al.* 2003; Cherian *et al.* 2012). PlsY is highly conserved in bacteria. In *S. aureus*, it was found that cell division was impaired in cells with *plsY* under the control of the IPTG-inducible promoter P_{Spac}, in the absence of IPTG (Garcia-Lara *et al.* 2005).

The localisation of PlsY in *S. aureus* has not previously been shown. A *S. aureus* chromosomal PlsY-GFP fusion strain was constructed by Jagath Kasturiarachchi (University of Sheffield) using the same strategy as used to construct JGL229 (*mreC-gfp*[+]). The ribosome binding site and coding sequence of *S. aureus plsY* were cloned into pMUTIN-GFP+ to create an in-frame fusion of *gpsB* to *gfp*. Integration of the plasmid into the chromosome results in a *plsY-gfp*[+] fusion under the control of the *plsY* promoter, and a native copy of *plsY* under the control of P_{Spac}. The plasmid insertion was transduced into an SH1000 background by phage transduction using Φ11.

The PlsY-GFP+ fusion was transduced into SJF4098 (*ΔmreC*), SJF2976 (*mreD::kan*) and SJF2625 (*mreCD::kan*) using a Φ11 lysate of SJF2164 *(plsY-gfp*[+]; P_{Spac}-*plsY)*. In order to determine the role of MreC and MreD in PlsY localisation, the subcellular localisation of PlsY in SJF4129 (*ΔmreC*; *plsY-gfp*[+]; P_{Spac}-*plsY*), SJF4127 (*mreD::kan*; *plsY-gfp*[+]; P_{Spac}-*plsY*) and SJF4128(*mreCD::kan*; *plsY-gfp*[+]; P_{Spac}-*plsY)* was analysed by fluorescence microscopy of fixed cells. Due to insufficient time, construction of an alternative PlsY-GFP+ strain via allelic replacement was not attempted. Therefore in order to verify that native PlsY is not required for localisation of PlsY-GFP+, and that alterations of PlsY-GFP+ localisation in SJF2164 (*plsY-gfp*[+]; P_{Spac}-*plsY*) are not due to the level of PlsY, a control strain was made by Φ11 transduction of pGL485 into SJF2164 (*plsY-gfp*[+]; P_{Spac}-*plsY*) resulting in JGL260 (*plsY-gfp*[+]; P_{Spac}-*plsY*; pGL485). Both SJF2164 (*plsY-gfp*[+]; P_{Spac}-*plsY*) and JGL260 (*plsY-gfp*[+]; P_{Spac}-*plsY*; pGL485) showed identical PlsY-GFP+ localisation (Garcia-Lara, unpublished).

Fluorescence microscopy of SJF2164 (*plsY-gfp*[+]; P_{Spac}-*plsY*) showed that PlsY was septally located (Fig. 5.27), but also distributed in a regular pattern of foci around the membrane throughout the cell cycle, 6 to 9 foci at the midcell focal plane was observed (Fig. 5.27 A). In the *mreC* mutant (Fig 5.27 B), the majority of cells preserved regular dotty pattern of PlsY-GFP+, despite the enlarged cell size (Fig. 5.28). The localisation of PlsY-GFP+ displayed a similar pattern in both *mreD* and *mreCD* mutants. The regular punctate PlsY-GFP+ distribution was significantly disrupted (Fig. 5.27 C & D). Amongst small cells (D<1.25μm), PlsY-GFP+ was dispersed in more than half of *mreD* mutant cells. Approximately 75% greatly enlarged cells lost regularly punctuated PlsY-GFP+ localisation.
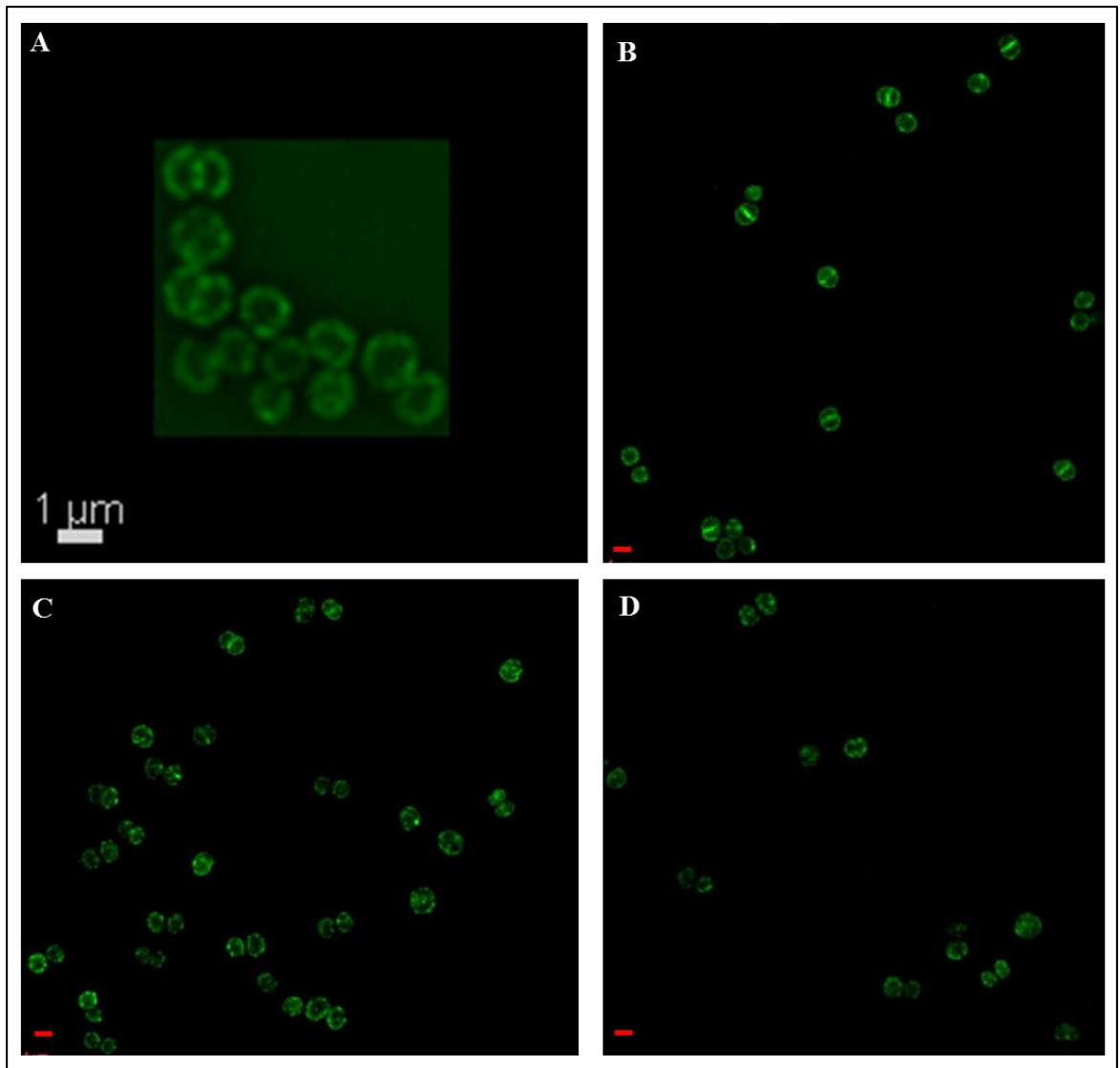
Figure 5-27 Localisation of PlsY-GFP+ in *mreC*, *mreD* or *mreCD* deleted *S. aureus*

Fluorescence images of SJF2164 (*plsY-gfp*$^+$; P$_{Spac}$-*gpsB*) (Panel A), Fluorescence images of SJF4129 (*ΔmreC*; *plsY-gfp*$^+$; P$_{Spac}$-*plsY*) (Panel B), SJF4127 (*mreD::kan*; *plsY-gfp*; P$_{Spac}$-*plsY*) (Panel C) and SJF4128 (*mreCD::kan*; *plsY-gfp*$^+$; P$_{Spac}$-*plsY*) (Panel D), until OD$_{600}$=0.3. The localisation of PlsY was determined by fluorescence microscopy of fixed cells. The PlsY-GFP+ signal is shown in green in the images. Images were acquired using an Olympus IX70 microscope and SoftWoRx 3.5.0 software (Applied Precision). Scale bar, 1μm.

Small cell (D<1.25 μm) with regular punctated PlsY-GFP+
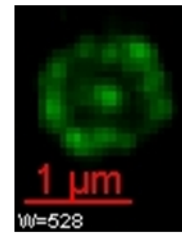
Small cell (D<1.25 μm) with irregular PlsY-GFP+ around cell periphery
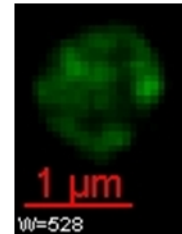
Big cell (D>1.25 μm) with regular punctated PlsY-GFP+

Big cell (D>1.25 μm) with irregular PlsY-GFP+

Big cell (D>1.25μm) with irregular PlsY-GFP+

Big cell (D>1.25) with regular punctated PlsY-GFP+

small cell (D<1.25μm) with irregular PlsY-GFP+
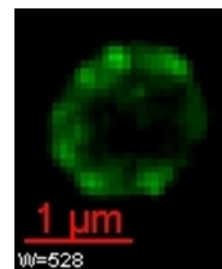
small cell (D<1.25) with regular punctated PlsY-GFP+
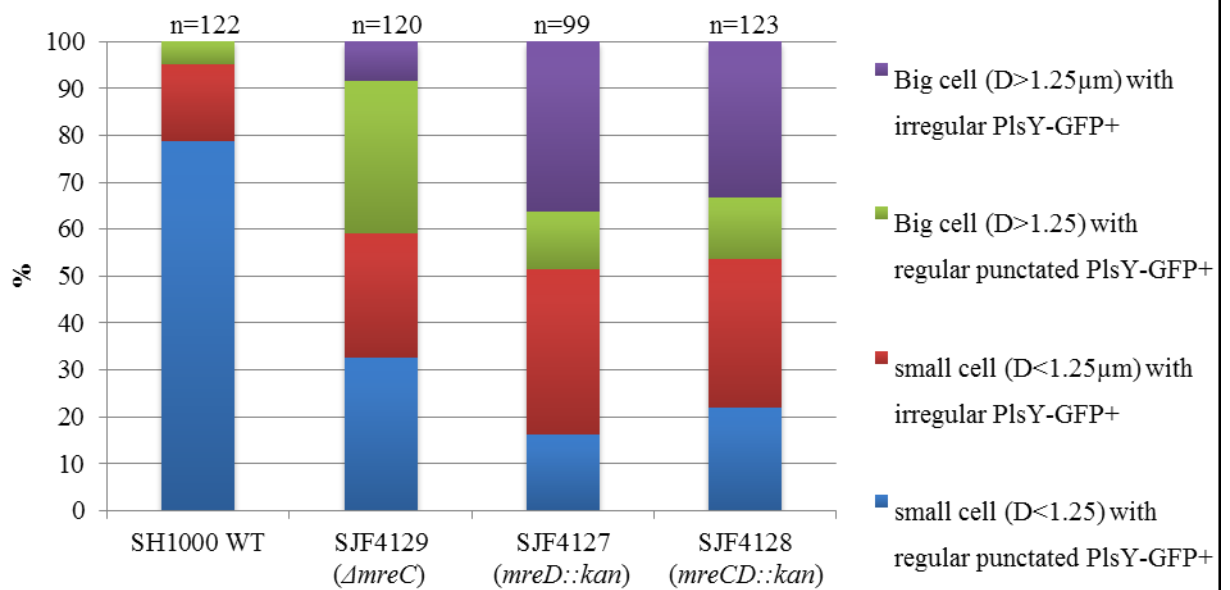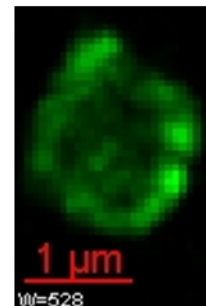
Figure 5-28 Frequency of phenotypes of PlsY-GFP+ in MreC, MreD or MreCD-deficient *S. aureus*

The localisation of PlsY-GFP+ was determined by fluorescence microscopy. Cells were given one of four phenotypes on the basis of their diameter (D) and PlsY-GFP+ distribution. Examples of the four phenotypes are shown above with PlsY-GFP+ shown in green. The frequency of phenotypes of SJF2164 (*plsY-gfp$^+$*; P$_{Spac}$-*plsY*) (Fig. 5.27 Panel B), SJF4129 (*ΔmreC*; *plsY-gfp$^+$*; P$_{Spac}$-*plsY*) (Panel D-F), SJF4127 (*mreD::kan*; *plsY-gfp$^+$*; P$_{Spac}$-*plsY*) (Fig. 5.27 Panel C) and SJF4128 (*mreCD::kan; plsY-gfp$^+$*; P$_{Spac}$-*plsY*) Fig. 5.27 (Panel D) are shown. The number of cells measured was 122, 120, 99 and 123 respectively. Cell measurements were made using SoftWoRx software. Scale bar: 1µm.

These results show that in *S. aureus*, MreD is required for the PlsY patterned distribution around the cell membrane. Due to the interaction between these two proteins (Fig. 3.4), it is likely that this recruitment is direct. It is possible that these PlsY foci represent membrane phospholipid biosynthesis complexes and that in the absence of any MreD these complexes are unable to form, resulting in large cells with dispersed PlsY localisation.

5.3.8.5 Role of MreC, MreD and MreCD in CdsA localisation

CTP-phosphatidic acid cytidylyltransferase (CDP-diacylglycerol synthase) is present across prokaryotes and eukaryotes. CdsA, encoding cytidine 5'-diphosphate (CDP)-diacylglycerol synthase, is responsible for the transformation of phosphatidic acid to CDP-diacylglycerol, which is a central intermediate in phospholipid synthesis (Dowhan 1997; Laczko-Dobos *et al.* 2008). Raetz and co-workers reported that mutations in *cdsA* leads to accumulation of phosphatidic acid in *E. coli* and defectiveness in phosphatidylglycerol synthesis in *Synechocystis* (Ganong & Raetz 1982; Sato *et al.* 2000). BACTH analysis has shown *S. aureus* MreC, MreD and PlsY interact with CdsA in *E. coli* (Fig. 3.4).

The localisation of CdsA remains unexplored in *S. aureus*. A *S. aureus* CdsA-GFP+ fusion strain was constructed by Jagath Kasturiarachchi (University of Sheffield) using the same strategy as used to construct JGL229 (*mreC-gfp*$^+$). The ribosome binding site and coding sequence of *S. aureus cdsA* were cloned into pMUTIN-GFP+ to create an in-frame fusion of *cdsA* to *gfp*$^+$. The resulting plasmid was introduced into *S. aureus* RN4220 by electroporation. Integration of the plasmid into the chromosome results in a *cdsA-gfp*$^+$ fusion under the control of the *cdsA* promoter, and a native copy of *cdsA* under the control of P$_{Spac}$. The plasmid insertion was transduced into an SH1000 background by phage transduction using Φ11. Jorge Garcia-Lara (University of Sheffield) discovered that CdsA-GFP+ fusion co-localized with PlsY which is involved in the same glycerophospholipid metabolic pathway as CdsA (Garcia-Lara *et al.* 2015).

The CdsA-GFP+ fusion was transduced into SJF4098 (*ΔmreC*), SJF2976 (*mreD::kan*) and SJF2625 (*mreCD::kan*) using a Φ11 lysate of SJF3933 (*cdsA-gfp*; P$_{Spac}$-*cdsA*). In order to determine the effect of MreC and MreD on CdsA localisation, the subcellular localisation of CdsA in SJF4105 (*ΔmreC*; *cdsA-gfp*$^+$; P$_{Spac}$-*cdsA*), SJF4123 (*mreD::kan*; *cdsA-gfp*$^+$; P$_{Spac}$-*cdsA*) and SJF4125 (*mreCD::kan; cdsA-gfp*$^+$; P$_{Spac}$-*cdsA*) was analysed by fluorescence microscopy of fixed cells. Due to insufficient time, construction of an alternative CdsA-GFP+ strain via allelic replacement was not attempted. Therefore, SJF3933 (*cdsA-gfp*; P$_{Spac}$-*cdsA*) was used as a control.

Fluorescence microscopy of SJF3933 (*cdsA-gfp*$^+$; P$_{Spac}$-*cdsA*) showed that in *S. aureus* SH1000, CdsA was predominantly localised at the division site in nearly all cells and also as punta around the cell periphery (Fig. 5.29A). The *mreC* mutant showed similar CdsA localisation pattern to the parental strain. In the particular case, CdsA-GFP+ localisation was not quantitatively compared across strains due to the poor resolution and florescence intensity. However, it is still apparent that the septal localisation of CdsA is lost in MreD deficient cells (Fig. 5.29 C).
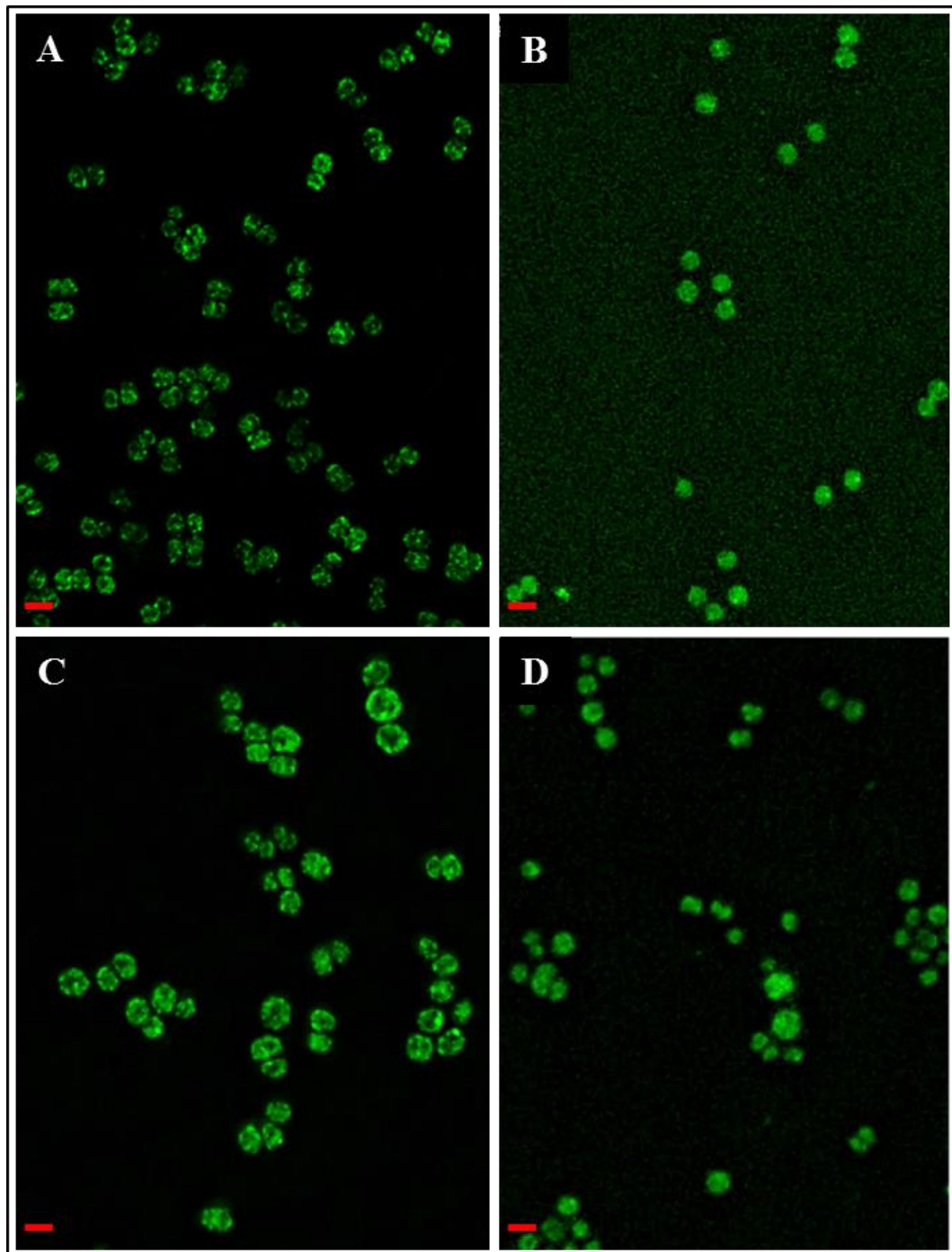
Figure 5-29 Localisation of CdsA-GFP+ in *mreC*, *mreD* and *mreCD S. aureus*

Fluorescence images of SJF3933 (*cdsA-gfp*+; P$_{Spac}$-*cdsA*) (Panel A), SJF4105 (*mreC*; *cdsA-gfpp*; P$_{Spac}$-*cdsA*) (Panel B), SJF4123 (*mreD::kan*; *cdsA-gfp*+; P$_{Spac}$-*cdsA*) (Panel C) and SJF4125 (*mreCD::kan; cdsA-gfp*+; P$_{Spac}$-*cdsA*) (Panel D). The localisation of CdsA was determined by fluorescent microscopy of fixed cells. All images are to the scale shown by the bar. The CdsA-GFP+ signal is shown in green in the images. Images were acquired using an Olympus IX70 microscope and SoftWoRx 3.5.0 software (Applied Precision). Scale bar, 2μm.

In *mreCD* mutant, CdsA was dispersed randomly and the punctate pattern was absent (Fig. 5.29D).

These results may suggest that in *S. aureus*, MreD is required for the recruitment of CdsA to puncta distribute around the cell. Due to the interaction between MreD and CdsA proteins (Fig. 3.4), it is likely that this recruitment is direct. It is possible that these CdsA foci represent membrane phospholipid biosynthesis complexes and that in the absence of any MreD these complexes are unable to form, resulting in large cells with dispersed CdsA localisation.

5.3.8.6   Role of MreC, MreD and MreCD in peptidoglycan biosynthesis

In WT *B. subtilis* peptidoglycan is synthesised at the mid cell during the division, and spots and transverse bands in the cylindrical side wall leading to cell elongation (Leaver & Errington 2005). Absence of MreC and MreD in *B. subtilis* resulted the loss or great reduction of PG in the side wall incorporation (Leaver & Errington 2005).

In *S. aureus*, PG synthesis appears mostly confined to the septum (Pinho & Errington 2003). My observations indicate that MreD is crucial for correct cell shape and probably involved in precise localisation of septum synthesis, in *S. aureus*. Thus, the localisation of nascent PG synthesis was determined, nascent cell wall was stained with a fluorescent derivative of vancomycin conjugated to BODIPY (Van-FL) (Pinho & Errington 2003) and visualised by fluorescent microscopy of fixed cells. Vancomycin binds the D-alanyl-D-alanine residues present in the carboxyl terminus of peptidoglycan precursors. Cross-linking of the cell wall via transpeptidation, catalysed by penicillin binding proteins, cleaves the D-ala-D-ala bond. Carboxypeptidases are also able to hydrolyse the D-ala-D-ala bond in order to control the extent of cross-linking. Therefore Van-FL preferentially labels nascent cell wall in various Gram-positive bacteria (Daniel & Errington 2003). The localisation of peptidoglycan synthesis in *S. aureus* by Van-FL staining was performed using the protocol based on Turner *et al.* (2010) as described in Chapter 2.14.

S. aureus WT SH1000 showed septal PG synthesis in the majority of cells (Fig. 5.30). Various stages of septum formation could be observed: the majority of cells displayed a fluorescent line across the cell, corresponding to newly synthesised peptidoglycan at the septum, a few cells showed a ring of fluorescence at the division site, corresponding to the septal ring viewed in another orientation. This phenotype is similar to that previously reported for WT *S. aureus* (Turner *et al.* 2010). A weak fluorescence of Van-FL was observed around the cell periphery (Fig. 5.30 A). In the absence of MreC, most SJF4098 (*ΔmreC*) cells showed a similar septal PG synthesis pattern as WT SH1000 (Fig. 5.30 B), given that SJF4098 (*ΔmreC*) has an increased proportion of enlarged cells. In contrast, septa were not present in most of the greatly enlarged cells of SJF2976 (*mreD::kan*) and SJF2625 (*mreCD::kan*). Van-FL was predominantly labelled to the cell periphery (Fig. 5.30 C) in SJF2976 (*mreD::kan*) (75%) and SJF2625 (*mreCD::kan*) (70%) (Fig. 5.31). This suggests that cell wall synthesis mainly occurs at division sites and that septal incorporation is lost or greatly reduced in the absence of MreD.
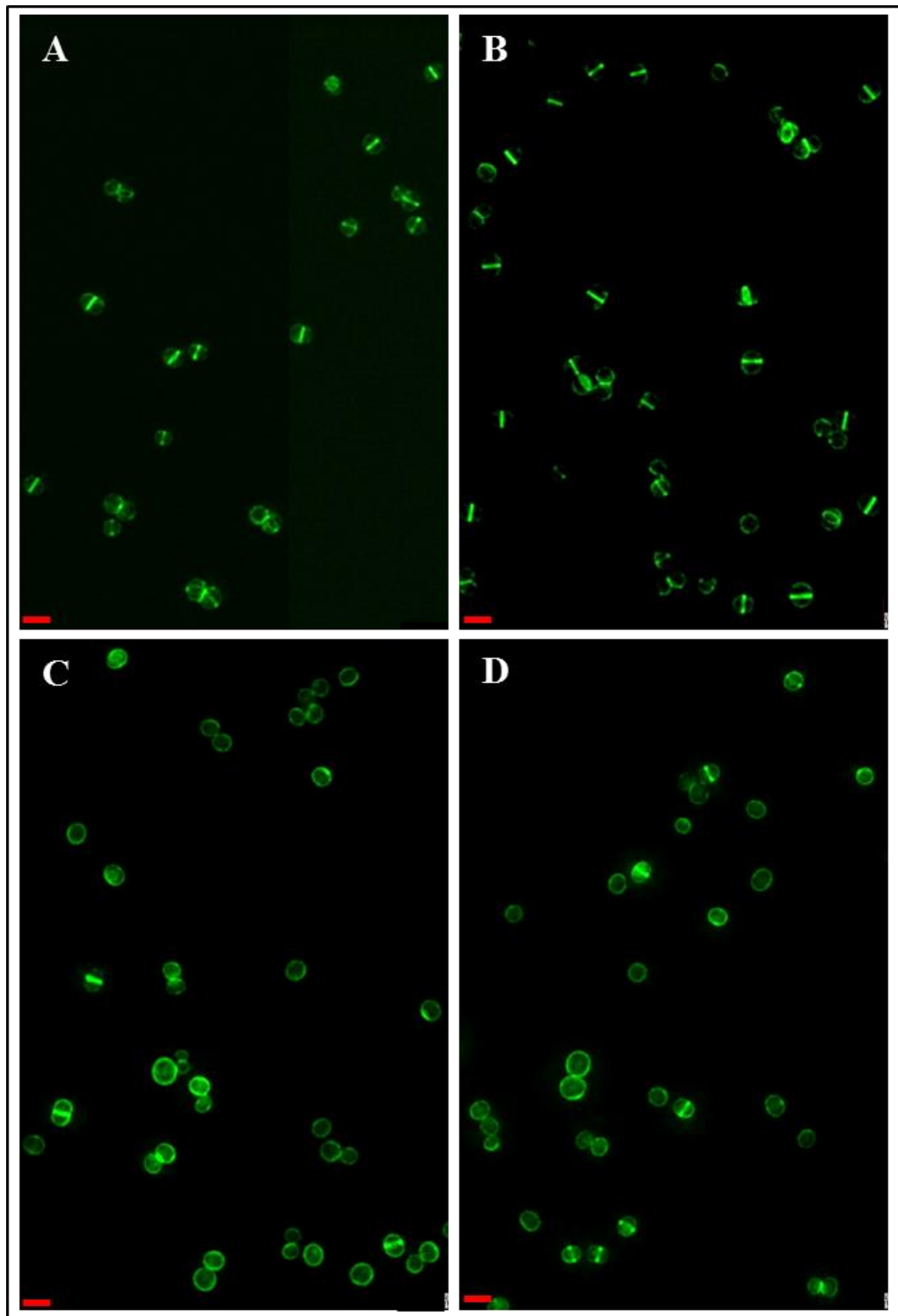
Figure 5-30 Localisation of PG synthesis in *mreC*, *mreD* and *mreCD* deleted *S. aureus*

SJF4098 (*ΔmreC*), SJF2976 (*mreD::kan*) and SJF2625 (*mreCD::kan*) were labelled with Van-FL. Panel A: WT; panel B: SJF4098 (*ΔmreC*); panel C: SJF2976 (*mreD::kan*) and panel D: SJF2625 (*mreCD::kan*). Different Van-FL labelling pattern was counted and analysed in Fig. 5.31. Images were acquired using an Olympus IX70 microscope and SoftWoRx 3.5.0 software (Applied Precision). Scale bar, 2μm.

Small cell (D<1.25 μm) with dispersed VAN-FL labelling around cell periphery

Small cell (D<1.25 μm) with midcell VAN-FL labelling

Big cell (D>1.25 μm) with midcell VAN-FL labelling

Big cell (D>1.25 μm) with dispersed VAN-FL labelling

Legend (chart):
- Big cell (D>1.25μm) with midcell VAN-FL labelling
- Big cell (D>1.25) with dispersed VAN-FL labelling
- small cell (D<1.25μm) with midcell VAN-FL labelling
- small cell (D<1.25) with dispersed VAN-FL labelling

Chart x-axis: SH1000 WT (n=69), SJF4098 (ΔmreC) (n=99), SJF2976 (mreD::kan) (n=246), SJF2625 (mreCD::kan) (n=189)

Y-axis: %

Figure 5-31 Phenotypes of WT SH1000, SJF4098 (*ΔmreC*), SJF2976 (*mreD::kan*) and SJF2625 (*mreCD::kan*).

The localisation of nascent cell wall was determined by fluorescence microscopy of Van-FL labelled cells. Cells were assigned one of four phenotypes on the basis of their diameter (D) and distribution of Van-FL labelling. Examples of the four phenotypes are shown above with Van-FL shown in green. The frequency of phenotypes of WT SH1000, SJF4098 (*ΔmreC*), SJF2976 (*mreD::kan*) and SJF2625 (*mreCD::kan*) is shown. The number of cells measured was 69, 99, 246 and 189 respectively. Cell measurements were made using SoftWoRx software. Scale bar, 1μm.

5.3.8.7 Role of MreC, MreD and MreCD in nucleoid segregation and membrane formation

Nucleoid occlusion is a crucial mechanism involved in selecting the correct cell division site (Wu & Errington 2012). Nucleoid occlusion blocks cell division at mid-cell until the sister chromosomes have segregated.

To analysis the chromosomal segregation in these mutants, fluorescent DAPI (blue) and FM4-64 stain (red) were used, which acts as a marker for areas of nucleoid and cell membrane respectively and visualised by fluorescent microscopy of fixed cells.

In WT *S. aureus* SH1000 fluorescent DAPI revealed strong labelling as spots (Fig. 5.32 A), almost all cells (93%) contained DNA bisected to opposite regions of the dividing cell (Fig. 5.33). In the absence of MreC, there were increased proportion of enlarged cells, however, all of those show bisected DNA and presence of membrane staining at midcell (Fig 5.32 B). In the *mreD* mutant, almost all cells (91.5%) contained DNA in an irregular pattern (Fig 5.32 C). DNA (blue) was condensed in the middle of the cells or partially bisected preventing septum formation in the mid-cell, cell membrane (red) was either absent from the mid cell or initiating in multiple places. The *mreCD* mutant showed similar morphology to the *mreD* strain (Fig 5.32 D), about 90% cells demonstrated irregular DAPI labelling. Notably, there were 35% more irregular DAPI labelling in enlarged cells of SJF2625 (*mreCD::kan*). There less than 2% measured cells has bisected DAPI labelling with cell diameter of just over 1μm. Membrane staining was also reduced or absent in the *mreCD* deficient cells.

In the absence of *mreD*, membrane formation was prohibited at the division sites due to nucleoid condensation in the middle of the cells, suggesting that *mreD* is required for accurate DNA segregation spatially and temporally.
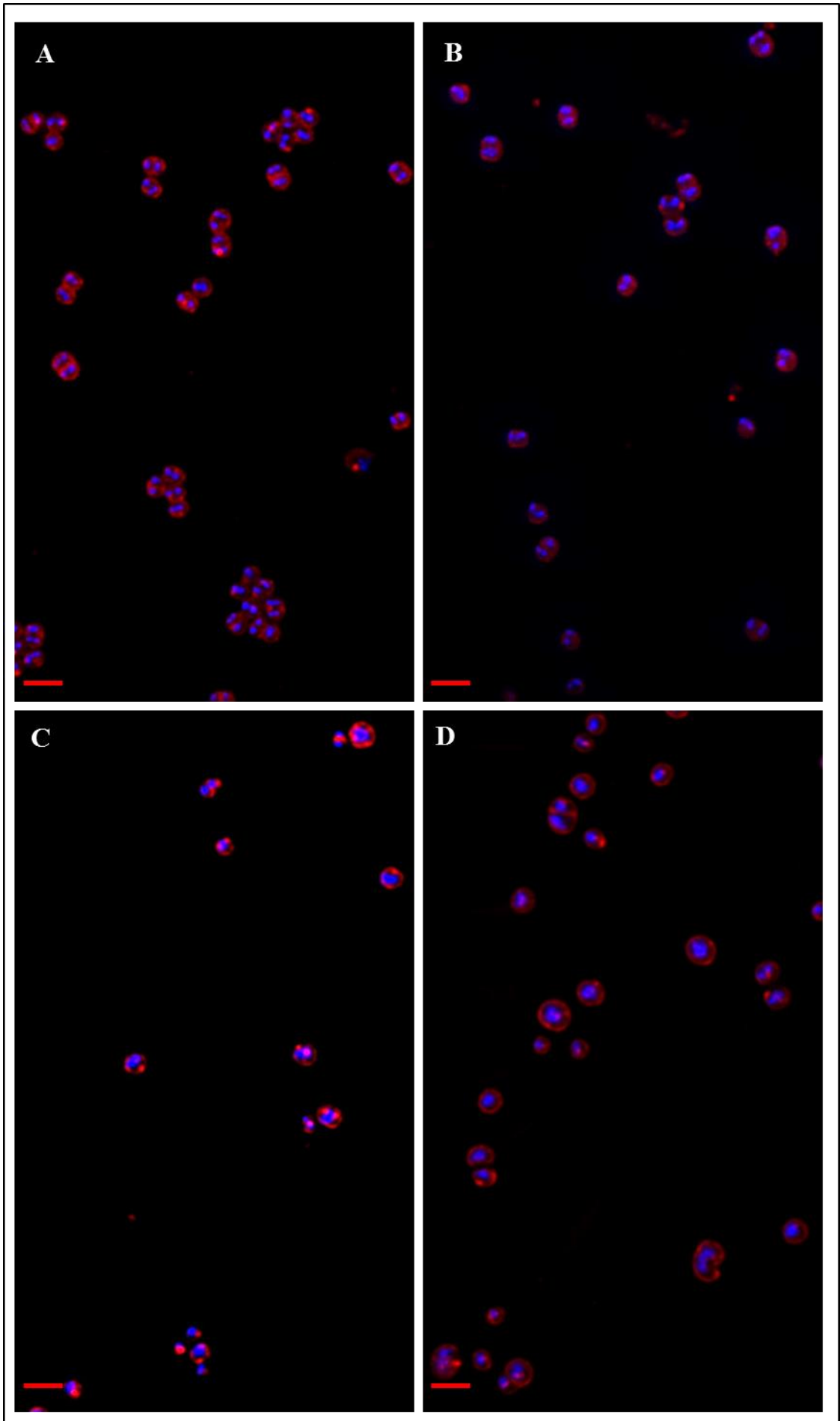
Figure 5-32 Role of MreC, MreD or MreCD in nucleoid and membrane topology in *S. aureus*

SJF4098 (*ΔmreC*), SJF2976 (*mreD::kan*) and SJF2625 (*mreCD::kan*) were labelled with DAPI (DNA) and FM4-64 (membrane). Panel A: WT; panel B: SJF4098 (*ΔmreC*); panel C: SJF2976 (*mreD::kan*) and panel D: SJF2625 (*mreCD::kan*). Different fluorescent DAPI and FM4-64 labelling pattern was counted and analysed in Fig. 5.33. Images were acquired using an Olympus IX70 microscope and SoftWoRx 3.5.0 software (Applied Precision). Scale bar, 2μm.

Small cell (D<1.25 μm)
with bisected DAPI labelling

Small cell (D<1.25 μm)
with mid-cell DAPI labelling
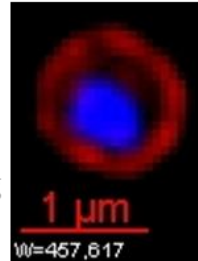
Big cell (D>1.25 μm)
with bisected DAPI labelling
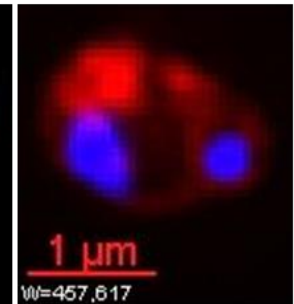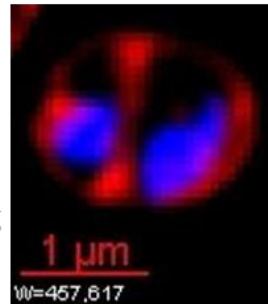
Big cell (D>1.25 μm)
with mid-cell labelling

Big cell (D>1.25μm) with
irregular DAPI labelling

Big cell (D>1.25) with
bisected DAPI labelling

small cell (D<1.25μm) with
irregular DAPI labelling

small cell (D<1.25) with
bisected DAPI labelling

n=110   n=106   n=117   n=131

Wild-type   SJF4098
(ΔmreC)   SJF2976
(mreD::kan)   SJF2625
(mreCD::kan)

239
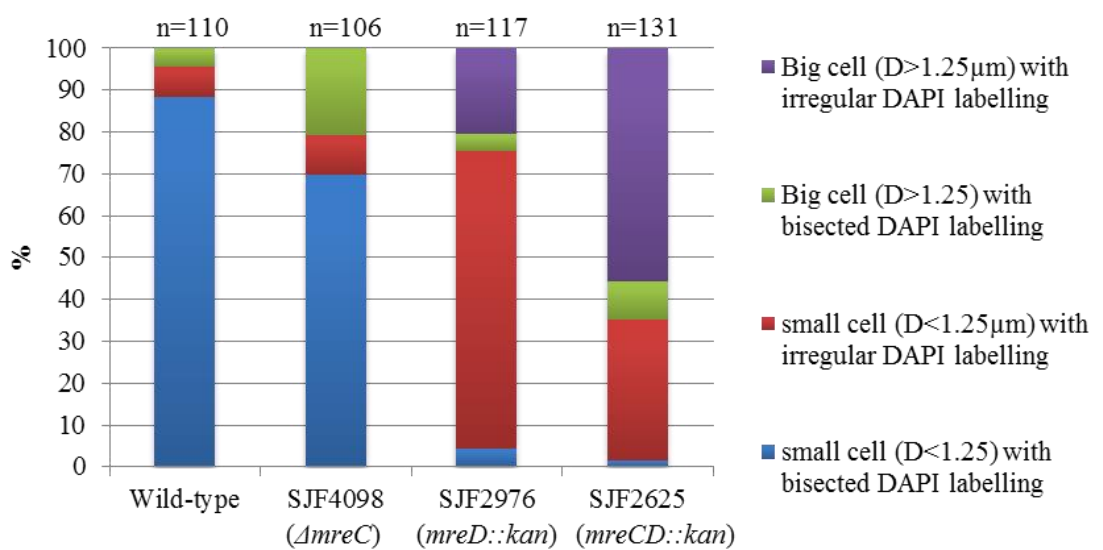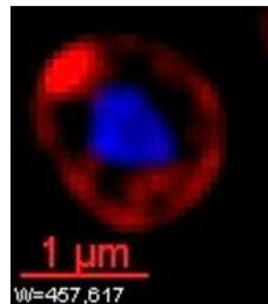
Figure 5-33 Role of MreC, MreD and MreCD in nucleoid and membrane topology.

The localisation of nucleoid and cell membrane was determined by fluorescence microscopy after DAPI and FM4-64 labelling. Cells were assigned one of four phenotypes on the basis of their diameter (D) and distribution of Van-FL labelling. Examples of the four phenotypes are shown above with DAPI shown in blue and FM4-64 shown in red. The frequency of phenotypes of WT SH1000, SJF4098 (*ΔmreC*), SJF2976 (*mreD::kan*) and SJF2625 (*mreCD::kan*) is shown. The number of cells measured was 110, 106, 117 and 131 respectively. Cell measurements were made using SoftWoRx software. Scale bar, 1µm.

5.4 Discussion

5.4.1 MreCD are cell shape determining proteins in *S. aureus*

The construction of deletions of *mreC*, *mreD* and *mreCD* revealed the operon is involved in cell growth and morphology of *S. aureus*. Previously, *mreC* and *mreD* has been shown not to be essential in *S. aureus* (Chaudhuri *et al.* 2009). In *B. subtilis* and *S. pneumoniae* (virulent serotype 2 strain D39), the genes are essential (Leaver & Errington 2005; Land & Winkler 2011).

Absence of MreC results in a larger cell diameter, although cells are still roughly spherical. The cell doubling time remains the same as WT *S. aureus*. Labelling of nascent cell wall with a fluorescent derivative of vancomycin showed that peptidoglycan synthesis was mainly observed at the septum. Successful complementation of episomic *mreD* of the *mreCD* deficient strain emphasised that the morphological alteration of *mreCD* double mutant was mainly due to the absence of *mreD* not *mreC*. From here, we conclude that MreC does not play a critical role in controlling cell shape.

In contrast, the absence of MreD results in the formation of non-spheroid cells that are significantly enlarged and possess a thicker uneven cell wall. These observations are consistent with Leaver & Errington's discovery in *B. subtilis* (Leaver & Errington 2005). This suggests that MreD has a role in cell wall peptidoglycan metabolism. Given the fact that the spherical bacterium *S. aureus* does not elongate and peptidoglycan synthesis only takes place at the septum (Pinho & Errington 2003), it seems loss of MreD results in delocalisation of peptidoglycan biosynthesis. Vancomycin labelling demonstrated that peptidoglycan synthesis did occur around the entire perimeter of the cells in which MreD was absent. Cell enlargement could be due to delocalisation of peptidoglycan synthesis and leading to *de novo* cell wall synthesis, reminiscent of *S. aureus* FtsZ-depleted phenotype (Pinho & Errington 2003). Enlarged MreD deficient cells carry distinct multi foci GpsB around their periphery that may coincide with patches of PBP2 and represent assembly of cell division components into complexes that are not correctly targeted to midcell. EzrA-GFP were also dispersed over the surface and showed a punctate pattern. This nonhomogeneous distribution of cell wall synthesis could be due to the presence of isolated complexes of peptidoglycan synthesising proteins that cannot localise to midcell in the absence of MreD. Delocalisation of GpsB and EzrA in the absence of *mreD* expression showed that assembly of the correct divisome requires MreD.

5.4.2 The role of MreCD in septum formation

In *S. aureus*, Noc acts as an inhibitor of FtsZ polymerization ensuring that chromosome is completely and equally bisected before septum formation (Veiga *et al.* 2011). Images of Noc-GFP+ localisation and DAPI labelling of *mreD* mutants showed condensation of nucleoids in the centre of regular sized cells and loss of axis of chromosome segregation. Membrane constriction asymmetrically initiates in free spaces resulted from condensed nucleoids, suggesting failure of septum formation at midcell. FM4-64 staining showed that cells were unable to form effective septa at midcell, instead, intense patches were accumulated around the cell periphery as multiple foci and TEM studies clearly showed that these foci contain cell wall material. Although the mutants were still able to accumulate Van-FL at midcell, they were mainly observed as swollen cells, implying a delay of peptidoglycan synthesis during septum formation. It seems likely that *S. aureus* cell division requires MreD to ensure placement of the division septum at the right place and time. MreD may play an important role in regulating Noc-dependent nucleoid occlusion prior to Z-ring formation in *S. aureus*, and provide a signal for septum formation in actively dividing cells. Interestingly, septa were still able to form in nucleoid free spaces or to overlay the nucleoids cutting unequal volumes of nucleoids into asymmetrical daughter cells. Therefore, it is likely that *S. aureus* also use other systems to activate membrane constriction as well as the role of MreD.

5.4.3 The role of MreD in cell membrane phospholipid synthesis

Perturbed localisation of PlsY-GFP+ and CdsA-GFP+ in the absence of MreD may indicate that MreD is required for the PlsY/CdsA metabolic pathway. PlsY is an essential acyltransferase involved in coupling of fatty acid and membrane phospholipid synthesis in Gram-positives (Cherian *et al.* 2012). PlsY depletion leads to larger cells, unable to divide, resulting in abnormal clusters, with misplaced cell division septa, altered peptidoglycan metabolism, and defective cytokinesis (Garcia-Lara *et al.* 2015). CdsA is responsible for the formation of CDP-diacylglycerol from phosphatidic acid in the same glycerophospholipid metabolic pathway as PlsY (Kobayashi *et al.* 2003). CdsA~GFP+ fusion co-localises with PlsY via immune-fluorescent microscopy (Garcia-Lara *et al.* 2015). In this study, MreD displayed abnormal morphology, reminiscent of the PlsY-depleted phenotype. It is possible that MreD guides the selection of position for PlsY/CdsA mediated phospholipid synthesis, its loss destabilises the PlsY/CdsA mediated metabolic pathway, therefore disrupting bacterial membrane biogenesis. The lipid bilayer may be synthesised at sites round the cell periphery at which PlsY and CdsA are colocalised.

Images of PlsY-GFP+ and membrane labelling in *S. aureus* deprived of MreC showed an identical localisation pattern to the parent WT SH1000, indicating that MreC is not required for cell membrane phospholipid synthesis.

5.4.4   Future directions

One of the key questions remaining to be answered about MreD function is the interdependence between FtsZ and MreD for the localisation to the division site. Colocalisation studies of the two proteins in wild type cells, the localisation of MreD in FtsZ depleted cells and the localisation of FtsZ in MreD deficient mutants are required to do this, and therefore optimisation of the protocol for FtsZ immunofluorescence must be achieved. Another question is if MreD is synthetically lethal with Noc? Combinations of *mreD* and *noc* mutations in *S. aureus* will test this hypothesis.

AFM studies on *S. aureus* peptidoglycan sacculus architecture revealed that epigenetic information is contained in a large belt of peptidoglycan with a 'piecrust' band which provide a template for division site recognition (Turner *et al.* 2010). Thus, it would be interesting to assess the piecrust footprint in *mreD* null mutants.

Measuring the rate of metabolic processes will help to understand why the *mreD* mutants grow slower than the wild type cells. It will be of great interest to determine the localisation pattern of other enzymes in phospholipid biosynthesis pathway and to extend this to further proteins involved in other metabolic processes and beyond, such as wall teichoic acid (WTA) biosynthetic pathway and peptidoglycan precursors synthesis, in which proteins involved have also been shown to directly interact with MreB, MreC and MreD in many organisms, including *S. aureus* (Mohammadi *et al.* 2007; Formstone *et al.* 2008; White *et al.* 2010; Kent 2014).

6   Chapter 6 General discussion

6.1   Overview

The cell wall is critical for controlling cell shape and preventing lysis by resisting the osmotic pressure within the cell. Maintenance of a consistent and yet dynamic cell shape is critical for bacteria since many cellular processes require precise spatial and temporal control. How bacteria manage to maintain the integrity of the wall as the cell grows and divides remains unclear. Identification of the cytoskeletal proteins MreB and FtsZ provide a framework for cell shape maintenance in rod shaped organisms. In most bacteria, MreB is associated with the membrane bound components MreC and MreD. Investigation into the role of MreC and MreD in cell shape determination in *S. aureus*, has contributed to a better understanding of the mechanisms, whereby membrane proteins are organised.

6.2   Conservation of bacterial cell wall growth mechanism

An analysis of cell wall growth in a range of organisms aids characterisation of the origin of the growth and division. The divisome in Eubacteria is assembled via the construction of a macromolecular complex consisting of more than twelve proteins (Margolin 2000a; Nikolaichik & Donachie 2000; Pinho *et al.* 2013). A comparison of the genomic sequences of Eubacteria has identified most of the cell division proteins are highly conserved (Nikolaichik & Donachie 2000). Ten cell division proteins identified in almost all cell wall-containing Eubacteria have been investigated: FtsZ, FtsA, FtsE, FtsX, FtsK, FtsL, FtsB, FtsQ, FtsW and FtsI. In addition, other proteins may be present (Table 6.1) (Margolin 2000b; Nikolaichik & Donachie 2000; Gamba *et al.* 2009; Pinho *et al.* 2013).

Although bacteria have a diverse range of shapes (Fig. 1.1), the conservation of many cell wall growth components (Fig. 1.1 & Table 6.1) suggests a degree of similarity in the recruitment and assemblage of the cell wall synthetic machinery. Indeed, the interactions between cell wall growth proteins are conserved in a range of organisms, and these proteins interact with either one partner or several partners (Reviewed in Chapter 1 & 3), suggesting that the cell wall synthetic machinery is stabilised by these interactions. The division complex in *S. aureus* investigated by BACTH has shown that nearly all the proteins interact with many partners (Steele *et al.* 2011).

In this study, MreC and MreD, interact with many cell division components and other proteins, suggesting a multicomponent division complex (Fig. 3.9 & 3.10). MreC and MreD are thought to be involved in the positioning of the peptidoglycan synthesis machinery in many species (van den Ent *et al.* 2006; Divakaruni *et al.* 2007; White *et al.* 2010). Interactions were

detected between MreC, MreD and DivIB by BACTH (Fig. 3.6), suggesting that DivIB may have a role linking with MreD localisation (Figure 6.1).

Species	Family	FtsZ	FtsA	ZipA	ZapA	EzrA	SepF	FtsW	FtsI	FtsK	FtsL	FtsB	FtsQ	FtsN	FtsEX	GpsB
Eco	γ-Proteobacteria	+	+	+	+	−	−	+	+	+	+	+	+	+	+	−
Hin	γ-Proteobacteria	+	+	+	+	−	−	+	+	+	+	+	+	+	+	−
Nme	β-Proteobacteria	+	+	−	+	−	−	+	+	+	+	+	+	+	+	−
Ccr	α-Proteobacteria	+	+	−	+	−	−	+	+	+	+	+	+	+	+	−
Hpy	ε-Proteobacteria	+	+	−	+	−	−	+	+	+	−	+	−	−	+	−
Ctr	Chlamydiae	−	−	−	−	−	−	+	+	+	+	−	−	−	−	−
Tpa	Spirochaetes	+	+	−	+	−	−	+	+	+	+	−	+	+	+	−
Mtu	+high GC	+	−	−	−	−	+	+	+	+	−	−	+	−	+	−
Mlu	+highGC	+	−	−	−	−	+	+	+	+	−	−	+	−	+	−
Bsu	+low GC	+	+	−	+	+	+	+	+	+	+	+	+	−	+	+
Efa	+lowGC	+	+	−	+	+	+	+	+	+	+	−	+	−	+	+
Sau	+low GC	+	+	−	+	+	+	+	+	+	+	+	+	−	+	+
Spn	+low GC	+	+	−	+	+	+	+	+	+	+	+	+	−	+	+
Ssp	Cyano/chlor	+	+	−	+	+	+	+	+	+	−	−	+	−	+	−
Mja	Euryarchaeota	+	−	−	−	−	+	−	−	−	−	−	−	−	+	+

Table 6.1 Conservation of divisome components across species

Eco, *E. coli*; Hin, *H. influenzae*; Nme, *N. meningitidis*; Ccr, *C. crescentus*; Hpy, *Helicobacter pylori*; Ctr, *Chlamydia trachomatis*; Tpa, *Treponema pallidum*; Mtu, *M. tuberculosis*; Mlu, *Micrococcus luteus*; Bsu, *B. subtilis*; Efu, *E. faecalis*; Sau, *S. aureus*; Spn, *S. pneumoniae*; Ssp, *Synechocystis* sp.; Mja, *M. jannaschii*.

Adapted from (Margolin, 2000; Nikolaichik and Donachie, 2000; Pinho *et al.*, 2013). The Protein Knowledgebase (UniprotKB), (http://www.uniprot.org/) was used to identify the presence (+) or absence (−) of protein homologues in the above-mentioned species.

6.3   *S. aureus*, a model of cell division

Lack of cylindrical elongation of the cell wall, make *S. aureus* a simpler model for studying cell growth and division (Turner *et al.* 2010). The synthesis of peptidoglycan predominantly occurs at the septum, which becomes the nascent hemi-ellipsoidal poles of the resulting daughter cells after the separation of the parent cell (Fig. 6.1) (Pinho & Errington 2003; Zhou *et al.* 2015). Absence of the Min system in *S. aureus* suggests that Noc plays an important role in placing the septum in the correct plane (Veiga *et al.* 2011). However, nucleoid occlusion is insufficient to initiate division in the next orthogonal plane (Turner *et al.* 2010). Thus, cell division proteins may recognise certain physical markers within the cell that guide the divisome to the presumptive division plane (Turner *et al.* 2010). AFM has demonstrated a thick ring of peptidoglycan termed the "piecrust" since it exhibited a piecrust texture at the presumptive site of septum formation (Turner *et al.* 2010). This piecrust was retained as an orthogonal "rib" after the completion of septum formation. When the cell divides in the next plane, division occurs across the previous septum, resulting in the sectoring of the cell wall material, whereby each sector is delineated by old piecrust material, the ribs. These ribs contain enough information to mark the previous plane and hence determine the location of the future division plane, maintaining the characteristic three-plane sequence (Turner *et al.* 2010). Thus, the dissimilarities in peptidoglycan structure throughout the cell cycle may be recognised by different components of the cell division machinery to form the septum. Indeed, the peptidoglycan architectural features of *S. aureus* (piecrust, septal plate and ribs) suggest that cell division is not a linear process and not all of the division components interact at the same time, which indicates that the division occurs in more than one stage (Turner *et al.* 2010). The synthesis of the septum in *S. aureus* has been shown to be disrupted in the absence of cell division components such as FtsZ (Pinho & Errington. 2003), EzrA (Steele *et al.* 2011) and DivIB (Bottomley *et al.* 2014). In this study, TEM has shown that MreD depletion led to the formation of enlarged "hamburger" cells with multiple or aberrant rings initiating at random positions (Fig. 5.20), suggesting that MreD may be involved in the initiation of septum formation. Surprisingly, MreCD double depletion led to a potentially more severe morphology defect (Fig. 5.20). Thus, the failure of MreD-depleted cells to form septa correctly suggests that it is required for septum initiation. A most recent study proposed that the scar (piecrust) of previous cell division plane cannot divide cells in quadrants, since it remains at 1/3 of the daughter cell surface area during cell wall remodelling and expansion (Fig. 6.1). Therefore, MreD may not necessarily interact with the piecrust, but may be involved in an alternative mechanism of initiation of septation. MreD in *S. aureus* SH1000 might play a role in recently reported minor peptidoglycan synthesis process around the cell periphery (Gautam *et al.* 2015; Monteiro *et al.* 2015; Zhou *et al.* 2015).
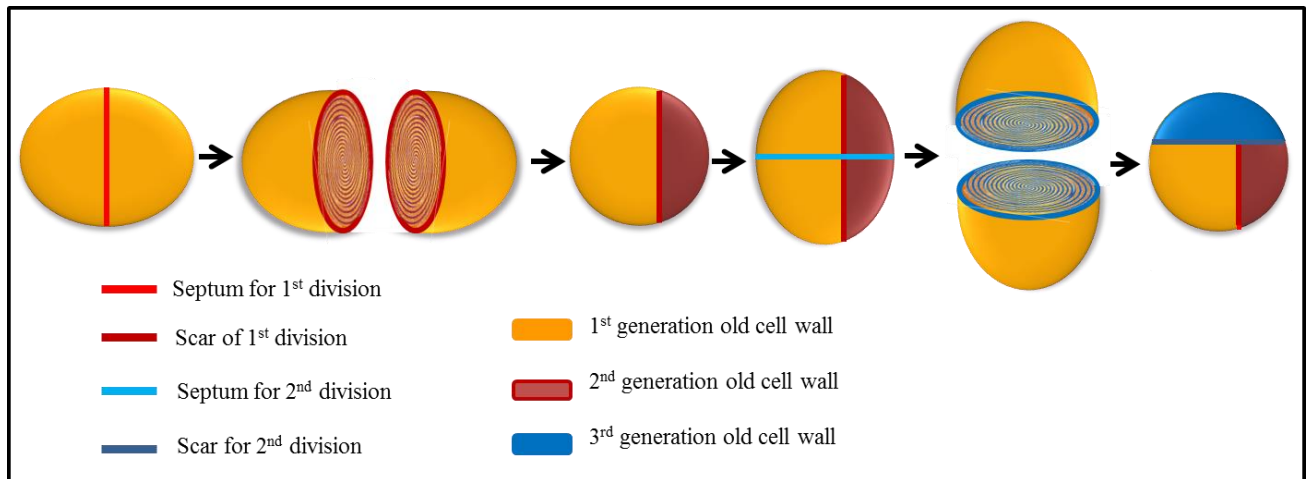
Figure 6-1*S. aureus* cell wall architecture and maturation

S. aureus cells illustrating the orthogonal planes of division. After the separation of the daughter cells, the peptidoglycan structure undergoes remodelling to allow expansion of the entire cell wall resulting in asymmetry in the regions composed of new and old cell wall. Modified from (Monteiro *et al.* 2015).

MreC depletion does not show any apparent morphological and growth defects on both solid and liquid medium (Fig. 5.14). However, the cell size is statistically significantly larger than the WT SH1000 (P<0.0001) (Fig. 5.31). MreC alone is not required for localisation and progression of divisome assembly but plays a different role. A recent study using wheat germ agglutinin and 3D structured illumination microscopy suggested that *S. aureus* undergoes continuous cell wall growth where the peptidoglycan is incorporated into the septum as well as the outer wall to sustain the continuous surface expansion required for cell size homeostasis generation after generation (Zhou *et al.* 2015). Another research group has also proposed that the remodelling and cell wall expansion occurs over the entire cell wall (Monteiro *et al.* 2015). Thus, MreC may play a subtle role in cell wall growth.

Very recently, a new study has been published which also shows that MreCD of *S. aureus* are not essential and in the tested strains, MreCD do not have a major role in cellular physiology (Tavares *et al.* 2015). However, the group was not able to delete the complete *mreD* gene from the genomes (Tavares *et al.* 2015). This may be due to the important role of MreD in the cell morphological control mechanism evidenced in this study and lost of MreD may leads to more severe morphological defects, implying that MreD maybe essential for cell viability and cell shape maintenance in Methicillin Resistan *S. aureus* strain COL.

6.4   The requirement of MreD for a supramolecular structure in the membrane of *S. aureus*

Recent studies have discovered that rod- and round-shaped bacteria can exist as wall-less forms with the ability to divide, called L-forms (Errington 2013). Surprisingly, FtsZ is not required for the division of L-forms of the rod-shaped bacterium *B. subtilis* (Leaver *et al.* 2009). L-forms appear to divide by scission after blebbing, tabulation, or vesiculation dependent on an altered rate of membrane biosynthesis (Mercier *et al.* 2014); this recalls a more evolutionary primitive mechanism allowing cellular proliferation. Therefore, maybe underlying organizational mechanisms maybe independent of apparent cytoskeletal elements. The fluid mosaic model proposing the free transport of proteins associated with membrane across the lipids has been questioned by increasing evidence of the subcellular heterogeneity within the membrane arising from a wide range of clustering of proteins and lipids (Lenn *et al.* 2008; Strahl & Hamoen 2012; Barak & Muchova 2013).

In *E. coli*, MreB, an essential cell wall organiser, is also required to regulate phospholipid and membrane biosynthesis (Bendezu & de Boer 2008). *S. aureus* lacks MreB, however MreC and MreD (encoded by the *mreBCD* operon) are present (Jones *et al.* 2001). The question arises as to whether MreC and MreD are the spatial organizers in *S. aureus*? My work has revealed that MreD is required for the formation of a supramolecular structure in *S. aureus* membrane (Garcia-Lara *et al.* 2015). PlsY, an essential acyltransferase required for the growth of *S. aureus* distributes in a punctate pattern in the membrane of *S. aureus*, providing evidence of an existence of a supramolecular structure (Garcia-Lara *et al.* 2015). In the absence of MreD, the punctate pattern of PlsY lost (Chapter 5.3.8.4) and so is the characteristic placement of EzrA (Chapter 5.3.8.2), an essential *S. aureus* cell division protein (Steele *et al.* 2011). CdsA, downstream of PlsY in the glycerophospholipid biosynthesis pathway, localises in a similar pattern as PlsY and colocalises with PlsY (Garcia-Lara *et al.* 2015). Depletion of MreD also leads to dispersed CdsA localisation. BACTH analysis demonstrated that MreD, PlsY and CdsA interact with each others *in vitro* (Chapter 3.5.2). A FRET based system in *S. aureus* using fluorescent protein fusions confirmed the interactions between these components at the molecular level (Garcia-Lara *et al.* 2015). These observations suggest that MreD may be involved in phospholipid and membrane biosynthesis via direct interaction with PlsY and CdsA, guiding their localisation pattern representing a supramolecular structure in the *S. aureus* membrane. MreD may serve as an organiser for optimal cell function and growth based on the intrinsic self-assembling properties of biological molecules.

6.5 Bacterial cytoskeleton as an antibacterial target

The essentiality and construction of the bacterial cytoskeleton in most bacteria, particularly those that are pathogenic, makes it an attractive target for development of antibiotics (McDevitt *et al.* 2002; Vollmer 2006). The tubulin-like cell division protein FtsZ, the actin-like cell division protein FtsA, and the actin-like multi-functional protein MreB have been extensively investigated as antibacterial targets (McDevitt *et al.* 2002; Vollmer 2006; Beuria *et al.* 2009; Schaffner-Barbero *et al.* 2012). Such inhibitors have been shown to have anti-tuberculosis (Kumar *et al.* 2010) and anti-staphylococcal (Haydon *et al.* 2008) activities. (Maira-Litran *et al.* 2005). A small-molecule inhibitor, S-(3,4-dichlorbenzyl) isothiourea, was developed to disrupt the MreB helical filament in many bacteria species (Gitai *et al.* 2005). The structural homology of FtsZ, FtsA and MreB to eukaryotic tubulin or actin could however result in host cell toxicity. Thus, cell shape proteins with unknown functions could serve as potential antimicrobial targets. MreC and MreD are putative targets because no homology to eukaryotic proteins has been identified, and they are conserved in bacteria with cell walls (Fig 1.1). MreC and MreD were shown to be essential in *B. subtilis* (Leaver & Errington 2005) and MreD is needed for optimal growth of *S. aureus.*

Immunological therapies, such as vaccination and therapeutic antibodies, can be used as alternatives to antibiotics. Available active and passive immunisation approaches for the development of *S. aureus* vaccines have targeted several antigens (Garcia-Lara & Foster 2009; Otto 2010). These antigens include the following: cell wall targets, including IsdB (V710, Merck), LTA (Pagimaximab, Biosynexus), clumping factor A (Veronate® & Aurexis®, Inhibitex), multi-component surface proteins, such as SdrE, IsdA, SdrD and IsdB (Stranger-Jones *et al.* 2006), anchorless cell wall proteins, such as enolase, oxoacyl reductase, putative esterase (Glowalla *et al.* 2009) and protein A (Elusys Therapeutics, Pfizer (ETI211)); capsular targets, including capsular polysaccharide type 5 and type 8 (StaphVAX™, Nabi); membrane targets, such as the ABC transporter GrfA (Aurograb®, Neutec Pharma); extracellular molecules, including α-toxin, H35L (Bubeck Wardenburg & Schneewind 2008), Panton-Valentine leucocidin (Bubeck Wardenburg & Schneewind 2008; Brown *et al.* 2009), enterotoxins and TSST (Nilsson *et al.* 1999; Hu *et al.* 2003); and surface-associated targets, such as poly-N-acetylglucosamine

Interactions of MreC and MreD, in particular MreD, with other proteins are likely to be important for cell division in *S. aureus* and therefore could also be targeted. Although, development of small-molecule inhibitors of PPIs is challenging to a lack of understanding of the specific molecular recognition between proteins and the thermodynamic and structural constraints involved in such a recognition (Cochran 2001). Characterisation of the binding

sites of MreC and MreD to essential cell division proteins is therefore important to enable the design of effective therapeutic agents. The ability to utilise membrane proteins as immunological targets for vaccine development suggests that MreC and MreD might be useful in this category.

6.6   Future directions

I have shown that MreC is found associated with the cell wall fraction. This suggests that the soluble domain may have affinity for cell wall components, such as peptidoglycan or teichoic acid. Ligand binding studies (Bottomley *et al.* 2014) would allow this to be investigated. Further analysis of MreC and MreD localisation and dynamics using super resolution techniques will give a more accurate picture of their relationship to other cellular structures and components. The observation that MreD may act as a subcellular organiser opens up the possibly of a much greater lever of membrane protein interaction that previously described. It will be of great interest to try to analyse potential self-assembly of MreD complicates *in vitro* as the beginnings of understanding how membrane proteins may organise themselves and therefore control cellular physiology and morphology.

7   Chapter 7 References

Aaron M., Charbon G., Lam H., Schwarz H., Vollmer W. & Jacobs-Wagner C. (2007) The tubulin homologue FtsZ contributes to cell elongation by guiding cell wall precursor synthesis in *Caulobacter crescentus*. *Mol Microbiol* **64**, 938-52.

Adams D.W. & Errington J. (2009) Bacterial cell division: assembly, maintenance and disassembly of the Z ring. *Nat Rev Microbiol* **7**, 642-53.

Adams D.W., Wu L.J. & Errington J. (2015) Nucleoid occlusion protein Noc recruits DNA to the bacterial cell membrane. *EMBO J* **34**, 491-501.

Addinall S.G., Bi E. & Lutkenhaus J. (1996) FtsZ ring formation in fts mutants. *J Bacteriol* **178**, 3877-84.

Addinall S.G., Cao C. & Lutkenhaus J. (1997) FtsN, a late recruit to the septum in *Escherichia coli*. *Mol Microbiol* **25**, 303-9.

Addinall S.G. & Lutkenhaus J. (1996a) FtsA is localized to the septum in an FtsZ-dependent manner. *J Bacteriol* **178**, 7167-72.

Alyahya S.A., Alexander R., Costa T., Henriques A.O., Emonet T. & Jacobs-Wagner C. (2009) RodZ, a component of the bacterial core morphogenic apparatus. *Proc Natl Acad Sci U S A* **106**, 1239-44.

Anderson D.E., Gueiros-Filho F.J. & Erickson H.P. (2004) Assembly dynamics of FtsZ rings in *Bacillus subtilis* and *Escherichia coli* and effects of FtsZ-regulating proteins. *J Bacteriol* **186**, 5775-81.

Angert E.R. (2005) Alternatives to binary fission in bacteria. *Nat Rev Microbiol* **3**, 214-24.

Archer G.L. (1998) *Staphylococcus aureus*: a well-armed pathogen. *Clin Infect Dis* **26**, 1179-81.

Arends S.J., Kustusch R.J. & Weiss D.S. (2009) ATP-binding site lesions in FtsE impair cell division. *J Bacteriol* **191**, 3772-84.

Arends S.J., Williams K., Scott R.J., Rolong S., Popham D.L. & Weiss D.S. (2010) Discovery and characterization of three new *Escherichia coli* septal ring proteins that contain a SPOR domain: DamX, DedD, and RlpA. *J Bacteriol* **192**, 242-55.

Arnaud M., Chastanet A. & Debarbouille M. (2004) New vector for efficient allelic replacement in naturally nontransformable, low-GC-content, Gram-positive bacteria. *Appl Environ Microbiol* **70**, 6887-91.

Aussel L., Barre F.X., Aroyo M., Stasiak A., Stasiak A.Z. & Sherratt D. (2002) FtsK Is a DNA motor protein that activates chromosome dimer resolution by switching the catalytic state of the XerC and XerD recombinases. *Cell* **108**, 195-205.

Baba T., Ara T., Hasegawa M., Takai Y., Okumura Y., Baba M., Datsenko K.A., Tomita M., Wanner B.L. & Mori H. (2006) Construction of *Escherichia coli* K-12 in-frame, single-gene knockout mutants: the Keio collection. *Mol Syst Biol* **2**, 2006 0008.

Bae T. & Schneewind O. (2006) Allelic replacement in *Staphylococcus aureus* with inducible counter-selection. *Plasmid* **55**, 58-63.

Barak I. & Muchova K. (2013) The role of lipid domains in bacterial cell processes. *Int J Mol Sci* **14**, 4050-65.

Barber M. & Rozwadowska-Dowzenko M. (1948) *Lancet* **2(6530)**, 641-4.

Battesti A. & Bouveret E. (2012) The bacterial two-hybrid system based on adenylate cyclase reconstitution in *Escherichia coli*. *Methods* **58**, 325-34.

Bayer A.S., Schneider T. & Sahl H.G. (2013) Mechanisms of daptomycin resistance in *Staphylococcus aureus*: role of the cell membrane and cell wall. *Ann N Y Acad Sci* **1277**, 139-58.

Beall B. & Lutkenhaus J. (1989) Nucleotide sequence and insertional inactivation of a *Bacillus subtilis* gene that affects cell division, sporulation, and temperature sensitivity. *J Bacteriol* **171**, 6821-34.

Beall B. & Lutkenhaus J. (1991) FtsZ in *Bacillus subtilis* is required for vegetative septation and for asymmetric septation during sporulation. *Genes Dev* **5**, 447-55.

Beall B. & Lutkenhaus J. (1992) Impaired cell division and sporulation of a *Bacillus subtilis* strain with the *ftsA* gene deleted. *J Bacteriol* **174**, 2398-403.

Beech P.L., Nheu T., Schultz T., Herbert S., Lithgow T., Gilson P.R. & McFadden G.I. (2000) Mitochondrial FtsZ in a chromophyte alga. *Science* **287**, 1276-9.

Bendezu F.O. & de Boer P.A. (2008) Conditional lethality, division defects, membrane involution, and endocytosis in mre and mrd shape mutants of *Escherichia coli*. *J Bacteriol* **190**, 1792-811.

Bendezu F.O., Hale C.A., Bernhardt T.G. & de Boer P.A. (2009) RodZ (YfgA) is required for proper assembly of the MreB actin cytoskeleton and cell shape in *E. coli*. *EMBO J* **28**, 193-204.

Bernard C.S., Sadasivam M., Shiomi D. & Margolin W. (2007) An altered FtsA can compensate for the loss of essential cell division protein FtsN in *Escherichia coli*. *Mol Microbiol* **64**, 1289-305.

Bernhardt T.G. & de Boer P.A. (2003) The *Escherichia coli* amidase AmiC is a periplasmic septal ring component exported via the twin-arginine transport pathway. *Mol Microbiol* **48**, 1171-82.

Bertsche U., Kast T., Wolf B., Fraipont C., Aarsman M.E.G., Kannenberg K., von Rechenberg M., Nguyen-Disteche M., den Blaauwen T., Holtje J.V. & Vollmer W. (2006) Interaction between two murein (peptidoglycan) synthases, PBP3 and PBP1B, in *Escherichia coli*. *Mol Microbiol* **61**, 675-90.

Beuria T.K., Mullapudi S., Mileykovskaya E., Sadasivam M., Dowhan W. & Margolin W. (2009) Adenine nucleotide-dependent regulation of assembly of bacterial tubulin-like FtsZ by a hypermorph of bacterial actin-like FtsA. *J Biol Chem* **284**, 14079-86.

Bi E.F. & Lutkenhaus J. (1991) FtsZ ring structure associated with division in *Escherichia coli*. *Nature* **354**, 161-4.

Bigot S., Sivanathan V., Possoz C., Barre F.X. & Cornet F. (2007) FtsK, a literate chromosome segregation machine. *Mol Microbiol* **64**, 1434-41.

Bolivar F., Rodriguez R.L., Greene P.J., Betlach M.C., Heyneker H.L., Boyer H.W., Crosa J.H. & Falkow S. (1977) Construction and characterization of new cloning vehicles. II. A multipurpose cloning system. *Gene* **2**, 95-113.

Bork P., Sander C. & Valencia A. (1992) An Atpase Domain Common to Prokaryotic Cell-Cycle Proteins, Sugar Kinases, Actin, and Hsp70 Heat-Shock Proteins. *Proc Natl Acad Sci U S A* **89**, 7290-4.

Bottomley A.L., Kabli A.F., Hurd A.F., Turner R.D., Garcia-Lara J. & Foster S.J. (2014) *Staphylococcus aureus* DivIB is a peptidoglycan-binding protein that is required for a morphological checkpoint in cell division. *Mol Microbiol*.

Boyle D.S., Khattar M.M., Addinall S.G., Lutkenhaus J. & Donachie W.D. (1997) *ftsW* is an essential cell-division gene in *Escherichia coli*. *Mol Microbiol* **24**, 1263-73.

Bramhill D. (1997) Bacterial cell division. *Annual Review of Cell and Developmental Biology* **13**, 395-424.

Bramkamp M., Emmins R., Weston L., Donovan C., Daniel R.A. & Errington J. (2008) A novel component of the division-site selection system of *Bacillus subtilis* and a new mode of action for the division inhibitor MinCD. *Mol Microbiol* **70**, 1556-69.

Bramkamp M., Weston L., Daniel R.A. & Errington J. (2006) Regulated intramembrane proteolysis of FtsL protein and the control of cell division in *Bacillus subtilis*. *Mol Microbiol* **62**, 580-91.

Brown E.L., Dumitrescu O., Thomas D., Badiou C., Koers E.M., Choudhury P., Vazquez V., Etienne J., Lina G., Vandenesch F. & Bowden M.G. (2009) The Panton-Valentine leukocidin vaccine protects mice against lung and skin infections caused by *Staphylococcus aureus* USA300. *Clin Microbiol Infect* **15**, 156-64.

Bubeck Wardenburg J. & Schneewind O. (2008) Vaccine protection against *Staphylococcus aureus* pneumonia. *J Exp Med* **205**, 287-94.

Buddelmeijer N. & Beckwith J. (2002) Assembly of cell division proteins at the *E. coli* cell center. *Curr Opin Microbiol* **5**, 553-7.

Buddelmeijer N. & Beckwith J. (2004) A complex of the *Escherichia coli* cell division proteins FtsL, FtsB and FtsQ forms independently of its localization to the septal region. *Mol Microbiol* **52**, 1315-27.

Burdett V. (1991) Purification and Characterization of Tet(M), a Protein That Renders Ribosomes Resistant to Tetracycline. *Journal of Biological Chemistry* **266**, 2872-7.

Buss J., Coltharp C., Huang T., Pohlmeyer C., Wang S.C., Hatem C. & Xiao J. (2013) In vivo organization of the FtsZ-ring by ZapA and ZapB revealed by quantitative super-resolution microscopy. *Mol Microbiol* **89**, 1099-120.

Buss J., Coltharp C., Shtengel G., Yang X., Hess H. & Xiao J. (2015) A multi-layered protein network stabilizes the *Escherichia coli* FtsZ-ring and modulates constriction dynamics. *PLoS Genet* **11**, e1005128.

Cafferkey M.T., Hone R. & Keane C.T. (1982) Severe Staphylococcal Infections Treated with Vancomycin. *Journal of Antimicrobial Chemotherapy* **9**, 69-74.

Carballido-Lopez R. & Errington J. (2003) A dynamic bacterial cytoskeleton. *Trends Cell Biol* **13**, 577-83.

Carballido-Lopez R. & Formstone A. (2007) Shape determination in *Bacillus subtilis*. *Curr Opin Microbiol* **10**, 611-6.

Carson M.J., Barondess J. & Beckwith J. (1991) The FtsQ protein of *Escherichia coli*: membrane topology, abundance, and cell division phenotypes due to overproduction and insertion mutations. *J Bacteriol* **173**, 2187-95.

Cha J.H. & Stewart G.C. (1997) The divIVA minicell locus of *Bacillus subtilis*. *J Bacteriol* **179**, 1671-83.

Chan K.E., Warren H.S., Thadhani R.I., Steele D.J., Hymes J.L., Maddux F.W. & Hakim R.M. (2012) Prevalence and outcomes of antimicrobial treatment for *Staphylococcus aureus* bacteremia in outpatients with ESRD. *J Am Soc Nephrol* **23**, 1551-9.

Charbonneau P., Parienti J.J., Thibon P., Ramakers M., Daubin C., du Cheyron D., Lebouvier G., Le Coutour X., Leclercq R. & Grp F.S. (2006) Fluoroquinolone use and methicillin-resistant *Staphylococcus aureus* isolation rates in hospitalized patients: A quasi experimental study. *Clinical Infectious Diseases* **42**, 778-84.

Chastanet A. & Carballido-Lopez R. (2012) The actin-like MreB proteins in *Bacillus subtilis*: a new turn. *Front Biosci (Schol Ed)* **4**, 1582-606.

Chaudhuri R.R., Allen A.G., Owen P.J., Shalom G., Stone K., Harrison M., Burgis T.A., Lockyer M., Garcia-Lara J., Foster S.J., Pleasance S.J., Peters S.E., Maskell D.J. & Charles I.G. (2009) Comprehensive identification of essential *Staphylococcus aureus* genes using Transposon-Mediated Differential Hybridisation (TMDH). *BMC Genomics* **10**, 291.

Chen J.C. & Beckwith J. (2001) FtsQ, FtsL and FtsI require FtsK, but not FtsN, for co-localization with FtsZ during *Escherichia coli* cell division. *Mol Microbiol* **42**, 395-413.

Chen Y. & Erickson H.P. (2005) Rapid in vitro assembly dynamics and subunit turnover of FtsZ demonstrated by fluorescence resonance energy transfer. *J Biol Chem* **280**, 22549-54.

Chepelev N., Chepelev L., Alamgir M.D. & Golshani A. (2008) Large-scale protein-protein interaction detection approaches: Past, present and future. *Biotechnology & Biotechnological Equipment* **22**, 513-29.

Cherian P.T., Yao J., Leonardi R., Maddox M.M., Luna V.A., Rock C.O. & Lee R.E. (2012) Acyl-sulfamates target the essential glycerol-phosphate acyltransferase (PlsY) in Gram-positive bacteria. *Bioorg Med Chem* **20**, 4985-94.

Chung K.M., Hsu H.H., Govindan S. & Chang B.Y. (2004) Transcription regulation of *ezrA* and its effect on cell division of *Bacillus subtilis*. *J Bacteriol* **186**, 5926-32.

Claessen D., Emmins R., Hamoen L.W., Daniel R.A., Errington J. & Edwards D.H. (2008) Control of the cell elongation-division cycle by shuttling of PBP1 protein in *Bacillus subtilis*. *Mol Microbiol* **68**, 1029-46.

Cooper E.L., Garcia-Lara J. & Foster S.J. (2009) YsxC, an essential protein in *Staphylococcus aureus* crucial for ribosome assembly/stability. *BMC Microbiol* **9**, 266.

Corbin B.D., Wang Y.P., Beuria T.K. & Margolin W. (2007) Interaction between cell division proteins FtsE and FtsZ. *J Bacteriol* **189**, 3026-35.

Costa C.S. & Anton D.N. (1999) Conditional lethality of cell shape mutations of *Salmonella typhimurium*: *rodA* and mre mutants are lethal on solid but not in liquid medium. *Curr Microbiol* **38**, 137-42.

Costa T., Priyadarshini R. & Jacobs-Wagner C. (2008) Localization of PBP3 in *Caulobacter crescentus* is highly dynamic and largely relies on its functional transpeptidase domain. *Mol Microbiol* **70**, 634-51.

Courvalin P. (2006) Vancomycin resistance in Gram-positive cocci. *Clinical Infectious Diseases* **42**, S25-S34.

Courvalin P. & Fiandt M. (1980) Aminoglycoside-Modifying Enzymes of Staphylococcus-Aureus - Expression in Escherichia-Coli. *Gene* **9**, 247-69.

Cui L.Z., Iwamoto A., Lian J.Q., Neoh H.M., Maruyama T., Horikawa Y. & Hiramatsu K. (2006) Novel mechanism of antibiotic resistance originating in vancomycin-intermediate *Staphylococcus aureus*. *Antimicrob Agents Chemother* **50**, 428-38.

Cui L.Z., Murakami H., Kuwahara-Arai K., Hanaki H. & Hiramatsu K. (2000) Contribution of a thickened cell wall and its glutamine nonamidated component to the vancomycin resistance expressed by *Staphylococcus aureus* Mu50. *Antimicrob Agents Chemother* **44**, 2276-85.

D'Ulisse V., Fagioli M., Ghelardini P. & Paolozzi L. (2007) Three functional subdomains of the *Escherichia coli* FtsQ protein are involved in its interaction With the other division proteins. *Microbiology-Sgm* **153**, 124-38.

Dai K. & Lutkenhaus J. (1991) *ftsZ* is an essential cell division gene in *Escherichia coli*. *J Bacteriol* **173**, 3500-6.

Dai K., Xu Y. & Lutkenhaus J. (1993) Cloning and characterization of ftsN, an essential cell division gene in *Escherichia coli* isolated as a multicopy suppressor of ftsA12(Ts). *J Bacteriol* **175**, 3790-7.

Dai K., Xu Y. & Lutkenhaus J. (1996) Topological characterization of the essential *Escherichia coli* cell division protein FtsN. *J Bacteriol* **178**, 1328-34.

Daniel R.A. & Errington J. (2000) Intrinsic instability of the essential cell division protein FtsL of *Bacillus subtilis* and a role for DivIB protein in FtsL turnover. *Mol Microbiol* **36**, 278-89.

Daniel R.A. & Errington J. (2003) Control of cell morphogenesis in bacteria: two distinct ways to make a rod-shaped cell. *Cell* **113**, 767-76.

Daniel R.A., Harry E.J. & Errington J. (2000) Role of penicillin-binding protein PBP 2B in assembly and functioning of the division machinery of *Bacillus subtilis*. *Mol Microbiol* **35**, 299-311.

Daniel R.A., Harry E.J., Katis V.L., Wake R.G. & Errington J. (1998) Characterization of the essential cell division gene *ftsL*(yIID) of *Bacillus subtilis* and its role in the assembly of the division apparatus. *Mol Microbiol* **29**, 593-604.

Daniel R.A., Noirot-Gros M.F., Noirot P. & Errington J. (2006) Multiple interactions between the transmembrane division proteins of *Bacillus subtilis* and the role of FtsL instability in divisome assembly. *J Bacteriol* **188**, 7396-404.

Daniel R.A., Williams A.M. & Errington J. (1996) A complex four-gene operon containing essential cell division gene *pbpB* in *Bacillus subtilis*. *J Bacteriol* **178**, 2343-50.

Datta P., Dasgupta A., Bhakta S. & Basu J. (2002) Interaction between FtsZ and FtsW of *Mycobacterium tuberculosis*. *J Biol Chem* **277**, 24983-7.

Datta P., Dasgupta A., Singh A.K., Mukherjee P., Kundu M. & Basu J. (2006) Interaction between FtsW and penicillin-binding protein 3 (PBP3) directs PBP3 to mid-cell, controls cell septation and mediates the formation of a trimeric complex involving FtsZ, FtsW and PBP3 in mycobacteria. *Mol Microbiol* **62**, 1655-73.

de Boer P., Crossley R. & Rothfield L. (1992a) The essential bacterial cell-division protein FtsZ is a GTPase. *Nature* **359**, 254-6.

de Boer P.A., Crossley R.E., Hand A.R. & Rothfield L.I. (1991) The MinD protein is a membrane ATPase required for the correct placement of the *Escherichia coli* division site. *EMBO J* **10**, 4371-80.

de Boer P.A., Crossley R.E. & Rothfield L.I. (1989) A division inhibitor and a topological specificity factor coded for by the minicell locus determine proper placement of the division septum in *E. coli*. *Cell* **56**, 641-9.

de Boer P.A., Crossley R.E. & Rothfield L.I. (1992b) Roles of MinC and MinD in the site-specific septation block mediated by the MinCDE system of *Escherichia coli*. *J Bacteriol* **174**, 63-70.

de Leeuw E., Graham B., Phillips G.J., ten Hagen-Jongman C.M., Oudega B. & Luirink J. (1999) Molecular characterization of *Escherichia coli* FtsE and FtsX. *Mol Microbiol* **31**, 983-93.

Deane C.M., Salwinski L., Xenarios I. & Eisenberg D. (2002) Protein interactions: two methods for assessment of the reliability of high throughput observations. *Mol Cell Proteomics* **1**, 349-56.

Defeu Soufo H.J. & Graumann P.L. (2004) Dynamic movement of actin-like proteins within bacterial cells. *EMBO Rep* **5**, 789-94.

DeLeo F.R., Diep B.A. & Otto M. (2009) Host defense and pathogenesis in *Staphylococcus aureus* infections. *Infect Dis Clin North Am* **23**, 17-34.

Den Blaauwen T., Buddelmeijer N., Aarsman M.E., Hameete C.M. & Nanninga N. (1999) Timing of FtsZ assembly in *Escherichia coli*. *J Bacteriol* **181**, 5167-75.

den Blaauwen T., de Pedro M.A., Nguyen-Disteche M. & Ayala J.A. (2008) Morphogenesis of rod-shaped sacculi. *FEMS Microbiol Rev* **32**, 321-44.

Di Lallo G., Castagnoli L., Ghelardini P. & Paolozzi L. (2001) A two-hybrid system based on chimeric operator recognition for studying protein homo/heterodimerization in *Escherichia coli*. *Microbiology* **147**, 1651-6.

Di Lallo G., Fagioli M., Barionovi D., Ghelardini P. & Paolozzi L. (2003) Use of a two-hybrid assay to study the assembly of a complex multicomponent protein machinery: bacterial septosome differentiation. *Microbiology* **149**, 3353-9.

Din N., Quardokus E.M., Sackett M.J. & Brun Y.V. (1998) Dominant C-terminal deletions of FtsZ that affect its ability to localize in Caulobacter and its interaction with FtsA. *Mol Microbiol* **27**, 1051-63.

Divakaruni A.V., Baida C., White C.L. & Gober J.W. (2007) The cell shape proteins MreB and MreC control cell morphogenesis by positioning cell wall synthetic complexes. *Mol Microbiol* **66**, 174-88.

Divakaruni A.V., Loo R.R., Xie Y., Loo J.A. & Gober J.W. (2005) The cell-shape protein MreC interacts with extracytoplasmic proteins including cell wall assembly complexes in *Caulobacter crescentus*. *Proc Natl Acad Sci U S A* **102**, 18602-7.

Dominguez-Escobar J., Chastanet A., Crevenna A.H., Fromion V., Wedlich-Soldner R. & Carballido-Lopez R. (2011) Processive movement of MreB-associated cell wall biosynthetic complexes in bacteria. *Science* **333**, 225-8.

Donachie W.D. & Begg K.J. (1989) Cell length, nucleoid separation, and cell division of rod-shaped and spherical cells of *Escherichia coli*. *J Bacteriol* **171**, 4633-9.

Dowding J.E. (1977) Mechanisms of Gentamicin Resistance in Staphylococcus-Aureus. *Antimicrob Agents Chemother* **11**, 47-50.

Dowhan W. (1997) CDP-diacylglycerol synthase of microorganisms. *Biochim Biophys Acta* **1348**, 157-65.

Draper G.C., McLennan N., Begg K., Masters M. & Donachie W.D. (1998) Only the N-terminal domain of FtsK functions in cell division. *J Bacteriol* **180**, 4621-7.

Drew R.H., Perfect J.R., Srinath L., Kurkimilis E., Dowzicky M. & Talbot G.H. (2000) Treatment of methicillin-resistant *Staphylococcus aureus* infections with quinupristin-dalfopristin in patients intolerant of or failing prior therapy. For the Synercid Emergency-Use Study Group. *J Antimicrob Chemother* **46**, 775-84.

Durand-Heredia J.M., Yu H.H., De Carlo S., Lesser C.F. & Janakiraman A. (2011) Identification and characterization of ZapC, a stabilizer of the FtsZ ring in *Escherichia coli*. *J Bacteriol* **193**, 1405-13.

Dye N.A., Pincus Z., Theriot J.A., Shapiro L. & Gitai Z. (2005) Two independent spiral structures control cell shape in Caulobacter. *Proc Natl Acad Sci U S A* **102**, 18608-13.

Ebersbach G., Galli E., Moller-Jensen J., Lowe J. & Gerdes K. (2008) Novel coiled-coil cell division factor ZapB stimulates Z ring assembly and cell division. *Mol Microbiol* **68**, 720-35.

Edwards D.H. & Errington J. (1997) The *Bacillus subtilis* DivIVA protein targets to the division septum and controls the site specificity of cell division. *Mol Microbiol* **24**, 905-15.

Edwards L.E. & Pojeto J., Jr. (1997) Fossils, Rocks, and Time. (ed. by Interior USDot). U.S. Geological Survey.

Ehlert K. & Holtje J.V. (1996) Role of precursor translocation in coordination of murein and phospholipid synthesis in *Escherichia coli*. *J Bacteriol* **178**, 6766-71.

El Ghachi M., Mattei P.J., Ecobichon C., Martins A., Hoos S., Schmitt C., Colland F., Ebel C., Prevost M.C., Gabel F., England P., Dessen A. & Boneca I.G. (2011) Characterization of the elongasome core PBP2: MreC complex of *Helicobacter pylori*. *Mol Microbiol* **82**, 68-86.

Erickson H.P. (2001) The FtsZ protofilament and attachment of ZipA--structural constraints on the FtsZ power stroke. *Curr Opin Cell Biol* **13**, 55-60.

Erickson H.P., Taylor D.W., Taylor K.A. & Bramhill D. (1996) Bacterial cell division protein FtsZ assembles into protofilament sheets and minirings, structural homologs of tubulin polymers. *Proc Natl Acad Sci U S A* **93**, 519-23.

Errington J. (2013) L-form bacteria, cell walls and the origins of life. *Open Biol* **3**, 120143.

Errington J., Daniel R.A. & Scheffers D.J. (2003) Cytokinesis in bacteria. *Microbiology and Molecular Biology Reviews* **67**, 52-+.

Espeli O., Lee C. & Marians K.J. (2003) A physical and functional interaction between *Escherichia coli* FtsK and topoisomerase IV. *Journal of Biological Chemistry* **278**, 44639-44.

Esue O., Cordero M., Wirtz D. & Tseng Y. (2005) The assembly of MreB, a prokaryotic homolog of actin. *J Biol Chem* **280**, 2628-35.

Fadda D., Pischedda C., Caldara F., Whalen M.B., Anderluzzi D., Domenici E. & Massidda O. (2003) Characterization of divIVA and other genes located in the chromosomal region downstream of the dcw cluster in *Streptococcus pneumoniae*. *J Bacteriol* **185**, 6209-14.

Fadda D., Santona A., D'Ulisse V., Ghelardini P., Ennas M.G., Whalen M.B. & Massidda O. (2007) *Streptococcus pneumoniae* DivIVA: Localization and interactions in a MinCD-free context. *J Bacteriol* **189**, 1288-98.

Feilmeier B.J., Iseminger G., Schroeder D., Webber H. & Phillips G.J. (2000) Green fluorescent protein functions as a reporter for protein localization in *Escherichia coli*. *J Bacteriol* **182**, 4068-76.

Ferrero L., Cameron B. & Crouset J. (1995) Analysis of Gyra and Grla Mutations in Stepwise-Selected Ciprofloxacin-Pesistant Mutants of Staphylococcus-Aureus (Vol 39, Pg 1556, 1995). *Antimicrob Agents Chemother* **39**, 2373-.

Feucht A., Lucet I., Yudkin M.D. & Errington J. (2001) Cytological and biochemical characterization of the FtsA cell division protein of *Bacillus subtilis*. *Mol Microbiol* **40**, 115-25.

Fields S. & Song O. (1989) A novel genetic system to detect protein-protein interactions. *Nature* **340**, 245-6.

Formstone A., Carballido-Lopez R., Noirot P., Errington J. & Scheffers D.J. (2008) Localization and interactions of teichoic acid synthetic enzymes in *Bacillus subtilis*. *J Bacteriol* **190**, 1812-21.

Foster T.J. (2005) Immune evasion by staphylococci. *Nat Rev Microbiol* **3**, 948-58.

Foster T.J. & Hook M. (1998) Surface protein adhesins of *Staphylococcus aureus*. *Trends Microbiol* **6**, 484-8.

Fraipont C., Alexeeva S., Wolf B., van der Ploeg R., Schloesser M., den Blaauwen T. & Nguyen-Disteche M. (2011) The integral membrane FtsW protein and peptidoglycan synthase PBP3 form a subcomplex in *Escherichia coli*. *Microbiology-Sgm* **157**, 251-9.

Fu G., Huang T., Buss J., Coltharp C., Hensel Z. & Xiao J. (2010) In vivo structure of the *E. coli* FtsZ-ring revealed by photoactivated localization microscopy (PALM). *PLoS One* **5**, e12682.

Fu X., Shih Y.L., Zhang Y. & Rothfield L.I. (2001) The MinE ring required for proper placement of the division site is a mobile structure that changes its cellular location during the *Escherichia coli* division cycle. *Proc Natl Acad Sci U S A* **98**, 980-5.

Fukushima T., Afkham A., Kurosawa S., Tanabe T., Yamamoto H. & Sekiguchi J. (2006) A new D,L-endopeptidase gene product, YojL (renamed CwlS), plays a role in cell separation with LytE and LytF in *Bacillus subtilis*. *J Bacteriol* **188**, 5541-50.

Galli E. & Gerdes K. (2010) Spatial resolution of two bacterial cell division proteins: ZapA recruits ZapB to the inner face of the Z-ring. *Mol Microbiol* **76**, 1514-26.

Galli E. & Gerdes K. (2012) FtsZ-ZapA-ZapB interactome of *Escherichia coli*. *J Bacteriol* **194**, 292-302.

Gamba P., Veening J.W., Saunders N.J., Hamoen L.W. & Daniel R.A. (2009) Two-step assembly dynamics of the *Bacillus subtilis* divisome. *J Bacteriol* **191**, 4186-94.

Ganong B.R. & Raetz C.R. (1982) Massive accumulation of phosphatidic acid in conditionally lethal CDP-diglyceride synthetase mutants and cytidine auxotrophs of *Escherichia coli*. *J Biol Chem* **257**, 389-94.

Garcia-Lara J. & Foster S.J. (2009) Anti-*Staphylococcus aureus* immunotherapy: current status and prospects. *Curr Opin Pharmacol* **9**, 552-7.

Garcia-Lara J., Masalha M. & Foster S.J. (2005) *Staphylococcus aureus*: the search for novel targets. *Drug Discov Today* **10**, 643-51.

Garcia-Lara J., Weihs F., Ma X., Walker L., Chaudhuri R.R., Kasturiarachchi J., Crossley H., Golestanian R. & Foster S.J. (2015) Supramolecular structure in the membrane of *Staphylococcus aureus*. *Proc Natl Acad Sci U S A*.

Garner E.C., Bernard R., Wang W., Zhuang X., Rudner D.Z. & Mitchison T. (2011) Coupled, circumferential motions of the cell wall synthesis machinery and MreB filaments in *B. subtilis*. *Science* **333**, 222-5.

Gautam S., Kim T. & Spiegel D.A. (2015) Chemical probes reveal an extraseptal mode of cross-linking in *Staphylococcus aureus*. *J Am Chem Soc* **137**, 7441-7.

Geissler B., Shiomi D. & Margolin W. (2007) The *ftsA** gain-of-function allele of *Escherichia coli* and its effects on the stability and dynamics of the Z ring. *Microbiology* **153**, 814-25.

Gerard P., Vernet T. & Zapun A. (2002) Membrane topology of the *Streptococcus pneumoniae* FtsW division protein. *J Bacteriol* **184**, 1925-31.

Gerding M.A., Liu B., Bendezu F.O., Hale C.A., Bernhardt T.G. & de Boer P.A. (2009) Self-enhanced accumulation of FtsN at Division Sites and Roles for Other Proteins with a SPOR domain (DamX, DedD, and RlpA) in *Escherichia coli* cell constriction. *J Bacteriol* **191**, 7383-401.

Ghigo J.M. & Beckwith J. (2000) Cell division in *Escherichia coli*: role of FtsL domains in septal localization, function, and oligomerization. *J Bacteriol* **182**, 116-29.

Ghigo J.M., Weiss D.S., Chen J.C., Yarrow J.C. & Beckwith J. (1999) Localization of FtsL to the *Escherichia coli* septal ring. *Mol Microbiol* **31**, 725-37.

Gibson C.W., Daneo-Moore L. & Higgins M.L. (1983) Cell wall assembly during inhibition of DNA synthesis in Streptococcus faecium. *J Bacteriol* **155**, 351-6.

Gitai Z., Dye N. & Shapiro L. (2004) An actin-like gene can determine cell polarity in bacteria. *Proc Natl Acad Sci U S A* **101**, 8643-8.

Gitai Z., Dye N.A., Reisenauer A., Wachi M. & Shapiro L. (2005) MreB actin-mediated segregation of a specific region of a bacterial chromosome. *Cell* **120**, 329-41.

Glowalla E., Tosetti B., Kronke M. & Krut O. (2009) Proteomics-based identification of anchorless cell wall proteins as vaccine candidates against *Staphylococcus aureus*. *Infect Immun* **77**, 2719-29.

Goehring N.W., Gueiros-Filho F. & Beckwith J. (2005) Premature targeting of a cell division protein to midcell allows dissection of divisome assembly in *Escherichia coli*. *Genes Dev* **19**, 127-37.

Goehring N.W., Robichon C. & Beckwith J. (2007) Role for the nonessential N terminus of FtsN in divisome assembly. *J Bacteriol* **189**, 646-9.

Goffin C. & Ghuysen J.M. (1998) Multimodular penicillin-binding proteins: an enigmatic family of orthologs and paralogs. *Microbiol Mol Biol Rev* **62**, 1079-93.

Goley E.D., Comolli L.R., Fero K.E., Downing K.H. & Shapiro L. (2010) DipM links peptidoglycan remodelling to outer membrane organization in Caulobacter. *Mol Microbiol* **77**, 56-73.

Goley E.D., Yeh Y.C., Hong S.H., Fero M.J., Abeliuk E., McAdams H.H. & Shapiro L. (2011) Assembly of the Caulobacter cell division machine. *Mol Microbiol* **80**, 1680-98.

Gonzalez M.D. & Beckwith J. (2009) Divisome under construction: distinct domains of the small membrane protein FtsB are necessary for interaction with multiple cell division proteins. *J Bacteriol* **191**, 2815-25.

Goranov A.I., Katz L., Breier A.M., Burge C.B. & Grossman A.D. (2005) A transcriptional response to replication status mediated by the conserved bacterial replication protein DnaA. *Proc Natl Acad Sci U S A* **102**, 12932-7.

Greenberg R.N., Kennedy D.J., Reilly P.M., Luppen K.L., Weinandt W.J., Bollinger M.R., Aguirre F., Kodesch F. & Saeed A.M.K. (1987) Treatment of Bone, Joint, and Soft-Tissue Infections with Oral Ciprofloxacin. *Antimicrob Agents Chemother* **31**, 151-5.

Grenga L., Luzi G., Paolozzi L. & Ghelardini P. (2008) The *Escherichia coli* FtsK functional domains involved in its interaction with its divisome protein partners. *FEMS Microbiol Lett* **287**, 163-7.

Grover N.B., Woldringh C.L., Zaritsky A. & Rosenberger R.F. (1977) Elongation of rod-shaped bacteria. *J Theor Biol* **67**, 181-93.

Grundling A. & Schneewind O. (2007a) Synthesis of glycerol phosphate lipoteichoic acid in *Staphylococcus aureus*. *Proc Natl Acad Sci U S A* **104**, 8478-83.

Guay G.G., Khan S.A. & Rothstein D.M. (1993) The Tet(K) Gene of Plasmid Pt181 of *Staphylococcus-Aureus* Encodes an Efflux Protein That Contains 14 Transmembrane Helices. *Plasmid* **30**, 163-6.

Gueiros-Filho F.J. & Losick R. (2002) A widely conserved bacterial cell division protein that promotes assembly of the tubulin-like protein FtsZ. *Genes Dev* **16**, 2544-56.

Guzman L.M., Barondess J.J. & Beckwith J. (1992) FtsL, an essential cytoplasmic membrane protein involved in cell division in *Escherichia coli*. *J Bacteriol* **174**, 7716-28.

Haeusser D.P., Garza A.C., Buscher A.Z. & Levin P.A. (2007) The division inhibitor EzrA contains a seven-residue patch required for maintaining the dynamic nature of the medial FtsZ ring. *J Bacteriol* **189**, 9001-10.

Hale C.A. & de Boer P.A. (1997) Direct binding of FtsZ to ZipA, an essential component of the septal ring structure that mediates cell division in *E. coli*. *Cell* **88**, 175-85.

Hale C.A. & de Boer P.A. (1999) Recruitment of ZipA to the septal ring of *Escherichia coli* is dependent on FtsZ and independent of FtsA. *J Bacteriol* **181**, 167-76.

Hale C.A., Shiomi D., Liu B., Bernhardt T.G., Margolin W., Niki H. & de Boer P.A.J. (2011) Identification of *Escherichia coli* ZapC (YcbW) as a Component of the Division Apparatus That Binds and Bundles FtsZ Polymers. *J Bacteriol* **193**, 1393-404.

Hamoen L.W., Meile J.C., de Jong W., Noirot P. & Errington J. (2006) SepF, a novel FtsZ-interacting protein required for a late step in cell division. *Mol Microbiol* **59**, 989-99.

Haney S.A., Glasfeld E., Hale C., Keeney D., He Z. & de Boer P. (2001) Genetic analysis of the *Escherichia coli* FtsZ.ZipA interaction in the yeast two-hybrid system. Characterization of FtsZ residues essential for the interactions with ZipA and with FtsA. *J Biol Chem* **276**, 11980-7.

Harris L.G., Foster S.J. & Richards R.G. (2002) An introduction to *Staphylococcus aureus*, and techniques for identifying and quantifying *S. aureus* adhesins in relation to adhesion to biomaterials: review. *Eur Cell Mater* **4**, 39-60.

Harry E.J., Stewart B. J. & Wake R.G. (1993) Characterization of Mutations in Divlb of *Bacillus-Subtilis* and Cellular-Localization of the Divlb Protein. *Mol Microbiol* **7**, 611-21.

Hartleib J., Kohler N., Dickinson R.B., Chhatwal G.S., Sixma J.J., Hartford O.M., Foster T.J., Peters G., Kehrel B.E. & Herrmann M. (2000) Protein A is the von Willebrand factor binding protein on *Staphylococcus aureus*. *Blood* **96**, 2149-56.

Hayden M.K., Rezai K., Hayes R.A., Lolans K., Quinn J.P. & Weinstein R.A. (2005) Development of Daptomycin resistance in vivo in methicillin-resistant *Staphylococcus aureus*. *J Clin Microbiol* **43**, 5285-7.

Haydon D.J., Stokes N.R., Ure R., Galbraith G., Bennett J.M., Brown D.R., Baker P.J., Barynin V.V., Rice D.W., Sedelnikova S.E., Heal J.R., Sheridan J.M., Aiwale S.T., Chauhan P.K., Srivastava A., Taneja A., Collins I., Errington J. & Czaplewski L.G. (2008) An inhibitor of FtsZ with potent and selective anti-staphylococcal activity. *Science* **321**, 1673-5.

Heidrich C., Templin M.F., Ursinus A., Merdanovic M., Berger J., Schwarz H., de Pedro M.A. & Holtje J.V. (2001) Involvement of N-acetylmuramyl-L-alanine amidases in cell separation and antibiotic-induced autolysis of *Escherichia coli*. *Mol Microbiol* **41**, 167-78.

Hennekinne J.A., De Buyser M.L. & Dragacci S. (2012) *Staphylococcus aureus* and its food poisoning toxins: characterization and outbreak investigation. *FEMS Microbiol Rev* **36**, 815-36.

Henriques A.O., Glaser P., Piggot P.J. & Moran C.P., Jr. (1998) Control of cell shape and elongation by the *rodA* gene in *Bacillus subtilis*. *Mol Microbiol* **28**, 235-47.

Hett E.C., Chao M.C., Deng L.L. & Rubin E.J. (2008) A mycobacterial enzyme essential for cell division synergizes with resuscitation-promoting factor. *PLoS Pathog* **4**, e1000001.

Hiramatsu K., Aritaka N., Hanaki H., Kawasaki S., Hosoda Y., Hori S., Fukuchi Y. & Kobayashi I. (1997) Dissemination in Japanese hospitals of strains of *Staphylococcus aureus* heterogeneously resistant to vancomycin. *Lancet* **350**, 1670-3.

Holtje J.V. (1998) Growth of the stress-bearing and shape-maintaining murein sacculus of *Escherichia coli*. *Microbiol Mol Biol Rev* **62**, 181-203.

Hope I.A. & Struhl K. (1986) Functional Dissection of a Eukaryotic Transcriptional Activator Protein, Gcn4 of Yeast. *Cell* **46**, 885-94.

Hope R., Mushtaq S., James D., Pllana T., Warner M. & Livermore D.M. (2010) Tigecycline activity: low resistance rates but problematic disc breakpoints revealed by a multicentre sentinel survey in the UK. *J Antimicrob Chemother* **65**, 2602-9.

Horsburgh M.J., Wharton S.J., Cox A.G., Ingham E., Peacock S. & Foster S.J. (2002) MntR modulates expression of the PerR regulon and superoxide resistance in *Staphylococcus aureus* through control of manganese uptake. *Mol Microbiol* **44**, 1269-86.

Hu D.L., Omoe K., Shimoda Y., Nakane A. & Shinagawa K. (2003) Induction of emetic response to staphylococcal enterotoxins in the house musk shrew (Suncus murinus). *Infect Immun* **71**, 567-70.

Hu Z. & Lutkenhaus J. (1999) Topological regulation of cell division in *Escherichia coli* involves rapid pole to pole oscillation of the division inhibitor MinC under the control of MinD and MinE. *Mol Microbiol* **34**, 82-90.

Hu Z. & Lutkenhaus J. (2000) Analysis of MinC reveals two independent domains involved in interaction with MinD and FtsZ. *J Bacteriol* **182**, 3965-71.

Hu Z., Mukherjee A., Pichoff S. & Lutkenhaus J. (1999) The MinC component of the division site selection system in *Escherichia coli* interacts with FtsZ to prevent polymerization. *Proc Natl Acad Sci U S A* **96**, 14819-24.

Huang W.M., Libbey J.L., van der Hoeven P. & Yu S.X. (1998) Bipolar localization of *Bacillus subtilis* topoisomerase IV, an enzyme required for chromosome segregation. *Proc Natl Acad Sci U S A* **95**, 4652-7.

Hunt A., Rawlins J.P., Thomaides H.B. & Errington J. (2006) Functional analysis of 11 putative essential genes in *Bacillus subtilis*. *Microbiology* **152**, 2895-907.

Ishikawa S., Kawai Y., Hiramatsu K., Kuwano M. & Ogasawara N. (2006) A new FtsZ-interacting protein, YlmF, complements the activity of FtsA during progression of cell division in *Bacillus subtilis*. *Mol Microbiol* **60**, 1364-80.

Ishino F., Jung H.K., Ikeda M., Doi M., Wachi M. & Matsuhashi M. (1989) New mutations fts-36, lts-33, and *ftsW* clustered in the mra region of the *Escherichia coli* chromosome induce thermosensitive cell growth and division. *J Bacteriol* **171**, 5523-30.

Iwai N., Nagai K. & Wachi M. (2002) Novel S-benzylisothiourea compound that induces spherical cells in *Escherichia coli* probably by acting on a rod-shape-determining protein(s) other than penicillin-binding protein 2. *Biosci Biotechnol Biochem* **66**, 2658-62.

Jevons M.P., Rolinson G.N. & Knox R. (1961) Celbenin-Resistant Staphylococci. *Br Med J* **1**, 124-&.

Ji Y., Zhang B., Van S.F., Horn, Warren P., Woodnutt G., Burnham M.K. & Rosenberg M. (2001) Identification of critical staphylococcal genes using conditional phenotypes generated by antisense RNA. *Science* **293**, 2266-9.

Jones L.J., Carballido-Lopez R. & Errington J. (2001) Control of cell shape in bacteria: helical, actin-like filaments in *Bacillus subtilis*. *Cell* **104**, 913-22.

Kaatz G.W., Seo S.M., Dorman N.J. & Lerner S.A. (1990) Emergence of Teicoplanin Resistance during Therapy of Staphylococcus-Aureus Endocarditis. *Journal of Infectious Diseases* **162**, 103-8.

Kaltwasser M., Wiegert T. & Schumann W. (2002) Construction and application of epitope- and green fluorescent protein-tagging integration vectors for *Bacillus subtilis*. *Appl Environ Microbiol* **68**, 2624-8.

Karimova G., Dautin N. & Ladant D. (2005) Interaction network among *Escherichia coli* membrane proteins involved in cell division as revealed by bacterial two-hybrid analysis. *J Bacteriol* **187**, 2233-43.

Karimova G., Pidoux J., Ullmann A. & Ladant D. (1998) A bacterial two-hybrid system based on a reconstituted signal transduction pathway. *Proc Natl Acad Sci U S A* **95**, 5752-6.

Katis V.L., Wake R.G. & Harry E.J. (2000) Septal localization of the membrane-bound division proteins of *Bacillus subtilis* DivIB and DivIC is codependent only at high temperatures and requires FtsZ. *J Bacteriol* **182**, 3607-11.

Kawai Y., Daniel R.A. & Errington J. (2009) Regulation of cell wall morphogenesis in *Bacillus subtilis* by recruitment of PBP1 to the MreB helix. *Mol Microbiol* **71**, 1131-44.

Keegan L., Gill G. & Ptashne M. (1986) Separation of DNA-Binding from the Transcription-Activating Function of a Eukaryotic Regulatory Protein. *Science* **231**, 699-704.

Kempf M.J. & McBride M.J. (2000) Transposon insertions in the Flavobacterium johnsoniae ftsX gene disrupt gliding motility and cell division. *J Bacteriol* **182**, 1671-9.

Kent V.L. (2014).

Khattar M.M., Addinall S.G., Stedul K.H., Boyle D.S., Lutkenhaus J. & Donachie W.D. (1997) Two polypeptide products of the *Escherichia coli* cell division gene *ftsW* and a possible role for FtsW in FtsZ function. *J Bacteriol* **179**, 784-93.

Kleinschnitz E.M., Heichlinger A., Schirner K., Winkler J., Latus A., Maldener I., Wohlleben W. & Muth G. (2011) Proteins encoded by the mre gene cluster in *Streptomyces coelicolor* A3(2) cooperate in spore wall synthesis. *Mol Microbiol* **79**, 1367-79.

Kobayashi K., Ehrlich S.D., Albertini A., Amati G., Andersen K.K., Arnaud M., Asai K., Ashikaga S., Aymerich S., Bessieres P., Boland F., Brignell S.C., Bron S., Bunai K., Chapuis J., Christiansen L.C., Danchin A., Debarbouille M., Dervyn E., Deuerling E., Devine K., Devine S.K., Dreesen O., Errington J., Fillinger S., Foster S.J., Fujita Y., Galizzi A., Gardan R., Eschevins C., Fukushima T., Haga K., Harwood C.R., Hecker M., Hosoya D., Hullo M.F., Kakeshita H., Karamata D., Kasahara Y., Kawamura F., Koga K., Koski P., Kuwana R., Imamura D., Ishimaru M., Ishikawa S., Ishio I., Le Coq D., Masson A., Mauel C., Meima R., Mellado R.P., Moir A., Moriya S., Nagakawa E., Nanamiya H., Nakai S., Nygaard P., Ogura M., Ohanan T., O'Reilly M., O'Rourke M., Pragai Z., Pooley H.M., Rapoport G., Rawlins J.P., Rivas L.A., Rivolta C., Sadaie A., Sadaie Y., Sarvas M., Sato T., Saxild H.H., Scanlan E., Schumann W., Seegers J.F., Sekiguchi J., Sekowska A., Seror S.J., Simon M., Stragier P., Studer R., Takamatsu H., Tanaka T., Takeuchi M., Thomaides H.B., Vagner V., van Dijl J.M., Watabe K., Wipat A., Yamamoto H., Yamamoto M., Yamamoto Y., Yamane K., Yata K., Yoshida K., Yoshikawa H., Zuber U. & Ogasawara N. (2003) Essential *Bacillus subtilis* genes. *Proc Natl Acad Sci U S A* **100**, 4678-83.

Koksharova O.A. & Wolk C.P. (2002) A novel gene that bears a DnaJ motif influences cyanobacterial cell division. *J Bacteriol* **184**, 5524-8.

Kreis C.A., Raschke M.J., Rosslenbroich S.B., Tholema-Hans N., Loffler B. & Fuchs T. (2013) Therapy of intracellular *Staphylococcus aureus* by tigecyclin. *BMC Infect Dis* **13**, 267.

Kreiswirth B.N., Lofdahl S., Betley M.J., O'Reilly M., Schlievert P.M., Bergdoll M.S. & Novick R.P. (1983) The toxic shock syndrome exotoxin structural gene is not detectably transmitted by a prophage. *Nature* **305**, 709-12.

Kruse T., Bork-Jensen J. & Gerdes K. (2005) The morphogenetic MreBCD proteins of *Escherichia coli* form an essential membrane-bound complex. *Mol Microbiol* **55**, 78-89.

Kumar K., Awasthi D., Berger W.T., Tonge P.J., Slayden R.A. & Ojima I. (2010) Discovery of anti-TB agents that target the cell-division protein FtsZ. *Future Med Chem* **2**, 1305-23.

Lacey R.W. & Chopra I. (1972) Evidence for Mutation to Streptomycin Resistance in Clinical Strains of Staphylococcus-Aureus. *J Gen Microbiol* **73**, 175-&.

Lackner L.L., Raskin D.M. & de Boer P.A. (2003) ATP-dependent interactions between *Escherichia coli* Min proteins and the phospholipid membrane in vitro. *J Bacteriol* **185**, 735-49.

Laczko-Dobos H., Ughy B., Toth S.Z., Komenda J., Zsiros O., Domonkos I., Parducz A., Bogos B., Komura M., Itoh S. & Gombos Z. (2008) Role of phosphatidylglycerol in the function and assembly of Photosystem II reaction center, studied in a *cdsA*-inactivated PAL mutant strain of Synechocystis sp. PCC6803 that lacks phycobilisomes. *Biochim Biophys Acta* **1777**, 1184-94.

Ladant D. (1988) Interaction of *Bordetella pertussis* adenylate cyclase with calmodulin. Identification of two separated calmodulin-binding domains. *J Biol Chem* **263**, 2612-8.

Land A.D., Tsui H.C., Kocaoglu O., Vella S.A., Shaw S.L., Keen S.K., Sham L.T., Carlson E.E. & Winkler M.E. (2013) Requirement of essential Pbp2x and GpsB for septal ring closure in *Streptococcus pneumoniae* D39. *Mol Microbiol* **90**, 939-55.

Land A.D. & Winkler M.E. (2011) The requirement for pneumococcal MreC and MreD is relieved by inactivation of the gene encoding PBP1a. *J Bacteriol* **193**, 4166-79.

Layec S., Gerard J., Legue V., Chapot-Chartier M.P., Courtin P., Borges F., Decaris B. & Leblond-Bourget N. (2009) The CHAP domain of Cse functions as an endopeptidase that acts at mature septa to promote Streptococcus thermophilus cell separation. *Mol Microbiol* **71**, 1205-17.

Le Gouellec A., Roux L., Fadda D., Massidda O., Vernet T. & Zapun A. (2008) Roles of pneumococcal DivIB in cell division. *J Bacteriol* **190**, 4501-11.

Le Marechal C., Seyffert N., Jardin J., Hernandez D., Jan G., Rault L., Azevedo V., Francois P., Schrenzel J., van de Guchte M., Even S., Berkova N., Thiery R., Fitzgerald J.R., Vautor E. & Le Loir Y. (2011) Molecular basis of virulence in *Staphylococcus aureus* mastitis. *PLoS One* **6**, e27354.

Leaver M., Dominguez-Cuevas P., Coxhead J.M., Daniel R.A. & Errington J. (2009) Life without a wall or division machine in *Bacillus subtilis*. *Nature* **457**, 849-53.

Leaver M. & Errington J. (2005) Roles for MreC and MreD proteins in helical growth of the cylindrical cell wall in *Bacillus subtilis*. *Mol Microbiol* **57**, 1196-209.

Lee J.C., Cha J.H., Zerbv D.B. & Stewart G.C. (2003) Heterospecific expression of the *Bacillus subtilis* cell shape determination genes mreBCD in *Escherichia coli*. *Curr Microbiol* **47**, 146-52.

Lee J.C. & Stewart G.C. (2003) Essential nature of the *mreC* determinant of *Bacillus subtilis*. *J Bacteriol* **185**, 4490-8.

Lenarcic R., Halbedel S., Visser L., Shaw M., Wu L.J., Errington J., Marenduzzo D. & Hamoen L.W. (2009) Localisation of DivIVA by targeting to negatively curved membranes. *EMBO J* **28**, 2272-82.

Lenn T., Leake M.C. & Mullineaux C.W. (2008) Clustering and dynamics of cytochrome bd-I complexes in the *Escherichia coli* plasma membrane in vivo. *Mol Microbiol* **70**, 1397-407.

Levin P.A., Kurtser I.G. & Grossman A.D. (1999) Identification and characterization of a negative regulator of FtsZ ring formation in *Bacillus subtilis*. *Proc Natl Acad Sci U S A* **96**, 9642-7.

Levin P.A. & Losick R. (1994) Characterization of a cell division gene from *Bacillus subtilis* that is required for vegetative and sporulation septum formation. *J Bacteriol* **176**, 1451-9.

Levin P.A. & Losick R. (1996) Transcription factor Spo0A switches the localization of the cell division protein FtsZ from a medial to a bipolar pattern in *Bacillus subtilis*. *Genes Dev* **10**, 478-88.

Levin P.A., Margolis P.S., Setlow P., Losick R. & Sun D. (1992) Identification of *Bacillus subtilis* genes for septum placement and shape determination. *J Bacteriol* **174**, 6717-28.

Lewis P.J. (2004) Bacterial subcellular architecture: recent advances and future prospects. *Mol Microbiol* **54**, 1135-50.

Lewis P.J. & Marston A.L. (1999) GFP vectors for controlled expression and dual labelling of protein fusions in *Bacillus subtilis*. *Gene* **227**, 101-10.

Liew A.T., Theis T., Jensen S.O., Garcia-Lara J., Foster S.J., Firth N., Lewis P.J. & Harry E.J. (2011) A simple plasmid-based system that allows rapid generation of tightly controlled gene expression in *Staphylococcus aureus*. *Microbiology* **157**, 666-76.

Lim D. & Strynadka N.C.J. (2002) Structural basis for the beta-lactam resistance of PBP2a from methicillin-resistant *Staphylococcus aureus*. *Nature Structural Biology* **9**, 870-6.

Lleo M.M., Canepari P. & Satta G. (1990) Bacterial-Cell Shape Regulation - Testing of Additional Predictions Unique to the 2-Competing-Sites Model for Peptidoglycan Assembly and Isolation of Conditional Rod-Shaped Mutants from Some Wild-Type Cocci. *J Bacteriol* **172**, 3758-71.

Lovering A.L. & Strynadka N.C. (2007) High-resolution structure of the major periplasmic domain from the cell shape-determining filament MreC. *J Mol Biol* **372**, 1034-44.

Lowe J. & Amos L.A. (1998) Crystal structure of the bacterial cell-division protein FtsZ. *Nature* **391**, 203-6.

Lowy F.D. (1998) *Staphylococcus aureus* infections. *N Engl J Med* **339**, 520-32.

Lu Y.J., Zhang F., Grimes K.D., Lee R.E. & Rock C.O. (2007) Topology and active site of PlsY: the bacterial acylphosphate:glycerol-3-phosphate acyltransferase. *J Biol Chem* **282**, 11339-46.

Ludwig W., Schleifer, K. H. & Whitman, W. B. (2009) *Revised road map to phylum firmicutes. In De Vos, G., Garrity, G., Jones, D., Krieg, N. R., Ludwing, W., Rainey, F. A., Schleifer, K. H. & Whitman, W. B. (Eds.).* Springer-Verlag., New York.

Lutkenhaus J. (2012) The ParA/MinD family puts things in their place. *Trends Microbiol* **20**, 411-8.

Lutkenhaus J.F., Wolf-Watz H. & Donachie W.D. (1980) Organization of genes in the *ftsA*-envA region of the *Escherichia coli* genetic map and identification of a new fts locus (*ftsZ*). *J Bacteriol* **142**, 615-20.

Ma L., King G.F. & Rothfield L. (2004) Positioning of the MinE binding site on the MinD surface suggests a plausible mechanism for activation of the *Escherichia coli* MinD ATPase during division site selection. *Mol Microbiol* **54**, 99-108.

Ma X., Ehrhardt D.W. & Margolin W. (1996) Colocalization of cell division proteins FtsZ and FtsA to cytoskeletal structures in living *Escherichia coli* cells by using green fluorescent protein. *Proc Natl Acad Sci U S A* **93**, 12998-3003.

Maggi S., Massidda O., Luzi G., Fadda D., Paolozzi L. & Ghelardini P. (2008) Division protein interaction web: identification of a phylogenetically conserved common interactome between *Streptococcus pneumoniae* and *Escherichia coli*. *Microbiology* **154**, 3042-52.

Maguin E., Duwat P., Hege T., Ehrlich D. & Gruss A. (1992) New thermosensitive plasmid for Gram-positive bacteria. *J Bacteriol* **174**, 5633-8.

Maira-Litran T., Kropec A., Goldmann D.A. & Pier G.B. (2005) Comparative opsonic and protective activities of *Staphylococcus aureus* conjugate vaccines containing native or deacetylated Staphylococcal Poly-N-acetyl-beta-(1-6)-glucosamine. *Infect Immun* **73**, 6752-62.

Malbruny B., Canu A., Bozdogan B., Fantin B., Zarrouk V., Dutka-Malen S., Feger C. & Leclercq R. (2002) Resistance to quinupristin-dalfopristin due to mutation of L22 ribosomal protein in *Staphylococcus aureus*. *Antimicrob Agents Chemother* **46**, 2200-7.

Mangili A., Bica I., Snydman D.R. & Hamer D.H. (2005) Daptomycin-resistant, methicillin-resistant *Staphylococcus aureus* bacteremia. *Clin Infect Dis* **40**, 1058-60.

Marbouty M., Mazouni K., Saguez C., Cassier-Chauvat C. & Chauvat F. (2009) Characterization of the Synechocystis strain PCC 6803 penicillin-binding proteins and cytokinetic proteins FtsQ and FtsW and their network of interactions with ZipN. *J Bacteriol* **191**, 5123-33.

Margolin W. (2000a) Green fluorescent protein as a reporter for macromolecular localization in bacterial cells. *Methods* **20**, 62-72.

Margolin W. (2000b) Themes and variations in prokaryotic cell division. *FEMS Microbiol Rev* **24**, 531-48.

Margolin W. (2001) Spatial regulation of cytokinesis in bacteria. *Curr Opin Microbiol* **4**, 647-52.

Margolin W. (2009) Sculpting the bacterial cell. *Curr Biol* **19**, R812-22.

Matsuhashi M., Wachi M. & Ishino F. (1990) Machinery for cell growth and division: penicillin-binding proteins and other proteins. *Res Microbiol* **141**, 89-103.

Mazouni K., Domain F., Cassier-Chauvat C. & Chauvat F. (2004) Molecular analysis of the key cytokinetic components of cyanobacteria: FtsZ, ZipN and MinCDE. *Mol Microbiol* **52**, 1145-58.

McCormick J.R. & Losick R. (1996) Cell division gene ftsQ is required for efficient sporulation but not growth and viability in *Streptomyces coelicolor* A3(2). *J Bacteriol* **178**, 5295-301.

McDevitt D., Payne D.J., Holmes D.J. & Rosenberg M. (2002) Novel targets for the future development of antibacterial agents. *Symp Ser Soc Appl Microbiol*, 28S-34S.

MenginLecreulx D., vanHeijenoort J. & Park J.T. (1996) Identification of the mpl gene encoding UDP-N-acetylmuramate: L-alanyl-gamma-D-glutamyl-meso-diaminopimelate ligase in *Escherichia coli* and its role in recycling of cell wall peptidoglycan. *J Bacteriol* **178**, 5347-52.

Mercer K.L. & Weiss D.S. (2002) The *Escherichia coli* cell division protein FtsW is required to recruit its cognate transpeptidase, FtsI (PBP3), to the division site. *J Bacteriol* **184**, 904-12.

Mercier R., Kawai Y. & Errington J. (2014) General principles for the formation and proliferation of a wall-free (L-form) state in bacteria. *Elife* **3**.

Mercier R., Petit M.A., Schbath S., Robin S., El Karoui M., Boccard F. & Espeli O. (2008) The MatP/matS site-specific system organizes the terminus region of the *E. coli* chromosome into a macrodomain. *Cell* **135**, 475-85.

Merino S., Altarriba M., Gavin R., Izquierdo L. & Tomas J.M. (2001) The cell division genes (ftsE and X) of Aeromonas hydrophila and their relationship with opsonophagocytosis. *FEMS Microbiol Lett* **198**, 183-8.

Migocki M.D., Freeman M.K., Wake R.G. & Harry E.J. (2002) The Min system is not required for precise placement of the midcell Z ring in *Bacillus subtilis*. *EMBO Rep* **3**, 1163-7.

Mir M.A., Rajeswari H.S., Veeraraghavan U. & Ajitkumar P. (2006) Molecular characterisation of ABC transporter type FtsE and FtsX proteins of *Mycobacterium tuberculosis*. *Arch Microbiol* **185**, 147-58.

Mohammadi T., Karczmarek A., Crouvoisier M., Bouhss A., Mengin-Lecreulx D. & den Blaauwen T. (2007) The essential peptidoglycan glycosyltransferase MurG forms a complex with proteins involved in lateral envelope growth as well as with proteins involved in cell division in *Escherichia coli*. *Mol Microbiol* **65**, 1106-21.

Mohammadi T., van Dam V., Sijbrandi R., Vernet T., Zapun A., Bouhss A., Diepeveen-de Bruin M., Nguyen-Disteche M., de Kruijff B. & Breukink E. (2011) Identification of FtsW as a transporter of lipid-linked cell wall precursors across the membrane. *EMBO J* **30**, 1425-32.

Moll A., Schlimpert S., Briegel A., Jensen G.J. & Thanbichler M. (2010) DipM, a new factor required for peptidoglycan remodelling during cell division in *Caulobacter crescentus*. *Mol Microbiol* **77**, 90-107.

Moll A. & Thanbichler M. (2009) FtsN-like proteins are conserved components of the cell division machinery in proteobacteria. *Mol Microbiol* **72**, 1037-53.

Monahan L.G., Robinson A. & Harry E.J. (2009) Lateral FtsZ association and the assembly of the cytokinetic Z ring in bacteria. *Mol Microbiol* **74**, 1004-17.

Monk I.R. & Foster T.J. (2012) Genetic manipulation of Staphylococci-breaking through the barrier. *Front Cell Infect Microbiol* **2**, 49.

Monk I.R., Shah I.M., Xu M., Tan M.W. & Foster T.J. (2012) Transforming the untransformable: application of direct transformation to manipulate genetically *Staphylococcus aureus* and Staphylococcus epidermidis. *MBio* **3**.

Monteiro J.M., Fernandes P.B., Vaz F., Pereira A.R., Tavares A.C., Ferreira M.T., Pereira P.M., Veiga H., Kuru E., VanNieuwenhze M.S., Brun Y.V., Filipe S.R. & Pinho M.G. (2015) Cell shape dynamics during the staphylococcal cell cycle. *Nat Commun* **6**, 8055.

Morlot C., Noirclerc-Savoye M., Zapun A., Dideberg O. & Vernet T. (2004) The D,D-carboxypeptidase PBP3 organizes the division process of *Streptococcus pneumoniae*. *Mol Microbiol* **51**, 1641-8.

Mosyak L., Zhang Y., Glasfeld E., Haney S., Stahl M., Seehra J. & Somers W.S. (2000) The bacterial cell-division protein ZipA and its interaction with an FtsZ fragment revealed by X-ray crystallography. *EMBO J* **19**, 3179-91.

Moy F.J., Glasfeld E., Mosyak L. & Powers R. (2000) Solution structure of ZipA, a crucial component of *Escherichia coli* cell division. *Biochemistry* **39**, 9146-56.

Mukherjee A. & Lutkenhaus J. (1994) Guanine nucleotide-dependent assembly of FtsZ into filaments. *J Bacteriol* **176**, 2754-8.

Mulder E. & Woldringh C.L. (1989) Actively replicating nucleoids influence positioning of division sites in *Escherichia coli* filaments forming cells lacking DNA. *J Bacteriol* **171**, 4303-14.

Muller P., Ewers C., Bertsche U., Anstett M., Kallis T., Breukink E., Fraipont C., Terrak M., Nguyen-Disteche M. & Vollmer W. (2007) The essential cell division protein FtsN interacts with the murein (peptidoglycan) synthase PBP1B in *Escherichia coli*. *J Biol Chem* **282**, 36394-402.

Murray I.A. & Shaw W.V. (1997) O-acetyltransferases for chloramphenicol and other natural products. *Antimicrob Agents Chemother* **41**, 1-6.

Murray T., Popham D.L. & Setlow P. (1997) Identification and characterization of *pbpA* encoding *Bacillus subtilis* penicillin-binding protein 2A. *J Bacteriol* **179**, 3021-9.

Murray T., Popham D.L. & Setlow P. (1998) *Bacillus subtilis* cells lacking penicillin-binding protein 1 require increased levels of divalent cations for growth. *J Bacteriol* **180**, 4555-63.

Mylotte J.M. & Tayara A. (2000) *Staphylococcus aureus* bacteremia: predictors of 30-day mortality in a large cohort. *Clin Infect Dis* **31**, 1170-4.

Naber C.K. (2009) *Staphylococcus aureus* bacteremia: epidemiology, pathophysiology, and management strategies. *Clin Infect Dis* **48 Suppl 4**, S231-7.

Naidoo J. & Noble W.C. (1978) Transfer of Gentamicin Resistance between Strains of Staphylococcus-Aureus on Skin. *J Gen Microbiol* **107**, 391-3.

Ng E.Y., Trucksis M. & Hooper D.C. (1996) Quinolone resistance mutations in topoisomerase IV: Relationship to the flqA locus and genetic evidence that topoisomerase IV is the primary target and DNA gyrase is the secondary target of fluoroquinolones in *Staphylococcus aureus. Antimicrob Agents Chemother* **40**, 1881-8.

Ng W.L., Kazmierczak K.M. & Winkler M.E. (2004) Defective cell wall synthesis in *Streptococcus pneumoniae* R6 depleted for the essential PcsB putative murein hydrolase or the VicR (YycF) response regulator. *Mol Microbiol* **53**, 1161-75.

Niba E.T., Li G., Aoki K. & Kitakawa M. (2010) Characterization of rodZ mutants: RodZ is not absolutely required for the cell shape and motility. *FEMS Microbiol Lett* **309**, 35-42.

Nikolaichik Y.A. & Donachie W.D. (2000) Conservation of gene order amongst cell wall and cell division genes in Eubacteria, and ribosomal genes in Eubacteria and Eukaryotic organelles. *Genetica* **108**, 1-7.

Nilsson I.M., Verdrengh M., Ulrich R.G., Bavari S. & Tarkowski A. (1999) Protection against *Staphylococcus aureus* sepsis by vaccination with recombinant staphylococcal enterotoxin A devoid of superantigenicity. *J Infect Dis* **180**, 1370-3.

Nishibori A., Kusaka J., Hara H., Umeda M. & Matsumoto K. (2005) Phosphatidylethanolamine domains and localization of phospholipid synthases in *Bacillus subtilis* membranes. *J Bacteriol* **187**, 2163-74.

Niu L. & Yu J. (2008) Investigating intracellular dynamics of FtsZ cytoskeleton with photoactivation single-molecule tracking. *Biophys J* **95**, 2009-16.

Noble W.C., Valkenburg H.A. & Wolters C.H. (1967) Carriage of *Staphylococcus aureus* in random samples of a normal population. *J Hyg (Lond)* **65**, 567-73.

Nogales E., Downing K.H., Amos L.A. & Lowe J. (1998) Tubulin and FtsZ form a distinct family of GTPases. *Nature Structural Biology* **5**, 451-8.

Noirclerc-Savoye M., Le Gouellec A., Morlot C., Dideberg O., Vernet T. & Zapun A. (2005) In vitro reconstitution of a trimeric complex of DivIB, DivIC and FtsL, and their transient co-localization at the division site in *Streptococcus pneumoniae*. *Mol Microbiol* **55**, 413-24.

Okuno T., Ogoh M., Tanina H., Funasaki N. & Kogure K. (2009) Direct monitoring of interaction between *Escherichia coli* proteins, MinC and monomeric FtsZ, in solution. *Biol Pharm Bull* **32**, 1473-5.

Osawa M., Anderson D.E. & Erickson H.P. (2008) Reconstitution of contractile FtsZ rings in liposomes. *Science* **320**, 792-4.

Osteryoung K.W., Stokes K.D., Rutherford S.M., Percival A.L. & Lee W.Y. (1998) Chloroplast division in higher plants requires members of two functionally divergent gene families with homology to bacterial *ftsZ*. *Plant Cell* **10**, 1991-2004.

Otto M. (2010) Novel targeted immunotherapy approaches for staphylococcal infection. *Expert Opin Biol Ther* **10**, 1049-59.

Otto M. (2012) Molecular basis of Staphylococcus epidermidis infections. *Semin Immunopathol* **34**, 201-14.

Paoletti L., Lu Y.J., Schujman G.E., de Mendoza D. & Rock C.O. (2007) Coupling of fatty acid and phospholipid synthesis in *Bacillus subtilis*. *J Bacteriol* **189**, 5816-24.

Patrick J.E. & Kearns D.B. (2008) MinJ (YvjD) is a topological determinant of cell division in *Bacillus subtilis*. *Mol Microbiol* **70**, 1166-79.

Peacock S.J., de Silva I. & Lowy F.D. (2001) What determines nasal carriage of *Staphylococcus aureus*? *Trends Microbiol* **9**, 605-10.

Pedersen L.B., Angert E.R. & Setlow P. (1999) Septal localization of penicillin-binding protein 1 in *Bacillus subtilis*. *J Bacteriol* **181**, 3201-11.

Pereira P.M., Filipe S.R., Tomasz A. & Pinho M.G. (2007a) Fluorescence ratio imaging microscopy shows decreased access of vancomycin to cell wall synthetic sites in vancomycin-resistant *Staphylococcus aureus*. *Antimicrob Agents Chemother* **51**, 3627-33.

Pereira P.M., Veiga H., Jorge A.M. & Pinho M.G. (2010) Fluorescent reporters for studies of cellular localization of proteins in *Staphylococcus aureus*. *Appl Environ Microbiol* **76**, 4346-53.

Pereira S.F., Henriques A.O., Pinho M.G., de Lencastre H. & Tomasz A. (2007b) Role of PBP1 in cell division of *Staphylococcus aureus*. *J Bacteriol* **189**, 3525-31.

Pereira S.F., Henriques A.O., Pinho M.G., de Lencastre H. & Tomasz A. (2009) Evidence for a dual role of PBP1 in the cell division and cell separation of *Staphylococcus aureus*. *Mol Microbiol* **72**, 895-904.

Peters N.T., Dinh T. & Bernhardt T.G. (2011) A fail-safe mechanism in the septal ring assembly pathway generated by the sequential recruitment of cell separation amidases and their activators. *J Bacteriol* **193**, 4973-83.

Peters P.C., Migocki M.D., Thoni C. & Harry E.J. (2007) A new assembly pathway for the cytokinetic Z ring from a dynamic helical structure in vegetatively growing cells of *Bacillus subtilis*. *Mol Microbiol* **64**, 487-99.

Petersen P.J., Jacobus N.V., Weiss W.J., Sum P.E. & Testa R.T. (1999) In vitro and in vivo antibacterial activities of a novel glycylcycline, the 9-t-butylglycylamido derivative of minocycline (GAR-936). *Antimicrob Agents Chemother* **43**, 738-44.

Pichoff S. & Lutkenhaus J. (2002) Unique and overlapping roles for ZipA and FtsA in septal ring assembly in *Escherichia coli*. *EMBO J* **21**, 685-93.

Pichoff S. & Lutkenhaus J. (2005) Tethering the Z ring to the membrane through a conserved membrane targeting sequence in FtsA. *Mol Microbiol* **55**, 1722-34.

Pinho M.G., de Lencastre H. & Tomasz A. (2000) Cloning, characterization, and inactivation of the gene pbpC, encoding penicillin-binding protein 3 of *Staphylococcus aureus*. *J Bacteriol* **182**, 1074-9.

Pinho M.G. & Errington J. (2003) Dispersed mode of *Staphylococcus aureus* cell wall synthesis in the absence of the division machinery. *Mol Microbiol* **50**, 871-81.

Pinho M.G. & Errington J. (2004) A divIVA null mutant of *Staphylococcus aureus* undergoes normal cell division. *FEMS Microbiol Lett* **240**, 145-9.

Pinho M.G. & Errington J. (2005) Recruitment of penicillin-binding protein PBP2 to the division site of *Staphylococcus aureus* is dependent on its transpeptidation substrates. *Mol Microbiol* **55**, 799-807.

Pinho M.G., Filipe S.R., de Lencastre H. & Tomasz A. (2001) Complementation of the essential peptidoglycan transpeptidase function of penicillin-binding protein 2 (PBP2) by the drug resistance protein PBP2A in *Staphylococcus aureus*. *J Bacteriol* **183**, 6525-31.

Pinho M.G., Kjos M. & Veening J.W. (2013) How to get (a)round: mechanisms controlling growth and division of coccoid bacteria. *Nat Rev Microbiol* **11**, 601-14.

Poggio S., Takacs C.N., Vollmer W. & Jacobs-Wagner C. (2010) A protein critical for cell constriction in the Gram-negative bacterium *Caulobacter crescentus* localizes at the division site through its peptidoglycan-binding LysM domains. *Mol Microbiol* **77**, 74-89.

Popham D.L. & Young K.D. (2003) Role of penicillin-binding proteins in bacterial cell morphogenesis. *Curr Opin Microbiol* **6**, 594-9.

Ramirez-Arcos S., Salimnia H., Bergevin I., Paradis M. & Dillon J.A. (2001) Expression of *Neisseria gonorrhoeae* cell division genes *ftsZ*, ftsE and minD is influenced by environmental conditions. *Res Microbiol* **152**, 781-91.

Rao V.S., Srinivas K., Sujini G.N. & Kumar G.N. (2014) Protein-protein interaction detection: methods and analysis. *Int J Proteomics* **2014**, 147648.

Rasigade J.P. & Vandenesch F. (2014) *Staphylococcus aureus*: a pathogen with still unresolved issues. *Infect Genet Evol* **21**, 510-4.

Raskin D.M. & de Boer P.A. (1999a) MinDE-dependent pole-to-pole oscillation of division inhibitor MinC in *Escherichia coli*. *J Bacteriol* **181**, 6419-24.

Raskin D.M. & de Boer P.A. (1999b) Rapid pole-to-pole oscillation of a protein required for directing division to the middle of *Escherichia coli*. *Proc Natl Acad Sci U S A* **96**, 4971-6.

Raskin D.M. & deBoer P.A.J. (1997) The MinE ring: An FtsZ-independent cell structure required for selection of the correct division site in E-coli. *Cell* **91**, 685-94.

RayChaudhuri D. (1999) ZipA is a MAP-Tau homolog and is essential for structural integrity of the cytokinetic FtsZ ring during bacterial cell division. *EMBO J* **18**, 2372-83.

Rice L.B. (2006) Antimicrobial resistance in Gram-positive bacteria. *Am J Infect Control* **34**, S11-S9.

Roberts M.C., Sutcliffe J., Courvalin P., Jensen L.B., Rood J. & Seppala H. (1999) Nomenclature for macrolide and macrolide-lincosamide-streptoGramin B resistance determinants. *Antimicrob Agents Chemother* **43**, 2823-30.

Robichon C., King G.F., Goehring N.W. & Beckwith J. (2008) Artificial septal targeting of *Bacillus subtilis* cell division proteins in *Escherichia coli*: an interspecies approach to the study of protein-protein interactions in multiprotein complexes. *J Bacteriol* **190**, 6048-59.

Robson S.A., Michie K.A., Mackay J.P., Harry E. & King G.F. (2002) The *Bacillus subtilis* cell division proteins FtsL and DivIC are intrinsically unstable and do not interact with one another in the absence of other septasomal components. *Mol Microbiol* **44**, 663-74.

Rosenbach A. (1884) *Mikro-Organismen bei den Wund-Infections-Krankheiten des*

Menschen.

Rothfield L., Taghbalout A. & Shih Y.L. (2005) Spatial control of bacterial division-site placement. *Nat Rev Microbiol* **3**, 959-68.

Rouch D.A., Byrne M.E., Kong Y.C. & Skurray R.A. (1987) The Aaca-Aphd Gentamicin and Kanamycin Resistance Determinant of Tn4001 from Staphylococcus-Aureus - Expression and Nucleotide-Sequence Analysis. *J Gen Microbiol* **133**, 3039-52.

Rowland S.L., Wadsworth K.D., Robson S.A., Robichon C., Beckwith J. & King G.F. (2010) Evidence from Artificial Septal Targeting and Site-Directed Mutagenesis that Residues in the Extracytoplasmic beta Domain of DivIB Mediate Its Interaction with the Divisomal Transpeptidase PBP 2B. *J Bacteriol* **192**, 6116-25.

Ruiz-Avila L.B., Huecas S., Artola M., Vergonos A., Ramirez-Aportela E., Cercenado E., Barasoain I., Vazquez-Villa H., Martin-Fontecha M., Chacon P., Lopez-Rodriguez M.L. & Andreu J.M. (2013) Synthetic inhibitors of bacterial cell division targeting the GTP-binding site of FtsZ. *ACS Chem Biol* **8**, 2072-83.

Sambrook J. & Russell D.W. (2001) *Molecular Cloning: A laboratory Manual*. Cold Spring Harbor Laboratory Press.

Sato N., Hagio M., Wada H. & Tsuzuki M. (2000) Requirement of phosphatidylglycerol for photosynthetic function in thylakoid membranes. *Proc Natl Acad Sci U S A* **97**, 10655-60.

Sauvage E., Kerff F., Terrak M., Ayala J.A. & Charlier P. (2008) The penicillin-binding proteins: structure and role in peptidoglycan biosynthesis. *FEMS Microbiol Rev* **32**, 234-58.

Schaffner-Barbero C., Martin-Fontecha M., Chacon P. & Andreu J.M. (2012) Targeting the assembly of bacterial cell division protein FtsZ with small molecules. *ACS Chem Biol* **7**, 269-77.

Schlag M., Biswas R., Krismer B., Kohler T., Zoll S., Yu W., Schwarz H., Peschel A. & Gotz F. (2010) Role of staphylococcal wall teichoic acid in targeting the major autolysin Atl. *Mol Microbiol* **75**, 864-73.

Schmidt K.L., Peterson N.D., Kustusch R.J., Wissel M.C., Graham B., Phillips G.J. & Weiss D.S. (2004) A predicted ABC transporter, FtsEX, is needed for cell division in *Escherichia coli*. *J Bacteriol* **186**, 785-93.

Sham L.T., Jensen K.R., Bruce K.E. & Winkler M.E. (2013) Involvement of FtsE ATPase and FtsX extracellular loops 1 and 2 in FtsEX-PcsB complex function in cell division of *Streptococcus pneumoniae* D39. *MBio* **4**.

Sharpe M.E., Hauser P.M., Sharpe R.G. & Errington J. (1998) *Bacillus subtilis* cell cycle as studied by fluorescence microscopy: constancy of cell length at initiation of DNA replication and evidence for active nucleoid partitioning. *J Bacteriol* **180**, 547-55.

Shen B. & Lutkenhaus J. (2010) Examination of the interaction between FtsZ and MinCN in E-coli suggests how MinC disrupts Z rings. *Mol Microbiol* **75**, 1285-98.

Shih Y.L., Le T. & Rothfield L. (2003) Division site selection in *Escherichia coli* involves dynamic redistribution of Min proteins within coiled structures that extend between the two cell poles. *Proc Natl Acad Sci U S A* **100**, 7865-70.

Shih Y.L. & Rothfield L. (2006) The bacterial cytoskeleton. *Microbiol Mol Biol Rev* **70**, 729-54.

Shiomi D. & Margolin W. (2007) The C-terminal domain of MinC inhibits assembly of the Z ring in *Escherichia coli*. *J Bacteriol* **189**, 236-43.

Shiomi D., Sakai M. & Niki H. (2008) Determination of bacterial rod shape by a novel cytoskeletal membrane protein. *EMBO J* **27**, 3081-91.

Sieradzki K. & Tomasz A. (1999) Gradual alterations in cell wall structure and metabolism in vancomycin-resistant mutants of *Staphylococcus aureus*. *J Bacteriol* **181**, 7566-70.

Sievers J. & Errington J. (2000) The *Bacillus subtilis* cell division protein FtsL localizes to sites of septation and interacts with DivIC. *Mol Microbiol* **36**, 846-55.

Sievert D.M., Rudrik J.T., Patel J.B., McDonald L.C., Wilkins M.J. & Hageman J.C. (2008) Vancomycin-resistant *Staphylococcus aureus* in the United States, 2002-2006. *Clinical Infectious Diseases* **46**, 668-74.

Silverman J.A., Perlmutter N.G. & Shapiro H.M. (2003) Correlation of daptomycin bactericidal activity and membrane depolarization in *Staphylococcus aureus*. *Antimicrob Agents Chemother* **47**, 2538-44.

Singh J.K., Makde R.D., Kumar V. & Panda D. (2007) A membrane protein, EzrA, regulates assembly dynamics of FtsZ by interacting with the C-terminal tail of FtsZ. *Biochemistry* **46**, 11013-22.

Singh J.K., Makde R.D., Kumar V. & Panda D. (2008) SepF increases the assembly and bundling of FtsZ polymers and stabilizes FtsZ protofilaments by binding along its length. *J Biol Chem* **283**, 31116-24.

Skinner D. & Keefer C. (1941) Significance of bacteremia caused by *Staphylococcus aureus*: A study of one hundred and twenty-two cases and a review of the literature concerned with experimental infection in animals. *Arch Intern Med* **68**, 851–75.

Slovak P.M., Porter S.L. & Armitage J.P. (2006) Differential localization of Mre proteins with PBP2 in Rhodobacter sphaeroides. *J Bacteriol* **188**, 1691-700.

Slovak P.M., Wadhams G.H. & Armitage J.P. (2005) Localization of MreB in Rhodobacter sphaeroides under conditions causing changes in cell shape and membrane structure. *J Bacteriol* **187**, 54-64.

Song J.H., Ko K.S., Lee J.Y., Baek J.Y., Oh W.S., Yoon H.S., Jeong J.Y. & Chun J. (2005) Identification of essential genes in *Streptococcus pneumoniae* by allelic replacement mutagenesis. *Mol Cells* **19**, 365-74.

Spratt B.G. (1975) Distinct penicillin binding proteins involved in the division, elongation, and shape of *Escherichia coli* K12. *Proc Natl Acad Sci U S A* **72**, 2999-3003.

Spratt B.G. (1977) Temperature-sensitive cell division mutants of *Escherichia coli* with thermolabile penicillin-binding proteins. *J Bacteriol* **131**, 293-305.

Steele V.R., Bottomley A.L., Garcia-Lara J., Kasturiarachchi J. & Foster S.J. (2011) Multiple essential roles for EzrA in cell division of *Staphylococcus aureus*. *Mol Microbiol* **80** 542-55.

Storrs M.J., Courvalin P. & Foster T.J. (1988) Genetic-Analysis of Gentamicin Resistance in Methicillin-Resistant and Gentamicin-Resistant Strains of Staphylococcus-Aureus Isolated in Dublin Hospitals. *Antimicrob Agents Chemother* **32**, 1174-81.

Strahl H. & Hamoen L.W. (2012) Finding the corners in a cell. *Curr Opin Microbiol* **15**, 731-6.

Stranger-Jones Y.K., Bae T. & Schneewind O. (2006) Vaccine assembly from surface proteins of *Staphylococcus aureus*. *Proc Natl Acad Sci U S A* **103**, 16942-7.

Stricker J., Maddox P., Salmon E.D. & Erickson H.P. (2002) Rapid assembly dynamics of the *Escherichia coli* FtsZ-ring demonstrated by fluorescence recovery after photobleaching. *Proc Natl Acad Sci U S A* **99**, 3171-5.

Studier F.W. (2005) Protein production by auto-induction in high density shaking cultures. *Protein Expr Purif* **41**, 207-34.

Suefuji K., Valluzzi R. & RayChaudhuri D. (2002) Dynamic assembly of MinD into filament bundles modulated by ATP, phospholipids, and MinE. *Proc Natl Acad Sci U S A* **99**, 16776-81.

Szeto T.H., Rowland S.L. & King G.F. (2001) The dimerization function of MinC resides in a structurally autonomous C-terminal domain. *J Bacteriol* **183**, 6684-7.

Tally F.P., Zeckel M., Wasilewski M.M., Carini C., Berman C.L., Drusano G.L. & Oleson F.B., Jr. (1999) Daptomycin: a novel agent for Gram-positive infections. *Expert Opin Investig Drugs* **8**, 1223-38.

Tamaki S., Matsuzawa H. & Matsuhashi M. (1980) Cluster of mrdA and mrdB genes responsible for the rod shape and mecillinam sensitivity of *Escherichia coli*. *J Bacteriol* **141**, 52-7.

Tavares A.C., Fernandes P.B., Carballido-Lopez R. & Pinho M.G. (2015) MreC and MreD Proteins Are Not Required for Growth of *Staphylococcus aureus*. *PLoS One* **10**, e0140523.

Tavares J.R., de Souza R.F., Meira G.L. & Gueiros-Filho F.J. (2008) Cytological characterization of YpsB, a novel component of the *Bacillus subtilis* divisome. *J Bacteriol* **190**, 7096-107.

Thanassi J.A., Hartman-Neumann S.L., Dougherty T.J., Dougherty B.A. & Pucci M.J. (2002) Identification of 113 conserved essential genes using a high-throughput gene disruption system in *Streptococcus pneumoniae*. *Nucleic Acids Res* **30**, 3152-62.

Thanedar S. & Margolin W. (2004) FtsZ exhibits rapid movement and oscillation waves in helix-like patterns in *Escherichia coli*. *Curr Biol* **14**, 1167-73.

Thibessard A., Fernandez A., Gintz B., Leblond-Bourget N. & Decaris B. (2002) Effects of *rodA* and pbp2b disruption on cell morphology and oxidative stress response of Streptococcus thermophilus CNRZ368. *J Bacteriol* **184**, 2821-6.

Tiyanont K., Doan T., Lazarus M.B., Fang X., Rudner D.Z. & Walker S. (2006) Imaging peptidoglycan biosynthesis in *Bacillus subtilis* with fluorescent antibiotics. *Proc Natl Acad Sci U S A* **103**, 11033-8.

Tjalsma H. & van Dijl J.M. (2005) Proteomics-based consensus prediction of protein retention in a bacterial membrane. *Proteomics* **5**, 4472-82.

Tonthat N.K., Arold S.T., Pickering B.F., Van Dyke M.W., Liang S., Lu Y., Beuria T.K., Margolin W. & Schumacher M.A. (2011) Molecular mechanism by which the nucleoid occlusion factor, SlmA, keeps cytokinesis in check. *EMBO J* **30**, 154-64.

Tsiodras S., Gold H.S., Sakoulas G., Eliopoulos G.M., Wennersten C., Venkataraman L., Moellering R.C. & Ferraro M.J. (2001) Linezolid resistance in a clinical isolate of *Staphylococcus aureus*. *Lancet* **358**, 207-8.

Turner R.D., Hurd A.F., Cadby A., Hobbs J.K. & Foster S.J. (2013) Cell wall elongation mode in Gram-negative bacteria is determined by peptidoglycan architecture. *Nat Commun* **4**, 1496.

Turner R.D., Ratcliffe E.C., Wheeler R., Golestanian R., Hobbs J.K. & Foster S.J. (2010) Peptidoglycan architecture can specify division planes in *Staphylococcus aureus*. *Nat Commun* **1**, 26.

Turner R.D., Vollmer W. & Foster S.J. (2014) Different walls for rods and balls: the diversity of peptidoglycan. *Mol Microbiol* **91**, 862-74.

Typas A., Banzhaf M., Gross C.A. & Vollmer W. (2012) From the regulation of peptidoglycan synthesis to bacterial growth and morphology. *Nat Rev Microbiol* **10**, 123-36.

Tzagoloff H. & Novick R. (1977) Geometry of cell division in *Staphylococcus aureus*. *J Bacteriol* **129**, 343-50.

Uehara T. & Bernhardt T.G. (2011) More than just lysins: peptidoglycan hydrolases tailor the cell wall. *Curr Opin Microbiol* **14**, 698-703.

Uehara T., Dinh T. & Bernhardt T.G. (2009) LytM-domain factors are required for daughter cell separation and rapid ampicillin-induced lysis in *Escherichia coli*. *J Bacteriol* **191**, 5094-107.

Uehara T., Parzych K.R., Dinh T. & Bernhardt T.G. (2010) Daughter cell separation is controlled by cytokinetic ring-activated cell wall hydrolysis. *EMBO J* **29**, 1412-22.

Urh M., Simpson D. & Zhao K. (2009) Affinity chromatography: general methods. *Methods Enzymol* **463**, 417-38.

Ursinus A., van den Ent F., Brechtel S., de Pedro M., Holtje J.V., Lowe J. & Vollmer W. (2004) Murein (peptidoglycan) binding property of the essential cell division protein FtsN from *Escherichia coli*. *J Bacteriol* **186**, 6728-37.

Uttley A.H.C., Collins C.H., Naidoo J. & George R.C. (1988) Vancomycin-Resistant Enterococci. *Lancet* **1**, 57-8.

van den Ent F., Amos L.A. & Lowe J. (2001) Prokaryotic origin of the actin cytoskeleton. *Nature* **413**, 39-44.

van den Ent F., Johnson C.M., Persons L., de Boer P. & Lowe J. (2010) Bacterial actin MreB assembles in complex with cell shape protein RodZ. *EMBO J* **29**, 1081-90.

van den Ent F., Leaver M., Bendezu F., Errington J., de Boer P. & Lowe J. (2006) Dimeric structure of the cell shape protein MreC and its functional implications. *Mol Microbiol* **62**, 1631-42.

van den Ent F., Vinkenvleugel T.M.F., Ind A., West P., Veprintsev D., Nanninga N., den Blaauwen T. & Lowe J. (2008) Structural and mutational analysis of the cell division protein FtsQ. *Mol Microbiol* **68**, 110-23.

Varley A.W. & Stewart G.C. (1992) The divIVB region of the *Bacillus subtilis* chromosome encodes homologs of *Escherichia coli* septum placement (minCD) and cell shape (mreBCD) determinants. *J Bacteriol* **174**, 6729-42.

Varma A., de Pedro M.A. & Young K.D. (2007) FtsZ directs a second mode of peptidoglycan synthesis in *Escherichia coli*. *J Bacteriol* **189**, 5692-704.

Vats P. & Rothfield L. (2007) Duplication and segregation of the actin (MreB) cytoskeleton during the prokaryotic cell cycle. *Proc Natl Acad Sci U S A* **104**, 17795-800.

Vats P., Shih Y.L. & Rothfield L. (2009) Assembly of the MreB-associated cytoskeletal ring of *Escherichia coli*. *Mol Microbiol* **72**, 170-82.

Vaughan S., Wickstead B., Gull K. & Addinall S.G. (2004) Molecular evolution of FtsZ protein sequences encoded within the genomes of archaea, bacteria, and eukaryota. *J Mol Evol* **58**, 19-29.

Veiga H., Jorge A.M. & Pinho M.G. (2011) Absence of nucleoid occlusion effector Noc impairs formation of orthogonal FtsZ rings during *Staphylococcus aureus* cell division. *Mol Microbiol* **80**, 1366-80.

Villafane R., Bechhofer D.H., Narayanan C.S. & Dubnau D. (1987) Replication control genes of plasmid pE194. *J Bacteriol* **169**, 4822-9.

Vollmer W. (2006) The prokaryotic cytoskeleton: a putative target for inhibitors and antibiotics? *Appl Microbiol Biotechnol* **73**, 37-47.

von Kockritz-Blickwede M., Rohde M., Oehmcke S., Miller L.S., Cheung A.L., Herwald H., Foster S. & Medina E. (2008) Immunological mechanisms underlying the genetic predisposition to severe *Staphylococcus aureus* infection in the mouse model. *Am J Pathol* **173**, 1657-68.

Wachi M., Doi M., Okada Y. & Matsuhashi M. (1989) New mre genes *mreC* and *mreD*, responsible for formation of the rod shape of *Escherichia coli* cells. *J Bacteriol* **171**, 6511-6.

Wachi M., Doi M., Tamaki S., Park W., Nakajima-Iijima S. & Matsuhashi M. (1987) Mutant isolation and molecular cloning of mre genes, which determine cell shape, sensitivity to mecillinam, and amount of penicillin-binding proteins in *Escherichia coli*. *J Bacteriol* **169**, 4935-40.

Wagner J.K., Setayeshgar S., Sharon L.A., Reilly J.P. & Brun Y.V. (2006) A nutrient uptake role for bacterial cell envelope extensions. *Proc Natl Acad Sci U S A* **103**, 11772-7.

Wang J.D. & Levin P.A. (2009) Metabolism, cell growth and the bacterial cell cycle. *Nat Rev Microbiol* **7**, 822-7.

Wang L., Khattar M.K., Donachie W.D. & Lutkenhaus J. (1998) FtsI and FtsW are localized to the septum in *Escherichia coli*. *J Bacteriol* **180**, 2810-6.

Wang Y., Jones B.D. & Brun Y.V. (2001) A set of *ftsZ* mutants blocked at different stages of cell division in Caulobacter. *Mol Microbiol* **40**, 347-60.

Weart R.B., Lee A.H., Chien A.C., Haeusser D.P., Hill N.S. & Levin P.A. (2007) A metabolic sensor governing cell size in bacteria. *Cell* **130**, 335-47.

Weart R.B. & Levin P.A. (2003) Growth rate-dependent regulation of medial FtsZ ring formation. *J Bacteriol* **185**, 2826-34.

Wedemeyer W.J., Welker E. & Scheraga H.A. (2002) Proline cis-trans isomerization and protein folding. *Biochemistry* **41**, 14637-44.

Wei Y., Havasy T., McPherson D.C. & Popham D.L. (2003) Rod shape determination by the *Bacillus subtilis* class B penicillin-binding proteins encoded by *pbpA* and pbpH. *J Bacteriol* **185**, 4717-26.

Weigel L.M., Clewell D.B., Gill S.R., Clark N.C., McDougal L.K., Flannagan S.E., Kolonay J.F., Shetty J., Killgore G.E. & Tenover F.C. (2003) Genetic analysis of a high-level vancomycin-resistant isolate of *Staphylococcus aureus*. *Science* **302**, 1569-71.

Weiss D.S. (2004) Bacterial cell division and the septal ring. *Mol Microbiol* **54**, 588-97.

Weiss D.S., Chen J.C., Ghigo J.M., Boyd D. & Beckwith J. (1999) Localization of FtsI (PBP3) to the septal ring requires its membrane anchor, the Z ring, FtsA, FtsQ, and FtsL. *J Bacteriol* **181**, 508-20.

Weiss D.S., Pogliano K., Carson M., Guzman L.M., Fraipont C., Nguyen-Disteche M., Losick R. & Beckwith J. (1997) Localization of the *Escherichia coli* cell division protein FtsI (PBP3) to the division site and cell pole. *Mol Microbiol* **25**, 671-81.

Werner G., Cuny C., Schmitz F.J. & Witte W. (2001) Methicillin-resistant, quinupristin-dalfopristin-resistant *Staphylococcus aureus* with reduced sensitivity to glycopeptides. *J Clin Microbiol* **39**, 3586-90.

White C.L., Kitich A. & Gober J.W. (2010) Positioning cell wall synthetic complexes by the bacterial morphogenetic proteins MreB and MreD. *Mol Microbiol* **76**, 616-33.

Williams R.E.O. (1959) Epidemic Staphylococci. *The Lancet* **273(7065)**, 190-5.

Woldringh C.L., Mulder E., Valkenburg J.A., Wientjes F.B., Zaritsky A. & Nanninga N. (1990) Role of the nucleoid in the toporegulation of division. *Res Microbiol* **141**, 39-49.

Wright C.L., Byrne M.E., Firth N. & Skurray R.A. (1998) A retrospective molecular analysis of gentamicin resistance in *Staphylococcus aureus* strains from UK hospitals. *J Med Microbiol* **47**, 173-8.

Wu L.J. & Errington J. (2004) Coordination of cell division and chromosome segregation by a nucleoid occlusion protein in *Bacillus subtilis*. *Cell* **117**, 915-25.

Wu L.J. & Errington J. (2012) Nucleoid occlusion and bacterial cell division. *Nat Rev Microbiol* **10**, 8-12.

Wu L.J., Ishikawa S., Kawai Y., Oshima T., Ogasawara N. & Errington J. (2009) Noc protein binds to specific DNA sequences to coordinate cell division with chromosome segregation. *EMBO J* **28**, 1940-52.

Yamada S., Sugai M., Komatsuzawa H., Nakashima S., Oshida T., Matsumoto A. & Suginaka H. (1996) An autolysin ring associated with cell separation of *Staphylococcus aureus*. *J Bacteriol* **178**, 1565-71.

Yang D.C., Peters N.T., Parzych K.R., Uehara T., Markovski M. & Bernhardt T.G. (2011) An ATP-binding cassette transporter-like complex governs cell-wall hydrolysis at the bacterial cytokinetic ring. *Proc Natl Acad Sci U S A* **108**, E1052-60.

Yang D.C., Tan K., Joachimiak A. & Bernhardt T.G. (2012) A conformational switch controls cell wall-remodelling enzymes required for bacterial cell division. *Mol Microbiol* **85**, 768-81.

Yanouri A., Daniel R.A., Errington J. & Buchanan C.E. (1993) Cloning and sequencing of the cell division gene *pbpB*, which encodes penicillin-binding protein 2B in *Bacillus subtilis*. *J Bacteriol* **175**, 7604-16.

Yao J. & Rock C.O. (2013) Phosphatidic acid synthesis in bacteria. *Biochim Biophys Acta* **1831**, 495-502.

Young K.H. (1998) Yeast two-hybrid: So many interactions, (in) so little time ... *Biology of Reproduction* **58**, 302-11.

Yu X.C. & Margolin W. (1999) FtsZ ring clusters in min and partition mutants: role of both the Min system and the nucleoid in regulating FtsZ ring localization. *Mol Microbiol* **32**, 315-26.

Yu X.C., Tran A.H., Sun Q. & Margolin W. (1998) Localization of cell division protein FtsK to the *Escherichia coli* septum and identification of a potential N-terminal targeting domain. *J Bacteriol* **180**, 1296-304.

Zapun A., Vernet T. & Pinho M.G. (2008) The different shapes of cocci. *FEMS Microbiol Rev* **32**, 345-60.

Zhou X., Halladin D.K., Rojas E.R., Koslover E.F., Lee T.K., Huang K.C. & Theriot J.A. (2015) Bacterial division. Mechanical crack propagation drives millisecond daughter cell separation in *Staphylococcus aureus*. *Science* **348**, 574-8.